

DIPLOMARBEIT

---

# A Measurement of the Electron Identification Efficiency using $W \rightarrow e\nu$ Decays in the ATLAS Experiment

Philip Sommer



---

Fakultät für Mathematik und Physik  
Albert-Ludwigs-Universität Freiburg

---



**A Measurement of the  
Electron Identification Efficiency using  
 $W \rightarrow e\nu$  Decays in the ATLAS Experiment**

DIPLOMARBEIT

Fakultät für Mathematik und Physik der

ALBERT-LUDWIGS-UNIVERSITÄT

Freiburg im Breisgau

vorgelegt von

Philip Sommer

Betreuer der Arbeit

Prof. Dr. Karl Jakobs

Juli 2012



## Erklärung

Hiermit versichere ich, dass ich die vorliegende Diplomarbeit selbstständig verfasst und keine anderen als die angegebenen Quellen und Hilfsmittel verwendet habe.

Freiburg, am 11. Juli 2012

---

Philip Sommer



---

# Contents

---

<b>0</b>	<b>Zusammenfassung/Abstract</b>	<b>1</b>
<b>1</b>	<b>Introduction</b>	<b>5</b>
<b>2</b>	<b>The Standard Model</b>	<b>9</b>
2.1	The Standard Model of Particle Physics . . . . .	9
2.1.1	Particle Content . . . . .	9
2.1.2	Fields and Gauge Interactions . . . . .	10
2.1.3	Quantum Chromodynamics . . . . .	11
2.1.4	Electroweak Theory . . . . .	12
2.2	Collider Physics . . . . .	14
2.2.1	Phenomenology . . . . .	14
2.2.2	Proton Structure . . . . .	15
2.2.3	Properties of the Gauge Bosons . . . . .	15
2.2.4	$W$ Boson Production at the LHC . . . . .	17
2.2.5	Cross-sections at the LHC . . . . .	18
2.3	Event Generation and Simulation . . . . .	20
<b>3</b>	<b>The ATLAS Detector at the LHC</b>	<b>21</b>
3.1	The Large Hadron Collider . . . . .	21
3.2	The ATLAS Detector . . . . .	22
3.2.1	The Inner Detector . . . . .	23
3.2.2	Calorimetry . . . . .	25
3.2.3	Muon Spectrometer . . . . .	27
3.2.4	Trigger . . . . .	27
<b>4</b>	<b>Motivation</b>	<b>29</b>
4.1	Electroweak Precision Measurements . . . . .	29
4.2	Usage of Scale-factors in Physics Analyses . . . . .	30
4.3	Relevance for the Higgs Boson Search . . . . .	31
<b>5</b>	<b>Event Reconstruction</b>	<b>33</b>
5.1	Track Reconstruction . . . . .	33
5.2	Vertex Reconstruction . . . . .	34
5.3	Electron Reconstruction . . . . .	34
5.4	Electron Identification . . . . .	35

5.5	Electron Trigger . . . . .	37
5.6	Electron Isolation . . . . .	38
5.7	Missing Transverse Energy . . . . .	38
5.8	$E_T^{\text{miss}}$ Significance Trigger . . . . .	39
5.9	Jet Reconstruction . . . . .	40
<b>6</b>	<b>Methodology of the Measurement</b>	<b>41</b>
6.1	The Tag & Probe Method . . . . .	41
6.2	Efficiency Definition . . . . .	42
6.3	Scale-factor Definition . . . . .	44
6.4	Combination of Different Measurements . . . . .	44
6.5	Measurement of Efficiencies . . . . .	45
6.5.1	Binning . . . . .	45
6.5.2	Background Subtraction . . . . .	47
6.5.3	Validation of the Background Templates . . . . .	51
6.6	Comparison of $J/\psi$ , $W$ and $Z$ Kinematics . . . . .	54
6.7	Statistical Uncertainties . . . . .	55
6.7.1	Background Subtracted Data . . . . .	55
6.7.2	Monte-Carlo . . . . .	58
6.7.3	Efficiency . . . . .	58
6.7.4	Treatment of Correlations and Calculation of Averages . . . . .	58
6.8	Systematic Uncertainties . . . . .	59
6.8.1	Systematic Variations . . . . .	59
6.8.2	Other Systematic Uncertainties Added . . . . .	60
<b>7</b>	<b>Data, Monte-Carlo Samples and Event Selection</b>	<b>61</b>
7.1	Data Samples . . . . .	61
7.2	Monte-Carlo Samples . . . . .	61
7.3	Event Selection . . . . .	63
7.3.1	Preselection . . . . .	63
7.3.2	Electron Selection . . . . .	66
7.3.3	$W$ Selection . . . . .	67
7.4	Monte-Carlo Specific Corrections and Selection . . . . .	67
7.4.1	Pile-up re-weighting . . . . .	68
7.4.2	Vertex Position Re-weighting . . . . .	69
7.4.3	Truth Matching . . . . .	69
7.4.4	Trigger Selection . . . . .	70
7.4.5	Energy Smearing . . . . .	70
7.5	Agreement between Data and Monte-Carlo . . . . .	70
<b>8</b>	<b>Systematic Studies</b>	<b>75</b>
8.1	Studies on $E_T^{\text{miss}}$ Significance Triggers . . . . .	75
8.2	Impact of the Vertex Position . . . . .	76
8.2.1	Efficiencies as a Function of the $z_{\text{vtx}}$ Position . . . . .	78

8.2.2	Differential Measurement in $\eta$ . . . . .	79
8.3	Pile-up Dependence . . . . .	79
8.3.1	Efficiencies vs. Pile-up . . . . .	81
8.3.2	Different Methods of Re-weighting . . . . .	81
8.3.3	Different Ways of Modelling . . . . .	82
8.4	Impact of Charge Misidentification . . . . .	83
8.4.1	ID Efficiency for Charge Misidentified Electrons . . . . .	84
8.4.2	$e^{+/-}$ -ratios for the Different Generators . . . . .	84
8.4.3	Charge Separated Measurements . . . . .	85
8.4.4	Systematic Uncertainties from Charge Asymmetry . . . . .	86
8.5	Impact of the Generator . . . . .	88
<b>9</b>	<b>Identification Efficiency Measurement</b>	<b>91</b>
9.1	Status 2010 and Improvements in the Present Analysis . . . . .	91
9.1.1	Status 2010 . . . . .	91
9.1.2	Improvements in Present Analysis . . . . .	92
9.1.3	1Dx1D vs. 2D Binning . . . . .	92
9.2	Efficiencies . . . . .	93
9.2.1	Measurement in $\eta$ , $E_T$ . . . . .	93
9.2.2	Measurement of Single Cut Efficiencies . . . . .	94
9.3	Scale-factors . . . . .	94
9.4	Efficiencies and Scale-factors in Different $\eta$ Granularities . . . . .	98
9.4.1	Coarse Binning . . . . .	98
9.4.2	Intermediate Binning . . . . .	98
9.4.3	Fine Binning . . . . .	102
9.5	Systematic Uncertainty from Variations . . . . .	102
9.6	Systematic Correlations Between the Different Bins . . . . .	106
<b>10</b>	<b>Conclusions</b>	<b>109</b>
<b>A</b>	<b>Tables of Efficiencies and Scalefactors</b>	<b>111</b>
<b>B</b>	<b>Derivation of the Statistical Formulae</b>	<b>127</b>
<b>C</b>	<b>Technicalities</b>	<b>131</b>
	<b>Bibliography</b>	<b>133</b>



Isolierte Elektronen hoher Energie treten als Bestandteil der Endzustände verschiedenster Prozesse des Standardmodells und neuer Physik in vielen Analysen am ATLAS-Experiment auf. Vorteile der Benutzung von Elektronen sind, dass diese eine im Gegensatz zu hadronischen Endzuständen an Hadron-Kollisionsbeschleunigern klare Signatur darstellen. Wie bei jedem Zählexperiment, ist die Kenntnis der Effizienz, mit der ein gewisser Prozess gemessen wird, von allergrößter Bedeutung. Die Messung von Elektronen erfolgt durch Forderung verschiedener Identifikationskriterien an die Signale im Detektor. Die vorliegende Arbeit befasst sich mit der Messung der Effizienz, mit der diese Kriterien Elektronen korrekt identifizieren.

Die Messung erfolgt mit einem Satz reiner Elektronen aus dem Zerfall von  $W$ -Bosonen in ein Elektron und ein Neutrino. Die Elektronen werden nur mithilfe der fehlenden Transversalenergie, verursacht durch das am Zerfall beteiligte Neutrino, ausgewählt. Hierfür wird ein spezieller Trigger verwendet. Das unverfälschte Elektron kann dann zur Untersuchung der Identifikationseffizienz herangezogen werden. Die so erhaltenen Elektronen sind stark mit Untergrundprozessen verunreinigt, die für die Messung abgezogen werden.

Je nach Entstehungsprozess unterscheiden sich Elektronen in ihren kinematischen Verteilungen. Die Messung wird daher als Funktion der Pseudorapidität  $\eta$  und der Transversalenergie  $E_T$  durchgeführt. Da die Effizienz der Identifikation von Elektronen besonders von diesen beiden Variablen abhängt, werden die Ergebnisse damit unabhängig vom Entstehungsprozess. Sie werden später mit weiteren, unabhängigen Messungen in  $J/\psi \rightarrow ee$  und  $Z \rightarrow ee$  Endzuständen kombiniert und den Mitgliedern der ATLAS-Kollaboration in Form von Skalenfaktoren, die simulierte Ereignisse entsprechend der Messung in Daten korrigieren, zur Verfügung gestellt. So finden die Ergebnisse Anwendung in physikalischen Analysen, wo sie verwendet, werden um die untersuchten Prozesse um Detektoreffekte zu korrigieren.

Die Messung wird doppelt-differenziell als Funktion der Transversalenergie  $E_T$  der Elektronen in 5 GeV Schritten im Bereich  $15 < E_T < 50$  GeV und als Funktion der Pseudorapidität  $\eta$  im Akzeptanzbereich der Spurdetektoren von  $-2.47 < \eta < 2.47$  durchgeführt. Um den Bedürfnissen verschiedener Analysegruppen gerecht zu werden, werden die Ergebnisse in zwei unterschiedlichen Granularitäten in  $\eta$  produziert. Die eine Granularität orientiert sich an der Detektorgeometrie und den Identifikationskriterien mit 20 Einteilungen in  $\eta$ . Sie bietet eine hohe Präzision bei einfacher Anwendung in physikalischen Analysen.

Die zweite Granularität hat 50 Einteilungen in  $\eta$  und infolgedessen größere statistische Unsicherheiten. Trotzdem wird eine Präzision von  $\lesssim 1\%$  in dem für Standardmodell-

Analysen wichtigen kinematischen Bereich erreicht. Zusätzlich werden detaillierte Informationen über die systematischen Korrelationen der Ergebnisse in den verschiedenen  $\eta \times E_T$  Bereichen zur Verfügung gestellt. Eine sorgfältige Fehlerbetrachtung mithilfe dieser Informationen ermöglicht eine maximale Präzision. Die feine Granularität und die Kenntnis der systematischen Korrelationen kommt besonders differenziellen Messungen zugute.

---

# Abstract

---

As a component of the final states of a variety of Standard Model processes, as well as new physics, isolated, high-energetic electrons are the cornerstones of many analyses at the ATLAS experiment. At hadron colliders they give a very clear signature in contrast to hadronic final states. Like in any counting experiment, the knowledge of the efficiency to register a certain process is of utmost importance. Electrons are measured by requiring the detector signals to fulfil a set of identification criteria. This thesis presents a measurement of the efficiency of these criteria to correctly identify electrons.

$W$  bosons serve as a source of a clean sample of electrons used in the measurement. These are selected by the missing transverse energy in the event. A special trigger is used to do that. The unbiased electron can then be used for the measurement of the identification efficiency. The electron sample obtained this way is largely contaminated with background processes. A subtraction technique is applied to account for that.

Depending on the production mechanism electrons have different kinematic distributions. Therefore, the measurement is carried out as a function of the pseudo-rapidity  $\eta$  and the transverse energy  $E_T$ . Since the efficiency to identify electrons depends especially on these variables, the results become process-independent this way. They are later combined with other, independent measurements in  $J/\psi \rightarrow ee$  and  $Z \rightarrow ee$  final states and provided to the other members of the ATLAS collaboration in form of scale-factors. These are calculated such that they correct simulated event samples according to the results of the measurement in data. This way the results find their way into all physics analyses involving electrons where they are used to correct the processes under investigation for detector effects.

The measurement is performed double differentially in constant 5 GeV bins of the transverse energy of the electron  $E_T$  covering the range  $15 < E_T < 50$  GeV and as a function of the pseudo-rapidity  $\eta$  in the acceptance region of the tracking system from  $-2,47 < \eta < 2,47$ . To fit the special needs of different analysis groups the results are provided in two different granularities in  $\eta$ . One is oriented at the detector geometry and identification requirements with 20 bins in  $\eta$ . This granularity provides a high precision with the possibility of a simple translation to physics analyses.

The other uses 50 bins in  $\eta$ , resulting in larger statistical uncertainties. Nevertheless, a precision of  $\lesssim 1\%$  was reached over the kinematic range that is most important for Standard Model analyses. Additionally, detailed information about the systematic correlations between the results in the different  $\eta \times E_T$  bins is provided. A thorough treatment of the uncertainties and the use of this information allows for a maximum of precision. The fine granularity and the knowledge of systematic correlations particularly benefits differential physics analyses.



Since March 2010 the ATLAS experiment at the European Centre of Nuclear Research CERN is recording collisions of protons at unprecedented energies. The physics programme is broad and ranges from Standard Model precision measurements, over the test of models beyond the Standard Model to model independent searches for unknown particles and phenomena.

High energy physics is investigating very short lived particles that eventually decay to light leptons or hadronic final states. They are produced in particle collisions and recorded by large detectors. Most of these particles decay even before they can interact with the detector. In order to analyse them they need to be identified by their decay products. Actual hits in the detector are caused by a hand full of baryons and mesons, by muons  $\mu$ , photons  $\gamma$  and electrons  $e$ . To examine any particle or process one, thus, relies on a precise determination of what kind of particles caused the hits in the detector. Physics analyses extensively rely on the three last-mentioned  $\mu$ ,  $\gamma$  and  $e$ , because the baryons and mesons usually come in sprays of collimated particles, so-called jets, and hence do not give clear signatures.

The physics processes of prime interest at the LHC suffer from large background and require an excellent capability in reconstructing and identifying these final state electrons, photons and muons. All analyses need to be translated into detector independent quantities, later. In order to do so, the knowledge of the efficiency to reconstruct and identify all the objects used is required, i.e. what fraction of the objects that were produced actually get reconstructed.

Both electrons and muons are equally important since they have very similar properties and thus are interchangeable in most physics processes. Corresponding physics measurements with muons and electrons, respectively, are frequently combined in order to increase precision, to cross-check each other or to overcome statistical limitations; the requirement of differing leptons in an event can be used to discriminate against background from pair-produced leptons of same flavour.

The thesis presented here is concerned with the measurement of the efficiency of identifying electrons based on algorithms that were developed independently before. With the large amount of data accumulated by the ATLAS experiment since the start of the LHC it is possible to perform measurements of the efficiency using data driven methods. A first measurement was already conducted with the data taken in 2010 [1]. The present analysis performs this measurement using the 2011 data. Apart from adapting to the new running conditions, improvements in reconstruction and identification algorithms, and to account for changes in the detector simulation and performance, the major objective has been the challenge of significantly improving the measurement.

This is desperately needed in order to allow for an improvement of existing precision measurements and to lay the groundwork necessary to render a whole set of future precision measurements possible. In general, the performance of the detector is monitored, adjusted and improved in dedicated measurements. The outcome is provided to the other members of the collaboration and find their way into physics analyses. Hence, the presented measurement benefits all analyses that use electrons.

At hadron colliders, electrons are produced at a high rate as the decay products of the resonances of  $pp \rightarrow Z/\gamma^*$  Drell-Yan processes and  $pp \rightarrow W$ . These serve as well-defined samples of isolated, high-energetic electrons for the efficiency measurements. In this thesis, the electron identification efficiency is measured using  $W \rightarrow e\nu$  processes, where a  $W$  boson is produced in a proton-proton collision and decays to an electron and a neutrino. A so-called tag-and-probe method is used, i.e. the  $W$  sample is selected using tight constraints on the neutrino or the missing transverse energy (tag), while only very loose constraints are made on the electron (probe) that is then used to measure the electron identification efficiency.

In physics measurements, Monte-Carlo simulations are used to correct the measured event counts for detector effects – amongst others the identification efficiency – to the number of events actually produced in the acceptance region of the detector. The Monte-Carlo simulation therefore needs to accurately describe the detector efficiency. This is achieved by correcting the simulated event samples with scale-factors that are calculated such that the true identification efficiency as measured in data is described in the simulation. Calculating these scale-factors is the major purpose of this analysis. It always has to be assured that these scale-factors are independent of the process they have been measured on (here  $W \rightarrow e\nu$ ). The identification efficiency typically varies in the different detector regions and depends on the energy of the electron. In order to assure the application of the results to other physics processes, the measurement is therefore performed double differentially as a function of the kinematic variables pseudo-rapidity  $\eta$  and transverse energy  $E_T$ . The scale-factors obtained from the measurement are combined with two other measurements that use electrons from  $J/\psi \rightarrow ee$  and  $Z \rightarrow ee$ . These are then provided to all analyses groups of the ATLAS collaboration.

The thesis starts with the very brief introductory Chapter 1. A reminder of the theory needed for the understanding of the physics at hadron colliders is given in Chapter 2. An overview of the experimental setup, the LHC and the ATLAS detector, follows in Chapter 3. Chapter 4 is concerned with the incentive of the performance measurements and the analyses most extensively relying on their results. After a description of the event reconstruction algorithms with a focus on missing transverse energy and the electron reconstruction and identification – particularly important for the analysis – in Chapter 5, the methodology of the measurement is explained in detail in Chapter 6. The used data samples and event selection criteria are described in Chapter 7. The next two chapters present the actual measurements; a collection of systematic studies on matters expected to affect either the efficiencies or their measurement is given in Chapter 8 and the actual measurement in Chapter 9. Finally all results are summarised and discussed in Chapter 10.

The results presented here are part of the official results of the 2011 run and will be

used in combination with two other measurements from  $Z \rightarrow ee$  and  $J/\psi \rightarrow ee$  by all future analyses by the ATLAS collaboration that involve electron final states in 2011 data at  $\sqrt{s} = 7$  TeV. The results are internally documented in Refs. [2, 3] where large parts of this thesis where incorporated.



This chapter introduces the theoretical and mathematical concepts used in high energy particle physics. Mankind's knowledge of subatomic particles and their interactions is described in a mathematical framework called the *Standard Model*. An overview is given in Section 2.1. Phenomenological aspects of proton-proton collisions are presented in Section 2.2. After that, a very brief introduction to Monte-Carlo generators, that are important tools of high energy physics analyses, is given in Section 2.3.

## 2.1 The Standard Model of Particle Physics

The Standard Model of particle physics represents today's knowledge of elementary particles and their interactions. Its fundamental ingredient is a  $SU(3) \times SU(2) \times U(1)$  gauge symmetry from which the laws of three fundamental forces can be deduced. It is a quantum field theory, incorporating quantum mechanics and special relativity. The three forces are the strong force, the weak force and the electromagnetic force. For the fourth known force, gravitation, no quantum theory could yet be developed. The basic constituents of all matter are 6 quarks and 6 leptons as listed in Table 2.1. Each of them has a corresponding anti-particle with opposite quantum numbers. The laws of nature are nearly symmetric between particles and anti-particles.

One of the most fundamental insights of theoretical physics is that for every symmetry there is a corresponding conservation law and vice versa. The connection will be discussed here in the framework of Lagrangian field theory. Only this much now:  $SU(3)$  is the symmetry group behind the strong interaction, whereas the electromagnetic and the weak force are unified in a  $SU(2) \times U(1)$  group. The associated quantum numbers are called colour, weak isospin and electric charge, respectively. They are conserved in all interactions.

Many textbooks have been written on the Standard Model. The following explanations are based on Refs. [4, 5, 6].

### 2.1.1 Particle Content

In the view of quantum field theory the terms particle and field become blurred and no differentiation is made between conventional particles and classical fields of forces. Both are described by fermionic and bosonic fields of spin- $\frac{1}{2}$  and spin-1 particles, respectively. An overview of the fermions, the constituents of all matter surrounding us, is given in Table 2.1. The bosons, the carriers of the fundamental forces, are listed in Table 2.2.

	1 <sup>st</sup> Generation	2 <sup>nd</sup> Generation	3 <sup>rd</sup> Generation	Charge [ $e$ ]
Quarks	Up ( $u$ )	Charm ( $c$ )	Top ( $t$ )	$\frac{2}{3}$
	Down ( $d$ )	Strange ( $s$ )	Bottom ( $b$ )	$-\frac{1}{3}$
Leptons	Electron neutrino ( $\nu_e$ )	Muon neutrino ( $\nu_\mu$ )	Tau neutrino ( $\nu_\tau$ )	0
	Electron ( $e$ )	Muon ( $\mu$ )	Tau ( $\tau$ )	-1

Table 2.1: Quarks and leptons, grouped in generations, with their electric charge.

Interaction	Mediator	Charge	Mass	associated quantum number
Electromagnetic	Photon ( $\gamma$ )	0	0	electric charge
Strong	8 Gluons	0	0	colour
Weak	$W^+$	+1	80.4 GeV	weak isospin
	$W^-$	-1	80.4 GeV	
	$Z$	0	91.2 GeV	

Table 2.2: The mediators of the three fundamental forces with their charge and mass.

There are a total of two different types of fermions and corresponding anti-fermions. Each fermion type comes in threefold family replication. Fermions of the three generations differ in their respective masses only. The two types are classified as quarks or leptons according to whether or not they interact via the strong force. The quarks come in triplets of colour, red, green or blue. There are up-type and down-type quarks. Leptons are colourless and hence do not participate in the strong interaction. Each electron-type lepton has a neutrino associated with it. These are the aforementioned basic constituents of matter. Throughout this thesis, when mentioning a particle the corresponding anti-particle will usually be implied. If this is not the case it will be clear from the context.

Each force has a force carrier and a quantum number associated to it. The electromagnetic force is mediated by the mass-less photon that couples to charge. Mediators of the strong force are a total of eight gluons, also mass-less, coupling to colour. The three mediators of the weak force are massive; two of them, the  $W^+$  and its charge conjugate  $W^-$ , have electric charge; the third,  $Z$ , is electrically neutral. They couple to weak isospin.

Of particular interest in the context of this thesis are the electron, the anti-electron called positron, and the two  $W$  bosons.

### 2.1.2 Fields and Gauge Interactions

A particle in the view of the Standard Model is not a localised entity, but a field, described by its Lagrangian density. For a freely propagating fermion this is

$$\mathcal{L} = \bar{\psi}(i\gamma^\mu\partial_\mu - m)\psi. \quad (2.1)$$

This Lagrangian density is invariant under so-called global gauge transformations of the field  $\psi \rightarrow e^{i\theta}\psi$ . The Standard Model postulates that the Lagrangian is also invariant under *local* gauge transformations, i.e. the phase factor  $\theta$  depends on space-time points  $x$

$$\psi \rightarrow e^{i\theta(x)}\psi. \quad (2.2)$$

In general, Eq. 2.1 is not invariant under a local gauge transformation, because  $e^{i\theta(x)}\psi$  picks up an extra term through the derivative. Local gauge invariance can be re-established by replacing the derivative  $\partial_\mu$  by the covariant derivative

$$\partial_\mu \rightarrow \partial_\mu - ieA_\mu \quad (2.3)$$

introducing a vector field  $A_\mu$  that transforms as  $A_\mu \rightarrow A_\mu + \frac{1}{e}\partial_\mu\theta$ . Requiring a free Lagrangian for this field, too, the new Lagrangian is

$$\mathcal{L} = \bar{\psi}(i\gamma^\mu\partial_\mu - m)\psi + e\bar{\psi}\gamma^\mu\psi A_\mu - \frac{1}{4}F_{\mu\nu}F^{\mu\nu} \quad (2.4)$$

where  $F_{\mu\nu} = \partial_\mu A_\nu - \partial_\nu A_\mu$ . It is invariant under a local gauge transformation.

The vector field  $A_\mu$  can be identified with the photon field, the gauge transformation corresponds to a  $U(1)$  symmetry and Eq. 2.4 is the Lagrangian of Quantum Electrodynamics (QED). The photon is mass-less. A mass term of the form  $\mathcal{L}_{\text{mass}} = \left(\frac{m}{2}\right)^2 A^\nu A_\nu$  would destroy local gauge invariance, which is the principle underlying assumption of the Standard Model.

### 2.1.3 Quantum Chromodynamics

The theory of the strong force is Quantum Chromodynamics (QCD). It is derived in similar manner as QED, this time requiring local gauge invariance under  $SU(3)$  transformations. The Lagrangian looks just like Eq. 2.1 but  $\psi$  is now a three column vector, representing the three quark colour fields

$$\psi = \begin{pmatrix} \psi_r \\ \psi_g \\ \psi_b \end{pmatrix} \quad (2.5)$$

The transformation then is

$$\psi \rightarrow e^{i\theta_a(x)\frac{\lambda_a}{2}}\psi \quad (2.6)$$

with a set of linearly independent, trace-less  $3 \times 3$  matrices  $\lambda_a$  – the summation over  $a$  with  $a = 1, \dots, 8$  is implied. Again, local gauge invariance is obtained by replacing the derivative with the covariant derivative and introducing gauge fields, that now take the form

$$\partial_\mu \rightarrow \partial_\mu + ig\frac{\lambda_a}{2}G_\mu^a \quad (2.7)$$

$$G_\mu^a \rightarrow G_\mu^a - \frac{1}{g}\partial_\mu\theta_a - f_{abc}\theta_a G_\mu^{bc} \quad (2.8)$$

where  $f_{abc}$  is the structure constant of the group. This results in the Lagrangian of QCD

$$\mathcal{L} = \bar{\psi} (i\gamma^\mu \partial_\mu - m) \psi - g(\bar{\psi}\gamma^\mu \frac{\lambda_a}{2} \psi) G_\mu^a - \frac{1}{4} G_{\mu\nu}^a G_a^{\mu\nu}. \quad (2.9)$$

The tensor  $G_{\mu\nu}^a$  is defined as  $G_{\mu\nu}^a = \partial_\mu G_\nu^a - \partial_\nu G_\mu^a - gf_{abc} G_\mu^b G_\nu^c$ . There are 8 vector gluon fields  $G_\mu^a$  in order to compensate the phase variation of three quark colour fields. Again, the vector fields are required to be mass-less. Compared to the QED field tensor there is an extra term in  $G_{\mu\nu}^a$ , causing self-interactions between the gauge bosons.

The strength of the strong force increases with distance between two coloured particles. Therefore, quarks exist only as colourless compounds. Allowed configurations for these compounds are a quark and anti-quark of opposite colour, classified as a Meson, and the combination of three quarks of red, green and blue (or corresponding anti-colours), classified as a Baryon. The production of a quark is accompanied by the creation of other quark-antiquark pairs from vacuum and a subsequent clustering process, called *hadronisation*. The result is a bundle of collimated, colourless particles, called a jet.

### 2.1.4 Electroweak Theory

The weak interaction is unified with the electromagnetic force in the electroweak model with a  $SU(2) \times U(1)$  gauge symmetry. Experimental observations suggest that charged weak currents act on left-handed fermions (and right-handed anti-fermions), only. These are represented by left-handed  $SU(2)_L$  doublets

$$\chi_L = \frac{1}{2}(1 - \gamma^5) \begin{pmatrix} \nu \\ e \end{pmatrix} \quad (2.10)$$

of weak isospin with  $I_3 = -\frac{1}{2}$  and  $I_3 = +\frac{1}{2}$  respectively. Eq. 2.10 refers to the doublet of electron and neutrino. All other fermions are treated accordingly. The right-handed fermions are represented by  $U(1)_Y$  singlets

$$\psi_R = \frac{1}{2}(1 + \gamma^5)e \quad (2.11)$$

that do not carry weak isospin. Right-handed neutrinos do not take part in any of the three interactions described by the Standard Model, since they do not carry any of the associated quantum numbers. The index  $L$  emphasises the left-handedness of the coupling, the index  $Y$  denotes the weak hypercharge that is related to the electric charge  $Q$  and the third component of the weak isospin  $I_3$  by the Gell-Mann-Nishijima equation  $Q = I_3 + \frac{Y}{2}$ .

The gauge transformations corresponding to a  $SU(2)_L \times U(1)_Y$  symmetry are

$$\chi_L \rightarrow e^{i\alpha \frac{Y}{2} + i\beta_a \frac{\tau_a}{2}} \chi_L \quad (2.12)$$

$$\psi_R \rightarrow e^{i\alpha \frac{Y}{2}} \psi_R. \quad (2.13)$$

This is again applied this to the Lagrangian

$$\mathcal{L} = \bar{\chi}_L (i\gamma^\mu \partial_\mu - m) \chi_L + \bar{\psi}_R (i\gamma^\mu \partial_\mu - m) \psi_R \quad (2.14)$$

and the covariant derivatives are constructed with the gauge fields  $W_\mu^a$  for  $SU(2)_L$  and  $B_\mu$  for  $U(1)_Y$ , analogously to Section 2.1.3

$$\partial_\mu \rightarrow \partial_\mu + ig \frac{\tau_a}{2} W_\mu^a + ig' \frac{Y}{2} B_\mu. \quad (2.15)$$

$$(2.16)$$

The kinetic terms of the gauge fields are

$$\mathcal{L} = -\frac{1}{4} W_{\mu\nu}^a W_a^{\mu\nu} - \frac{1}{4} B_{\mu\nu} B^{\mu\nu}. \quad (2.17)$$

Eq. 2.14 is *not* invariant under the transformation. Neither are mass terms for the gauge bosons but the gauge bosons of the weak interaction  $W^{+/-}$  and  $Z$  are known to be very massive.

Mass terms are introduced by breaking this symmetry. This can be achieved by adding a complex scalar field  $\phi$  to the Lagrangian in Eq. 2.17 with a potential such that  $\phi$  has a non-zero vacuum expectation value

$$\mathcal{L}_\phi = \frac{1}{2} (\partial_\mu \phi)^* (\partial^\mu \phi) + \frac{\mu^2}{2} (\phi^* \phi) - \frac{\lambda}{4} (\phi^* \phi)^2. \quad (2.18)$$

With the parameters  $\mu^2 < 0$  and  $\lambda > 0$  the vacuum expectation value is  $|\phi|^2 = -\frac{\mu^2}{2\lambda}$ . Requiring local gauge invariance under  $SU(2)_L \times U(1)_Y$  for this field at some arbitrarily chosen minimum, three of the four extra degrees of freedom give a longitudinal polarisation state to the gauge bosons, allowing mass terms and thus retaining local gauge invariance, the other results in a massive Spin-0 particle, the Higgs boson.

The kinetic terms in Eq. 2.18 after the gauge transformation can be diagonalised. Their eigenvalues are

$$W_\mu^+ = \frac{1}{\sqrt{2}} (W_\mu^1 - iW_\mu^2) \quad (2.19)$$

$$W_\mu^- = \frac{1}{\sqrt{2}} (W_\mu^1 + iW_\mu^2) \quad (2.20)$$

and

$$\begin{pmatrix} A_\mu \\ Z_\mu \end{pmatrix} = \begin{pmatrix} \cos \theta_W & \sin \theta_W \\ -\sin \theta_W & \cos \theta_W \end{pmatrix} \begin{pmatrix} B^\mu \\ W^{3\mu} \end{pmatrix} \quad (2.21)$$

in agreement with the gauge bosons  $\gamma$ ,  $W^+$ ,  $W^-$  and  $Z$  that are observed experimentally. The weak mixing angle  $\theta_W$  is defined as  $\tan \theta_W = \frac{g'}{g}$ ; the coupling constants  $g$  and  $g'$  are related to the electric charge by  $e = g \sin \theta$ . The masses of the gauge bosons are predicted in terms of the vacuum expectation value  $v$  and the coupling constants  $g$  and  $g'$  to be

$$M_W = \frac{1}{2} v g \quad \text{and} \quad M_Z = \frac{1}{2} v \sqrt{g^2 + g'^2} \quad (2.22)$$

leaving the photon mass-less.

Electroweak symmetry breaking has been proposed forty-eight years ago and the search for the Higgs boson has been a major goal of the physics programme at the ATLAS experiment. A resonance of a previously unknown boson has been observed at 126 GeV in July 2012 by the ATLAS and CMS collaborations at the LHC[7, 8]. The cross-section of this resonance is compatible with the Standard-Model Higgs boson. Whether it has the precise properties of the Standard Model Higgs boson remains to be experimentally validated.

## 2.2 Collider Physics

The mathematical formulation of the Standard Model needs to be translated into observables that can actually be measured. The experimental quantities, needed to verify and test the Standard Model, are described here, based on Refs. [5, 9, 10]. Moreover, the proton is introduced as a compound of the elementary particles from the previous chapter. The properties and the production of the  $W$  bosons are discussed afterwards.

### 2.2.1 Phenomenology

A transition amplitude  $\mathcal{M}$  of a well defined physics process can be obtained from the Lagrangian density using perturbation theory. The transition amplitude contains all the dynamical information of the process under investigation. A measure of the probability of this process to occur is the differential cross-section  $d\sigma$

$$d\sigma = \frac{|\mathcal{M}|^2}{F} dQ \quad (2.23)$$

with the incident particle flux  $F$  and a phase-space factor  $dQ$  that contains the kinematic information of the particles participating in the interaction. In the context of scattering processes the transition amplitude  $\mathcal{M}$  is often referred to as matrix-element of the scattering matrix.

The event rate  $n$  can be measured experimentally and is related to the total cross-section  $\sigma$  by

$$n = L \cdot \sigma. \quad (2.24)$$

$L$  denotes the luminosity, i.e. the number of particles scattering per unit area per unit time. For a particle collider it can be calculated to

$$L = f \frac{N_1 N_2}{4\pi\sigma_x\sigma_y} \quad (2.25)$$

if two beams, filled with bunches, containing  $N_1$  and  $N_2$  particles, collide with frequency  $f$  and Gaussian beam profiles with widths of  $\sigma_x$ ,  $\sigma_y$ . Integrated over a larger timescale the total number of collected events  $N$  is

$$N = L_{\text{int}} \cdot \sigma, \quad \text{where } L_{\text{int}} = \int L dt. \quad (2.26)$$

### 2.2.2 Proton Structure

The proton is a composite particle. In order to calculate the cross-section of a certain process at proton colliders one has to consider all possible interactions between the constituents of the proton. These constituents cannot be identified with the three quarks  $uud$  only. Experiments at high energies observe a variety of partons – quarks and gluons – inside the proton. This is due to the permanent exchange of gluons between the nominal constituents. At any time such a gluon can split into a quark-antiquark pair. Thus, the proton structure can only be described on a probabilistic level. The substructure visible to a probing object depends on the momentum transfer  $Q^2$  between the proton and the probe and the fraction of the momentum of the proton that is carried by the struck parton,  $x$ , called Bjorken- $x$ .

The structure of the proton is parameterised via parton distribution functions  $f$ . These cannot be calculated analytically and are a phenomenological approximation. They are obtained using global fits to data and are performed by various theoretical groups. An example of a PDF from the MSTW group is shown in Fig. 2.1 for two different  $Q^2$ . All existing flavours of quarks can be regarded as constituents of the proton. However, not surprisingly, the nominal constituents are more likely to carry the momentum of the proton. This is seen in Fig. 2.1 as an enhancement of  $u$ -quarks and  $d$ -quarks at large  $x$ .

The cross-section for two protons  $p_1$  and  $p_2$  to scatter into a final state  $Y$  can be calculated as

$$d\sigma(p_1 p_2 \rightarrow Y + X) = \int_0^1 dx_1 \int_0^1 dx_2 \sum_{q_1, q_2} f_{q_1}(x_1, Q^2) f_{q_2}(x_2, Q^2) \cdot d\sigma(q_1 q_2 \rightarrow Y) \quad (2.27)$$

where the sum runs over all quarks, anti-quarks and gluons  $q_1$  and  $q_2$  in the two protons that can produce the final state  $Y$ . Any hadronic final states that are formed by the remnants of the protons that were broken up in the interaction are denoted by  $X$ . The remnants lead to additional activity in the event.

### 2.2.3 Properties of the Gauge Bosons

The masses of the gauge bosons have been measured to be  $m_W = 80.40 \pm 0.03$  GeV and  $m_Z = 91.188 \pm 0.002$  GeV [9]. Since the  $W$  boson couples to weak isospin it can be produced by either of the isospin doublets and decay to either of the ones kinematically allowed. The  $W$  boson decays to every isospin doublet with equal probability when the kinematics of the phase-space are neglected. The decay to quarks is enhanced by a colour factor of three, the decay to a top and a bottom-quark is kinematically forbidden – the top-quark is heavier than the  $W$  boson. From this simplified approach it follows, that the decay to any lepton and corresponding neutrino is equally likely with a fraction of 11%. The so-called hadronic decay-modes into quarks contribute with 67%. The measured branching fractions as listed in Table 2.3 are in agreement with the results from precise calculations.

The  $Z$  boson decays to all fermion-antifermion pairs kinematically allowed. The decay to top-quarks is, again, kinematically forbidden. Compared to the photon  $\gamma$  the  $Z$  boson

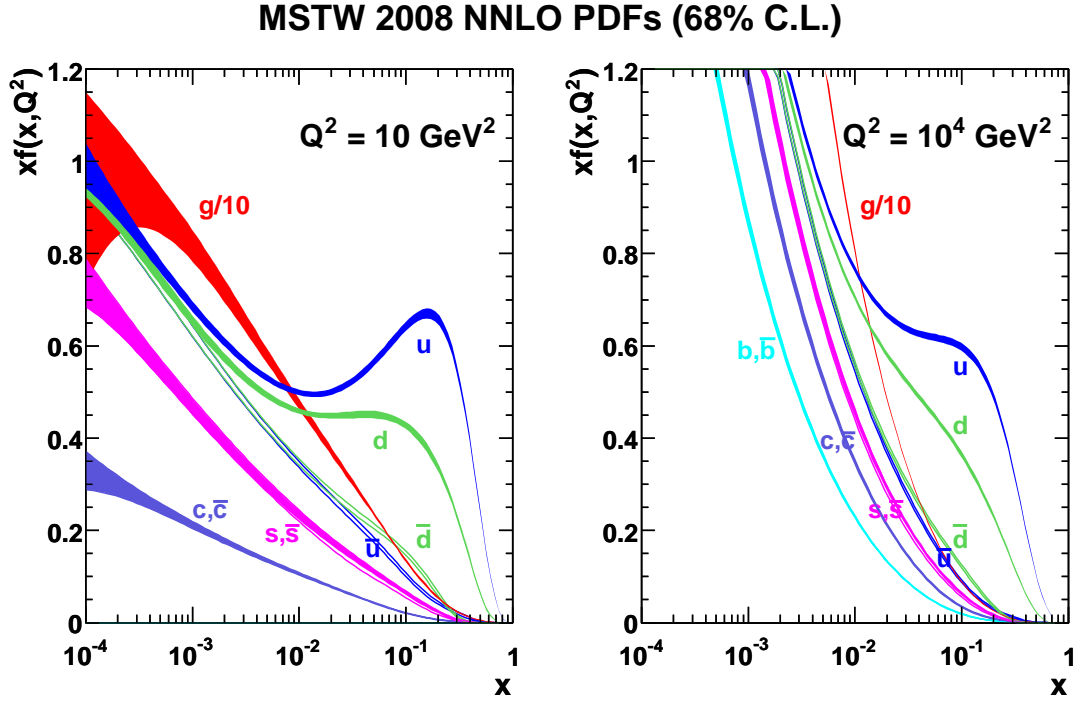


Figure 2.1: Parton distribution functions  $xf_q(x, Q^2)$  for  $Q^2 = 10 \text{ GeV}^2$  (left) and  $Q^2 = 10^4 \text{ GeV}^2$  (right), calculated to next-to-next-to-leading order by the global PDF fitting group MSTW, taken from Ref. [11].

$W^+$ decay-modes	Fraction ( $\Gamma_i/\Gamma$ ) [%]
$e^+\nu_e$	$10.75 \pm 0.13$
$\mu^+\nu_\mu$	$10.57 \pm 0.15$
$\tau^+\nu_\tau$	$11.25 \pm 0.20$
hadrons	$67.60 \pm 0.27$

Table 2.3:  $W^+$  decay-modes and their branching fractions  $\Gamma_i/\Gamma$ , taken from Ref. [9]. The  $W^-$  decay-modes are charge conjugates of the modes given.

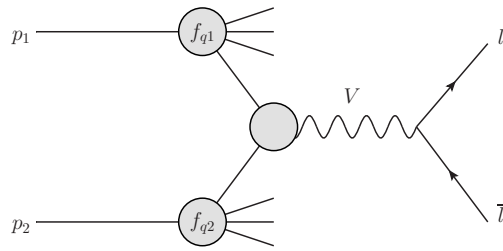


Figure 2.2: The production of a vector boson in proton-proton scattering.

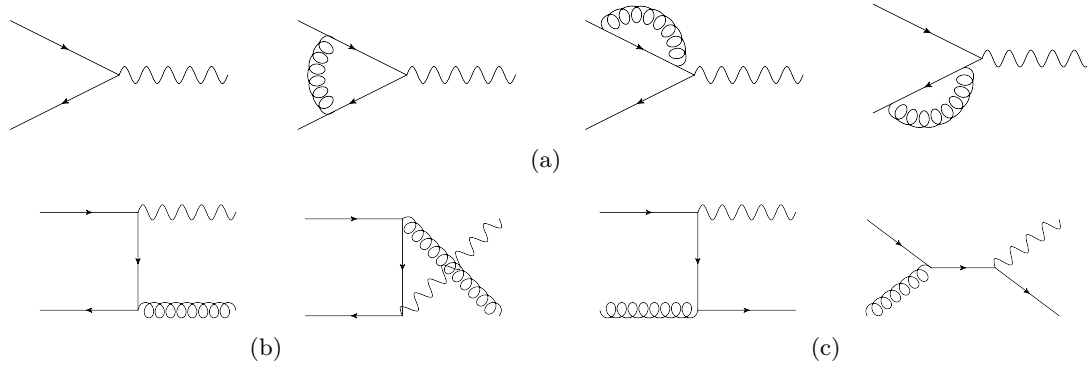


Figure 2.3: Perturbative corrections to the Drell-Yan cross-section. Shown are the leading- and next-to-leading order diagrams [10].

decay features a special mode: since neutrinos carry weak isospin but no electric charge, the  $Z$  boson unlike the photon can decay to a neutrino-antineutrino pair.

### 2.2.4 $W$ Boson Production at the LHC

The prototype of a hard-scattering process in hadron collisions is the Drell-Yan production of a lepton pair via quark-antiquark annihilation and the exchange of a photon,  $q\bar{q} \rightarrow \gamma^* \rightarrow l^+l^-$ . In place of the photon, a vector boson can be exchanged. The production and the subsequent leptonic decay of a  $W$  boson can be considered as Drell-Yan like, where the incoming quarks have to be of different flavour. The Drell-Yan process is illustrated in Fig. 2.2. It is the process at lowest-order QCD in perturbation theory. When the perturbation series is expanded to higher orders additional contributions to  $W$  boson production arise. They can be grouped into virtual gluon corrections to the leading-order contribution (a), radiative gluon corrections (b) and quark-gluon scattering processes (c) [10].

The cross-section of the  $W$  boson production with a subsequent decay to an electron and a neutrino  $W \rightarrow e\nu$  has been calculated to next-to-next-to-leading order QCD to 6.16 nb for  $W^+$  and 4.30 nb for  $W^-$  [12]. These cross-sections are different because of the different probabilities of finding a  $u$ - or a  $d$ -quark inside the proton. The asymmetry

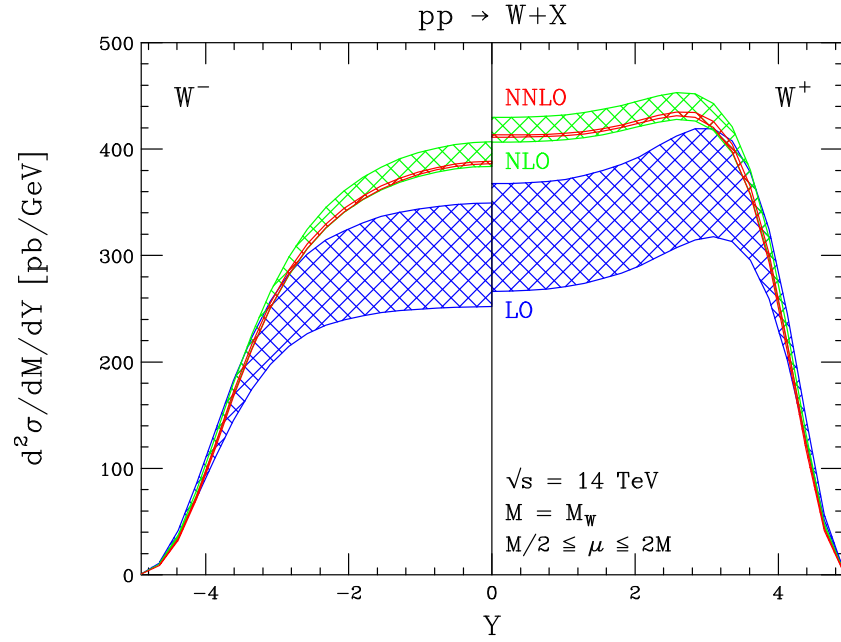


Figure 2.4: Theoretical prediction of the rapidity distribution of an on-shell  $W^-$  boson (left) and a  $W^+$  boson (right) at LO, NLO and NNLO and  $\sqrt{s} = 14$  TeV, taken from Ref. [13].

between  $W^{+/-}$  boson production is a function of the rapidity of the bosons. This is due to the different  $x$  values contributing; as can be seen in Fig. 2.1  $u$ -quarks in general carry more momentum than  $d$ -quarks. The rapidity distributions of  $W^+$  and  $W^-$  bosons produced in  $pp$  collisions are shown in Fig. 2.4. In addition the figure illustrates the perturbative behaviour of the theory, i.e. the convergence of the perturbation series when higher orders are included in the calculation.

For electrons originating from a  $W$  decay the asymmetry is smaller. Since the weak interaction involves left-handed particles (and right-handed anti-particles) only, the electrons are not produced isotropically in the  $W$  boson rest frame.

### 2.2.5 Cross-sections at the LHC

In the collisions of protons with protons most of the interactions are soft, i.e. at very low momentum transfer  $Q^2$ . Such processes constitute the overwhelming majority of processes. But eventually, two quarks or gluons will exchange a large momentum. These processes are the interesting ones. The cross-section for a variety of processes have been calculated for the LHC and are shown in Fig. 2.5. At the current (2011) centre-of-mass energy at the LHC of  $\sqrt{s} = 7$  TeV the production of the two vector bosons amounts for  $\sim 10^{-6}$  of the total  $pp$  cross-section.

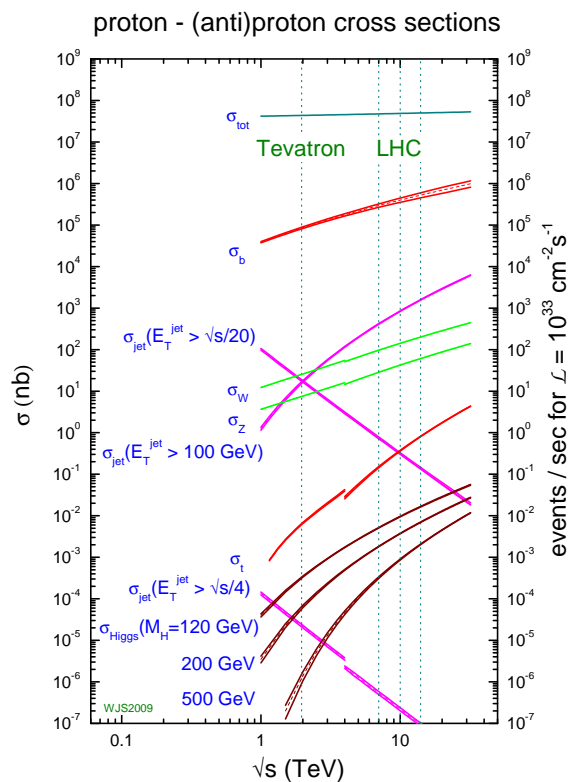


Figure 2.5: Cross-sections of different Standard Model processes at hadron colliders as a function of the centre-of-mass energy  $\sqrt{s}$ . The lower-energy range is shown for a proton-antiproton collider (Tevatron), the high-energy range for a proton-proton collider like the LHC, taken from Ref. [14].

## 2.3 Event Generation and Simulation

The calculation of a cross-section involves the integration of Eq. 2.23. Also the hadronisation of quarks and the decay of particles happen on a probabilistic basis and matrix-elements  $\mathcal{M}$  have to be integrated. Solving these integrals analytically is possible in very rare and simple cases, only. In order to evaluate them, Monte-Carlo techniques are used.

Particle physics experiments like the ATLAS experiment make extensive use of simulation. The selection of events of interest in data and the identification of objects in the detector are only two examples of steps in an analysis that are optimised by using simulated event samples. The event generation process as well as the simulation infrastructure at the ATLAS experiment is summarised in Ref. [15]. The simulation is closely matched to the conditions in data, regarding e.g. beam profile, luminosity or detector structure and even detector defects.

The starting point is the generation of the hard interaction of the proton-proton collision. The samples used in this thesis were produced with the POWHEG [16] or PYTHIA6 [17] packages. While POWHEG computes the matrix-element to next-to-leading order precision, PYTHIA is limited to leading-order processes. POWHEG, however, is incapable of simulating hadronisation processes. For that purpose it is interfaced with PYTHIA6. Electromagnetic radiation processes of e.g. the final state electron is handled by a dedicated package, called PHOTOS [18]. Such processes distort the electron energy distribution and can therefore bias the correct identification.

In a given bunch-crossing, multiple interactions occur due to the high luminosity, so-called pile-up. The simulated hard interaction is therefore overlaid with simulations of low  $Q^2$  di-jet processes, so-called minimum bias events. These events are produced by PYTHIA6 or PYTHIA8 [19]. The main difference between both is that PYTHIA8 uses  $p_T$ -ordered showers whereas PYTHIA6 uses mass-ordered showers.

Furthermore, a very integral part of the simulation process is the detector simulation, i.e. the passage of the produced particles through and the interaction with the detector. The full detector simulation is done using GEANT4 [20].

---

# 3 The ATLAS Detector at the LHC

---

Located on the outskirts of Geneva, Switzerland, the Large Hadron Collider (LHC) accelerates and collides protons in a 26.7 km circumference synchrotron ring with unprecedented energies and instantaneous luminosities. Along the ring there are four interaction points where the actual collisions take place. Around the interaction points experimental caverns are excavated, each hosting a different experiment. The largest in size is the ATLAS (A Toroidal LHC Apparatus) detector, designed to explore yet unknown and unobserved physics phenomena.

The accelerator complex and detector structure are outlined below. Unless stated otherwise, the explanations are based on Refs. [21, 22]. How the reconstruction algorithms make use of the various detector components is described in Chapter 5.

## 3.1 The Large Hadron Collider

The LHC is a proton-proton accelerator and collider installed in a tunnel 100 m underground. The accelerator consists of eight arcs and eight straight sections of superconducting magnets. The operation of two beams, one clockwise, the other counter-clockwise, of equally charged particles necessitates two opposite magnetic dipole fields to bend the particles on a circular path. For the LHC, a design has been realised where both beams run in two adjacent pipes. The collider has been designed for a centre-of-mass energy of 14 TeV. To reach this energy protons are accelerated in a number of successive accelerators with increasing energy until they are injected into the LHC ring at 450 GeV. The LHC has been designed to reach an instantaneous luminosity of  $L = 10^{34} \text{ cm}^{-2}\text{s}^{-1}$ . This high luminosity is delivered to the two multi-purpose experiments ATLAS and CMS. There is also a low luminosity experiment LHCb, dedicated to b-physics and designed for  $L = 10^{32} \text{ cm}^{-2}\text{s}^{-1}$ . The LHC is also capable of colliding lead ions at a design energy  $\sqrt{s} = 1.15 \text{ PeV}$ . These collisions are recorded by the two multi-purpose detectors and the ALICE experiment, designed specifically for the analysis of Pb-Pb collisions and intending to study the quark-gluon-plasma.

Throughout 2011 the LHC was operating at a centre-of-mass energy of 7 TeV. The luminosity was steadily increased from  $L = 10^{32} \text{ cm}^{-2}\text{s}^{-1}$  up to  $L = 3.9 \cdot 10^{33} \text{ cm}^{-2}\text{s}^{-1}$ . The total integrated luminosity delivered to ATLAS was  $L_{\text{int}} = 5.6 \text{ fb}^{-1}$ . The evolution of the luminosity as a function of time can be seen in Fig. 3.1.

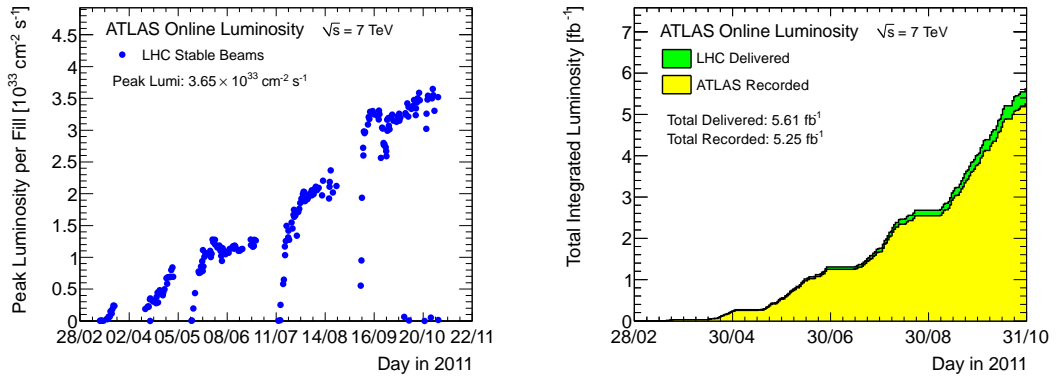


Figure 3.1: The maximum instantaneous luminosity versus day delivered to ATLAS (left) and the cumulative luminosity versus day delivered to, and recorded by ATLAS (right), taken from Ref. [23].

## 3.2 The ATLAS Detector

The ATLAS experiment has been designed to record and analyse the proton-proton interactions delivered by the LHC. A cut-away view of the detector is given in Fig. 3.2. It is assembled in several layers around the nominal interaction point and symmetric in forward and backward direction along the beam pipe w.r.t. the interaction point. The inner detector consists of three tracking sub-systems and is embedded in a superconducting solenoid magnet that produces a magnetic field of  $B = 2$  T. The combination of magnetic field and tracking system allows for the momentum measurement of charged particles. Around it, the calorimeter system is built as a cylindrical barrel with caps at each end. It is divided into an electromagnetic (EM) and a hadronic calorimeter part, designed according to their purpose of providing a high resolution measurement of electrons and photons through electromagnetic showers and an adequate resolution measurement for hadronic particles. The detector is completed by the muon spectrometer, consisting of another magnetic system with a barrel and two end-cap toroid magnets, producing a field of  $B = 0.5$  T and  $B = 1$  T respectively, and a number of different muon chambers and drift tubes assembled inside and around the toroids. In order to record the collisions, the event rate has to be reduced from 40 MHz to 200 Hz. This is achieved by a three-level trigger system.

The nominal interaction point is taken as the origin of a right-handed coordinate system with the  $z$ -axis defined by the beam direction. Perpendicular to it is the  $x$ - $y$  plane, with the  $x$ -axis pointing towards the centre of the LHC ring and the  $y$ -axis pointing upwards. With that, the azimuth and polar angles  $\phi$  and  $\theta$  are measured from the positive  $x$ -axis counter-clockwise in the  $x$ - $y$ -plane and from the  $z$ -axis, respectively. Throughout

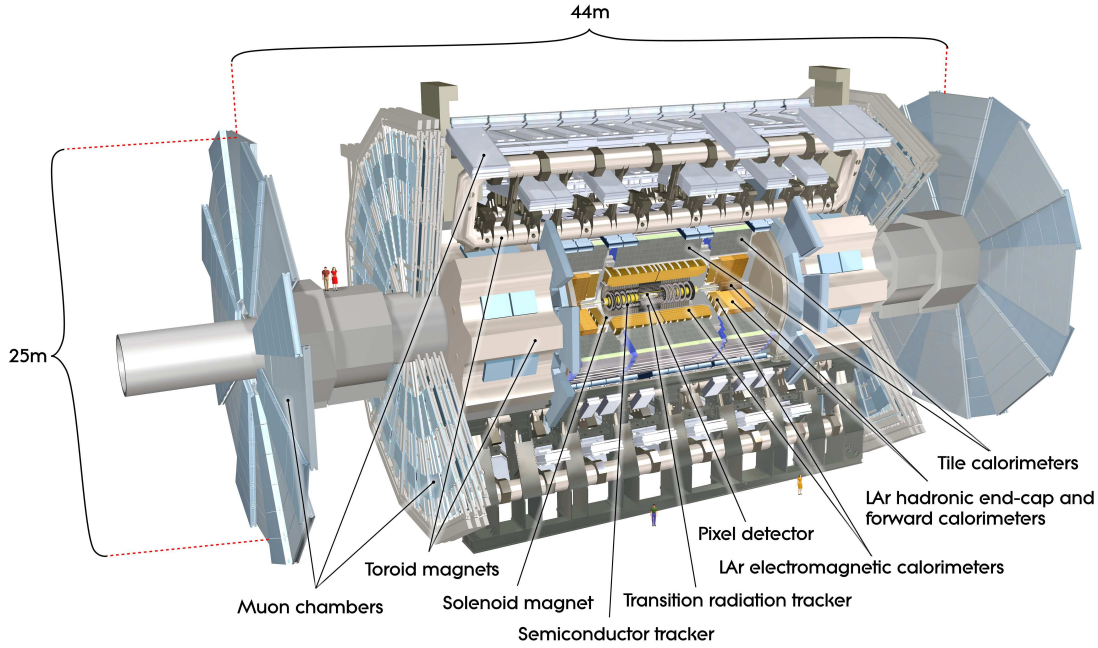


Figure 3.2: Cut-away view of the ATLAS detector, taken from Ref. [22].

this thesis, further quantities will be used repeatedly: the pseudo-rapidity  $\eta$ , defined as

$$\eta = -\ln \tan \left( \frac{\theta}{2} \right), \quad (3.1)$$

and the distance in pseudorapidity-azimuth-angle-space  $\Delta R$

$$\Delta R = \sqrt{\Delta\eta^2 + \Delta\phi^2}. \quad (3.2)$$

### 3.2.1 The Inner Detector

The inner detector is designed for high resolution measurements of the momentum of charged particles and the reconstruction of primary and secondary vertices. It consists of three independent but complementary sub-detectors: the Pixel detector, the Semiconductor Tracker (SCT) and the Transition Radiation Tracker (TRT). The different parts are depicted in Fig. 3.3.

The Pixel detector comes in three cylindrical silicon layers and three end-cap discs on each side. The nominal pixel size is  $50 \times 400 \mu\text{m}^2$ . It constitutes the sub-detector with the highest spatial resolution and the highest number of readout channels. The layer closest to the beam-pipe is referred to as the b-layer since through its proximity to the beam pipe it reaches the highest resolution and plays an important part in the identification of jets from  $b$ -quarks. The SCT consists of a barrel part of four layers and a total of 9 discs in the end-cap region, again on each side, with silicon strip detectors. For

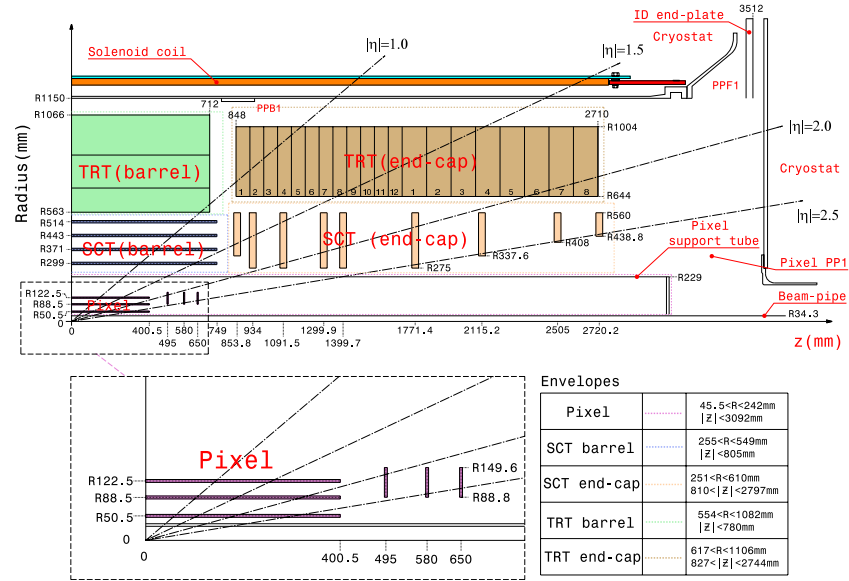


Figure 3.3: Sketch of the inner detector, taken from Ref. [22].

a three-dimensional measurement of the trajectory of a particle each layer has two silicon strips that are oriented under a 40 mrad angle. Both systems are commonly referred to as silicon trackers. They span a pseudo-rapidity range up to  $|\eta| < 2.5$ . Beyond that no track reconstruction is possible. Without the possibility of track reconstruction, electrons cannot be distinguished from photons above a pseudo-rapidity of  $|\eta| > 2.5$ .

The third part of the inner detector is the TRT, a combination of tracking and transition radiation detector. It consists of straw drift tubes, 4 mm in diameter, that are interleaved with polyimide fibres in the barrel and foils in the end-cap as a transition radiation element. The straws are filled with a Xenon-based gas mixture. A tungsten wire is used as an anode for the drift tube. The barrel straws are divided in two in the middle at  $\eta = 0$ . They are read out at each end and at the centre. The TRT front-end electronics can discriminate between signals from tracking hits from minimum-ionising particles and transition radiation hits, that yield higher signal amplitudes, by using separate low and high thresholds. It covers a range up to  $|\eta| < 2.0$  with a gap for the readout at  $|\eta| < 0.1$ . The tubes are aligned parallel to the beam pipe. Therefore, the TRT has only very limited resolution in  $\eta$ .

The amount of material a particle has to pass in order to penetrate the inner detector and reach the electromagnetic calorimeter is given in Fig. 3.4. Additionally, it has to traverse the solenoid magnet that is surrounding the three sub-detectors. By passing through the material, electrons lose large fractions of their energy by bremsstrahlung; large fractions of photons convert to electron-positron pairs, becoming a background for genuine electrons.

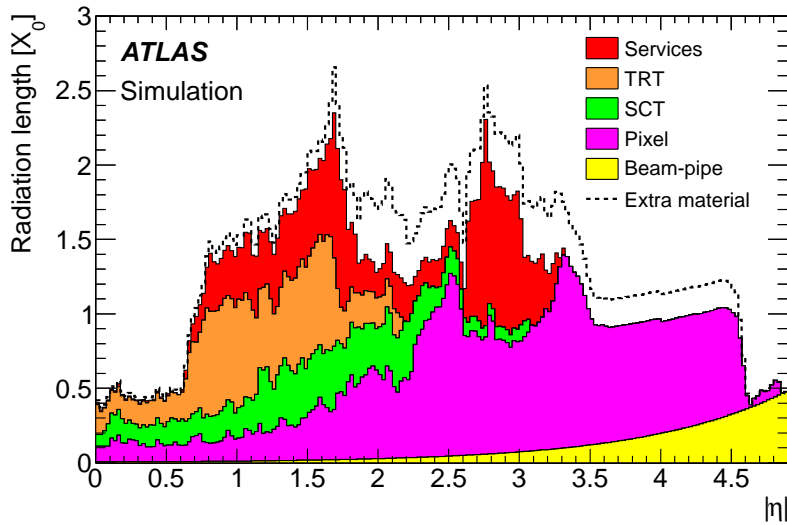


Figure 3.4: Amount of material a particle has to traverse in order to reach the electromagnetic calorimeter in units of radiation lengths  $X_0$ , taken from Ref. [1].

### 3.2.2 Calorimetry

The calorimeters cover a range  $|\eta| < 4.9$  using different techniques for the measurement of the energy of electrons and photons, and jets. An overview is given in Fig. 3.5.

#### Electromagnetic Calorimeter

The electromagnetic calorimeter is a lead-liquid-argon calorimeter and provides a fine granularity. It is suited for a high-resolution measurement of the energy of electrons and photons. It is divided into a barrel and two end-cap parts, covering  $|\eta| < 1.475$  and  $1.375 < |\eta| < 3.2$ , respectively. The cells consist of alternating layers of accordion-shaped lead absorbers, readout electrodes and liquid argon as a sampling material. The accordion structure provides symmetry in  $\phi$  without azimuth cracks. The calorimeter is made up of three longitudinal layers in the barrel and two in the end-caps with different granularity. A sketch of a barrel module is given in Fig. 3.6 with the dimensions of the individual layers.

The front layer, also called strip layer, has a very fine granularity in  $\eta$  and only very limited resolution in  $\phi$ . The size of the cells is  $\Delta\eta \times \Delta\phi = 0.0031 \times 0.1$  for  $|\eta| < 1.8$  and coarser beyond that. The middle layer amounts to the largest part of the whole system and has almost equal granularity in  $\eta$  and  $\phi$  with cells of size  $\Delta\eta \times \Delta\phi = 0.025 \times 0.025$ . This layer is also used in the trigger, where  $4 \times 4$  cells are combined. The electromagnetic calorimeter is completed by the back layer, that has the same granularity as the middle layer in  $\phi$ , but only half the granularity in  $\eta$ .

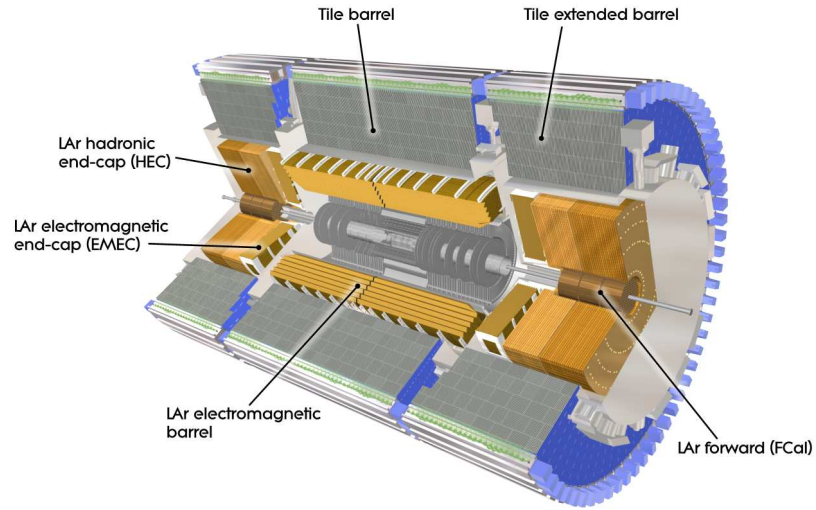


Figure 3.5: Cut-away view of the calorimeter system, taken from Ref. [22].

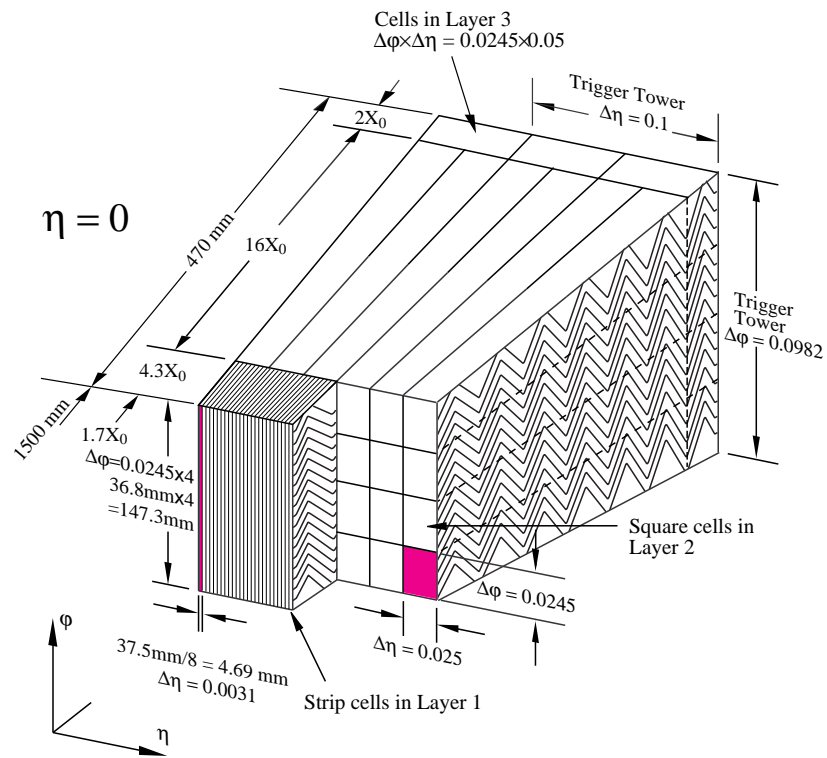


Figure 3.6: A single barrel module of the electromagnetic calorimeter, taken from Ref. [22].

### Hadronic Calorimeter

Hadronic showers usually penetrate the material further and partly shower in the consecutive hadronic calorimeter, that surrounds the electromagnetic calorimeter. The ATLAS hadronic calorimeter is a sampling calorimeter, too. In the barrel region it is made of steel absorbers and scintillating tiles. In the end-caps it consists of two independent wheels per end-cap of copper plates, that are interleaved with liquid-argon gaps.

### Forward Calorimeter

The forward region is covered by the Forward Calorimeter (FCAL) in the pseudo-rapidity range of  $3.1 < |\eta| < 4.9$ . As already mentioned, electrons outside the acceptance of the tracking system are not discussed in this analysis. With regard to this analysis, the forward calorimeter contributes to the measurement of the missing transverse energy  $E_T^{\text{miss}}$ . The FCAL is, again, a liquid argon sampling calorimeter consisting of three layers, the first with copper, the other two with tungsten as the absorber material.

### 3.2.3 Muon Spectrometer

The central part of the muon momentum measurement are the barrel toroid magnet, covering the range  $|\eta| < 1.4$ , and the two smaller end-cap toroid magnets, covering  $1.6 < |\eta| < 2.7$ . This configuration causes a bending of the trajectories of muons in the  $(r,z)$  plane rather than in  $(r,\phi)$ . In combination with three cylindrical layers of muon chambers and three layers of planes of chambers, perpendicular to the beam axis, this allows for a precise measurement of the muon momentum over nearly the full solid angle. The barrel layers consists of drift tubes for precision tracking, and resistive plate chambers with very fast response for triggering. The end-cap uses drift tubes and cathode strip chambers for precision tracking and thin gap chambers for triggering.

### 3.2.4 Trigger

The collision rate of the proton bunches is 40 MHz. The vast majority of interactions is through low energetic QCD processes and of limited experimental interest. The rate at which events can be written to disk is limited to around 200 Hz. To pick the interesting ones is the task of a three-level trigger system.

The first level trigger L1 looks for high  $E_T$  objects, large missing transverse energy and total transverse energy. It uses only a subset of the detector with reduced granularity and simplified algorithms. These are used to define one or more Regions of Interest (RoIs) in  $\eta \times \phi$  that are passed to the higher level triggers. At this stage the event rate is reduced to  $\sim 75$  kHz.

At second level, L2, the RoIs are further analysed, using all detector sub-systems at full granularity but, again, with highly simplified algorithms. The event rate is reduced to  $\sim 3.5$  kHz. For an event that passed L2 the full information is passed to the last trigger level, a processing farm called Event Filter (EF). At EF level, offline-like algorithms as given in Chapter 5 are used, further reducing the event rate to the designated 200 Hz.

Examples of trigger algorithms are given in Sections 5.5 and 5.8. In order to make optimal use of the available bandwidth the trigger system can be pre-scaled at each level.

The important Standard Model quantities need to be measured independently of the detector response to enable meaningful comparisons of theory and experiment. Therefore, the efficiencies of detecting all relevant physics objects need to be known and measurements need to be corrected using Monte-Carlo and detector simulation. The efficiency to reconstruct and identify electrons in data has already been measured in 2010, providing scale-factors as a function of pseudo-rapidity  $\eta$  and transverse energy  $E_T$  to adjust the efficiencies predicted by simulation to reflect data efficiencies.

After the “rediscovery” of all known Standard Model particles by the ATLAS experiment in first data-taking the next round of analyses has already been probing the precision of theoretical predictions. In Standard Model analyses with  $36 \text{ pb}^{-1}$  of data – less than 1% of the data available today – the results in the electroweak sector are already dominated by systematic uncertainties in the electron sector, rather than statistical uncertainties. To account for new identification requirements, changing simulation and detector performance and to improve on statistical uncertainties the measurement has to be continuously updated. The major part of the work done for this thesis was concerned with an improvement of the measurement technique, since the previously achieved precision is unsatisfactory.

The next three sections give examples of physics measurements and how they rely on a precise knowledge in the electron sector.

## 4.1 Electroweak Precision Measurements

One of the first milestones in the electroweak sector has been the measurement of the  $W^\pm$  and  $Z/\gamma^*$  cross-sections and their ratios using  $36 \text{ pb}^{-1}$  of data. The dominant source of uncertainty of the measurement is systematic rather than statistical. Table 4.1 gives an overview of the sources of the systematic uncertainty in the electron channel. The single largest uncertainty comes from the luminosity measurement (this uncertainty has undergone significant improvement already [24]). For the measurements of the ratios of  $W^+/W^-$  or  $W/Z$  it cancels entirely.

Apart from that, both  $W$  and  $Z$  are dominated by the uncertainties on electron reconstruction and electron identification. For the  $Z$  boson this uncertainty doubles since it involves two electrons. For the  $W$  boson there is another major source of uncertainty, the missing transverse energy originating from the neutrino.

Aside from the large uncertainty, the correction factors for the efficiencies on Monte-Carlo were found to be not valid: applying the  $\eta \times E_T$  dependent scale-factors proved to be responsible for disagreement between data and Monte-Carlo simulation in a kin-

	$\delta\sigma_{W^\pm}$	$\delta\sigma_{W^+}$	$\delta\sigma_{W^-}$	$\delta\sigma_Z$
Trigger	0.4	0.4	0.4	<0.1
Electron reconstruction	0.8	0.8	0.8	1.6
Electron identification	0.9	0.8	1.1	1.8
Electron isolation	0.3	0.3	0.3	—
Electron energy scale and resolution	0.5	0.5	0.5	0.2
Non-operational LAr channels	0.4	0.4	0.4	0.8
Charge misidentification	0.0	0.1	0.1	0.6
QCD background	0.4	0.4	0.4	0.7
Electroweak+ $t\bar{t}$ background	0.2	0.2	0.2	<0.1
$E_T^{\text{miss}}$ scale and resolution	0.8	0.7	1.0	—
Pile-up modelling	0.3	0.3	0.3	0.3
Vertex position	0.1	0.1	0.1	0.1
$C_{W/Z}$ theoretical uncertainty	0.6	0.6	0.6	0.3
Total experimental uncertainty	1.8	1.8	2.0	2.7
$A_{W/Z}$ theoretical uncertainty	1.5	1.7	2.0	2.0
Total excluding luminosity	2.3	2.4	2.8	3.3
Luminosity	3.4			

Table 4.1: Summary of relative systematic uncertainties from the 2010  $W^\pm$  and  $Z/\gamma^*$  cross-section measurement, taken from Ref. [26].

matic region, where no physics-related cause for the discrepancy could be found. As a consequence, the result of a one-dimensional measurement of the efficiencies in  $\eta$  was used for the differential cross-section measurement as a function of the pseudo-rapidity [25].

The large uncertainty in this analysis has been the major incentive for this thesis. There is no motivation to repeat the measurement with a larger event sample unless there is significant improvement in the electron systematic uncertainties.

In addition, there are other measurements of  $W$  and  $Z$  properties foreseen that are almost impossible without the precise knowledge of the electron performance. To match the higher statistical precision, sub-percent precision on the scale-factors is needed in the next round of Standard Model  $W/Z$  measurements [27].

## 4.2 Usage of Scale-factors in Physics Analyses

In order to provide a maximum of precision to the analysis groups it should be recognised how the values in Table 4.1 were obtained. For the example in Section 4.1 the analysis is corrected for detector effects by calculating correction factors  $C_{W/Z}$  as defined and explained in detail in Sec 6.2. They are obtained from Monte-Carlo simulation using generator-level information. The efficiency is the fraction of events reconstructed

after detector simulation w.r.t. the events generated in the geometrical and kinematic acceptance of the detector.

The simulated signal event sample is corrected with the results of the efficiency measurements in advance by applying scale-factors to all events that have an electron in it. The same is done with the results of other performance measurements. This way the correction factors  $C_{W/Z}$  describe the detector efficiency even if the kinematics of the process of interest are different from the ones of the process the scale-factors were obtained from. Additionally, the efficiency of the detector is still reproduced when only slices of phase-space are analysed, e.g. in differential measurements.

The uncertainty of the scale-factors is translated to  $C_{W/Z}$  by recalculating  $C_{W/Z}$  with the scale-factors varied up and down within their uncertainty. The difference of the resulting correction factors is taken as the uncertainty of the final result.

The method is improved by providing statistical and systematic uncertainties on scale-factors separately and making use of their different natures. Usually, the systematic uncertainty is assumed to be fully correlated between different  $\eta \times E_T$  bins. Therefore, all scale-factors are varied up and down by their systematic uncertainty simultaneously in all bins. Following Ref. [25] the statistical uncertainty is propagated to  $C_{W/Z}$  by doing pseudo-experiments, making use of its stochastic nature. Each scale-factor is varied individually according to a Gaussian distribution with a width of the statistical uncertainty. In the above example this was done 1000 times. The mean of all  $C_{W/Z}$  factors obtained this way is taken as the result of the variation. The procedure assumes that all scale-factors are statistically independent.

All other analyses extrapolate their measurements in a very similar way. The precision could further be improved by providing detailed information of the systematic correlation of the different scale-factors. The above method thus overestimates the uncertainty.

### 4.3 Relevance for the Higgs Boson Search

Probably the most important effort ongoing at the LHC is the search for the Standard Model Higgs boson [8]. Events with final state electrons contribute to this search, that is suffering from a very limited number of expected events. Electrons are e.g. used in the decay-modes of the Higgs boson to two  $W$  or  $Z$  bosons  $H \rightarrow WW^{(*)}$  and  $H \rightarrow ZZ^{(*)}$  that have excluded the existence of a Standard Model Higgs boson over a wide mass range. These decay modes are the only contributors to the search for a Higgs boson with a mass beyond  $m_h > 150$  GeV but are also used in the search at lower masses. Electron are used in the channels  $WW^{(*)} \rightarrow e\nu e\nu, e\nu\mu\nu, e\nu q\bar{q}$  and  $ZZ^{(*)} \rightarrow eeee, ee\mu\mu, eeq\bar{q}, ee\nu\nu$ . Electron final states give a very clean signal, compared to the hadronic decay-modes. Depending on the channel one to four final state leptons are selected. The current limits on the production cross-section of a Standard-Model Higgs boson are given in Fig. 4.1 for a number of channels.

In the low mass region where a resonance compatible with a Higgs boson at 126.5 GeV has been observed recently [7, 8], the Higgs strahlung processes  $W \rightarrow WH$  and  $Z \rightarrow ZH$  are used among other production mechanisms. Electrons originating from

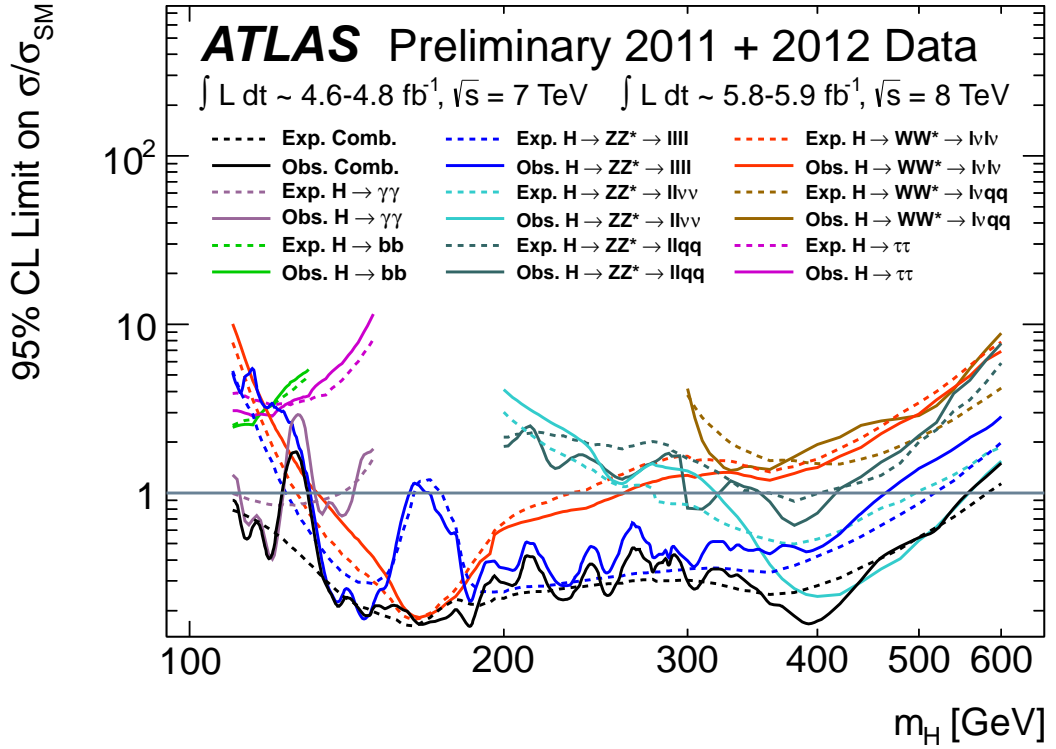


Figure 4.1: The observed (solid) and expected (dashed) 95% CL cross section upper limits for a set of individual search channels for the SM Higgs boson as a function of the Higgs boson mass in units of the SM Higgs boson production cross-section, taken from Ref. [8].

the vector bosons are used as tags for these events, with e.g. the Higgs decay-mode  $H \rightarrow bb$ . Electrons will this way contribute to future measurements of the properties of the observed boson, i.e. whether or not it is the Higgs boson predicted by the Standard Model.

The measurements in the Higgs sector are, however, not dominated by electron systematic uncertainties. For the analysis with  $4.8 \text{ fb}^{-1}$  of data taken in 2011 it reaches up to 8% in the  $H \rightarrow ZZ \rightarrow 4e$  channel that of all channels is most sensitive to the uncertainties of the electron efficiency. This number is compared to a  $\pm 15 - 20\%$  theoretical uncertainty on the production cross-section of the dominant gluon fusion production mechanism and a  $\pm 15\%$  uncertainty on the background determination, see. Ref. [28].

For a physics analysis the signals in the various detector components need to be translated to physics objects like electrons, muons, jets, and other particles. This is done by a dedicated offline reconstruction software. All data recorded by the ATLAS triggers are passed to this software. The algorithms used for reconstruction have to be designed carefully. They are required to collect a large fraction of signal and at the same time reject as much background as possible.

This chapter gives an introduction to the reconstruction algorithms most important for the  $W$  and electron selection. The first two sections address the more general topics of track and vertex reconstruction as described in Refs. [29, 30]. The electron reconstruction is split into several steps, i.e. candidate reconstruction, identification, trigger and additional isolation requirements. The respective algorithms are described in Ref. [31] and have received major updates in Ref. [32, 33]. An overview on the reconstruction, identification, triggers and isolation is given in Subsections 5.3 to 5.6 for electrons in the acceptance region of the tracking system  $|\eta| < 2.5$ . Electrons outside this  $\eta$  region are not discussed since they are not subject to this thesis. The electron reconstruction and identification are of particular interest in this thesis. Finally, the last two sections are concerned with the reconstruction of the missing transverse energy, which is vital for the event selection for this analysis.

## 5.1 Track Reconstruction

The hits in the three subsystems of the inner detector are used to reconstruct charged-particle tracks. Track seeds are formed from a combination of space-points in the three pixel layers and the first SCT layer. These are then extrapolated back to the outer SCT layers. The track candidates are fitted and quality cuts are applied. All tracks are extended to the TRT, TRT hits are associated and the tracks are refitted using the full information of the inner detector.

A complementary approach starts from unused tracks in the TRT that are then extended to the SCT and pixel sub-detectors. It aims to recover tracks from photon conversions and long lived particles.

Tracks are a key ingredient for the reconstruction of electrons. Furthermore, the curvature is the only way to determine the sign of the charge of an electron. In the electron reconstruction and identification algorithms these tracks are matched to energy deposits in the calorimeter, called clusters. This track-cluster matching is affected by bremsstrahlung losses. A radiated photon does not leave a track in the inner detector but deposits energy in the calorimeters. Both can easily be clustered together, shifting

the cluster position w.r.t. the electron (a photon does not get bent in the magnetic field). Therefore, the  $\Delta\phi$  distribution between the extrapolated track and the cluster used for the track-cluster matching is asymmetric between electrons and positrons. For the electron identification, the track is extrapolated from the point with the closest approach to the primary vertex. It was found that the  $\Delta\phi$  distribution between the cluster and a track re-fitted like this is symmetric.

## 5.2 Vertex Reconstruction

The reconstruction of the interaction vertex is based on the reconstructed tracks. It is subdivided into a finding and a fitting algorithm. A number of requirements on the quality of the tracks considered for the vertex finding is applied. The global maximum in the distribution of  $z$  coordinates of the tracks at the point of closest approach to the beam-spot centre is taken as a vertex seed. A re-fit is performed forcing them to originate from the vertex seed. Tracks that are incompatible with the vertex seed by more than seven standard-deviations are used to seed a new vertex.

The vertices selected this way are ordered according to the sum of  $p_T^2$  of the associated tracks. The one that yields the highest value is taken as the primary vertex.

## 5.3 Electron Reconstruction

Electrons deposit their energy in the LAr calorimeter cells leaving tracks on their way through the inner detector. There are a total of three different reconstruction algorithms used to reconstruct the electrons, one calorimeter seeded, dedicated to high  $E_T$  isolated electrons, one seeded by a track in the inner detector, dedicated mostly to low  $E_T$  electrons in jets, and one for the forward region not subject to this thesis.

The cluster-based reconstruction algorithm is seeded by energy deposits in the electromagnetic calorimeter which exceed 2.5 GeV in a certain number of cells grouped together, so-called clusters. These clusters are formed in  $3 \times 5$  middle layer cells in  $\eta \times \phi$ , formed by a sliding window algorithm. These seed clusters are then very loosely matched to tracks in  $\eta$  and  $\phi$  where the tracks are extrapolated to the second calorimeter layer from their last measurement point. Of the tracks that fulfil the track-cluster matching requirement, the one with the smallest  $\Delta R = \sqrt{\Delta\eta^2 + \Delta\phi^2}$  is considered the best match. In order to reject photons that have converted to an electron-positron pair, tracks with hits in the silicon tracker have priority over those that do not. For tracks reconstructed in the TRT only, no  $\eta$  information is available. Such tracks are matched to the seed clusters in  $\phi$  only.

The track seeded algorithm starts from a track with  $p_T > 2$  GeV. A minimum of two hits in the pixel detector, one of them in the b-layer, and a total of seven hits in the pixel and SCT detector are required. A ratio of hits above and below a certain threshold is required in the TRT. The reconstructed tracks are extrapolated to the middle layer of the calorimeter where clusters around the extrapolated position are built. Close-by

tracks are removed by the algorithm, more precisely the track with the highest transverse momentum is chosen based on track-cluster matching .

Objects reconstructed in either of the above ways are labelled electron candidates. Finally, the energy of each electron candidate is determined in a  $3 \times 7$  (barrel) or  $5 \times 5$  (end-cap) window and corrected for modulations in the calorimeter response and leakage outside the cluster.

The sample of electron candidates is still highly contaminated with photon conversions. Dedicated cuts to reject the latter are applied in the electron identification.

## 5.4 Electron Identification

In contrast to the electron reconstruction, that is concerned with the reconstruction of a high fraction of the electrons produced in the  $pp$ -collision, the identification algorithms are intended to reject a large number of background candidates with little loss of real signal electrons. There are three sets of criteria, that differ in background rejection and signal efficiency. Each criterion involves a set of cuts on shower shape variables, track variables and the combination of both. They are applied on top of the electron reconstruction and successively built upon each other. They are labelled LoosePP, MediumPP and TightPP, where the suffix ‘‘PP’’ stands for PlusPlus and is used to differentiate from the set of cuts used for the ATLAS analyses in 2010.

The cuts on the shower shape variables are optimised in pseudo-rapidity  $\eta$  and transverse energy  $E_T$  by a multivariate analysis programme. The precise binning in  $\eta$  is given in Table 6.2 and complies with the detector geometry. In  $E_T$ , a constant 5 GeV binning is used for  $5 < E_T < 20$  GeV and a 10 GeV binning for  $20 < E_T < 80$  GeV.

The variables used for the three identification criteria are listed in Table 5.1. The *LoosePP* requirements use information from the middle layer of the calorimeter, the energy leakage into the hadronic calorimeter, the pixel and SCT tracking system and a matching of a track to the cluster in  $\eta$ . The *MediumPP* requirement additionally makes use of the b-layer and the TRT. The same shower shape cuts as for the LoosePP requirement are used but at tighter values. Finally, the *TightPP* criterion has an additional cut on the ratio of cluster energy to track momentum, as well as tighter requirements on track-related variables. In particular, the track-cluster matching involves the  $\phi$  direction.

Some of the variables are of special importance for the analysis. The hadronic leakage fraction  $R_{\text{had}}$  is the ratio of the transverse energy deposited in the first layer of the hadronic calorimeter to the one in the electromagnetic cluster. Since hadrons cannot be stopped as efficiently as leptons they penetrate through the electromagnetic into the hadronic calorimeter. Consequently, this cut effectively rejects hadrons and non-isolated electrons inside jets. Showers of isolated electrons with very high  $E_T$  leak into the hadronic calorimeter and the variable loses some of its discrimination power. The variable is highly correlated with the calorimeter isolation that is introduced in Section 5.6.

Type	Description	Name
<b>LoosePP selection</b>		
Acceptance	$ \eta  < 2.47$	
Hadronic leakage	Ratio of $E_T$ in the first layer of the hadronic calorimeter to $E_T$ of the EM cluster (used over the range $ \eta  < 0.8$ and $ \eta  > 1.37$ )	$R_{\text{had1}}$
	Ratio of $E_T$ in the hadronic calorimeter to $E_T$ of the EM cluster (used over the range $ \eta  > 0.8$ and $ \eta  < 1.37$ )	$R_{\text{had}}$
Middle layer of EM calorimeter	Ratio of the energy in 3x7 cells over the energy in 7x7 cells centred at the electron cluster position	$R_\eta$
	Lateral width of the shower	$w_{\eta 2}$
Track quality	Number of hits in the pixel detector ( $\geq 1$ )	$n_{\text{pixel}}$
	Number of total hits in the pixel and SCT detectors ( $\geq 7$ )	$n_{\text{Si}}$
Track-cluster matching	$\Delta\eta$ between the cluster position in the strip layer and the extrapolated track ( $ \Delta\eta  < 0.015$ )	$\Delta\eta$
Strip layer of EM calorimeter	Total shower width	$w_{\text{stot}}$
	Ratio of the energy difference between the largest and second largest energy deposits in the cluster over the sum of these energies	$E_{\text{ratio}}$
<b>MediumPP selection (includes LoosePP)</b>		
Shower-shapes	All LoosePP shower shape cuts but at tighter values	
Track-cluster matching	Tighter $\Delta\eta$ track-cluster matching ( $ \Delta\eta  < 0.005$ )	$\Delta\eta$
Track quality	Transverse impact parameter ( $ d_0  < 5$ mm)	$d_0$
	Number of b-layer hits ( $\geq 1$ ) for $ \eta  < 2.01$	$n_{\text{BL}}$
	Stricter requirements for pixel hits ( $> 1$ ) above $ \eta  > 2.01$	$n_{\text{pixel}}$
TRT	Ratio of the number of high-threshold hits to the total number of hits in the TRT	$f_{\text{HT}}$
<b>TightPP selection (includes MediumPP)</b>		
Track-cluster matching	$\Delta\phi$ between the cluster position in the middle layer and the extrapolated track ( $ \Delta\phi  < 0.02$ )	$\Delta\phi$
	Ratio of the cluster energy to the track momentum	$E/p$
	Tighter $\Delta\eta$ requirement ( $ \Delta\eta  < 0.005$ )	$\Delta\eta$
Track quality	Tighter transverse impact parameter requirement ( $ d_0  < 1$ mm)	$d_0$
	Number of b-layer hits ( $\geq 1$ ) over the full $\eta$ range	$n_{\text{BL}}$
TRT	Total number of hits in the TRT	$n_{\text{TRT}}$
Conversions	Number of hits in the b-layer ( $\geq 1$ )	$n_{\text{BL}}$
	Veto electron candidates matched to reconstructed photon conversions	

Table 5.1: List of variables used for the three identification criteria LoosePP, MediumPP and TightPP. The shower shape cut values vary in  $\eta$  and  $E_T$  and are therefore not explicitly stated, assembled from Refs. [1, 32, 34].

The finely grained strip layer can separate between two photons from  $\pi^0 \rightarrow \gamma\gamma$  decays. The total shower width in the strip layer  $w_{\text{stot}}$  is used to reject those. The ratio of the number of high threshold hits to the total number of hits in the TRT  $f_{\text{HT}}$  makes use of the ability of the TRT to detect additional charge caused by transition radiation. The probability of leaving transition radiation hits increases with the Lorentz factor  $\gamma$  of a particle. Since electrons are by far the lightest detectable particles, this variable is well suited for electron identification.

Electron identification in the transition region between the barrel and end-cap calorimeters  $1.37 < |\eta| < 1.52$  is very challenging. It is excluded from the efficiency measurement and also from all physics analyses that use electrons.

## 5.5 Electron Trigger

It seems natural to use the same criteria as for reconstruction and identification to select electrons at trigger level. However, on trigger level one is facing the problem of very high event rates, that need to be reduced fast and effectively. At the same time only limited computing power is available. Thus, simplifications in the algorithms used have to be made.

The first level trigger L1 uses the information in the calorimeter with reduced granularity of  $0.1 \times 0.1$  in  $\eta \times \phi$ , so-called trigger towers, in order to identify Regions of Interest (RoIs). This is done in  $4 \times 4$  groups of trigger towers, while the energy deposited in the central  $2 \times 2$  trigger towers pass a certain threshold. For the most important triggers used in electron analyses, i.e. e20\_medium, e22\_medium and e22vh\_medium1, depending on the data period, this threshold is 14 or 16 GeV. The suffix vh in the last trigger denotes an  $\eta$  dependent threshold and a hadronic leakage requirement.

The RoIs built at L1 are passed to the level two trigger L2. There, cell clusters are built within the RoI, using the second layer of the electromagnetic calorimeter. The final energy is calculated in a  $3 \times 7$  (barrel) or  $5 \times 5$  (end-cap) grid around the cell with the largest deposited transverse energy. At L2, information from the tracking becomes available. The fast tracking algorithms used here start from the inner silicon detectors and are extended to the TRT volume. Finally, at event filter level (EF) track reconstruction and electron identification algorithms are used that are very similar to the offline selection, i.e. medium selection in the case of the above-mentioned triggers. A selection on the transverse energy of  $E_{\text{T}} > 20$  GeV or  $E_{\text{T}} > 22$  GeV is applied.

Trigger loss arises mainly due to the L2 tracking algorithm. Also, there is a number of corrections applied offline that cannot be applied at trigger level. Of the shower shape variables the hadronic leakage cut is the main source of trigger inefficiency. The trigger performance, as it is measured in this thesis for the offline identification, is documented in Ref. [35] using a tag-and-probe method as well.

## 5.6 Electron Isolation

In order to achieve an even higher background rejection, special isolation requirements can be used on top of the identification criteria. The variables used for discrimination are constructed out of the transverse energy or momentum in a cone of  $\Delta R = 0.3$  around the electron candidate direction. The energy of the candidate that was calculated in  $3 \times 7$  or  $5 \times 5$  cells is removed.

The calorimetric isolation, as defined in Ref. [36]

$$E_T^{\text{cone}}(0.3) = \left( \sum_{\substack{\text{cells} \\ \Delta R < 0.3}} E_T(\text{cell}) \right) - E_T^{\text{el}} \quad (5.1)$$

has the advantage of being sensitive to charged and neutral particles whereas the tracking isolation

$$p_T^{\text{cone}}(0.3) = \sum_{\substack{\text{good tracks} \\ \text{track} \neq \text{electron} \\ \Delta R < 0.3}} p_T(\text{track}) \quad (5.2)$$

is only sensitive to charged particles but capable of differentiating between tracks from the primary vertex of the hard interaction and tracks from pile-up events by applying quality requirements on the tracks. The variables are normalised to the transverse energy or momentum of the electron, i.e.  $E_T^{\text{cone}}(0.3)/E_T$  and  $p_T^{\text{cone}}(0.3)/p_T$ . They are used separately or in combination.

Isolation requirements are not used in this thesis. The calorimetric isolation is used in cones of  $\Delta R = 0.3$  and  $\Delta R = 0.4$  to discriminate signal from background.

## 5.7 Missing Transverse Energy

The missing transverse energy is the key signature of neutrinos that escape the detector without interacting. It is defined as the negative vectorial sum of all energy deposits in the detector [37] and thus is a measure of the transverse energy of the particles that escape the detector without interacting.

$$E_x^{\text{miss}} = - \sum_i E_i \sin \theta_i \cos \phi_i \quad (5.3)$$

$$E_y^{\text{miss}} = - \sum_i E_i \sin \theta_i \sin \phi_i \quad (5.4)$$

$$E_T^{\text{miss}} = \sqrt{(E_x^{\text{miss}})^2 + (E_y^{\text{miss}})^2} \quad (5.5)$$

The  $E_T^{\text{miss}}$  is calculated from three-dimensional topological clusters with energies  $E_i$ . In order to suppress energy from calorimeter noise, these clusters are built iteratively, seeded by cells with  $|E_i| > 4\sigma_{\text{noise}}^2$  and expanded to neighbouring cells. The reconstruction algorithm accounts for the energy deposited in the calorimeters, energy loss

in the cryostat and the energy of muons, measured in the outermost detector layers. Cluster shape variables are used to classify the topological clusters as electromagnetic or hadronic [38]. Each topocluster gets corrected for invisible or escaped energy fractions from nuclear interactions or neutrinos in the shower, accounting also for the dead material. The correction weights are obtained in dedicated calibration studies.

The muon energy is taken from the measurement in the muon spectrometers and added. Only good muons with associated tracks are used and the energy deposited in the calorimeters is removed from the calorimeter term.

## 5.8 $E_T^{\text{miss}}$ Significance Trigger

As will be explained in detail in Chapter 6 it is essential for the analysis presented in this thesis to select events by their missing transverse energy  $E_T^{\text{miss}}$  at trigger level. However,  $E_T^{\text{miss}}$  is not a distinct feature of particles not interacting with the detector. Any object, whose energy is mismeasured causes missing transverse energy in the detector. Either in transverse direction of this object if its energy fluctuates down, or in opposite transverse direction if its energy fluctuates up. On trigger level, where the precision of the event reconstruction is only limited a pure  $E_T^{\text{miss}}$  trigger, capable of selecting  $W \rightarrow e\nu$  events, would record at a too high rate. To prevent automatic pre-scaling a different quantity, called  $E_T^{\text{miss}}$  significance, is used instead.

The  $E_T^{\text{miss}}$  significance (XS) is defined as the ratio of the missing transverse energy to its resolution. With more objects in the detector the individual energy fluctuations cancel partially. As a result the resolution of the  $E_T^{\text{miss}}$  measurement is a function of the total energy deposited in the detector  $\sum E_T$ . The  $E_T^{\text{miss}}$  resolution can be fitted with a function  $f = a \cdot (\sqrt{\sum E_T} - b)$ , see Ref. [29]. A simple  $E_T^{\text{miss}}$  significance can be defined as the ratio

$$\text{XS} = \frac{E_T^{\text{miss}}}{a \cdot (\sqrt{\sum E_T} - b)} \quad (5.6)$$

Depending on the period and trigger level, values of 0.46-1.12 are used for the parameter  $a$  and values of 0.5-1.28 for the parameter  $b$  [39]. The triggers that will be used for this analysis apply a selection such that events with  $\text{XS} > 4.5\sqrt{\text{GeV}}$  pass L1 and events with  $\text{XS} > 6.0\sqrt{\text{GeV}}$  pass the event filter. Because of the limited computing power on trigger level no correction for the possible presence of muons is applied, i.e. the information from the muon spectrometer is not used for the trigger decision. Therefore  $E_T^{\text{miss}}$  and  $\sum E_T$  do not include any muon  $p_T$ , measured in the muon system. This results in a significance on trigger level quite different from the significance calculated offline.

The analysis does not use pure  $E_T^{\text{miss}}$  significance triggers. More details about the selection applied by the trigger and the triggers used are given in Section 7.3.1. A few studies on the trigger performance are done in Section 8.1

## 5.9 Jet Reconstruction

Jets that are used in the analysis are reconstructed using the anti- $k_t$  algorithm. Like in Section 5.7 topological clusters are built from the energy deposits in adjacent calorimeter cells. These clusters are then combined pair-wise to jets starting with the closest one according to the following distance definition

$$d_{ij} = \min \left( \frac{1}{p_{T,i}^2}, \frac{1}{p_{T,j}^2} \right) \frac{\Delta R_{ij}^2}{R^2} \quad (5.7)$$

where  $R = 0.4$ . If there is no cluster with  $d_{ij} < \frac{1}{p_{T,i}^2}$  the jet clustering is discontinued.  $\frac{1}{p_{T,i}^2}$  can be interpreted as the distance to the beam axis.

---

# 6 Methodology of the Measurement

---

A clean sample of genuine electrons is needed for the measurement of electron efficiencies. Such electrons are known to be produced at high rate as the products of  $W$  bosons decaying to an electron and a neutrino, and the resonances of the  $Z$  boson and  $J/\psi$  meson decaying to an electron-positron pair. At the ATLAS experiment all these three decay modes are used for a variety of performance measurements. The measurements with  $W$  and  $Z$  bosons complement each other over a large kinematic range; the  $J/\psi$  channel completes the measurement to lower transverse energies.

The full efficiency measurement is factorised in similar way as the electron reconstruction and identification described in Chapter 5. From the calorimeter seed to the electron object used in physics analyses it is performed in three steps:

- reconstruction;
- identification (ID);
- trigger.

For all of them the data samples are contaminated with events from background processes that need to be subtracted. For  $Z \rightarrow ee$  events a variety of background subtraction techniques have been established. For  $W \rightarrow e\nu$  events on the other hand, the background subtraction is known to be notoriously difficult. This is not only because of the lack of a good subtraction technique; the background is much larger for  $W$  than for  $Z$  events. Given the severe background contamination, the measurements of the trigger and reconstruction efficiencies are only performed with  $Z \rightarrow ee$  events. All three channels use a so-called tag-and-probe method to select the events of interest. The thesis presented here is only concerned with the  $W \rightarrow e\nu$  channel and thus only with the measurement of the identification efficiencies. In the following, the abbreviations  $WT\&P$  or  $ZT\&P$  are used to refer to the efficiency measurements in a certain channel.

## 6.1 The Tag & Probe Method

When performing efficiency measurements one is confronted with the problem of selecting an unbiased, well defined sample of objects, here electrons, to test the cut of interest. Putting prior selection criteria on these objects carelessly can easily distort the measurement. The principle of selecting a test sample is formalised in the so-called tag-and-probe method.

It is best explained for processes that have two particles in the final state but is easily extendable to processes with more final states or single particles. With this approach

	$W$ tag-and-probe	$Z$ tag-and-probe
Tag	$E_T^{\text{miss}} > 30 \text{ GeV}$ $\Delta\phi(E_T^{\text{miss}}, 2\text{jets}) > 0.7$	one MediumPP electron $E_T > 20 \text{ GeV}$
Trigger	$E_T^{\text{miss}}$ significance trigger	single electron trigger (matched to tag electron)
Boson selection	$M_T > 40 \text{ GeV}$	$80 < M_{ee} < 100 \text{ GeV}$

Table 6.1: Tag requirements for  $W$  and  $ZT\&P$  measurements.

the event selection has to involve objects other than the object to be tested. The basic idea is to select such an event by setting strict requirements on *one* of the two final state particles, the tag object. The other particle serves as a probe for the measurement. The cut of interest can be tested on this unbiased probe. Its efficiency  $\varepsilon_{\text{cut}}$  is the fraction of all probes considered that pass the cut

$$\varepsilon_{\text{cut}} = \frac{N_{\text{probes, passing cut}}}{N_{\text{probes}}}. \quad (6.1)$$

In  $ZT\&P$ , one of the electrons is used to tag the event. Cuts are tested on the other electron. Similarly, for  $WT\&P$ , high missing transverse energy, caused by the neutrino that escapes the detector undetected, is used as the tag. The selection applied to tag the event is different from the selection used in a physics analysis of the respective process. The selection cuts on the tag object are tightened while no selection is applied on the probe. The reason for the tighter selection is that only the tag object can be used to reject background processes and improve on the signal-to-background ratio – the probe electron has to remain untouched. A juxtaposition of the tag requirements for the  $W$  and  $ZT\&P$  measurements is given in Table 6.1.

The procedure requires some care in selecting the triggers. Following the tag-and-probe idea no selection on the probe must be applied on trigger level. In case of the identification efficiency measurements, this thesis is concerned with, a selection on the probe is applied beforehand: electrons are required to be reconstructed and fulfil certain additional criteria listed in the following section.

## 6.2 Efficiency Definition

The production cross-section times branching-ratio of a certain physics process, e.g. a  $W$  or  $Z$  decay, is measured using the formula:

$$\sigma_{W/Z} \times BR(W/Z \rightarrow e\nu/ee) = \frac{N^{\text{data}} - N^{\text{bkg}}}{A_{W/Z} \cdot C_{W/Z} \cdot L_{\text{int}}} \quad (6.2)$$

with

- $N^{\text{data}}$  the number of events observed in data;
- $N^{\text{bkg}}$  the number of expected background events;
- $A_W$  and  $A_Z$  the correction factors to account for the geometrical and kinematic acceptance of the detector;
- $C_W$  and  $C_Z$  the correction factors to account for the efficiency of the event being reconstructed in the detector;
- $L_{\text{int}}$  the integrated luminosity.

Both the acceptance  $A_{W/Z}$  and efficiency  $C_{W/Z}$  are obtained from Monte-Carlo simulations of the signal process. They are defined as

$$A_{W/Z} = \frac{N_{\text{MC,gen,fid}}}{N_{\text{MC,gen,all}}} \quad \text{and} \quad C_{W/Z} = \frac{N_{\text{MC,rec}}}{N_{\text{MC,gen,fid}}}. \quad (6.3)$$

The acceptance  $A_{W/Z}$  is the fraction of Monte-Carlo events that are generated in the geometrical and kinematic range of the detector, the so-called fiducial phase-space. This number is obtained using generator-level information only. The efficiency  $C_{W/Z}$  is the fraction of these events that get reconstructed correctly.

All detector effects and the impact of QED final state radiation is included in  $C_{W/Z}$ . The correction factors  $C_{W/Z}$  are obtained from Monte-Carlo simulation, too, but the simulation is corrected for differences between data and Monte-Carlo with the results of dedicated measurements of the efficiency to trigger, reconstruct and identify the  $W/Z$  decay products. The factor  $C_W$  can be further decomposed into [40]:

$$C_W = \varepsilon_{\text{event}} \cdot \alpha_{\text{reco}} \cdot \varepsilon_{\text{ID}} \cdot \varepsilon_{\text{trig}} \cdot \varepsilon_{\text{iso}} \quad (6.4)$$

where

- $\varepsilon_{\text{event}}$  is the efficiency of the signal events passing the event preselection cuts, e.g. primary vertex requirements;
- $\alpha_{\text{reco}}$  accounts for the differences between applying the geometrical and kinematic selection at generator or reconstruction level, i.e. the reconstruction efficiency;
- $\varepsilon_{\text{ID}}$  is the efficiency of an electron passing the identification criteria as mentioned in Section 5.4; this is the efficiency this thesis addresses;
- $\varepsilon_{\text{trig}}$  is the efficiency of an event being triggered;
- $\varepsilon_{\text{iso}}$  is the efficiency of possible isolation cuts.

It was mentioned in Section 4.1 that the uncertainties on the electron efficiencies are larger for the  $Z \rightarrow ee$  than for the  $W \rightarrow e\nu$  cross-section measurement. This is reflected in the corresponding equation for  $C_Z$ , that accounts for the fact, that two electrons have

to be identified and either of the electrons can trigger the event (in case a single electron trigger is employed):

$$C_Z = \varepsilon_{\text{event}} \cdot \alpha_{\text{reco}} \cdot \varepsilon_{\text{ID}}^2 \cdot \varepsilon_{\text{iso}}^2 \left(1 - (1 - \varepsilon_{\text{trig}})^2\right). \quad (6.5)$$

For cross-section measurements other than that of  $W \rightarrow e\nu$  and  $Z \rightarrow ee$ , definitions similar to  $C_{W/Z}$  are used.

Also the number of expected background events  $N^{\text{bkg}}$  is usually obtained from Monte-Carlo (with the exception of background from QCD multi-jet processes). The samples used to estimate the background processes are also corrected with the results from measurements on data, so the efficiencies measured in this thesis do not only contribute to the calculation of events produced but also to correct the estimation of the number of background events.

The exact factorisation of  $\alpha_{\text{reco}}$  and  $\varepsilon_{\text{ID}}$  in the  $C_{W/Z}$  factors is determined by technicalities in the efficiency measurement and slightly differs from the different event reconstruction steps. It was found that  $WT\&P$  suffers from large background contamination from non-collision beam background [41]. This can be reduced by quality requirements on the tracks of the probe electrons. For reasons that are discussed in Section 6.5.2, the background subtraction technique for  $WT\&P$  is inapplicable to the measurement of the efficiency of the cut on the hadronic leakage fraction  $R_{\text{had}}$ . Because of that, the factorisation is changed to:

- reconstruction+track-quality+ $R_{\text{had}}$ ;
- all other identification criteria;

where track-quality and  $R_{\text{had}}$  are the identification cuts usually applied on LoosePP level. Throughout this thesis, the term identification efficiency is used as the efficiency of identifying an electron that was reconstructed and passed the track-quality and  $R_{\text{had}}$  requirements. For consistency and in order to arrive at comparable results the same factorisation is used for the measurement in  $ZT\&P$ .

### 6.3 Scale-factor Definition

The efficiencies are calculated for data and Monte-Carlo as a function of the pseudorapidity  $\eta$  and the transverse energy  $E_T$ . In order to use the results in analyses, scale-factors that correct the efficiencies measured in Monte-Carlo to the results from data are defined as

$$\text{SF}(\eta, E_T) = \frac{\varepsilon_{\text{data}}(\eta, E_T)}{\varepsilon_{\text{MC}}(\eta, E_T)} \quad (6.6)$$

### 6.4 Combination of Different Measurements

As mentioned above the measurement of the identification efficiencies is performed via three different decay processes. The central value is taken as the weighted mean of the

three channels

$$\overline{\text{SF}} = \frac{\sum_i \frac{\text{SF}_i}{\delta_{\text{SF}_i}^2}}{\sum_i \frac{1}{\delta_{\text{SF}_i}^2}}, \quad i = J/\psi, W, Z, \quad (6.7)$$

$$\delta_{\overline{\text{SF}}} = \frac{1}{\sqrt{\sum_i \frac{1}{\delta_{\text{SF}_i}^2}}} \quad (6.8)$$

For electrons with a transverse energy of  $5 < E_T < 15$  GeV only the values obtained from the  $J/\psi$  measurement are used. Between  $15 < E_T < 20$  GeV all three measurements are combined, and above, the results from  $WT\&P$  and  $ZT\&P$  measurements are combined.

## 6.5 Measurement of Efficiencies

After these introductory sections, valid for all efficiency measurements, this section is concerned with more technical questions, to large extent specific for the  $W$  channel.

### 6.5.1 Binning

The identification efficiencies are expected to depend on a set of variables. The identification requirements are optimised in pseudo-rapidity  $\eta$  and transverse energy  $E_T$ . Hence, a dependence of the identification efficiencies is expected and also the efficiency measurements have to be performed as a function of these variables.

Different physics processes have different distributions in these variables. The measurement needs to be universal for electrons no matter where they are originating from. Since physics is a function of these variables as well, one might want to do a differential physics measurement in  $\eta$  or  $E_T$ . Associated with that, the dependence of the identification efficiencies is of interest. Thus, there is also a technical motivation to measure the identification efficiencies differentially.

As a third variable, the measurement is performed for electrons and positrons separately in the  $WT\&P$  channel.

#### Pseudo-rapidity $\eta$

The detector geometry changes with the pseudo-rapidity  $\eta$  and predetermines some of the  $\eta$  bins:

- $|\eta| < 2.47$ , the outermost bin borders where the silicon tracking system ends;
- $|\eta| < 2.01$ , the end of the transition radiation tracker (TRT);
- $1.37 < |\eta| < 1.52$ , the crack between barrel and end-cap calorimeters;
- $|\eta| < 0.1$ , the very central region where the readout electronics of the TRT are located.

	<b>barrel</b>														
fine	0.0	0.1	0.2	0.3	0.4	0.5	0.6	0.7	0.8	0.9	1.0	1.1	1.2	1.3	1.37
intermediate	0.0	0.1					0.6		0.8				1.15		1.37
coarse		0.1							0.8						1.37
ID		0.1					0.6		0.8						1.37
	<b>end-cap</b>														
fine	1.52	1.6	1.7	1.8	1.9	2.0	2.1	2.2	2.3	2.4	2.47				
intermediate	1.52			1.81		2.01				2.37	2.47				
coarse	1.52					2.01					2.47				
ID	1.52			1.81		2.01				2.37	2.47				

Table 6.2: Binning of the efficiency measurements in pseudo-rapidity  $\eta$ . For the performance measurements the same binning is used in  $-\eta$  direction to account for detector effects that are asymmetric in  $\eta$ . The optimisation of identification requirements assumes forward-backward asymmetry.

More bins are predetermined by the electron identification cuts. The measurement is performed in three  $\eta$  granularities, fine, intermediate and coarse. They are listed in Table 6.2 together with the binning of the identification cuts. The coarse binning with 11 bins is a remainder of the 2010 analysis and kept for systematic and future studies with a smaller number of events, e.g. the 2012 analysis. The intermediate binning with 18 bins is the default binning provided to physics analyses, intended for those who do not need a high precision in the electron sector. The fine binning with 50 bins is intended for Standard Model analyses with electrons that require a high precision. In order to achieve maximum precision, methods to treat the individual statistical uncertainties and the systematic correlation between the different bins are under development.

While the identification cuts are chosen symmetric in  $\eta$ , efficiencies are not necessarily expected to be symmetric. Effects from misalignment of the detector, displacement in the beam-spot position and detector effects can cause an asymmetry; therefore the measurement is performed for positive and negative values of  $\eta$  separately.

### Transverse energy

The second variable for the differential measurement is the transverse energy. With increasing energy the electrons are more likely to radiate photons influencing the track-based identification cuts. The electromagnetic showers in the calorimeters become wider with some impact on the calorimeter-based identification cuts. Furthermore, the background processes change over the kinematic range. Therefore, the electron identification is optimised for different electron energies and for the rejection of different background processes. The binning is particularly important to provide portability to other processes and comparability to  $ZT\&P$ . A binning in constant, 5 GeV steps is used from 15 to 50 GeV.

## Charge

At last, the efficiencies are calculated for electrons and positrons separately. Although for the single object there is no difference expected, there is a subtle effect related to charge misidentification causing differences in the efficiencies of identifying electrons and positrons. Due to the initial asymmetry in the production of  $W^+$  and  $W^-$  bosons, charge misidentified particles contribute to the efficiency measurements of electrons and positrons in different proportions. Namely, the fraction of misidentified particles is higher in the measured electron sample than in the positron sample. This effect is further studied in Section 8.4. It causes the efficiencies of positrons to be larger than for electrons.

Both electrons and positrons enter the efficiency measurements with the same weight, i.e. the arithmetic mean of electron and positron identification efficiencies is used in order to derive general, charge independent electron efficiencies.

## Considerations on the choice of the binning

The final choice of the granularity of the binning is driven by the uncertainties of the resulting scale-factors. A very fine separation of the measurement into bins would result in large statistical uncertainties. If on the other hand a very coarse granularity is chosen, the statistical uncertainties get very small, leaving only systematic uncertainties.

Since, the scale factors have been measured in specific physics processes with specific kinematic distributions, the scale factors might not be valid for other physics processes with other kinematic distributions, if they are integrated over a too large kinematic region using a very coarse granularity. If this was the case, the systematic uncertainties would have to be enlarged to make sure kinematic biases are accounted for in the uncertainties. In order to assure portability of the scale-factors to other analyses the granularity should be chosen such that neighbouring bins overlap within their uncertainty. For an optimal binning, precision and portability should therefore be balanced.

### 6.5.2 Background Subtraction

The  $W$  sample is selected by applying a hard selection on the tag while only few requirements on the electron are made. This results in a high background contamination, especially on reconstruction level. For the efficiency measurements the residual background has to be subtracted.

#### Sources of background

There are two categories of background processes to be considered. Background from genuine electrons in events that can easily be mistaken for a  $W \rightarrow e\nu$  decay, like a  $Z \rightarrow ee$  decay where one electron is outside the detectors acceptance and thus induces  $E_T^{\text{miss}}$ , or  $W \rightarrow \tau\nu$  with the  $\tau$  decaying leptonically  $\tau \rightarrow e\nu_e\nu_\tau$ . These represent the most important background processes from real electrons in Standard Model analyses.

Here, they are not subtracted. Such electrons are allowed to contribute to the efficiency measurements and do not represent background in the ordinary sense.

The second group is background from QCD processes faking an electron. The high cross-section of QCD processes that is roughly six orders of magnitude higher than the one of the  $W \rightarrow e\nu$  process leads to a considerable contamination of the electron sample with jets. These processes cannot be predicted reliably by Monte-Carlo simulation. This is because regions of rare processes which are not reliably modelled contribute. These are very extreme cases with large fluctuations in the showers. Instead, a data driven method is used to subtract the residual background from QCD fakes in the numerator as well as the denominator.

To give an idea of the amount of background to be subtracted, Tables A.1 to A.3 show the number of signal and background events obtained with the subtraction technique explained in the following.

### Background templates

The difficulty the analysis is confronted with is to find a background template that is suitable for all bins – 350 in the case of the fine binning. It was decided to use an object-based method considering the characteristics of the fake electron itself. This means that background templates are constructed out of the selected probes, using the same binning in  $\eta$  and  $E_T$ , by inverting at least two of the electron identification criteria with the intention of selecting objects that are not electrons. The reverted criteria are the requirements on the total shower width  $w_{stot}$  and the TRT ratio  $f_{HT}$  that are described in detail in Section 5.4. Electron candidates that do not leave hits in the TRT pass the latter cut by definition, so in the region not covered by the TRT no templates are selected. An alternative, second template is constructed by applying a cut on  $R_\phi < 0.9$  (similar to  $R_\eta$  as defined in Section 5.4) on top of the first template. Moreover, in order to increase the number of events in the templates, no charge selection is applied and the templates obtained from the two bins in negative and positive pseudo-rapidity  $|\eta|$  are summed.

This way of template selection causes statistical correlations that need to be considered later in the analysis. Each template is used for the background subtraction on reconstruction level and all three ID levels. The same template is used to obtain the efficiencies for electrons and positrons. The template in a certain  $\eta$  bin is also used in  $-\eta$ . In the end-cap bins not covered by the TRT, the given selection does not yield templates, so for a pseudo-rapidity  $|\eta| > 2.01$  the template from the closest bin with  $|\eta| < 2.01$  is used repeatedly. This means that a single template can be used up to ten times in the fine  $\eta$  granularity.

### Subtraction technique

The isolation variables  $E_T^{\text{cone}}(0.3)/E_T$  and  $E_T^{\text{cone}}(0.4)/E_T$  are used to discriminate between signal and background. The candidate probes in each  $\eta \times E_T$  bin are subdivided

into a signal dominated and a background dominated region at a certain isolation value, typically 0.40. Assuming the region with an isolation energy higher than this threshold, called *control region*, is free of signal, the background templates obtained as described above are normalised to the number of selected probes using the range up to  $E_T^{\text{cone}}/E_T = 1.5$ . The number of background events found after normalisation in the *signal region*, defined by  $E_T^{\text{cone}}/E_T$  below the threshold, is then subtracted. The result of that procedure is shown in Fig. 6.1 for a low  $E_T$  bin and for the different identification criteria.

The central value of the efficiencies in each bin is not defined by a single choice of the threshold between signal and control region but by averaging over five configurations and the two template variations, explained earlier. Furthermore the kinematic selection of the probes is varied. The background-only assumption above the isolation threshold causes an implicit cut on the discriminating variable in the process of the background subtraction. Because of that, a cut on isolation is applied on Monte-Carlo at the value of the isolation threshold although no background is present.

What seems to be very problematic here is the isolation threshold. Judging from Fig. 6.1, there seems to be a considerable amount of signal present in the control region, with the isolation threshold chosen at 0.40 in the plots. This means that there is supposedly too much background subtracted. Because of that, the threshold is varied as a part of the estimation of the systematic uncertainty down to 0.30, with a very little amount signal in the (now smaller) control region, and up to 0.50, with a larger amount of signal. This way, the effect is expected to be accounted for by the systematic uncertainty, see Section 6.8.1.

There is a strong correlation between the calorimeter isolation and the hadronic leakage fraction  $R_{\text{had}}$  that is applied in every set of identification criteria but not for reconstruction. Because of the implicit cut at the isolation threshold, the efficiency of this cut cannot be measured with the presented background subtraction technique. Instead, it is measured together with the reconstruction efficiencies. With this factorisation, the variables used for electron identification can be regarded as uncorrelated with the calorimeter isolation and the shape of the calorimeter isolation remains unaffected by the application of electron identification requirements. This also means that the same templates can be used for background subtraction on reconstruction and all three identification levels.

Above a transverse energy of  $E_T > 40$  GeV the probes tend to be very isolated. This is causing problems in the background subtraction. In a large number of bins there are no events in the control region with the consequence that no background is subtracted at all. To account for the high isolation in these high  $E_T$  bins the discriminating variable is replaced by the transverse energy in a cone of 0.3 or 0.4 divided by a value of 25 GeV, i.e.  $E_T^{\text{cone}}/25$  GeV. This way the background can be subtracted, keeping the isolation thresholds used in the lower  $E_T$  bins. An alternative would be the modification of the isolation threshold.

There have been attempts to construct signal templates for the background subtraction. This would allow an alternative, fit-based background subtraction technique. Until today these attempts were unsuccessful since the trigger used for the analysis seems to distort the shape of the signal in the distributions of the discriminating variables. A sig-

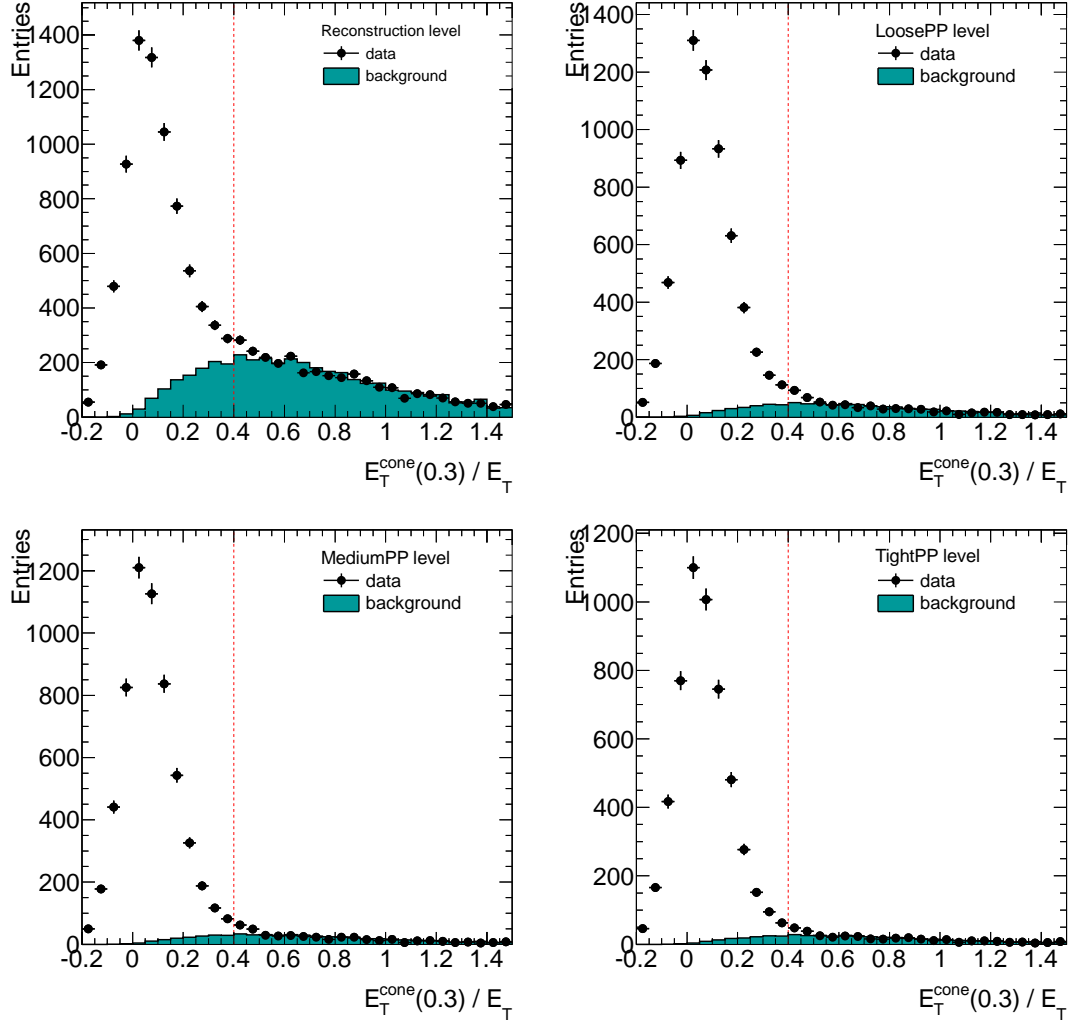


Figure 6.1: Example distributions of the calorimeter isolation variable  $E_T^{\text{cone}}(0.3)/E_T$  in the low  $E_T$  region with the background estimate for a barrel bin,  $15 < E_T < 20$  GeV and  $-0.8 < \eta < -0.1$ . The red line marks the isolation threshold used for normalisation.

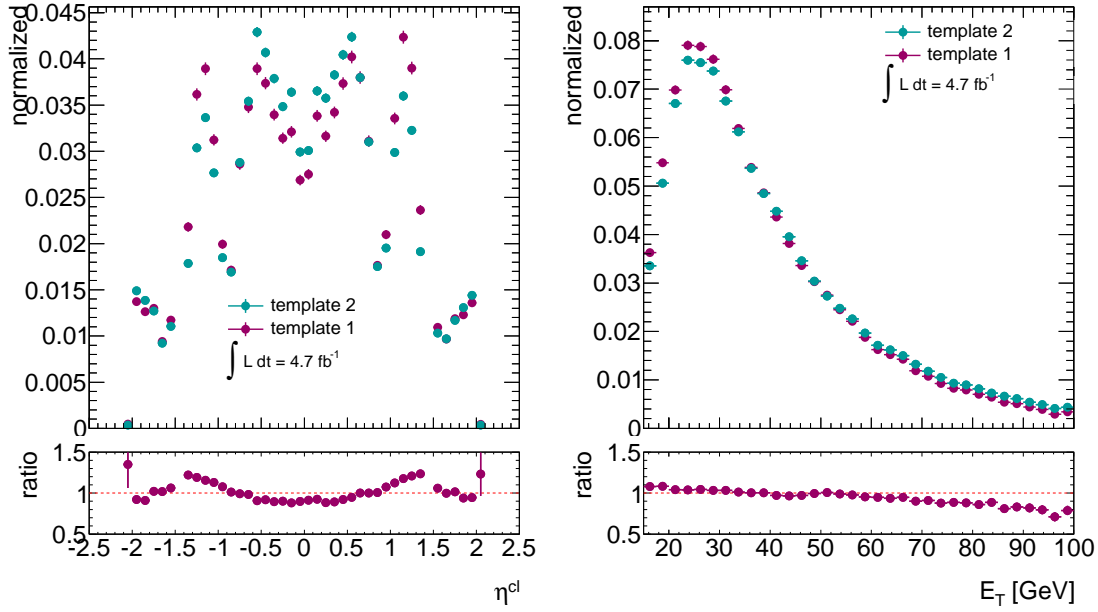


Figure 6.2: The distributions of pseudo-rapidity  $\eta$  and transverse energy  $E_T$  of the two background templates.

nal template would not only make the problematic implicit cut at the isolation threshold obsolete, it might also make a measurement of the efficiency of the cut on the hadronic leakage fraction  $R_{\text{had}}$  possible.

### 6.5.3 Validation of the Background Templates

A validation of the background templates with Monte-Carlo is very difficult and has never been carried out properly, because of the lack of a large di-jet Monte-Carlo sample. The largest sample available gave a total of 34 electron fakes on reconstruction level. Clearly, this is not enough to validate the template selection, especially not in each of the up to 350 bins. The choice of the template therefore only follows theoretical considerations, agreement to the probe distributions in the control region and studies of the signal contamination based on Monte-Carlo simulation of the signal process.

#### Kinematic distributions of the background templates

The kinematic distributions in  $\eta$  and  $E_T$  for both template variations are compared in Fig. 6.2. They are slightly different, however this disagreement is not a problem, since the measurement is performed in bins of these variables. More problematic is the disagreement in the distributions of the two discriminating variables used for the background subtraction. These are compared in Fig. 6.3 for the two template selections. Their ratios are flat in the background dominated region but there is significant disagreement

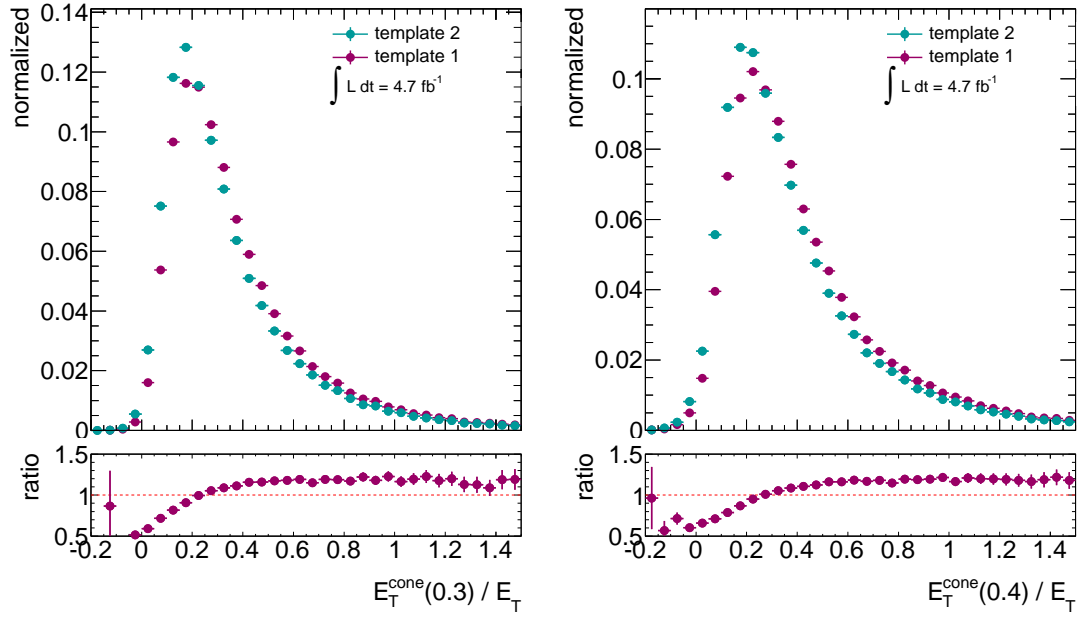


Figure 6.3: The distribution of the discriminating variables  $E_T^{\text{cone}}(0.3)/E_T$  and  $E_T^{\text{cone}}(0.4)/E_T$  of the two background templates.

in the signal dominated region, affecting the amount of background to be subtracted. In a large number of  $\eta \times E_T$  bins the disagreement of the two templates give the largest contribution to the estimated systematic uncertainties. More studies on the template shape could improve the measurement. However, for now there is no way to judge which of the templates is better.

The choice of the template is mainly driven by looking at background subtraction plots like Fig. 6.1. In the control region the templates agree very well with the selected probes.

### Signal contamination

For statistical reasons the following studies were done in coarse  $\eta$  granularity. They are believed to remain valid in the finer binning.

The question whether it is enough to revert only two identification cuts to reject real electrons in the template has been raised repeatedly. A Monte-Carlo study has been performed in order to address this. By applying the template selection on the signal Monte-Carlo, the amount of real electrons that leak into the template can be estimated. This approach is valid, since electromagnetic showers of real electrons are generally described quite well in Monte-Carlo simulations. The fraction of signal in the templates was found to be largest in the middle  $E_T$  range where the signal-to-background ratio is large. The signal-to-background ratios for the different bins is given in Table A.3. An

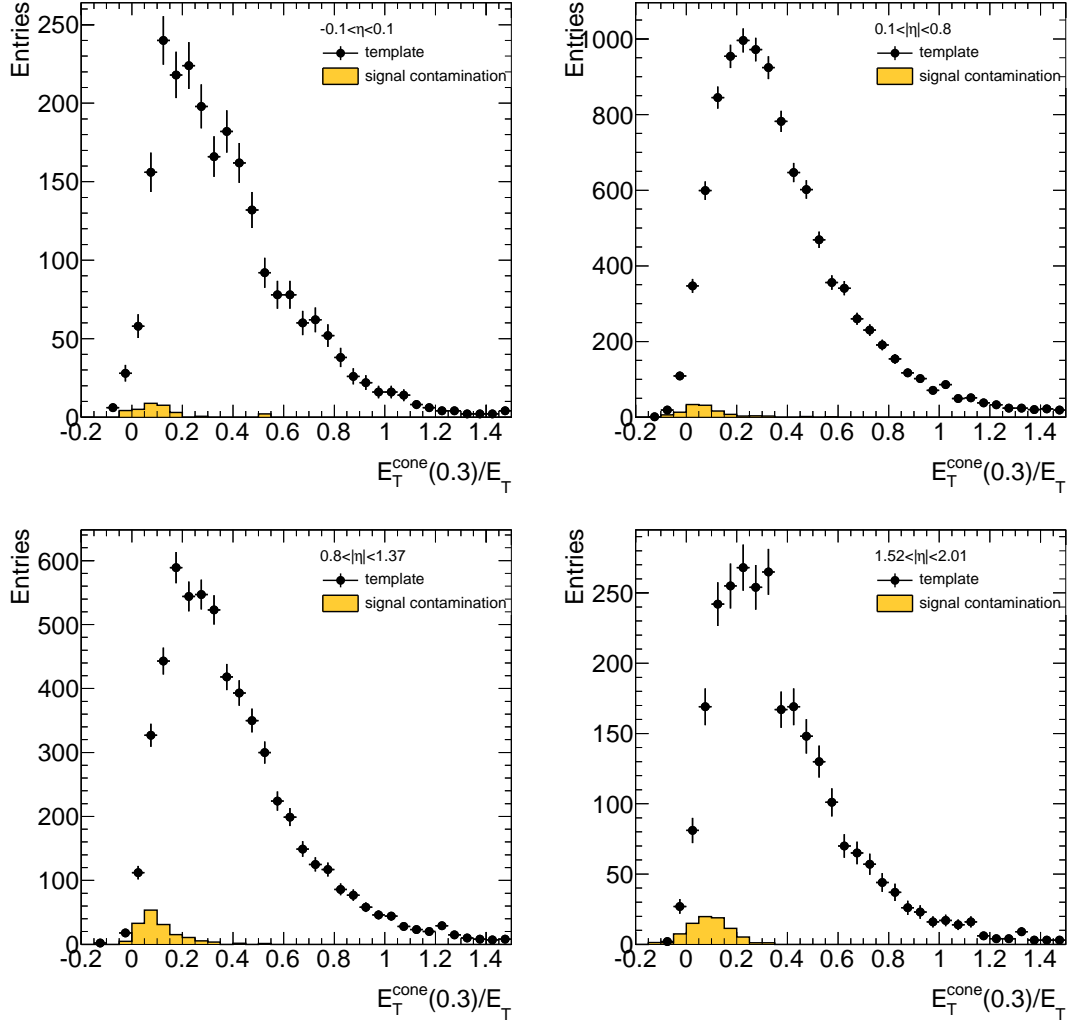


Figure 6.4: Signal contamination in the background templates for one of the more affected  $E_T$  bins  $25 < E_T < 30$  GeV for all  $\eta$  bins in coarse granularity. Signal from POWHEG Monte-Carlo is expected to be overestimated by  $\sim 10 - 15$  %.

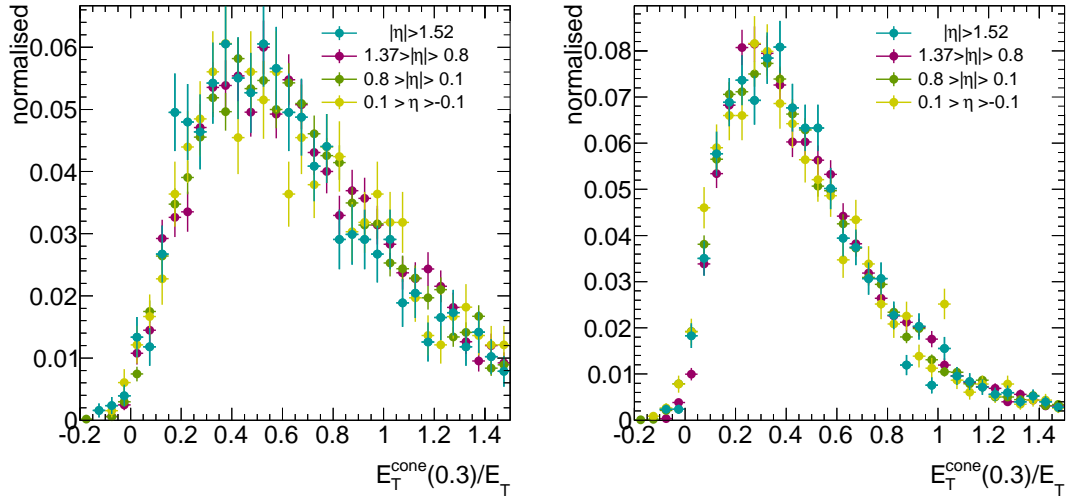


Figure 6.5: Templates for the different  $\eta$  bins for the two lowest  $E_T$  bins.  $15 < E_T < 20$  GeV (left) and  $20 < E_T < 25$  GeV (right).

example of the signal contamination study is shown for a specific  $E_T$  bin in Fig. 6.4. Note, that Monte-Carlo is expected to be overestimated by approx. 10 – 15 % because of trigger mismodelling, as will be discussed in Section 7.5.

There are signal events present in the templates and they are not spread evenly over the full range of the isolation but localised in the signal region. Therefore, there is too much background subtracted on both reconstruction and ID level. The signal contamination is of the same order for the other discriminating variables and the other template (cutting on  $R_\phi$  does not reject signal more efficiently). Looking at the different template shapes in Fig. 6.3 the systematic effect of subtracting too much background is believed to be well covered by the systematic variations.

### Replacement of the templates in the outermost $\eta$ bins

The replacement of the templates in the end-caps by the one from the closest bin, still in the acceptance region of the TRT, would introduce a bias in case there is a dependence of the templates vs.  $\eta$ . For the two most background contaminated  $E_T$  bins and one of the template variations, templates for different  $\eta$  bins are compared in Fig. 6.5. They are indeed compatible within statistical uncertainties. The corresponding plots for the other template variation and for the other  $E_T$  bins have been checked as well with the same conclusion: it is safe to replace the templates.

## 6.6 Comparison of $J/\psi$ , $W$ and $Z$ Kinematics

As mentioned before, the measurement of electron identification efficiencies using  $W \rightarrow e\nu$  decays is complemented by measurements using the decay products of  $J/\psi$  and  $Z$ .

The three channels all have strengths and weaknesses. A big setback in *WT&P* is that a  $W \rightarrow e\nu$  event cannot be fully reconstructed because of the neutrino in the event. Additionally, the  $E_T^{\text{miss}}$  used as the tag can have causes other than neutrinos, most notably fluctuations in energy measurements of jets. As a consequence, it is difficult to select a sample of  $W$  events with high purity. Both the impossibility of fully reconstructing the event and the poor purity result in difficulties in the background subtraction. Furthermore, no background subtraction technique was found that could measure the efficiency of the cut on the hadronic leakage fraction  $R_{\text{had}}$ . As a consequence, the factorisation of the measurement was changed.

However, there are numerous advantages in using  $W$  events. Each of the three decay channels  $J/\psi$ ,  $W$  and  $Z$  covers a different kinematic range. With the much lower mass of the  $J/\psi$  the electrons have a lower transverse energy and cover the range  $7 < E_T < 20$  GeV. The major advantage of the  $W$  boson w.r.t.  $Z$  is its high production rate.  $W \rightarrow e\nu$  events are produced at a rate of 10.46 nb compared to 0.99 nb for  $Z \rightarrow ee$ . Because of the slightly lower mass of the  $W$  boson its electrons can probe a lower  $E_T$  range; because of the boost in  $z$ -direction, the production rate is particularly larger in the end-cap bins. The distributions in probe  $E_T$  and  $\eta$  for  $J/\psi$ ,  $W$  and  $Z$  are shown in Fig. 6.6 for TightPP probes, selected with the tag-and-probe technique.

## 6.7 Statistical Uncertainties

This section states the equations used for the calculation of statistical uncertainties. The equations for the number of signal events and for the treatment of statistical correlations are specific for the background subtraction technique of *WT&P* and thus derived here.

### 6.7.1 Background Subtracted Data

The statistical uncertainty on the background subtracted data has three sources: the statistical uncertainty on the probes, the statistical uncertainty on the normalisation of the template to the number of probes in the control region and the statistical uncertainty on the number of template events. Especially on reconstruction level, the number of events in the background template is very limited. This is because the templates are selected as a subset of the probes they are normalised to.

All data events are split into signal and control region,  $N_{\text{dataL}}$  for events below and  $N_{\text{dataR}}$  for events above the isolation threshold. Assuming Poissonian errors the statistical uncertainties on these numbers are

$$\delta_{\text{dataL}} = \sqrt{N_{\text{dataL}}} \quad (6.9)$$

$$\delta_{\text{dataR}} = \sqrt{N_{\text{dataR}}}. \quad (6.10)$$

The same is done for the templates with corresponding errors

$$\delta_{\text{templL}} = \sqrt{N_{\text{templL}}} \quad (6.11)$$

$$\delta_{\text{templR}} = \sqrt{N_{\text{templR}}}. \quad (6.12)$$

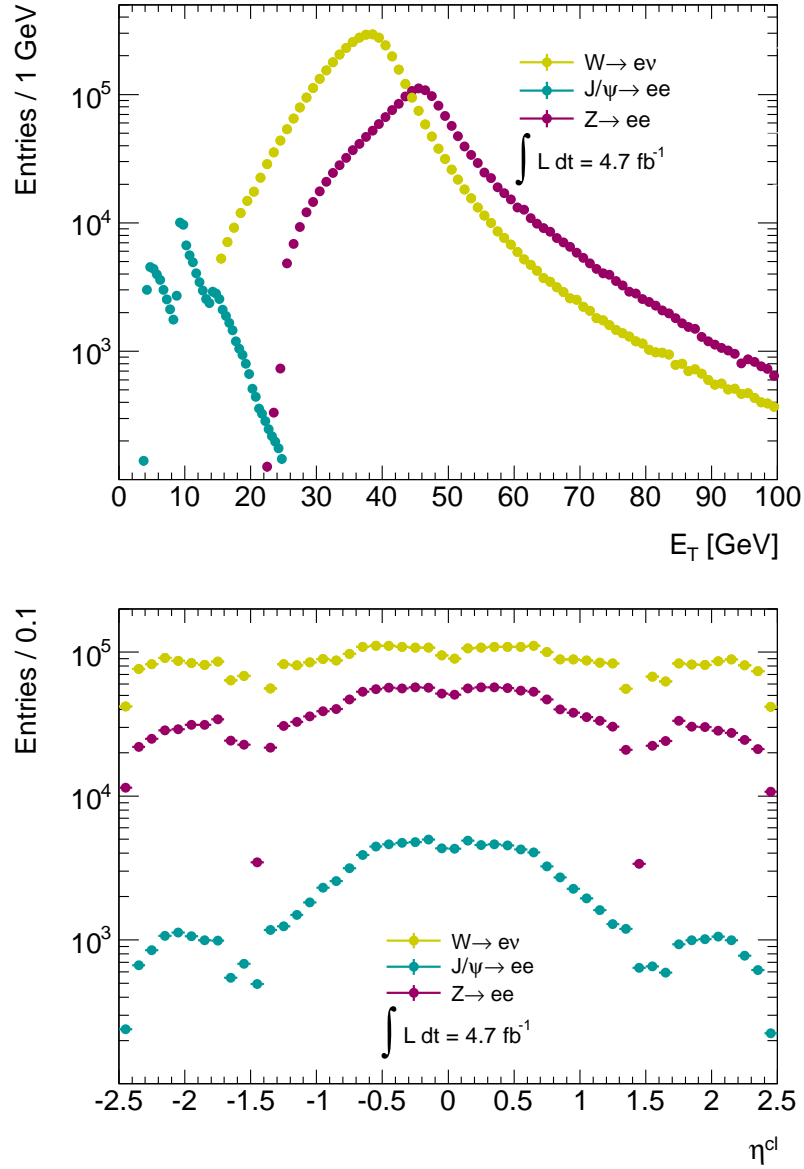


Figure 6.6: The distributions in transverse energy (top) and pseudo-rapidity (bottom) of the probes selected in the three different channels  $J/\psi$ ,  $W$  and  $Z$  on TightPP level. In order to increase the number of probes and avoid biases all possible tag-probe combinations are used in  $ZT\&P$ . The three peaks in  $J/\psi \rightarrow ee$  are caused by three different triggers with different pre-scales, used in  $J/\psi T\&P$ . The trigger thresholds are set to 4, 9 and 14 GeV. The  $J/\psi$  histograms have been provided by Ref. [42].

It is assumed that there is only background in the control region. The number of background events there is then identical to the number of data events and so is the statistical uncertainty

$$N_{\text{bkgR}} = N_{\text{dataR}} \quad (6.13)$$

$$\delta_{\text{bkgR}} = \delta_{\text{dataR}} = \sqrt{N_{\text{dataR}}}. \quad (6.14)$$

To determine the amount of background in the signal region together with its statistical uncertainty, the ratio of the number of events in signal and control region of the background template is introduced

$$\beta = \frac{N_{\text{templL}}}{N_{\text{templR}}} \quad (6.15)$$

$$\delta_{\beta} = \beta \sqrt{\left(\frac{\delta_{\text{templL}}}{N_{\text{templL}}}\right)^2 + \left(\frac{\delta_{\text{templR}}}{N_{\text{templR}}}\right)^2}. \quad (6.16)$$

Using explicit values for the statistical uncertainties from Eqs. 6.9-6.12, the number of background events in the signal region is

$$N_{\text{bgdL}} = \beta N_{\text{bgdR}} \quad (6.17)$$

$$\delta_{\text{bgdL}} = \sqrt{(\delta_{\beta} N_{\text{bgdR}})^2 + (\beta \delta_{\text{bgdR}})^2} \quad (6.18)$$

$$= \left[ \frac{N_{\text{templL}}}{1} \frac{N_{\text{dataR}}^2}{N_{\text{templR}}^2} \left( 1 + \frac{N_{\text{templL}}}{N_{\text{dataR}}} + \frac{N_{\text{templL}}}{N_{\text{templR}}} \right) \right]^{1/2} \quad (6.19)$$

The first term in brackets accounts for the uncertainty on the template in the signal region, the second for the uncertainty on the template in the control region and the last term for the uncertainty on the data in the control region. Any correlation between template and probes is neglected. Especially on reconstruction level, where the background template is a subset of the probes, the correlation is clearly non-negligible but it should be noted that after charge averaging and symmetrising the template in  $\eta$ , on average only one quarter of the selected template events is constructed out of the data it is normalised to. In general one would expect a positive correlation. Hence, Eq. 6.19 overestimates the uncertainty.

From  $N_{\text{dataL}}$  and  $N_{\text{bkgL}}$  the number of signal events is calculated

$$N_{\text{sig}} = N_{\text{dataL}} - N_{\text{bkgL}} \quad (6.20)$$

$$\delta_{\text{sig}} = \sqrt{(\delta_{\text{dataL}})^2 + (\delta_{\text{bkgL}})^2} \quad (6.21)$$

again neglecting the correlation between template and probes (this time in the signal region). Here the assumption is justified. Only a small fraction of data in the signal region is expected to be background.

### 6.7.2 Monte-Carlo

To account for differences between experimental conditions and simulation conditions event weights  $w_i$  are used on Monte-Carlo for every event  $i$ . The statistical uncertainty on the number of Monte-Carlo events  $N_{MC}$  therefore is

$$\delta_{MC} = \sqrt{\sum w_i^2} \quad (6.22)$$

### 6.7.3 Efficiency

In the simple case of a counting experiment the efficiency  $\varepsilon$  of a cut is given by

$$\varepsilon = \frac{N_P}{N_0} \quad (6.23)$$

where  $N_0$  is the number of total events and  $N_P$  is the number of events passing a certain cut. The statistical uncertainty of the efficiency derived there and used in this thesis is

$$(\delta_\varepsilon)^2 = \frac{\varepsilon(1-\varepsilon)}{N_0} \quad (6.24)$$

assuming a binomial distribution with the total number  $N_0$  and the probability  $\varepsilon$  of passing a cut. If  $N_0$  and  $N_P$  are the result of a background subtraction the assumption of a binomial problem is not justified. In Ref. [43] an alternative derivation of Eq. 6.24 is given using Poissonian errors. It is also shown how to obtain the statistical uncertainty if  $N_0$  and  $N_P$  are the result of a background subtraction. The statistical uncertainty of the efficiency then is

$$(\delta_\varepsilon)^2 = \frac{(1-2\varepsilon)\delta_P^2 + \varepsilon^2\delta_0^2}{N_0^2} \quad (6.25)$$

### 6.7.4 Treatment of Correlations and Calculation of Averages

The equation stated above neglects the correlation between the templates on probe and ID level. This is obviously wrong since the templates used are the same with just a different normalisation. Considering these correlations a term

$$+ 2 \frac{\varepsilon(1-\varepsilon)}{N_0^2} \cdot \text{cov}(N_{\text{bkg,P}}, N_{\text{bkg,0}} - N_{\text{bkg,P}}) \quad (6.26)$$

is added to Eq. 6.25. The derivation is given in Appendix B together with a directive on how to obtain the covariance. It should be noted that  $N_0$  and  $N_P$  are the number of signal events *after* background subtraction.  $N_{\text{bkg,0}}$  and  $N_{\text{bkg,P}}$  is the amount of background that is subtracted.

The effect on the efficiencies is found to be rather small. However, there is another correlation to be considered, i.e. the correlation between the background subtracted for positive and negative charge. Again, the same template is used. Since all efficiencies are averaged the correlations have to be taken into account. The equation used to derive the full statistical uncertainty is explicitly given in Appendix B.

## 6.8 Systematic Uncertainties

The systematic uncertainties on the efficiency measurements are mainly assumed to originate from the background subtraction technique. The main effort of estimating the systematic uncertainties is therefore put into this. Since one of the main objectives of the measurement is the preparation of scale-factors to correct the efficiencies simulated on Monte-Carlo, a number of systematic uncertainties are estimated to account for mismodelling of variables in Monte-Carlo that are specific for  $W$  events. Here just a brief overview on the extra systematic uncertainties is given. Details on their size and derivation are given in Chapter 8.

### 6.8.1 Systematic Variations

The main difficulty in estimating the systematic uncertainty is to give a directive that is valid for all three identification levels in each of the 77, 126 or 350  $\eta \times E_T$  bins, depending on the  $\eta$  granularity. To estimate the systematic uncertainties of the measurement in data the parameters of the background subtraction are varied. Some of these variations have already been mentioned in the preceding sections and are summarised again here. The varied parameters are:

- variation of the kinematic selection: considered as a variation of the signal-over-background ratio and the  $\eta$ ,  $E_T$  distributions – four different sets of  $E_T^{\text{miss}}$ ,  $M_T$  cuts are used:  
 $(E_T^{\text{miss}}, M_T) = (30,45), (40,40), (30,50), (35,50)$ ;
- variation of the isolation threshold, i.e. the threshold between signal and control region in the background subtraction: five thresholds from 0.30 to 0.50 in steps of 0.05 are used;
- variation of the discriminating variable: calorimeter isolation in cones of 0.3 and 0.4 are used, divided by the electron transverse energy for  $E_T < 40$  GeV and divided by 25 GeV for  $E_T > 40$  GeV;
- variation of the background template: two different background templates, reverting either two or three of the electron ID cuts.

All possible combinations of these variations give the 80 measurements mentioned before.

The estimation of the systematic uncertainties is closely related to the determination of the central value of the efficiencies in each bin. Rather than having a default configuration the efficiencies are calculated as the arithmetic mean of a total of 80 variations for each individual  $\eta \times E_T$  bin, with the statistical uncertainty taken as the arithmetic mean of all statistical uncertainties and the systematic uncertainty taken as the RMS of all 80 variations.

On Monte-Carlo the efficiency calculation follows the method on data. No background needs to be subtracted, but still the Monte-Carlo efficiencies are obtained as the central

value of 40 variations – naturally the variation of the background template has no application on Monte-Carlo. Instead of the variation of the isolation threshold a simple cut is applied on the two isolation variables  $E_T^{\text{cone}}(0.3)/E_T$  and  $E_T^{\text{cone}}(0.4)/E_T$ . With the variations of the kinematic selection these are then 40 variations.

The scale-factors are obtained by dividing the results of individual, matching efficiency measurements in data and Monte-Carlo by one another. The central values are obtained analogously to the procedure explained for data and Monte-Carlo efficiencies from the 80 individual scale-factors. With this procedure the central value of the scale-factor does not necessarily agree with the ratio of the central values of data and Monte-Carlo efficiency. This is unproblematic and the effect was found to be much smaller than the uncertainty, anyway.

With the approach just given, any study to be done on the measurement is rather extensive since it always has to involve a number of variations. For the purpose of illustration, all plots in this thesis showing kinematic distributions were done for one specific set of parameters, i.e. the working point  $(E_T^{\text{miss}}, M_T) = (30, 50)$ , isolation threshold at 0.40,  $E_T^{\text{cone}}(0.3)/E_T$  as a discriminating variable and the template with  $w_{\text{tot}}$  and  $f_{\text{HT}}$  reverted. A full set of data efficiencies in fine  $\eta$  granularity involves 224 000 of the background subtraction plots as shown in Fig. 6.1.

### 6.8.2 Other Systematic Uncertainties Added

Pile-up and generator effects are discussed and accounted for in Section 8.3. The charge dependence of the efficiencies is further explained and investigated in Section 8.4.

The requirements applied to obtain a clean sample of electrons from  $W \rightarrow e\nu$  decays are listed and described in detail in the following. A number of corrections has to be applied on the Monte-Carlo samples in order to match the simulation to the conditions in data.

## 7.1 Data Samples

The data analysed in this thesis were recorded between April and October 2011. The data-set is subdivided into periods D-M. Data within one period were recorded with a consistent configuration of the ATLAS detector system, the trigger and LHC machine parameters. The total data set corresponds to an integrated luminosity of  $L_{\text{int}} = 4.7 \text{ fb}^{-1}$  after detector quality requirements.

## 7.2 Monte-Carlo Samples

One of the major purposes of the performance measurements is the correction of mis-modelling in Monte-Carlo. In order to derive scale-factors and to investigate systematic effects, three Monte-Carlo samples are available, each with 40 million generated events. They differ in the generator used and some specific simulation conditions. One sample was generated using POWHEG, with the parton shower and the minimum-bias events being modelled with PYTHIA6. It is referred to as POWHEG in the following. The other two samples were generated using PYTHIA6. They differ in the modelling of the minimum-bias events that were modelled with PYTHIA6 in one case and PYTHIA8 in the other. The generation of the hard interaction is identical for both. In the following these two samples are referred to as PYTHIA6 and PYTHIA8, although the name corresponds to the generator of the minimum-bias events only.

The most important difference in the simulation conditions is the width of the distribution of the vertex position of the hard interaction. This is explained in detail in Section 7.4.2.

All three samples were generated as four independent “Monte-Carlo runs”, each with simulation conditions corresponding to LHC machine parameters and ATLAS detector status in a certain data-taking period. These simulation conditions are LHC luminosity, pile-up and detector defects like LAr calorimeter read-out problems, tile and pixel data-taking conditions. The different Monte-Carlo runs and their corresponding data periods

	data 2011		POWHEG Monte-Carlo	
Preselection: processed	385456027		39991926	
Preselection: GRL	355593081	92%	–	–
Preselection: Vertex	355441351	100%	39979767	100%
Preselection: Trigger	22923695	6%	–	–
Preselection: LAr	22845663	100%	39979767	100%
Preselection: MET cleaning	21873961	96%	35630685	89%
Electron selection: Author	20108530	92%	28809669	81%
Electron selection: Eta	20084181	100%	28462944	99%
Electron selection: Otx	20022506	100%	28319565	99%
Electron selection: Pt	19060716	95%	23026079	81%
Electron selection: TQ+pass Rhad	9406334	49%	21400412	93%
$W$ selection: Veto 2nd ele	9394372	100%	21388604	100%
$W$ selection: $E_T^{\text{miss}} > 25$ GeV	8214064	87%	16500533	77%
$W$ selection: $M_T > 40$ GeV	8065506	98%	16139073	98%
$W$ selection: All	6768763	84%	13990292	87%
→ e+	3945900	58%	8246894	59%
→ e-	2822863	42%	5743398	41%

Table 7.1: Number of events after the application of different selection criteria for data and POWHEG Monte-Carlo. For Monte-Carlo the number of generated events is shown with pile-up weights applied. Further, no trigger selection has been applied on Monte-Carlo.

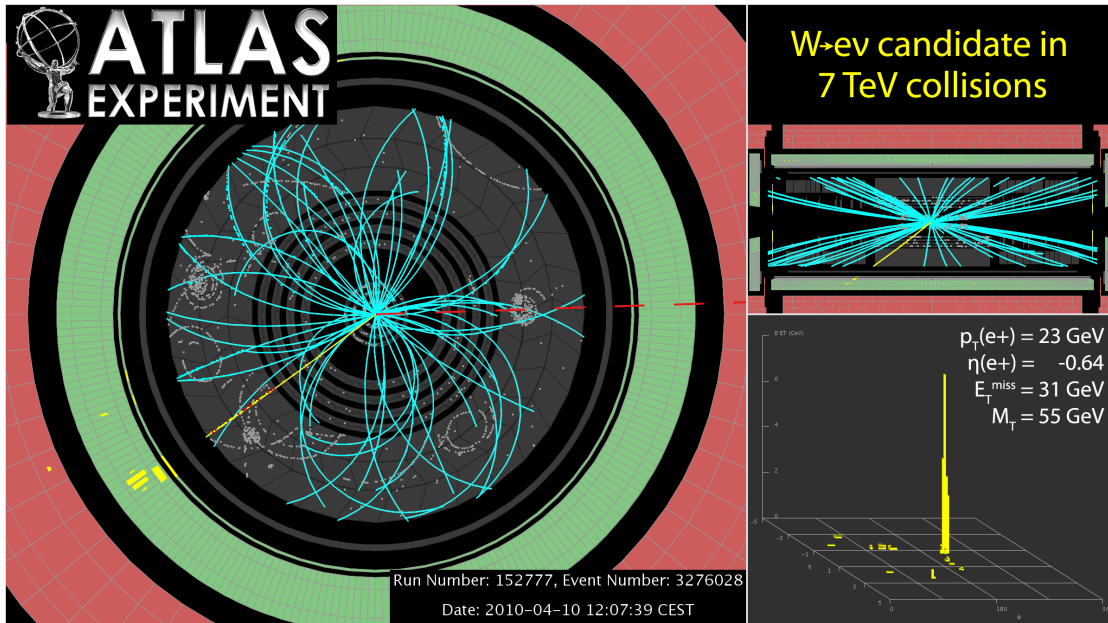


Figure 7.1: Event display of a  $W \rightarrow e\nu$  candidate event. Indicated are the electron candidate (yellow), the missing transverse energy from the neutrino (dashed red) and other tracks from hadrons (cyan).

can be found in Table 7.2. A detailed list of the configurations and the fractions of generated events of the four runs is given in Ref. [44].

The overall normalisation of the Monte-Carlo samples is irrelevant for the analysis. The POWHEG sample comes split into a sample of  $W^+$  and a sample of  $W^-$  events. They are normalised according to the theoretical next-to-next-to-leading order cross sections, as calculated in Ref. [12], of 6.16 nb and 4.30 nb, respectively.

## 7.3 Event Selection

This section lists the requirements used to select a  $W \rightarrow e\nu$  candidate event. They are adopted from the  $W \rightarrow e\nu$  Standard Model analysis in Ref. [26] and modified according to the needs of the tag-and-probe analysis. The number of selected events at each step is listed in Table 7.1. The terms used are explained below. A visualisation of a  $W \rightarrow e\nu$  candidate event recorded in early data from 2010 is given in Fig. 7.1.

### 7.3.1 Preselection

The preselection event cuts are mainly concerned with the detector status and the quality of an event as a whole.

trigger name	first Run	corresponding data period	pre-scale
EF_xs60_noMu_L1EM10XS45	179710	D-F	0.88
EF_e13_etcut_xs60_noMu	182726	G-H	1.00
EF_e13_etcut_xs60_noMu_dphi2j10xe07	185353	I-L4	0.91
EF_e13_etcutTrk_xs60_noMu_dphi2j10xe07	189639	L5-M	1.00

trigger name	MC run	corresponding data period	weight
EF_xs60_noMu_L1EM10XS45	180164	D	0.88
EF_xs60_noMu_L1EM10XS45	183003	E-H	0.17
EF_e13_etcut_xs60_noMu	183003	E-H	0.81
EF_e13_etcut_xs60_noMu	186169	I-K	0.87
EF_e13_etcutTrk_xs60_noMu_dphi2j10xe07	189751	L-M	0.99

Table 7.2: Overview of the triggers used in data with their pre-scale (top) and the triggers used in the different Monte-Carlo runs with the weights assigned as described in Section 7.4.4 (bottom). All triggers are pre-scaled. The entries with 1.00 are due to rounding when the pre-scale is very small.

### GRL and Vertex

It is required that all detector sub-systems needed in the analysis are working nominally. Events are further required to have at least one reconstructed vertex with more than two associated tracks with  $p_T > 400$  MeV.

### Trigger

Dedicated tag-and-probe triggers are used to record the data for the efficiency measurement. Triggers have to be chosen such, that they do not affect the probe electron and at the same time keep the trigger rate low by selecting  $W \rightarrow e\nu$  events with a high purity. This eliminates the single-electron triggers used in other  $W$  and  $Z$  analyses with electron final states. These triggers apply electron identification cuts on event filter level and clearly cannot be used here.  $ZT\&P$  in contrast can use single-electron triggers, as long as it is the tag electron that set the trigger.

In line with the tag-and-probe philosophy, the missing transverse energy is used to select events of interest. Throughout data-taking four different  $E_T^{\text{miss}}$  significance triggers were used. They are listed in Table 7.2. In order to reduce the event rate to prevent automatic pre-scaling the  $E_T^{\text{miss}}$  significance is combined with a low  $E_T$  EM cluster trigger element with  $E_T > 10$  GeV and  $E_T > 13$  GeV in periods D-F and G-M respectively. Additional selection criteria on trigger level include a number of hits on a matched track from period G on. From period I on a cut on the azimuthal separation of the missing transverse energy from the two leading jets,  $\Delta\phi(E_T^{\text{miss}}, 2\text{jets}) > 0.7$ , is applied. The latter cut is also applied offline and further discussed in Section 7.3.3. Note that the two

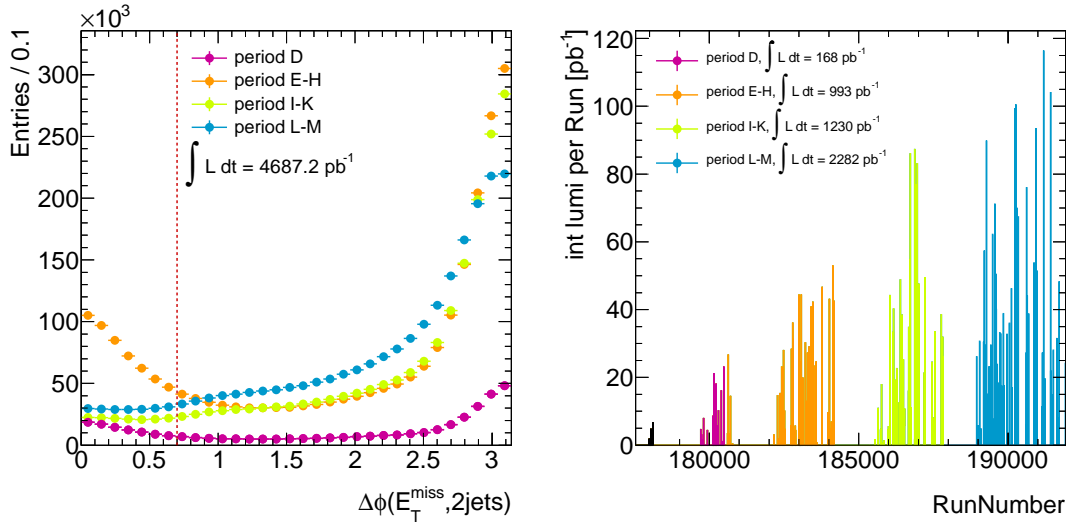


Figure 7.2: Number of selected probes in different data taking periods as a function of  $\Delta\phi(E_T^{\text{miss}}, 2\text{jets})$  (left). The selection on  $\Delta\phi(E_T^{\text{miss}}, 2\text{jets}) > 0.7$  is the major difference between the triggers. The integrated luminosity as a function of the run number (right) is shown in different colours.

triggers in periods I-M are identical. The track cut indicated by the name `etcutTrk` has also been applied before.

With an increasing number of interactions in one bunch-crossing the total transverse energy  $\sum E_T$  increases. Therefore, a smaller and smaller fraction of  $W \rightarrow e\nu$  events is triggered by the  $E_T^{\text{miss}}$  significance triggers. This is shown in Fig. 7.2. Since the triggers differ mainly in the cut on  $\Delta\phi(E_T^{\text{miss}}, 2\text{jets})$  the number of selected events above the cut value have to be compared. While almost half of the integrated luminosity has been recorded in periods L and M the number of selected probes in the periods is much smaller. This behaviour is further discussed in Section 8.1. No offline cut on  $E_T^{\text{miss}}$  significance or a similar quantity is applied.

### $E_T^{\text{miss}}$ cleaning and LAr quality cuts

In order to ensure, that the  $E_T^{\text{miss}}$  in the selected events is caused by real missing transverse energy, cleaning cuts are applied that remove events with jets that are most likely due to coherent noise in the electromagnetic calorimeters, noise bursts in the hadronic end-cap calorimeter and non-collision backgrounds or cosmic rays. The jets considered for this procedure are reconstructed from topological clusters with the anti- $k_T$  algorithm. Trips in the high voltage power supply and frequent noise bursts affect a large number of channels in the same detector partition. An additional cut, the so-called LAr quality flag, removes events with severe noise bursts in the electromagnetic calorimeters, independent of the jet reconstruction.

### 7.3.2 Electron Selection

In a given event, the electron with the highest  $E_T$ , satisfying a set of requirements, is chosen as the probe electron on which the identification cuts are to be tested. An object in the detector is considered an electron candidate if it fulfils the following four selection criteria.

#### Author

Only electrons that have been reconstructed by two of the standard algorithms are considered, i.e. either the cluster-based or the combined cluster and track-based algorithm, see Section 5.3.

#### Eta

The efficiency measurement is only concerned with electrons that are in the acceptance region of the inner detector of  $\eta < 2.47$ .

#### Object quality

A nominal operation of the electromagnetic calorimeter is particularly important for the reconstruction of electrons. A malfunctioning crate controller caused defects in some of the readout electronics. Electrons which are reconstructed in the vicinity of temporarily non-functional regions of the calorimeters due to damaged read-out electronics are removed.

#### Transverse energy

The kinematic range of the electrons covered by the *WT&P* measurement reaches down to  $E_T > 15$  GeV. Electrons with smaller transverse energy are discarded. The transverse energy receives an additional correction: depending on the number of hits in the silicon trackers the energy is recalculated to

$$E_T = \frac{E^{\text{cl}}}{\cosh \eta^{\text{trk}}}. \quad (7.1)$$

The motivation for this correction is the better spacial resolution of the inner detector compared to the calorimeter. The transverse energy is afterwards corrected with the latest results from calibration measurements.

#### Identification cuts

Since the measurement of the efficiency of the identification is the purpose of this analysis no identification requirements can be applied on electrons in the preselection. Given the difficulty of the background subtraction in *WT&P*, two loose identification cuts were moved to the reconstruction efficiency measurement and are included in the probe definition of *all* identification measurements. Electrons are required to pass the loose

track quality criteria, i.e. that the number of hits in the pixel layer and the combined number of hits in pixel layer and SCT exceed one and seven, respectively. Outlier hits are taken into account in this calculation. Furthermore, electrons are required to pass the cut on hadronic leakage.

### 7.3.3 $W$ Selection

Considering only events where at least one electron was reconstructed, further cuts are applied in order to separate the  $W \rightarrow e\nu$  signal from background events. In order to suppress events from  $Z \rightarrow ee$ ,  $t\bar{t}$  or di-boson processes, an event is rejected from the selection if it has two or more MediumPP electrons.

#### Kinematic selection on $E_T^{\text{miss}}$ and $W$ $M_T$

A selection on the missing transverse energy  $E_T^{\text{miss}}$ , originating from the neutrino, and the transverse mass of the  $W$  candidate  $M_T$  is applied. The transverse mass is calculated from  $E_T^{\text{miss}}$  and the selected electron  $E_T$ :

$$M_T = \sqrt{2E_T E_T^{\text{miss}} (1 - \cos \Delta\phi)} \quad (7.2)$$

with the azimuthal separation between the electron and the missing transverse energy  $\Delta\phi$ . In the preselection the missing transverse energy is required to be  $E_T^{\text{miss}} > 25$  GeV, the transverse mass is required to be  $M_T > 40$  GeV. For the final probe selection a set of cuts is used in order to measure the efficiency with different signal-over-background ratios. These are  $(E_T^{\text{miss}}, M_T) = (30, 45)$ ,  $(40, 40)$ ,  $(30, 50)$  and  $(35, 50)$ .

#### Isolation from jets

As mentioned in Section 5.8 an object whose energy is mismeasured causes missing transverse energy in the detector. The energy measurement is inherently difficult for jets. To suppress fake  $E_T^{\text{miss}}$ , induced by fluctuations in the energy measurement of jets, the missing transverse energy is required to be isolated in azimuthal direction by  $\Delta\phi(E_T^{\text{miss}}, 2\text{jets}) > 0.7$ , where only the two jets with the highest  $p_T$  above 10 GeV are considered.

Similarly, the selected electron candidate is required to be isolated from jets in a cone of  $\Delta R < 0.4$ . This is meant to suppress electrons, that are part of a jet and e.g. originate from a heavy flavour decay and fake electrons from hadrons. Here jets above  $p_T > 25$  GeV are considered.

## 7.4 Monte-Carlo Specific Corrections and Selection

Usually, Monte-Carlo samples are produced during data-taking. Assumptions about future pile-up conditions or beam-spot dimensions have to be made. To obtain the right composition of the four Monte-Carlo runs the amount of data to be recorded had to be

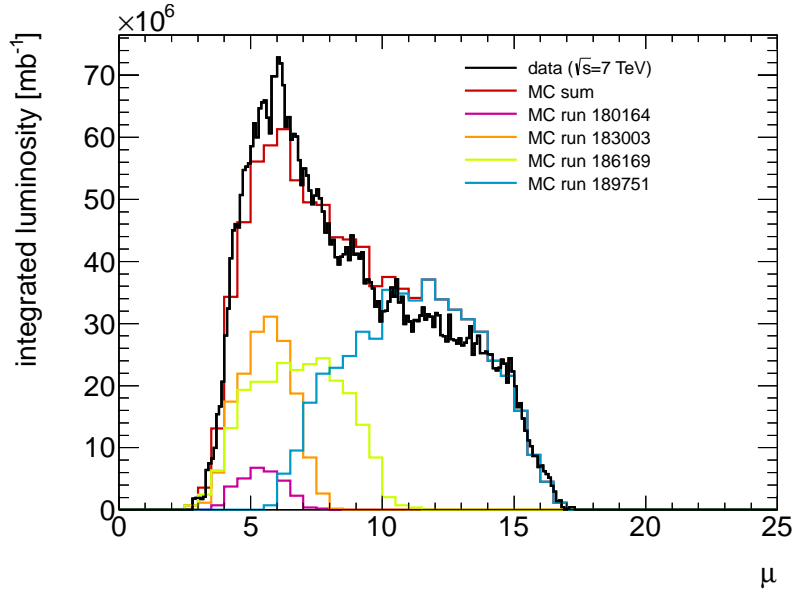


Figure 7.3: Distributions of the average interactions per bunch-crossing  $\mu$  in data and the four individual Monte-Carlo runs. For the re-weighting procedure the distribution in data is split up corresponding to the Monte-Carlo runs.

estimated, too. A set of corrections is applied on the Monte-Carlo samples, to account for differences in the expectations of machine parameters and simulation conditions or the mismodelling of parameters. Furthermore, the trigger selection has to be adapted to the special conditions in Monte-Carlo.

#### 7.4.1 Pile-up re-weighting

For each Monte-Carlo run, the simulated distributions of the interactions per bunch-crossing  $\mu$  is re-weighted to the distribution observed in the corresponding data period. Included in these weights is the re-weighting of the single Monte-Carlo runs to each other according to the total integrated luminosity delivered by the LHC in the corresponding data periods. The distributions that are used for the re-weighting procedure are shown in Fig. 7.3.

Another quantity related to pile-up is the number of reconstructed vertices  $nV_{xp}$ . For Monte-Carlo samples that were overlaid with pile-up simulation from PYTHIA8 a known issue is that the distribution of  $nV_{xp}$  does not agree well between data and Monte-Carlo when  $\mu$ -reweighting is applied. Because of that, the  $\mu$ -distribution of data was shifted w.r.t Monte-Carlo for the re-weighting procedure.

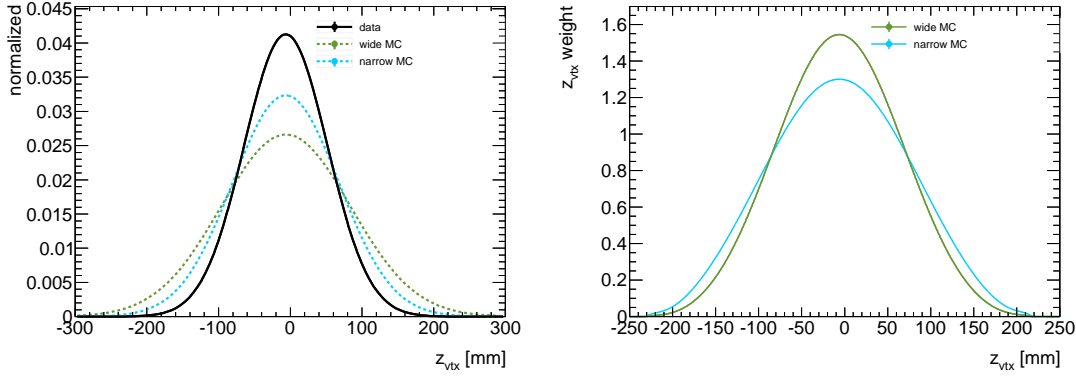


Figure 7.4: Results of the fits of the  $z_{vtx}$  distribution to data and Monte-Carlo samples with wide and narrow  $z_{vtx}$  distribution (left), weights obtained from these fits (right) for re-weighting Monte-Carlo to data.

### 7.4.2 Vertex Position Re-weighting

The position of the beam-spot follows a Gaussian distribution in  $x$ -,  $y$ - and  $z$ -direction. This is simulated on Monte-Carlo, but the precise position and the width of this distribution differs from the one observed in data. In addition, there are two different simulation conditions realised on Monte-Carlo. There are samples with a wide (90 mm) and a narrow (74 mm)  $z_{vtx}$  distribution available, both wider than the width measured in data (58 mm). The results of a fit to these distributions is shown in Fig. 7.4. The mean vertex position in  $z$ -direction is -6.3 mm in data, -6.2 mm in the sample with the wide and -6.4 mm in the samples with the narrow  $z_{vtx}$  distribution.

The effect on electron efficiencies is studied in Section 8.2. A re-weighting is applied to correct for this effect and make the efficiencies independent of the  $z_{vtx}$  distribution.

### 7.4.3 Truth Matching

The simulation of  $W$  production includes the production of additional, associated jets resulting from higher order QCD corrections, bremsstrahlung processes, pile-up jets and the decay of the  $W$  boson into the electron and the neutrino. Especially on reconstruction level, non-isolated electrons in jets represent a significant background and should not be considered for the efficiency measurement since in data they are removed in the background subtraction. By using generator level information of the process, only electrons originating from a  $W$  boson are considered. Photon conversions are also included in the measurement if they originate from a  $W$  decay electron. Since the effects of QED final state radiation are also included in the factorisation introduced in Section 6.2.

#### 7.4.4 Trigger Selection

The trigger selection that is applied on data cannot be applied on Monte-Carlo in exactly the same way. Firstly, the data-taking periods covered by the triggers do not correspond to the four Monte-Carlo runs, secondly all triggers have a pre-scale that is changing over time – the pre-scales are not simulated on Monte-Carlo. Thirdly, not all triggers used are simulated on Monte-Carlo. Rather than emulating these triggers they are substituted by other, very similar ones. This affects mainly Monte-Carlo run 186169 where the trigger EF\_e13\_etcut\_xs60\_noMu\_dphi2j10xe07 has to be replaced by its predecessor without the  $\Delta\phi(E_T^{\text{miss}}, 2\text{jets})$  cut. Apart from a possible effect on event-filter level this is unproblematic since the cut is applied offline.

To account for the pre-scales and the mismatch of trigger and Monte-Carlo periods a method of applying weights has been developed. For each Monte-Carlo run a weight of the delivered luminosity, divided by the total luminosity in the corresponding data period, is assigned to the different triggers. These weights are then the inverse (luminosity weighted) pre-scale in case there is only one trigger in a Monte-Carlo run. In case of overlapping triggers (run 183003) the weights correspond to the luminosity fraction covered by the different trigger (times inverse pre-scale). The weight assigned to a given event is the sum of trigger weights of the triggers the event passed. The big advantage of this method is that it keeps a maximum of statistical precision compared to competing methods described in Ref. [45]. The triggers used in data and Monte-Carlo are listed in Table 7.2.

#### 7.4.5 Energy Smearing

The fluctuations of the energy measurement in the calorimeters are smaller in the simulated Monte-Carlo sample than in data. Therefore, the electron energy in the Monte-Carlo samples is smeared using random numbers from a Gaussian distribution. The width of the Gaussian is determined from a sample of  $Z$  events, such that the width of the  $Z$  resonance in data is reproduced by Monte-Carlo.

### 7.5 Agreement between Data and Monte-Carlo

A number of kinematic distributions for the selected events are shown in Figs. 7.6, 7.5 and 7.7 after TightPP selection. Only the events selected in data and POWHEG Monte-Carlo are shown, since there is no large di-jet Monte-Carlo sample for the background description available. Background processes in data are of the order of 5%. Distortions in the shape of data are therefore expected.

The total transverse energy deposited in the detector  $\sum E_T$  is shown in Fig. 7.6. Compared to the distribution in data, the distribution on Monte-Carlo is slightly shifted towards lower values. This affects the trigger decision. It was found that the Monte-Carlo prediction yields  $\sim 10 - 15\%$  more events than there are in data. Therefore, all three figures show the Monte-Carlo prediction normalised to the number of events in data. The overestimation of the selected events by the Monte-Carlo prediction is only

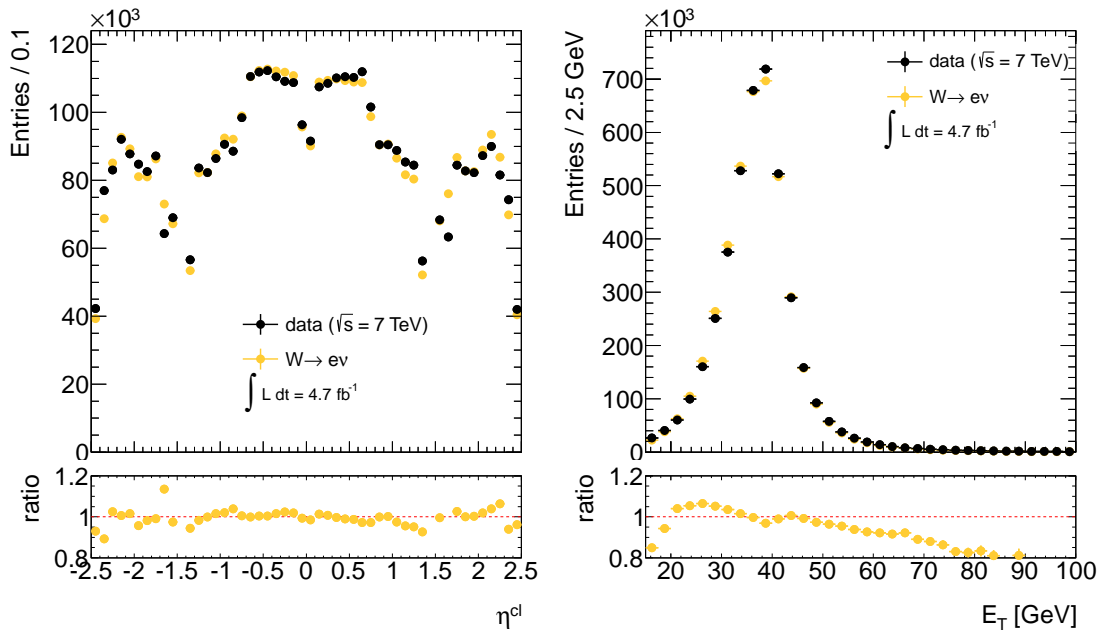


Figure 7.5: Distributions of the pseudo-rapidity  $\eta$  and the transverse energy  $E_T$  of the selected electrons for POWHEG Monte-Carlo on TightPP level. Events were selected with  $E_T^{\text{miss}} > 30$  GeV and  $M_T > 50$  GeV. The Monte-Carlo prediction is normalised to the number of data events.

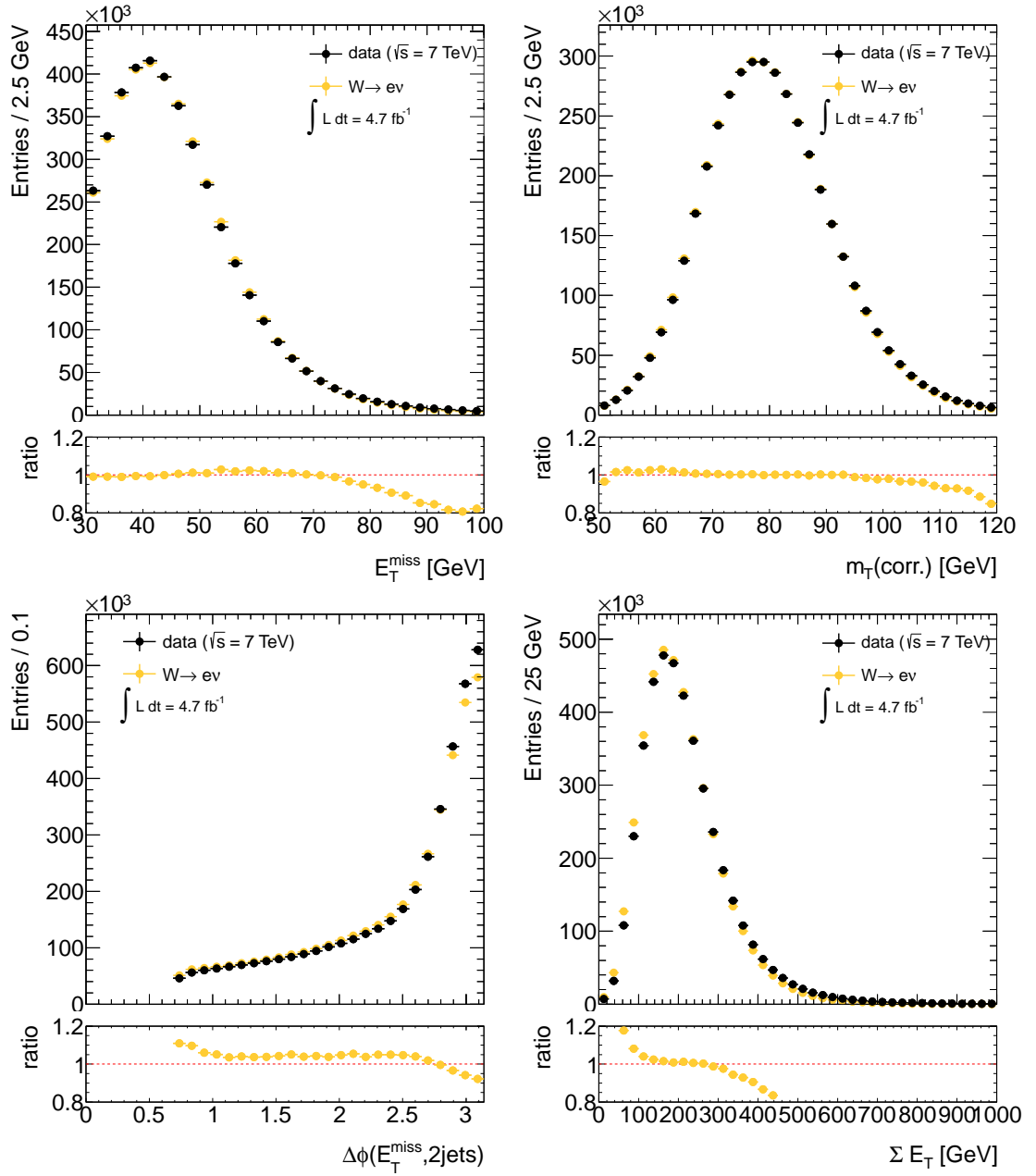


Figure 7.6: Distributions of the missing transverse energy  $E_T^{\text{miss}}$  (top left), the  $W$  transverse mass (top right), the isolation of the  $E_T^{\text{miss}}$  from the two leading jets  $\Delta\phi(E_T^{\text{miss}}, 2\text{jets})$  (lower left) and the sum of transverse energy deposited in the detector (lower right) for data and POWHEG Monte-Carlo on TightPP level. Events were selected with  $E_T^{\text{miss}} > 30$  GeV and  $M_T > 50$  GeV. The Monte-Carlo prediction is normalised to the number of data events.

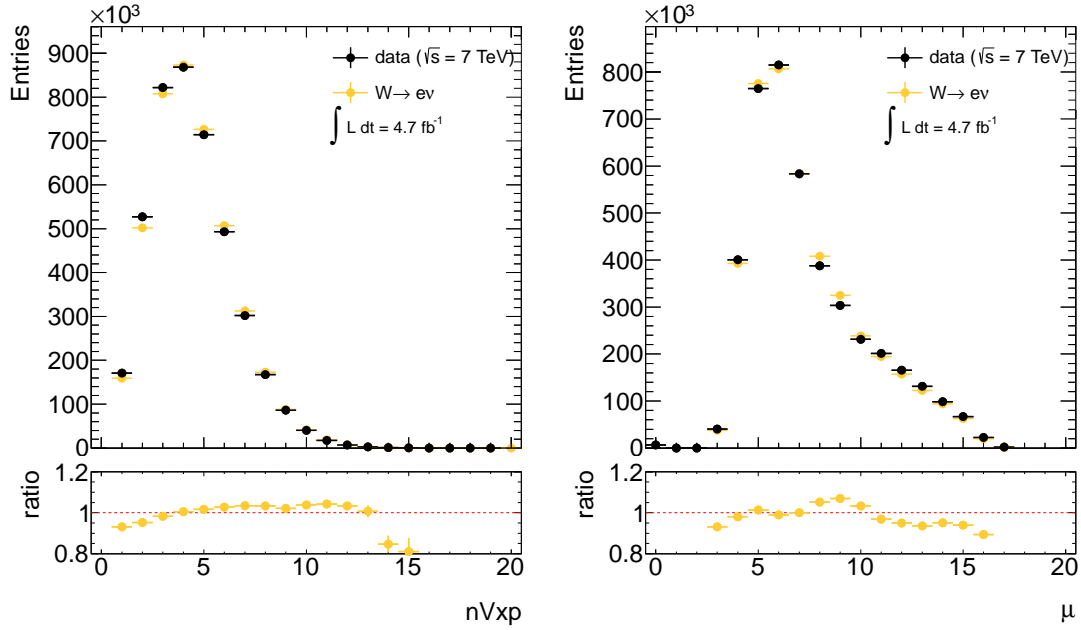


Figure 7.7: The pile-up related distributions of the number of primary vertices in an event  $nV_{xp}$  (left) and the average interactions per bunch-crossing  $\mu$  (right) for data and POWHEG Monte-Carlo on TightPP level. Events were selected with  $E_T^{\text{miss}} > 30$  GeV and  $M_T > 50$  GeV. The Monte-Carlo prediction is normalised to the number of data events.

a minor flaw. When calculating efficiencies the overall normalisation in the numerator and the denominator cancel.

The variables that were used for the event selection,  $E_T^{\text{miss}}$ ,  $M_T$  and  $\Delta\phi(E_T^{\text{miss}}, 2\text{jets})$  are shown, too. The agreement of the shape of the distributions is very good. This is seen in the lower parts in the single sub-figures where the ratio of data to the Monte-Carlo prediction is shown. The variables of the differential measurement  $\eta$  and  $E_T$  are shown in Fig. 7.5. The disagreement is much worse. Any disagreement in  $\eta$  or  $E_T$  is not too relevant to this analysis, since the measurement is performed in bins of these variables.

This chapter describes studies on systematic effects on the electron identification efficiencies or their measurement. They are mostly concerned with the modelling on Monte-Carlo samples. Since the results of the measurement are provided to physics analyses through scale-factors, it is as important to measure the efficiency on Monte-Carlo accurately as it is to measure it on data. Biases that stem from choosing one Monte-Carlo sample over another one in the calculation of the scale-factors need to be understood and accounted for.

### 8.1 Studies on $E_T^{\text{miss}}$ Significance Triggers

All triggers used in the analysis are  $E_T^{\text{miss}}$  significance triggers. This section studies their behaviour and their description in Monte-Carlo. The two input parameters  $E_T^{\text{miss}}$  and  $\sum E_T$  are known to be difficult to model in the simulation. They are known to have a large impact on the pile-up related variables  $nV_{\text{xp}}$  and  $\mu$ . Since there is no unrescaled pure  $E_T^{\text{miss}}$  significance (XS) trigger available over a longer time period the trigger decision was emulated using the trigger level information stored offline for all three trigger levels.

The events used for this study have been selected using a tag-and-probe method, as well. Here, however, the electron is used as a tag whereas the cut of interest – the trigger decision – is emulated using the total and the missing transverse energy reconstructed in the specific event on trigger level. Events are selected using the single-electron triggers EF\_e20\_medium, EF\_e22\_medium and EF\_e22vh\_medium1 that are described in Section 5.5. Electrons are required to have a transverse energy  $E_T > 20$  GeV and to be reconstructed in the acceptance region of the tracking system  $|\eta| < 2.47$ . In combination with the missing transverse energy, a cut on the transverse mass window of the  $W$  boson of  $40 < M_T < 80$  GeV is applied. No background subtraction is applied.

The trigger turn-on curve for data and Monte-Carlo plotted against the significance calculated offline is shown Fig. 8.1. From this plot it is obvious that the trigger is highly inefficient. For an offline  $E_T^{\text{miss}}$  significance that corresponds to the event-filter level cut only approx. 50% of the events pass. The plateau, which is below 100%, is reached only at values much higher than the cut value. The reasons for this inefficiency become clear when comparing the missing and total transverse energy,  $E_T^{\text{miss}}$ , on event filter level and offline in Fig. 8.2. Whereas the missing transverse energy seems to be reconstructed quite well on trigger level, the sum of the energy,  $\sum E_T$ , deposited in the detector is much lower online, dramatically reducing the significance. The event filter does not use the full detector information, in particular it does not use the information from the muon

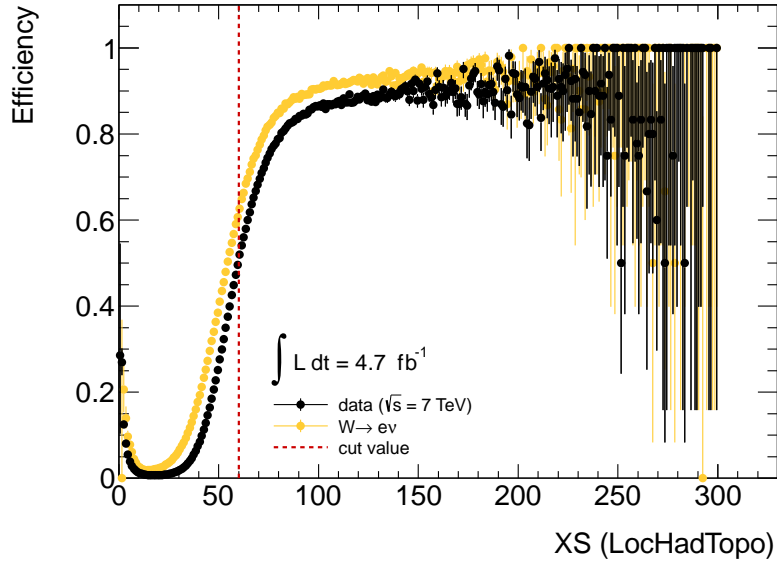


Figure 8.1: Trigger efficiency plotted against the  $E_T^{\text{miss}}$  significance (XS) for a EF\_xs60\_noMu trigger. The trigger decision has been emulated. Bayesian error propagation has been used. The red line shows the cut value applied on trigger level.

spectrometer. To some extent this is accounted for in the choice of the parameters  $a$  and  $b$  in Eq. 5.6. It does, however, not restore the energy of muons, escaping the inner detector and the calorimeters.

The shift of the turn-on curve in Monte-Carlo w.r.t. data can be explained when looking at the  $\sum E_T$  distributions in Fig. 7.6. With a shift in  $\sum E_T$  to lower values an event is more likely to get triggered on Monte-Carlo. This is the main reason why the Monte-Carlo prediction yields a higher number of events of about 10 – 15%, as already mentioned in Section 7.5. But, for the efficiency calculation the absolute normalisation of Monte-Carlo cancels in the numerator and denominator. Also, the identification efficiency does not depend on the  $E_T^{\text{miss}}$  significance itself, thus the mismodelling is not accounted for with a systematic uncertainty.

The method described above can easily be extended to an efficiency measurement of  $E_T^{\text{miss}}$  significance triggers similar to the identification measurement presented in this thesis. This way, one could provide scale-factors that could benefit the electron identification efficiency measurement.

## 8.2 Impact of the Vertex Position

The Monte-Carlo samples are generated with a specific beam-spot. The position is assumed to be distributed Gaussian with a specific width. The beam-spot position is reflected in the position of the primary vertex of the hard interaction in  $z$  direction  $z_{\text{vtx}}$ .

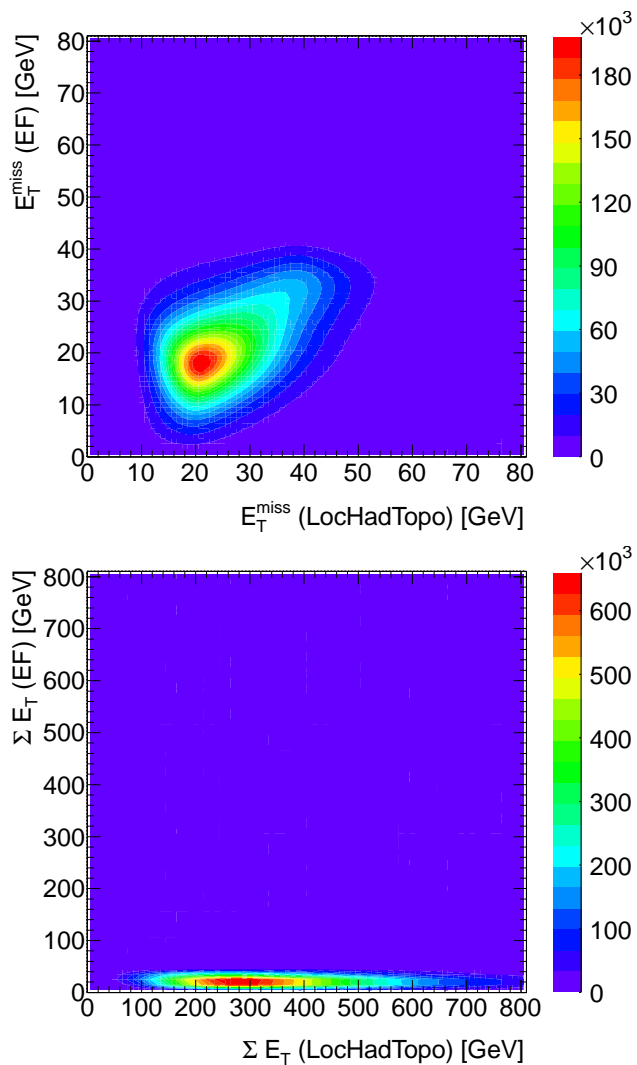


Figure 8.2: Missing transverse energy (top) and total transverse energy in the detector (bottom) as measured offline versus the values measured at event-filter level (EF).

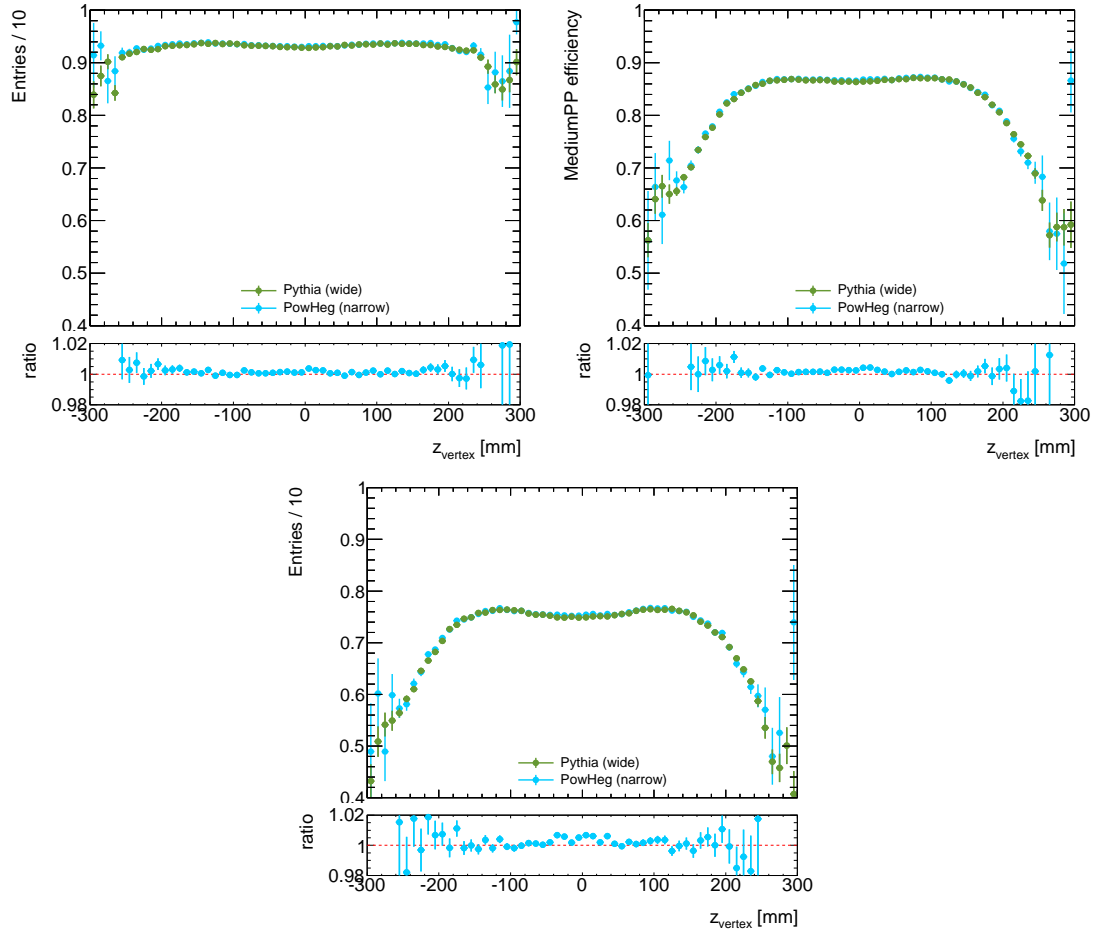


Figure 8.3: Electron ID efficiency as a function of  $z_{\text{vtx}}$  for LoosePP (upper left), MediumPP (upper right) and TightPP (bottom).

For the simulation at ATLAS two different distributions of the vertex position are used, see Fig. 7.4. For both configurations the position of the beam-spot differs only little from the one measured in data. The width of its distribution, however, is very different. As already mentioned in Section 7.4.2 there are Monte-Carlo samples with a wide and a narrow beam-spot distribution. With the coexistence of two different simulation conditions the impact on the electron identification needs to be checked.

### 8.2.1 Efficiencies as a Function of the $z_{\text{vtx}}$ Position

The provided scale-factors should be universal for all samples. With the PYTHIA and POWHEG samples used throughout this analysis, samples with a narrow (POWHEG) and a wide (PYTHIA) beam spot are available. The wide sample is better suited to investigate the effect of re-weighting to data and is used in this section. A clear dependence

of the identification efficiency as a function of the vertex position  $z_{\text{vtx}}$  is seen in Fig. 8.3 for all identification criteria. The dependence as a function of  $z_{\text{vtx}}$  is small for LoosePP and much larger for MediumPP and TightPP. Consequently, re-weighting the  $z_{\text{vtx}}$  distribution changes the efficiency obtained in Monte-Carlo as well as the scale-factors.

As can be seen in the lower part of each sub-figure the difference between both generators is well below 1%. However, the measured efficiencies over the full  $z_{\text{vtx}}$  range differ by up to 2% for MediumPP efficiencies in the central barrel  $|\eta| < 0.5$  and the end-cap region  $|\eta| > 2.0$ . This is because the  $z_{\text{vtx}}$  width is different in the two generators. Re-weighting the  $z_{\text{vtx}}$  distribution reduces the difference dramatically.

### 8.2.2 Differential Measurement in $\eta$

It is expected that the re-weighting affects all rapidity related variables, such as  $\eta$  and the number of reconstructed primary vertices  $n_{\text{Vxp}}$ . Of the variables used for identification, the track related ones are expected to be most affected.

Measurements of the efficiencies of the single identification requirements has been performed in fine  $\eta$  granularity. These efficiencies were calculated w.r.t reconstructed electrons. The difference between the efficiencies obtained with the re-weighted and the non-reweighted PYTHIA6 sample is shown in Fig. 9.4 with the numbering scheme for the identification cuts as listed in Appendix C. The affected identification cuts, together with the corresponding number in Fig. 8.4, are described in the following.

The detector regions that see the largest effect from the re-weighting procedure are the very central barrel region ( $|\eta| < 0.6$ ) and the outermost end-cap ( $|\eta| > 2.1$ ). The identification cuts most affected are different for the barrel and end-cap region. In the barrel these are the cuts on track-cluster matching (20,28),  $n_{\text{TRT}}$  hits (24) and the TRT-ratio  $f_{\text{HT}}$  (26). The effect on the TRT related variables is opposite of the others. This is why the effect of re-weighting is smaller for TightPP efficiencies than it is for LoosePP and MediumPP, which do *not* use the number of hits in the TRT; some of the effects of re-weighting cancel. In the end-cap region the largest effect is seen on the isolation cuts not used for identification and only in the outermost bin ( $2.4 < |\eta| < 2.47$ ). The other affected cut variables are again the track related ones, the conversion match (1),  $n_{\text{PIX}}$  (17) and  $E/p$  track-match (22).

As a result of this analysis the re-weighting of the  $z_{\text{vtx}}$  position to data was included in the official recommendations to physics analyses, using the truth vertex position, and is applied in the performance measurements, as well. With the consistent usage of  $z_{\text{vtx}}$  re-weighting in all analyses a systematic effect is avoided and therefore no systematic uncertainties due to this effect are assigned to the efficiency measurements.

## 8.3 Pile-up Dependence

The instantaneous luminosity of the LHC was steadily increased resulting in an increasing number of interactions per bunch-crossing. Therefore, the energy deposited in the calorimeters is higher and there are more tracks in the tracking system. This then affects

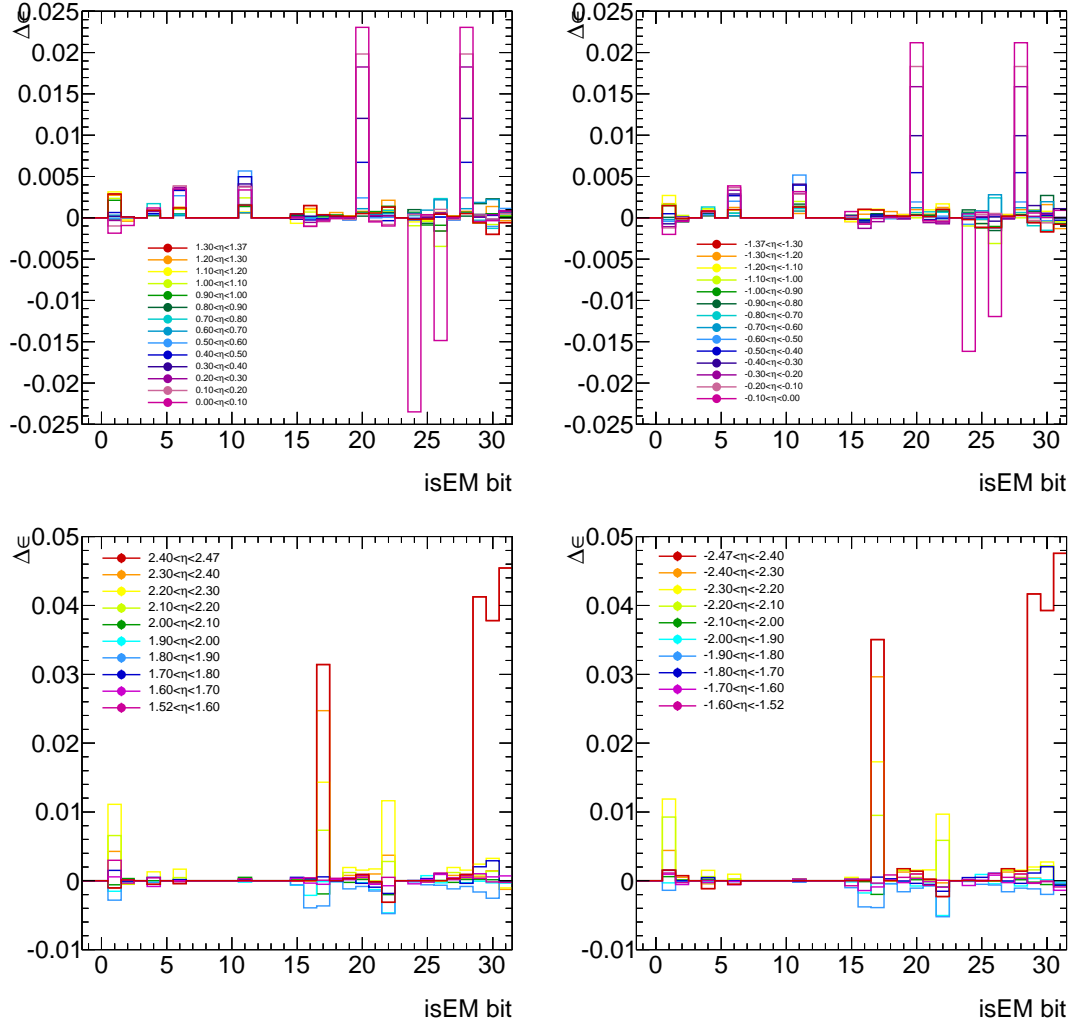


Figure 8.4: Difference between the efficiencies obtained with the PYTHIA Monte-Carlo sample that was re-weighted or not re-weighted in  $z_{\text{vtx}}$ . Shown are the individual identification requirements for MediumPP cut values. Each number on the  $x$ -axis corresponds to a certain identification cut, the so-called isEM bit that is an arbitrary numbering scheme for the identification cuts listed in Table C.

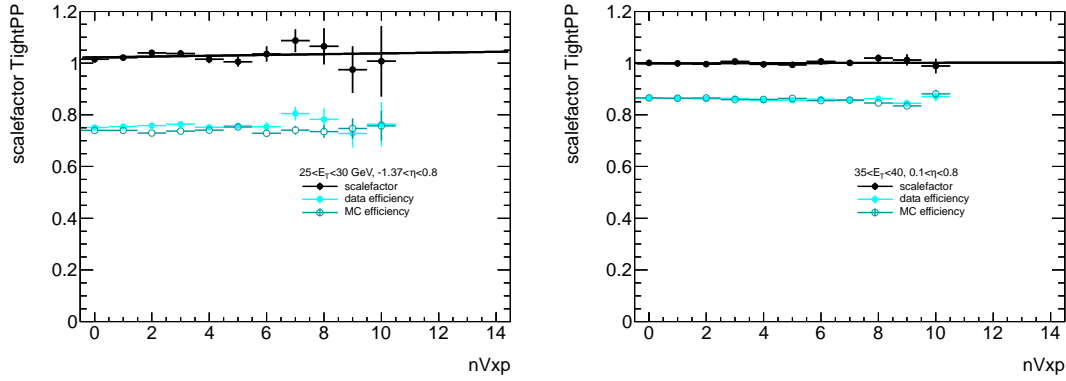


Figure 8.5: Scale-factors, Monte-Carlo and data efficiency for TightPP as a function of primary vertices in the event.

the track reconstruction and the energy measurement of the electron. With more pile-up a decrease in the electron identification efficiency is expected.

The  $E_T^{\text{miss}}$  significance triggers preferably select events with only few pile-up jets due to correlation with the input parameter  $\sum E_T$ . Since the results are combined later with the results from  $ZT\&P$ , where electron triggers are used, this does not need to be accounted for. What needs to be accounted for is a potential mismatch of the pile-up effects in data compared to Monte-Carlo.

### 8.3.1 Efficiencies vs. Pile-up

A measurement of the efficiencies has been performed as a function of the number of primary vertices. Due to the limited number of probes the measurement was performed using the coarse  $\eta$  granularity. The results are shown for two exemplary bins in Fig. 8.5. The study indicates that the efficiencies decrease with an increasing number of vertices  $nV_{xp}$ . For the scale-factors calculated subsequently there is no clear behaviour or pattern visible. Linear fits in every  $\eta \times E_T$  bin vs.  $nV_{xp}$  give a slope, different from 0 within one standard deviation, in 18 out of 63 bins. This is compatible with what is expected from statistical fluctuations for the null hypothesis, assuming no pile-up dependence of the scale-factors. The decrease seen in efficiencies is very little. It is typically larger for higher values of  $nV_{xp}$ . These are not accessible in  $WT\&P$  because of the use of  $E_T^{\text{miss}}$  significance triggers and their correlation with pile-up.

The study indicates that the behaviour of the efficiencies vs. pile-up is modelled well. Whether the description of pile-up itself is correct remains to be checked.

### 8.3.2 Different Methods of Re-weighting

As stated in Section 7.4.1 the  $\mu$  distribution of the Monte-Carlo samples are re-weighted to match the distribution in data. In order to account for systematic effects in the re-weighting method a second method has been tested that is fundamentally different from

$E_T$ [GeV]	mean ( $\times 10^{-4}$ )	RMS ( $\times 10^{-4}$ )
15-20	-4.16	25.14
20-25	-7.22	18.13
25-30	-4.67	16.03
30-35	-2.28	17.27
35-40	-0.56	12.87
40-45	-0.24	16.33
45-50	1.93	11.27

Table 8.1: Difference between two methods of pile-up re-weighting, with  $\mu$  or  $nVxp$  re-weighted to data, for TightPP efficiencies for the PYTHIA6 sample as a function of  $E_T$ , averaged over  $\eta$ .

the first. Instead of the distribution of average interactions per bunch-crossing  $\mu$  the number of primary vertices has been used to re-weight Monte-Carlo to data. To avoid effects from mismodelling of e.g. the trigger,  $E_T^{\text{miss}}$  or  $\sum E_T$ , the weights are obtained *after* the full TightPP selection. This way, by construction, the  $nVxp$  distribution is flat for the specific kinematic selection used to obtain the weights and almost flat for the other ID levels and working points. At the same time this gives an estimate of the wrong modelling of  $\sum E_T$  on Monte-Carlo, since it affects the trigger decision and shifts the pile-up distributions.

The difference between the efficiencies obtained with the two approaches is calculated in the fine  $\eta$  granularity. As stated in the introduction of this section, mainly the transverse energy of the electron is expected to be affected by pile-up. Therefore, the differences of the efficiencies measured using two re-weighting methods are averaged over  $\eta$  and investigated as a function of  $E_T$ . The means and RMS values of the differences, averaged over  $\eta$ , are listed in Table 8.1 where the efficiencies obtained after  $nVxp$  re-weighting are subtracted from the efficiencies obtained after  $\mu$  re-weighting.

Except for the highest  $E_T$  bin re-weighting in  $\mu$  gives lower efficiencies. The effect is decreasing with higher transverse energy of the electron. This is also seen in the RMS values. One has to keep in mind, that the statistical uncertainties for both methods are highly correlated since they use the same events only with different event weights. Therefore, the RMS is not a statistical quantity but is the real mean squared difference of one method to the other. The average difference between two methods is found to be completely negligible and below per-mille level.

### 8.3.3 Different Ways of Modelling

A second systematic effect comes from the pile-up description in Monte-Carlo. With the PYTHIA samples, two samples that differ only in the modelling of pile-up are available. It has been shown in Ref. [46] that the modelling provided by PYTHIA6 is better. Since there are still some samples in use that have been generated with PYTHIA8 any systematic effect has to be added as an uncertainty.

$E_T$ [GeV]	mean ( $\times 10^{-4}$ )	RMS ( $\times 10^{-4}$ )
15-20	53.15	187.55
20-25	54.51	123.57
25-30	-22.75	89.54
30-35	12.12	58.82
35-40	-6.41	46.94
40-45	16.05	47.46
45-50	0.43	89.08

Table 8.2: Difference between two methods of pile-up modelling, pile-up generated with PYTHIA6 or PYTHIA8, for TightPP efficiencies as a function of  $E_T$ , averaged over  $\eta$ .

The systematic effect of the pile-up modelling is investigated in the same manner as it has been done for the two re-weighting methods in the preceding section. This time the difference between the efficiencies obtained with two different samples is computed using either PYTHIA6 or PYTHIA8 for the pile-up modelling. The result is shown in Table 8.2, again as a function of  $E_T$ . In contrast to Section 8.3.2 the samples are not fully statistically correlated. Although the generated events of the hard-scattering are identical, the detector simulation has been redone with the new pile-up description.

The high values for the RMS are now originating from statistical fluctuations. The average difference does not follow a clear pattern like before. The moduli are of the same order as the RMS values were before when comparing the different pile-up re-weighting methods. It has been decided to add the moduli of the difference between efficiencies in PYTHIA6 and PYTHIA8 as a systematic uncertainty to account for both the systematic effects of the re-weighting method and the systematic effect from the description in the generator.

This systematic uncertainty is added *after* combining the results with the  $Z$  and  $J/\psi$  channels to also account for any mismodelling there. Otherwise the  $W$  channel would enter the combination with a lower weight which in the case of the uncertainty of pile-up is unjustified.

## 8.4 Impact of Charge Misidentification

The efficiency is calculated for electrons and positrons separately and averaged for each of the 80 variations. As described in Section 6.5.1, a dependence of the charge is expected, originating from charge misidentification.

There is a correlation between the efficiency of identifying electrons and the probability to identify its charge correctly. A misidentification of the charge typically happens to electrons that interact early in the detector, creating multiple high  $p_T$  tracks. In the track-cluster matching the primary track is then either not available or a wrong alternative is chosen [1]. Charge misidentified positrons are migrating into the electron sample and electrons are migrating into the positron sample. Since track-cluster matching cuts

are used in the electron identification, and since near-by secondary photons or electrons also distort the shower shapes in the calorimeter, generally, electrons whose charge is identified incorrectly have a lower probability to pass all identification cuts and being identified as electrons. The process is more likely to occur in the end-cap region where more material has to be traversed.

This happens to all electrons regardless of their origin but it features a subtlety that is specific for  $WT&P$ . In  $Z \rightarrow ee$  decays electrons and positrons obviously are produced at the same rate. Moreover, in  $Z$  analyses misidentified electrons are rejected by requiring a negative charge product for the selected tag- and probe-electrons in an event, suppressing the fraction of charge-misidentified particles to the square of the misidentification probability.

The situation for the  $WT&P$  measurement is fundamentally different. No such selection can be applied and due to the correlation with the identification requirements the efficiencies measured in  $WT&P$  are generally lower. Moreover, the  $W^+$  bosons are produced with a larger cross-section than  $W^-$  bosons but their decay products have equal rates of charge misidentification. As a result, the fraction of charge-misidentified particles is larger in the electron sample than it is in the positron sample. Therefore, in the  $WT&P$  measurement, one relies on a good description of the misidentified electrons and the  $W^+/W^-$  ratio, when calculating efficiencies on Monte-Carlo.

#### 8.4.1 ID Efficiency for Charge Misidentified Electrons

To illustrate the above facts, a pure Monte-Carlo study has been performed. The fraction of electrons with misidentified charge is shown in Fig. 8.6 on the left hand side. The probability of incorrectly identifying the charge of an electron is below 1% in the barrel region and increases up to 3 – 10% in the end-caps. On the right hand side the efficiency of identifying electrons with correctly and incorrectly identified charge is compared. For the latter the identification efficiency drops below 40% compared to more than 80% for correctly charge-identified electrons.

There are dedicated measurements of the charge misidentification probability done with  $ZT&P$ , using a same-sign sample of  $Z \rightarrow ee$  decays. As an improvement for this analysis, the Monte-Carlo misidentification rate could be re-weighted to match the one in data. The correlation of reconstruction efficiency and charge measurement has not yet been measured. In principle, the differences in reconstruction efficiencies for electrons with correctly and incorrectly identified charge should not be very small since the track-cluster matching is much looser. The measurement here therefore captures the full effect of charge misidentification.

#### 8.4.2 $e^{+/-}$ -ratios for the Different Generators

The asymmetry in the production of  $W^+$  and  $W^-$  is largest in the end-caps, where also the probability of misidentifying the charge of an electron is largest. Since the asymmetry changes with higher order effects, as shown for theoretical calculations in Fig. 2.4, a

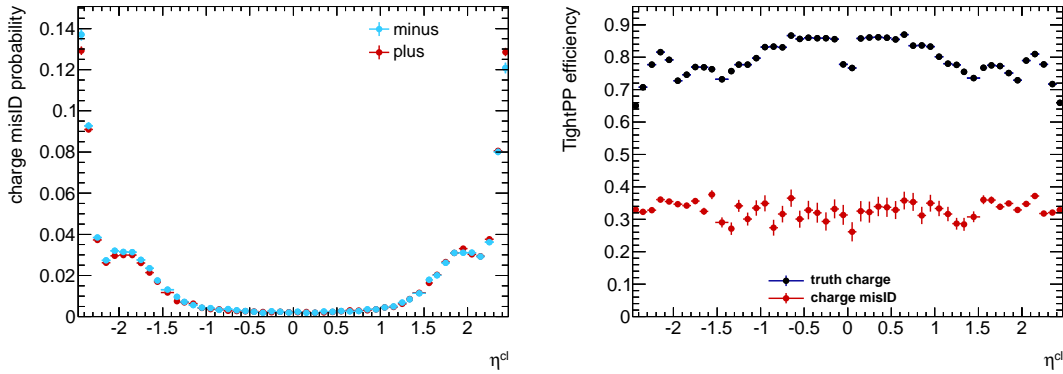


Figure 8.6: Charge misidentification probability for reconstructed electrons (left) and TightPP identification efficiency of charge misidentified and correctly identified electrons (right), pure Monte-Carlo.

careful choice of the generator is necessary. Whereas PYTHIA calculates the matrix-element to leading-order only, POWHEG includes next-to-leading-order calculations.

The  $e^+/e^-$ -ratios of the probes selected in data and two Monte-Carlo samples is shown in Fig. 8.7 for one typical selection out of the 80 variations used in the analysis. For data the background has been subtracted, for Monte-Carlo the implicit cut on isolation is applied. The description of data is much better for POWHEG than it is for PYTHIA, as expected. The agreement is not perfect, however. To account for any residual differences a method has been developed to estimate the effect on the scale-factors in Section 8.4.4. There, the two generators available are compared again. Since it was found that the efficiency measurement is sensitive to the effects of the charge asymmetry the figure determines the choice of POWHEG as the default Monte-Carlo generator used for the analysis.

### 8.4.3 Charge Separated Measurements

As just discussed there is an asymmetry in the efficiency measured in WT&P for positron and electron samples, caused by the migration of electrons of one sample into the other through charge misidentification. This section is devoted to any residual mismodelling of this asymmetry or mismodelling of the charge misidentification probability.

In order to see how large the effect actually is, the full efficiency measurement is run for data and Monte-Carlo for electrons and positrons separately. Then scale-factors are calculated. The result is compared to the ordinary, averaged efficiencies and scale-factors in Fig. 8.8. The efficiency of identifying a positron is clearly higher than that of identifying electrons. This is expected and seen on both data and Monte-Carlo. When looking at the scale-factors the difference between electrons and positrons diminishes but persists. This is the effect to be accounted for. It is caused by a mismodelling of either the  $e^+/e^-$ -ratio, the charge identification efficiency or the efficiency of identifying an electron whose charge was incorrectly identified.

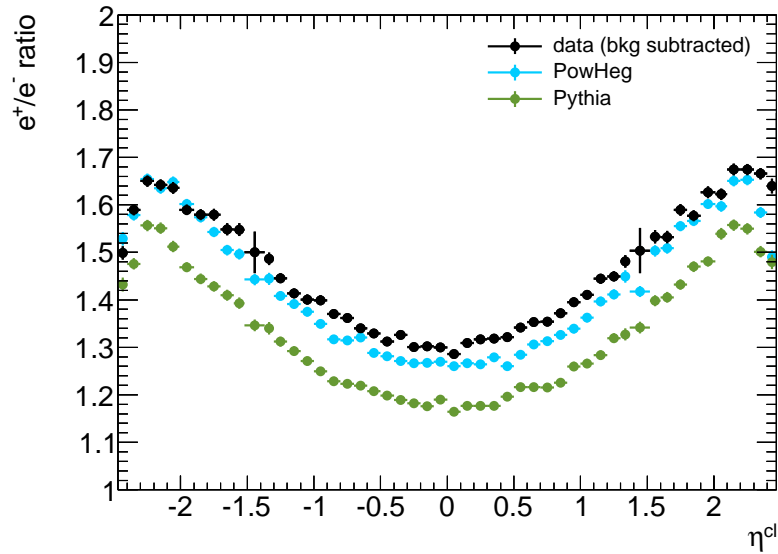


Figure 8.7:  $e^+/e^-$  ratio for data (background subtracted) and Monte-Carlo.

Moreover the mismodelling is asymmetric in  $\eta$ . In the past, similar asymmetries have been seen and were traced back to originate from issues in the alignment. In order to account for all of these differences an extra systematic uncertainty is added.

#### 8.4.4 Systematic Uncertainties from Charge Asymmetry

The systematic uncertainty added is calculated using an enhanced version of what the Particle Data Group uses for “unconstrained averaging” in Ref. [9]. The  $\chi^2/(N - 1)$  of  $N$  uncorrelated measurements is expected to be equal to 1. The error of the average of these measurements is increased by a factor

$$S = \left[ \frac{\chi^2}{N - 1} \right]^{\frac{1}{2}} \quad (8.1)$$

if the  $\chi^2/(N - 1)$  of the individual measurements is  $> 1$

The individual measurements in this analysis are taken as the average of two efficiencies and two Monte-Carlo efficiencies that are used to calculate a scale-factor. With 350 bins in the fine  $\eta$  granularity there will always be bins where for some statistical fluctuation the averaged value does not cover the individual value even if the modelling of Monte-Carlo was perfect. This is because the  $\chi^2$  distribution for  $N = 1$  is very steep at  $\chi^2 = 1$ . In the same manner the statistical fluctuation can be such that there is perfect agreement even though the modelling is bad. To account for that a  $\chi^2$  is calculated for 24 different kinematic regions, summing over all bins in the given region. Three bins in  $E_T$  were chosen, matching the binning used for the measurement of charge misidentification, and

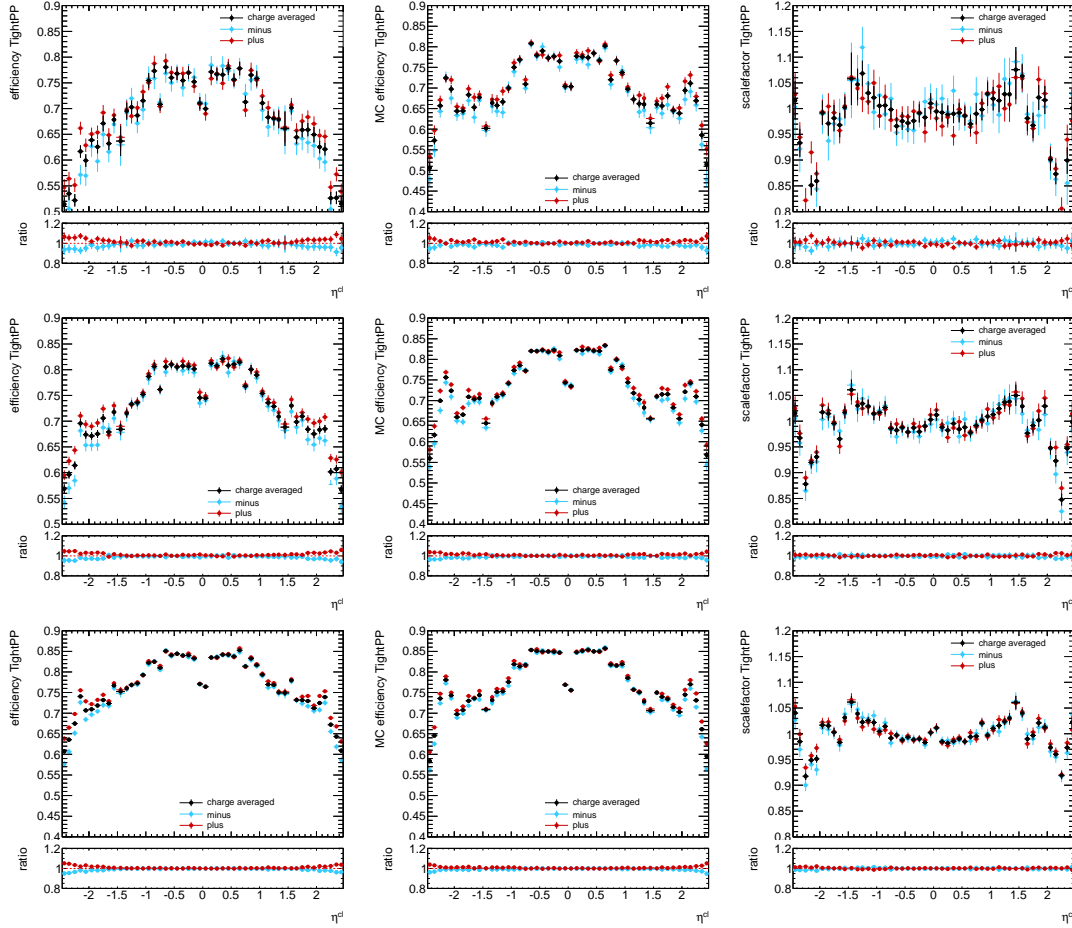


Figure 8.8: Efficiencies and scale-factors measured separately for electrons and positrons together with the charge averaged values. Efficiencies for data (left), Monte-Carlo (middle) and scale-factors (right) of the TightPP criterion as a function of pseudo-rapidity  $\eta$  for three specific  $E_T$  bins. From top to bottom these are  $20 < E_T < 25$  GeV,  $25 < E_T < 30$  GeV,  $35 < E_T < 40$  GeV.

eight different  $\eta$  bins because the asymmetry is expected to be larger in the end-caps than in the barrel region and an asymmetry was seen between forward and backward region.

For each of the 80 variations on data and 40 variations on Monte-Carlo the difference between electron and positron efficiency  $\Delta\varepsilon$  is calculated, considering the statistical correlation of the two efficiencies as discussed in Section 6.7.3. The individual measurements are then averaged in the same way as it is done for the 80 individual efficiencies, i.e.  $\Delta\varepsilon$  is the arithmetic mean of the individual measurements and the statistical uncertainty is the arithmetic mean of the individual statistical uncertainties.

The  $\chi^2$  in one of the 24 kinematic regions is then defined as

$$\chi^2 = \sum_{\text{bins}} \frac{(\Delta\varepsilon(\text{data})_i - \Delta\varepsilon(\text{MC})_i)^2}{\delta_{\Delta}(\text{data})_{\text{stat},i}^2 + \delta_{\Delta}(\text{MC})_{\text{stat},i}^2} \quad (8.2)$$

with the statistical uncertainty  $\delta_{\Delta}(\text{data})_{\text{stat},i}$  of the measurement in data and  $\delta_{\Delta}(\text{MC})_{\text{stat},i}$  on Monte-Carlo. The single differences between the efficiencies  $\Delta\varepsilon$  in data and Monte-Carlo are not expected to vanish – this is the insight of Section 8.4 – only the full numerator  $\Delta\varepsilon(\text{data}) - \Delta\varepsilon(\text{MC})$  is, provided the effect of the charge asymmetry is modelled well on Monte-Carlo. A  $\chi^2/N_{\text{bins}} = 1$  is expected for this hypothesis. The systematic uncertainties are then calculated in units of the statistical uncertainties as  $\delta_{\text{charge}} = \sqrt{S-1} \cdot \delta_{\text{stat}}$ . Hence, the systematic uncertainty is different in every bin. The correction factor  $S$  is

$$S = \left[ \frac{\chi^2}{N_{\text{bins}}} \right]^{\frac{1}{2}}. \quad (8.3)$$

Table 8.3 shows the factors  $S$  obtained by this method for different identification criteria and Monte-Carlo generators. The correction to be applied is larger in the end-cap region than it is in the barrel. Also, it is larger the tighter the cuts on track-cluster matching are for the different identification criteria. Since the correction is calculated in units of the statistical uncertainty, larger correction factors are applied in the coarser granularities where the statistical uncertainties are smaller. The numbers obtained for PYTHIA6 are shown for illustration only since the nominal scale-factors for analysis use are calculated using POWHEG. The higher values w.r.t. POWHEG confirm the wrong modelling of the  $W^+/W^-$  ratio as discussed in Section 8.4.2.

The asymmetry between forward and backward region already seen in Fig. 8.8 is reflected, too. The sudden changes of the correction factors especially in the end-cap regions are also seen in Fig. 8.8 and related to the sudden change of the charge misidentification probability.

## 8.5 Impact of the Generator

Apart from small residual differences due to disagreement of the distributions of the transverse energy and pseudo-rapidity within one bin, the efficiencies measured on Monte-Carlo should be independent of the generator used. All generators are interfaced with Photos and the full detector simulation is the same for all generators used

$E_T$ [GeV]	Fine $\eta$ granularity			Intermediate $\eta$ granularity			Coarse $\eta$ granularity			Fine with PYTHIA		
	15-20	20-30	30-50	15-20	20-30	30-50	15-20	20-30	30-50	15-20	20-30	30-50
	LoosePP			LoosePP			LoosePP			LoosePP		
[-2.47, -2.01]	1	1.20	1	1	2.09	1	1	3.24	1.22	1	1.52	1
[-2.01, -1.52]	1	1	1	1	1	1	1	1	1	1	1	1
[-1.37, -0.8]	1.31	1	1	1	1	1	1.85	1	1	1.12	1	1
[-0.8, 0]	1	1	1	1	1	1	1	1	1	1	1	1
[0, 0.8]	1	1	1	1	1.05	1	2.26	2.81	1	1	1	1
[0.8, 1.37]	1	1	1	1	1	1	1	1	1	1	1	1
[1.52, 2.01]	1	1	1	1	1	1	1	1	1	1	1	1
[2.01, 2.47]	1.34	1	1	2.06	1	1	4.47	2.25	1	1.65	1.04	1
	MediumPP			MediumPP			MediumPP			MediumPP		
[-2.47, -2.01]	1	1.52	1.39	1	2.01	2.47	1	4.73	3.74	1.12	2.24	1.36
[-2.01, -1.52]	1.07	1	1.18	1.51	1.52	1.47	2.48	2.81	1.70	1.98	1.45	1.09
[-1.37, -0.8]	1	1	1	1	1	1	1	1	1	1	1.15	1
[-0.8, 0]	1	1.07	1	1.05	1	1	1.84	1	1	1	1	1.34
[0, 0.8]	1.14	1.13	1	1.51	1.08	1	2.18	3.04	1	1	1	1
[0.8, 1.37]	1.19	1	1.11	1	1	1	1	1	1	1	1	1
[1.52, 2.01]	1.26	1	1	1	1	1.35	1	1	1.75	1.44	1	1
[2.01, 2.47]	1	1.14	1	1	1.32	1	1	3.10	1.26	2.27	2.63	1
	TightPP			TightPP			TightPP			TightPP		
[-2.47, -2.01]	1	1.55	2.18	2.09	2.07	3.43	3.51	4.01	5.46	1.56	4.28	2.05
[-2.01, -1.52]	1.78	1	1	3.44	1	1.30	5.06	1	1.38	2.73	1.27	1.12
[-1.37, -0.8]	1	1	1.57	1	1	1.61	1	1	2.80	1	1.16	1.05
[-0.8, 0]	1	1	1	1.21	1	1	2.56	1	1	1	1.17	1.37
[0, 0.8]	1.29	1.71	1	1	1.41	1	1.89	3.38	1	1	1	1
[0.8, 1.37]	1.11	1	1	1.47	1	1	1	1	1	1	1	1
[1.52, 2.01]	1	1	1	1	1.91	1	1.13	1.41	1.15	1	1	1
[2.01, 2.47]	1	1.34	1.24	1	1.62	1.49	1	2.72	2.35	2.65	3.24	1.67

Table 8.3: Charge correction factors for all  $\eta$  granularities and ID level calculated for 24  $\eta \times E_T$  regions. For coarse granularity the bin  $-0.1 < |\eta| < 0.1$  is not considered. The last column shows the correction factors obtained for PYTHIA Monte-Carlo in fine granularity for comparison.

at ATLAS. The efficiency measurement heavily relies on the correct description of the underlying physics processes. As presented in Section 8.4 a good description of the  $e^{+/-}$ -ratio is crucial for *WT&P*. The measurement is clearly sensitive to effects from charge misidentification. Because of that POWHEG was chosen as a default to calculate scale-factors and no systematic uncertainty is added for the impact of the generator.

---

# 9 Identification Efficiency Measurement

---

The results of the efficiency measurement in different  $\eta$  granularities and for the three different identification criteria are given in the following. This chapter is loosely divided into four parts. It starts with a retrospective look at the 2010 measurement, followed by a qualitative overview over the measured efficiencies, which is interesting from the performance point-of-view. Then the scale-factors, interesting from the simulation point-of-view, are listed before the detailed results are discussed with their uncertainties. This last part is what is used in physics analyses and has been the main motivation for this analysis.

## 9.1 Status 2010 and Improvements in the Present Analysis

The measurement has received changes in a number of aspects compared to the 2010 measurement. The results of various improvements have been discussed in Chapters 6-8. The changes made will be summarised below, probably the most important one being the transition to a double differential measurement.

### 9.1.1 Status 2010

With the luminosity recorded in 2010, only a very small fraction of data available today was on hand. A double differential measurement like the one introduced in Section 6.5.1 was not possible at the time. Instead, the efficiencies had been measured as a function of  $E_T$  and then separately as a function of  $\eta$ . The scale-factors have been provided in 2D but with a 1D×1D approximation, where the value for a certain  $\eta \times E_T$  bin is obtained by

$$\text{SF}(\eta, E_T) = \frac{\text{SF}(\eta) \cdot \text{SF}(E_T)}{\overline{\text{SF}}} \quad (9.1)$$

where  $\overline{\text{SF}}$  is the average of the scale-factors in the numerator.

With the increasing number of recorded events it was possible to use a real 2D binning. The 1D×1D approximation is compared to the results from a real 2D measurement in Section 9.1.3 for TightPP efficiencies. However, this cannot really be compared to the status in 2010. Back then the uncertainties were dominated by statistical uncertainties and one did not have to worry about systematic effects so much. Despite a significant improvement in statistical precision the approximation has still been used for all intermediate results throughout 2011 data-taking. This was done on account of the  $J/\psi$  and  $Z \rightarrow ee$  channels. They are much more limited by statistical uncertainties because of the lower cross-sections of the processes.

### 9.1.2 Improvements in Present Analysis

With an increasing amount of data available the analysis has been overwhelmed by its own increasing precision. Since the kinematic distributions in  $\eta$  and  $E_T$  are sensitive to some of the systematic variations the systematic uncertainties decreased in the 2D measurement. Additionally, an optimisation of the event selection proposed in the context of this thesis increased the number of selected probes by a factor of two with regard to the previous selection, with only slightly increasing background.

Within this thesis efforts have been made to match the Monte-Carlo selection more closely to data. An improved trigger selection on Monte-Carlo led to improvements in the agreement of all variables in data and Monte-Carlo, in particular the  $E_T^{\text{miss}}$  and pile-up related variables. With that, the standard techniques for the pile-up re-weighting could be used and for the first time in *WT&P*, Monte-Carlo could be scaled to luminosity uncovering the trigger mismodelling. It also provided the possibility to estimate the signal leaking into the templates used for the background subtraction. Subsequent adjustments in the template selection resulted in a better agreement of the probes with the template and reduced the signal contamination.

A study on  $e^+/e^-$  ratios for a variety of Monte-Carlo generators favoured a transition from the *PYTHIA* to the *POWHEG* Monte-Carlo for the calculation of Monte-Carlo efficiencies and scale-factors. A method to account for residual effects has been developed. The procedure of averaging the charge split efficiencies has been improved and the statistical tools to account for the correlations between numerator and denominator, and the measurement of both charges were applied.

Finally, the data sample is now large enough to move the cut on the hadronic leakage fraction  $R_{\text{had}}$ , that caused problems in the background subtraction, into the measurement of the reconstruction efficiencies.

### 9.1.3 1Dx1D vs. 2D Binning

A measurement is performed in the binning used in 2010, i.e. a  $1\text{D}\times 1\text{D}$  approximation. The resulting scale-factors translated to 2D are shown in Fig. 9.1 compared to the ones obtained from the coarse 2D binning. It is notable that the distribution of the scale-factors, both in  $\eta$  and  $E_T$ , are more uniform for the  $1\text{D}\times 1\text{D}$  binning resulting in a spread of up to 10%. The extreme values in the end-caps are not present. Also notable is, that the agreement of both methods is better in the higher  $E_T$  bin that is closer to the maximum of the Jacobian peak of the electron  $E_T$  spectrum. This can easily be explained by the kinematic distributions of the probes in Fig. 7.5.

A 1D measurement cannot capture the full structure in  $\eta$  since the pattern of the  $\eta$  distributions in the different  $E_T$  bins is the same by construction. The  $1\text{D}\times 1\text{D}$  scale-factors in both  $E_T$  bins in Fig. 9.1 just have different normalisation. Naturally, the results of the 1D measurement in  $\eta$  is shifted towards the electron  $E_T$  peak region at  $\sim 40$  GeV whereas the values of the measurement in  $E_T$  is shifted towards the barrel region. The latter is an even larger effect for *ZT&P* since the  $Z$  is less boosted along the beam axis, as it is discussed in Section 6.6.

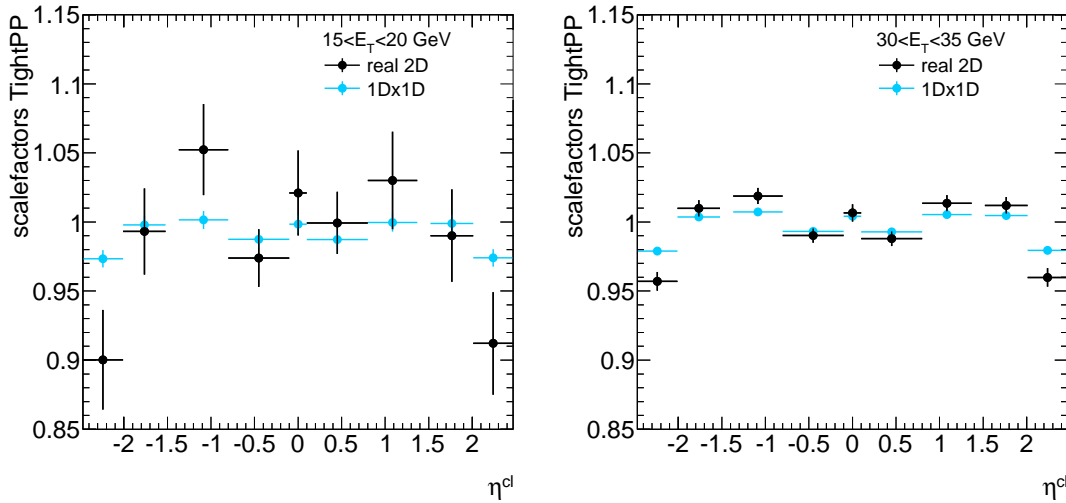


Figure 9.1: Comparison of scale-factors in coarse binning, obtained in 1D $\times$ 1D (cyan) and real 2D measurements (black), for the lowest  $E_T$  bin  $15 < E_T < 20$  GeV (left) and  $30 < E_T < 35$  GeV (right). The scale-factors of the 1D $\times$ 1D approximation in a certain bin are calculated according to Eq. 9.1.

Also, most of the scale-factors do not agree within their uncertainties. However, it should be noted that the results given here cannot directly be compared to the results given back in 2010. The uncertainties used to be much larger. It is clear that the measurement cannot be used in the 1D $\times$ 1D approximation if the precision is high enough to be sensitive to the effects.

The values obtained in the 1D $\times$ 1D approximation are systematically biased. Supposedly, the disagreement is the reason the 2010  $W^\pm$  and  $Z/\gamma^*$  cross section measurement [26] had to use scale-factors from a simple 1D measurement in  $\eta$ , as already explained in Section 4.1.

## 9.2 Efficiencies

The measurement is performed in three  $\eta$  granularities. In the following, a general overview of the efficiencies for the different identification criteria and kinematic regions is given.

### 9.2.1 Measurement in $\eta$ , $E_T$

The efficiencies are compared in two selected  $E_T$  bins as a function of  $\eta$  for all  $\eta$  granularities in Fig. 9.2. The TightPP identification criterion has been chosen since it involves all detector parts. Comparing the different granularities, the efficiencies do *not* follow a step-like pattern that is oriented at the detector geometry and the optimisation of the

electron identification. The transition is rather smooth with smaller jumps at the edges of the bins of the identification menu.

The efficiencies of all three identification criteria are shown in Fig. 9.3. In the given factorisation with reconstructed electrons already fulfilling the track-quality and  $R_{\text{had}}$  requirements the LoosePP identification requirements are  $> 90\%$  efficient over the full kinematic range. Going to tighter identification requirements these efficiencies drop and reveal a plateau of maximum efficiency between  $35 < E_T < 45$  GeV in the barrel region where typically only few background processes are present. This is a clear consequence of the fact, that the identification requirements are not optimised for gathering a maximum fraction of electrons but for a given rejection of background. The signal-to-background ratios in coarse granularity using the usual background estimation are listed in Table A.3. The efficiency is correlated with the signal-to-background ratio.

The lowest efficiency is reached in the end-caps for lower  $E_T$  electrons. In general the efficiency drops dramatically as a function of  $\eta$ . Very conspicuous is the massive drop in the region of the TRT readout at  $|\eta| < 0.1$ . Its position is clearly visible as a small central region with decreased efficiency for MediumPP and TightPP efficiencies. It is not present for LoosePP that does not make use of the TRT. The efficiencies are typically largest, where only few material has to be traversed and all detector parts can be used.

### 9.2.2 Measurement of Single Cut Efficiencies

A pure Monte-Carlo study of measuring the efficiency of single identification cuts was performed. The Monte-Carlo efficiencies of the single cuts as defined in Appendix C are depicted in Fig. 9.4 for PYTHIA6. Unfortunately the same measurement cannot be performed on data, primarily because of the limited precision.

The most inefficient cuts are the track related ones, the conversion match (1), pixel hits (17) and track-match  $E/p$  (22). In the readout region of the TRT the requirement of TRT hits (24) is particularly inefficient; shown is the TightPP cut value. Note that the very inefficient TRT ratio 90 cut (26) is not used in the standard identification menu. It uses an increased upper threshold.

Particularly inefficient are the isolation cuts (29-31). This is expected, since these cuts were designed to have an efficiency of 95% w.r.t. MediumPP electrons. This analysis is not concerned with the measurement of the efficiency of those cuts. They are typically evaluated on tags with regards to electrons passing all other identification cuts using a ZT&P method.

### 9.3 Scale-factors

The extracted scale-factors between data and Monte-Carlo simulation are depicted in Figs. 9.5 and 9.6. They are all very close to unity. This indicates a good simulation of the detector and a good description of the showering of the electron. There are, however, regions where the scale-factors deviate from 1. This is especially the case in the end-cap regions for which the electrons have to traverse a lot of material and for the regions

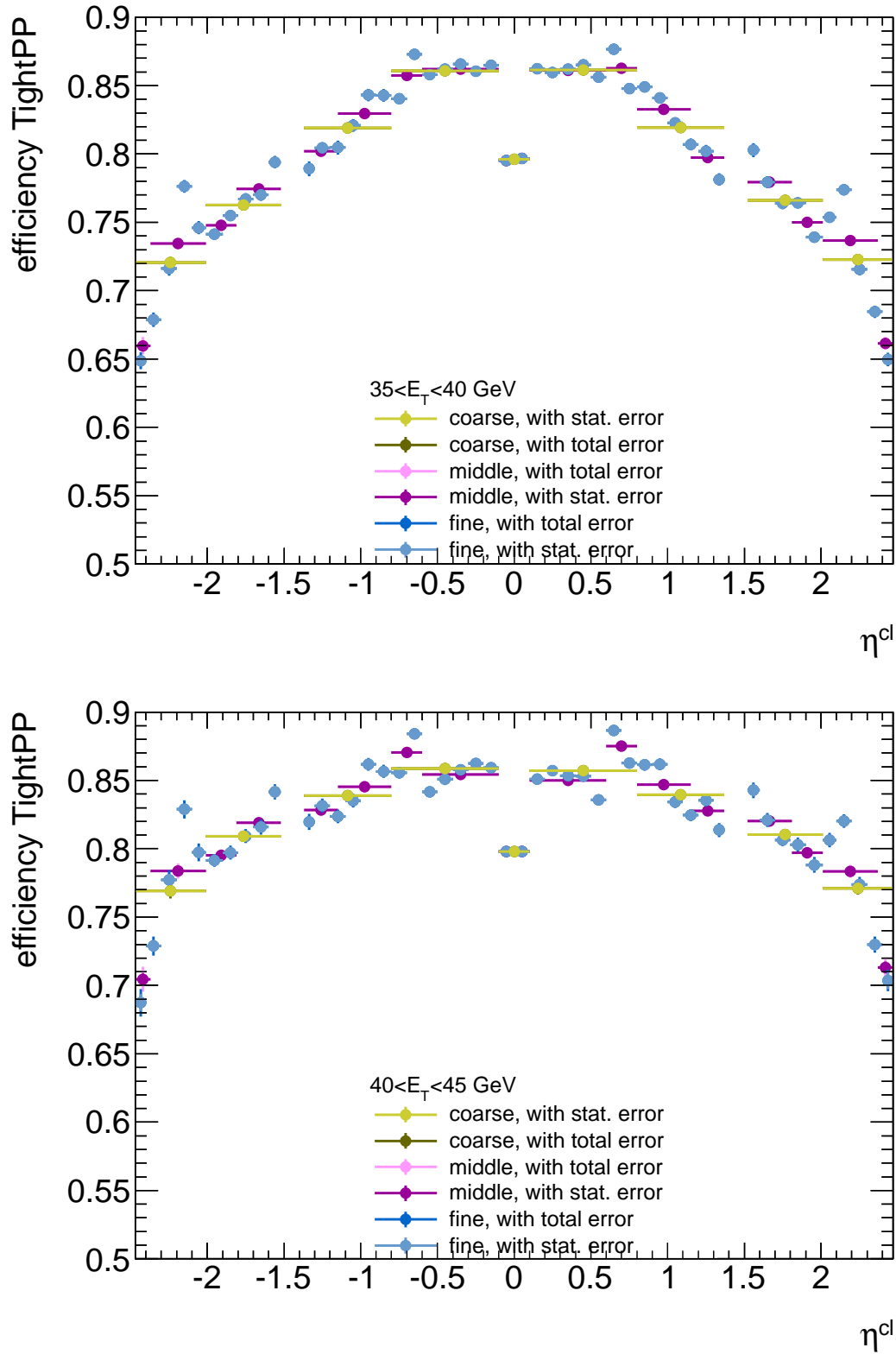


Figure 9.2: TightPP efficiency measured in the  $E_T$  bins with highest statistical precision for three  $\eta$  granularities and for  $35 < E_T < 40$  GeV (top) and  $40 < E_T < 45$  GeV (bottom).

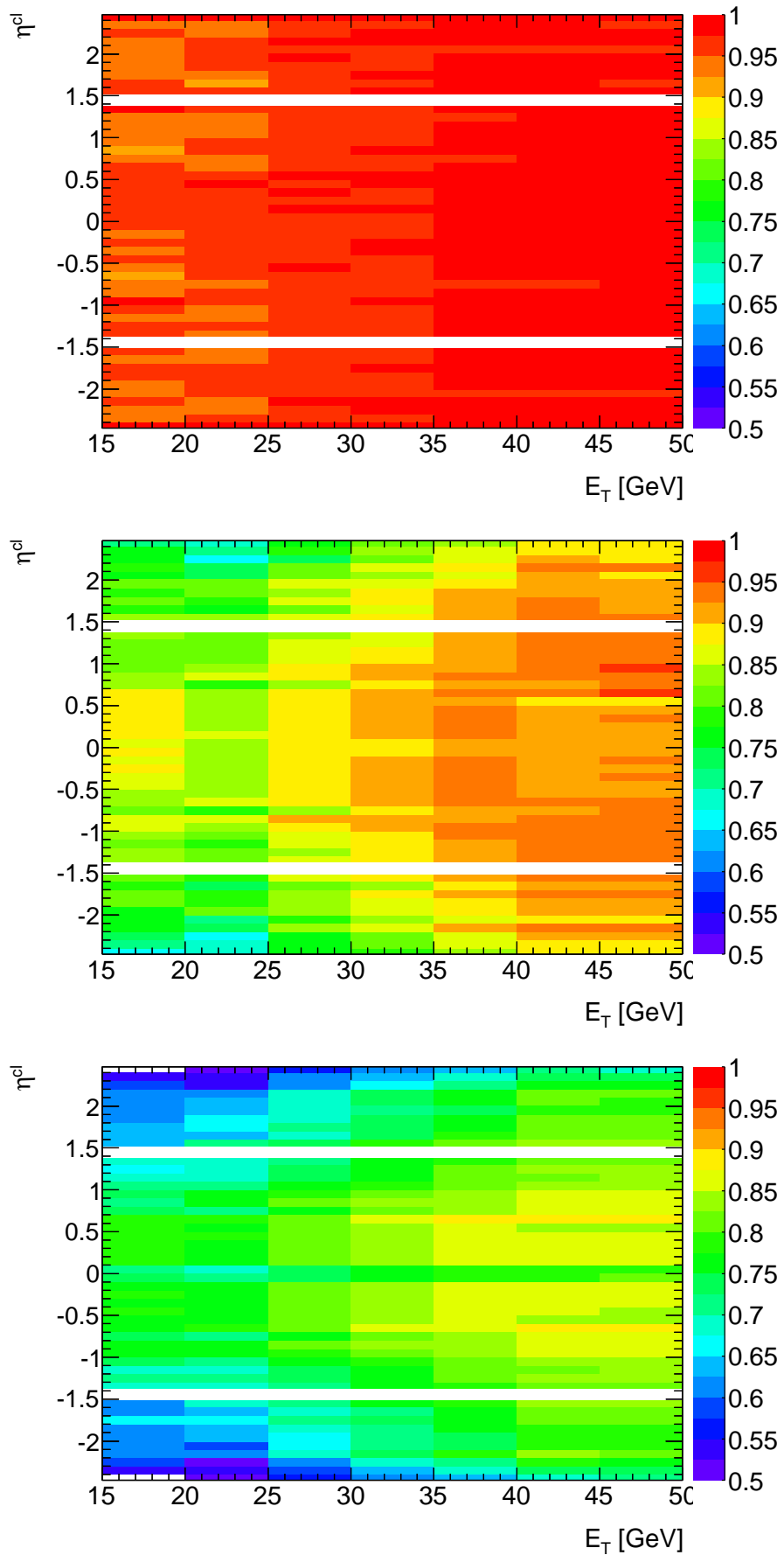


Figure 9.3: Efficiencies as a function of  $E_T$  and  $\eta$  for the fine granularity for LoosePP (top), MediumPP (middle) and TightPP (bottom). To allow for comparison, the colour scale is chosen to be the same in the three sub-figures.

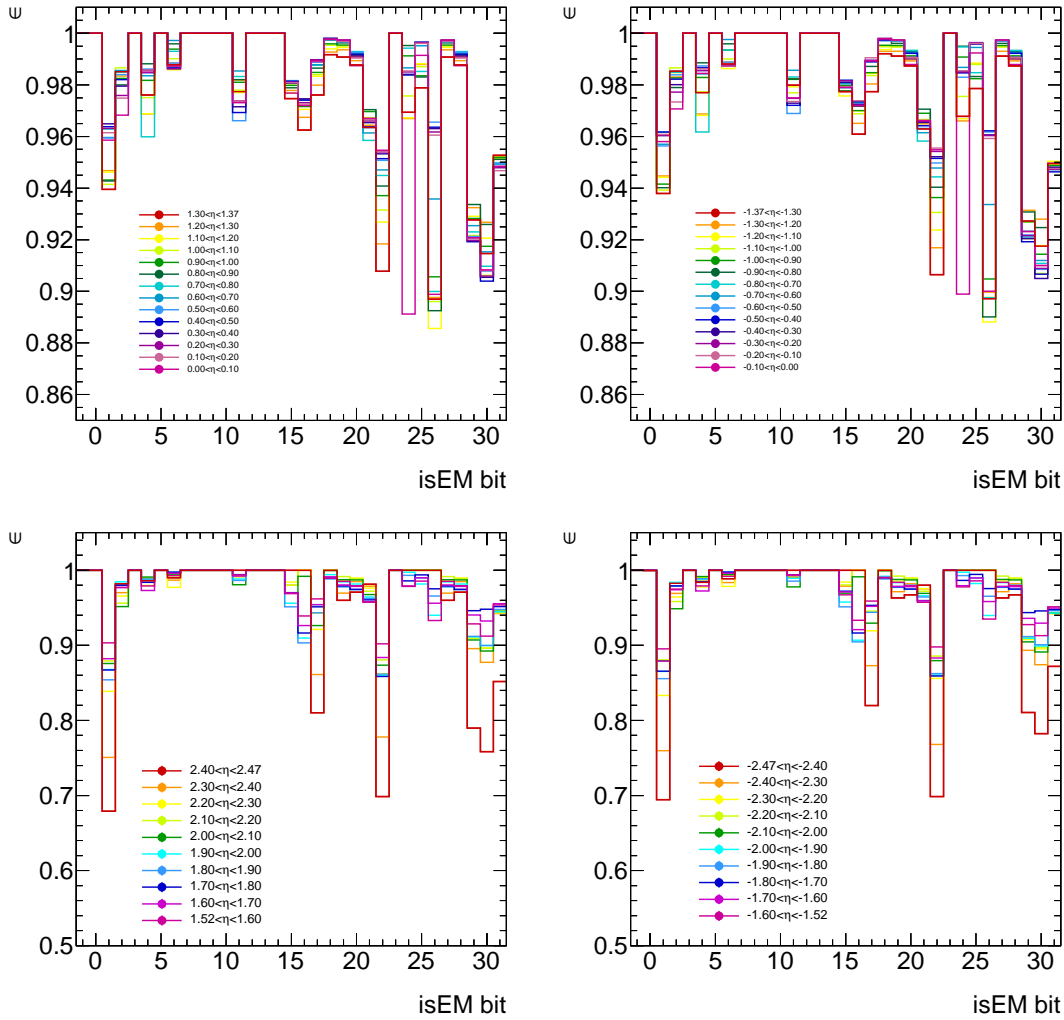


Figure 9.4: Measurement of the efficiency of individual identification requirements for PYTHIA Monte-Carlo for MediumPP cut values. Each number on the  $x$ -axis corresponds to a certain identification cut, the so-called isEM bit that is an arbitrary numbering scheme for the identification cuts that are listed in Table C.

close to the crack between the barrel and end-cap calorimeters. Also the very low  $E_T$  region seems to be rather difficult to model. The lowest scale-factors are obtained in  $20 < E_T < 25$  GeV. Here, major changes in the identification requirements are made. For higher transverse energies the scale-factors increase. Results based on  $J/\psi$  events show higher scale-factors for a transverse energy lower than 15 GeV.

The pattern seen in the scale-factors is mostly unrelated to the efficiencies. Apart from a general drop for low  $E_T$  the scale-factors seem to be mostly detector geometry dependent. This is likely to be caused by the amount of material that has to be traversed, as shown in Fig. 3.4. Especially in the end-cap region above  $\eta > 2.01$  the pattern of the scale-factors shown in Fig. 9.5 follow closely the material distribution.

## 9.4 Efficiencies and Scale-factors in Different $\eta$ Granularities

A general overview has been given in the previous sections. In the following the results are discussed in the context of their usage in physics analyses. Tables with the efficiencies, Monte-Carlo efficiencies and scale-factors for all identification criteria and  $\eta$  granularities are given in Appendix A together with the statistical and the systematic uncertainties estimated from the 80 variations. The systematic uncertainties listed in Chapter 8 are not included in these tables.

### 9.4.1 Coarse Binning

This granularity was used in the past for the  $1D \times 1D$  measurement, in the process of developing the double differential measurement and for systematic studies that are limited in their statistical precision. The results of the measurement are very different for neighbouring bins and the portability to other physics processes is not secured. Only processes with very similar distributions in  $\eta \times E_T$  could profit from the precision.

The results in this granularity really illustrates that the precision of the provided scale-factors is limited by the accuracy of the simulation and the requirement of neighbouring bins to overlap. There are no intentions to use these results.

### 9.4.2 Intermediate Binning

The medium granularity is intended for the majority of physics analyses that do not require a high precision in the electron sector. The finer granularity w.r.t. the coarse binning provides the portability to other physics processes. Although the aforementioned overlap between neighbouring bins is not observed over the full range it is believed that the residual differences are due to changes in the identification requirements or the detector geometry from one bin to another. The fine granularity follows a pattern that is very close to the one seen in this intermediate binning. It has lower statistical uncertainties compared to the fine binning. The scale-factors for MediumPP and TightPP identification criteria are listed in Tables 9.1 and 9.2 with their total (statistical and systematic) uncertainties, including also the systematic uncertainties for pile-up and modelling of charge effects described in Chapter 8.

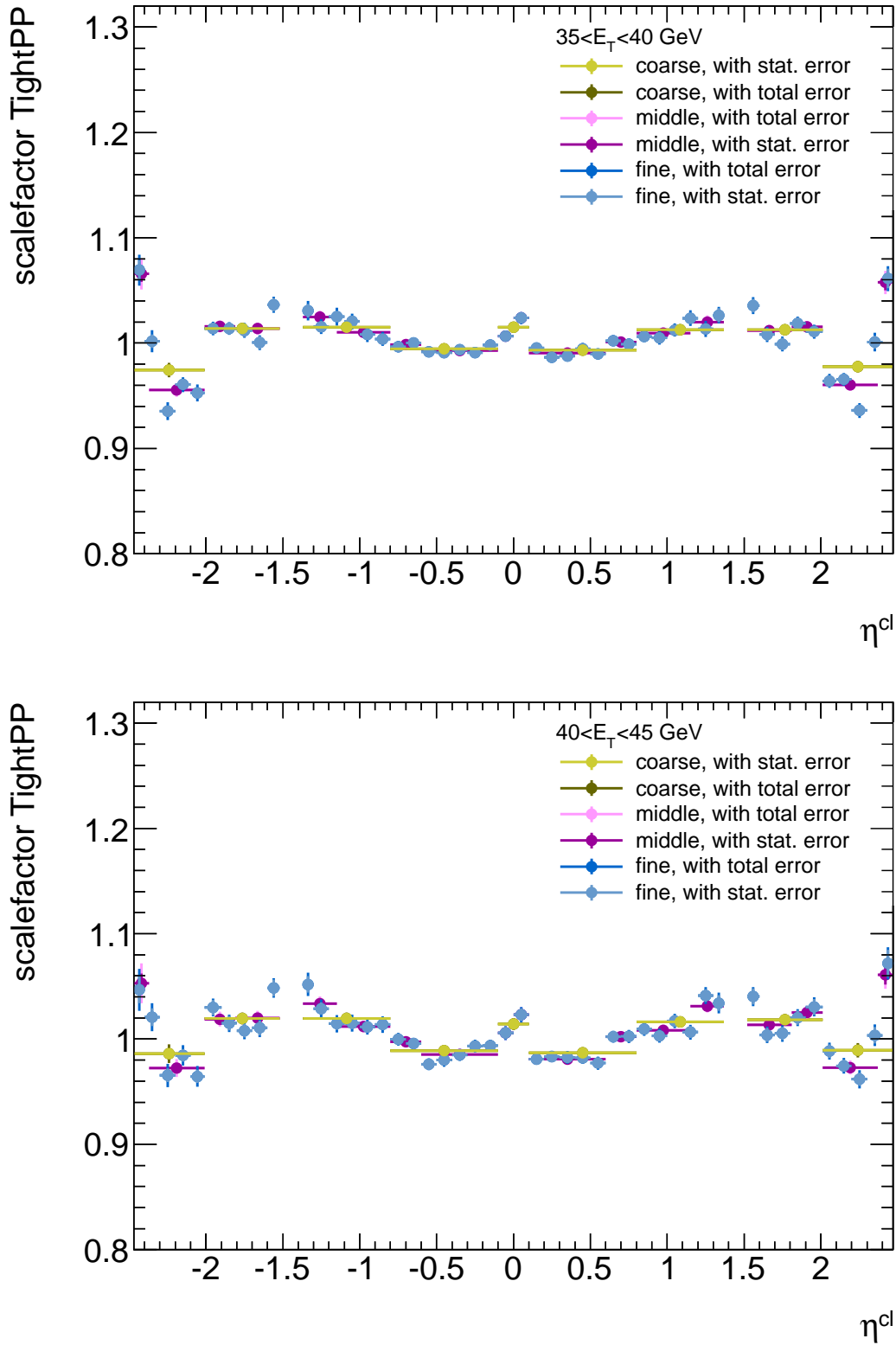


Figure 9.5: TightPP scale-factors measured in the  $E_T$  bins with highest statistical precision for three  $\eta$  granularities and for  $35 < E_T < 40$  GeV (top) and  $40 < E_T < 45$  GeV (bottom).

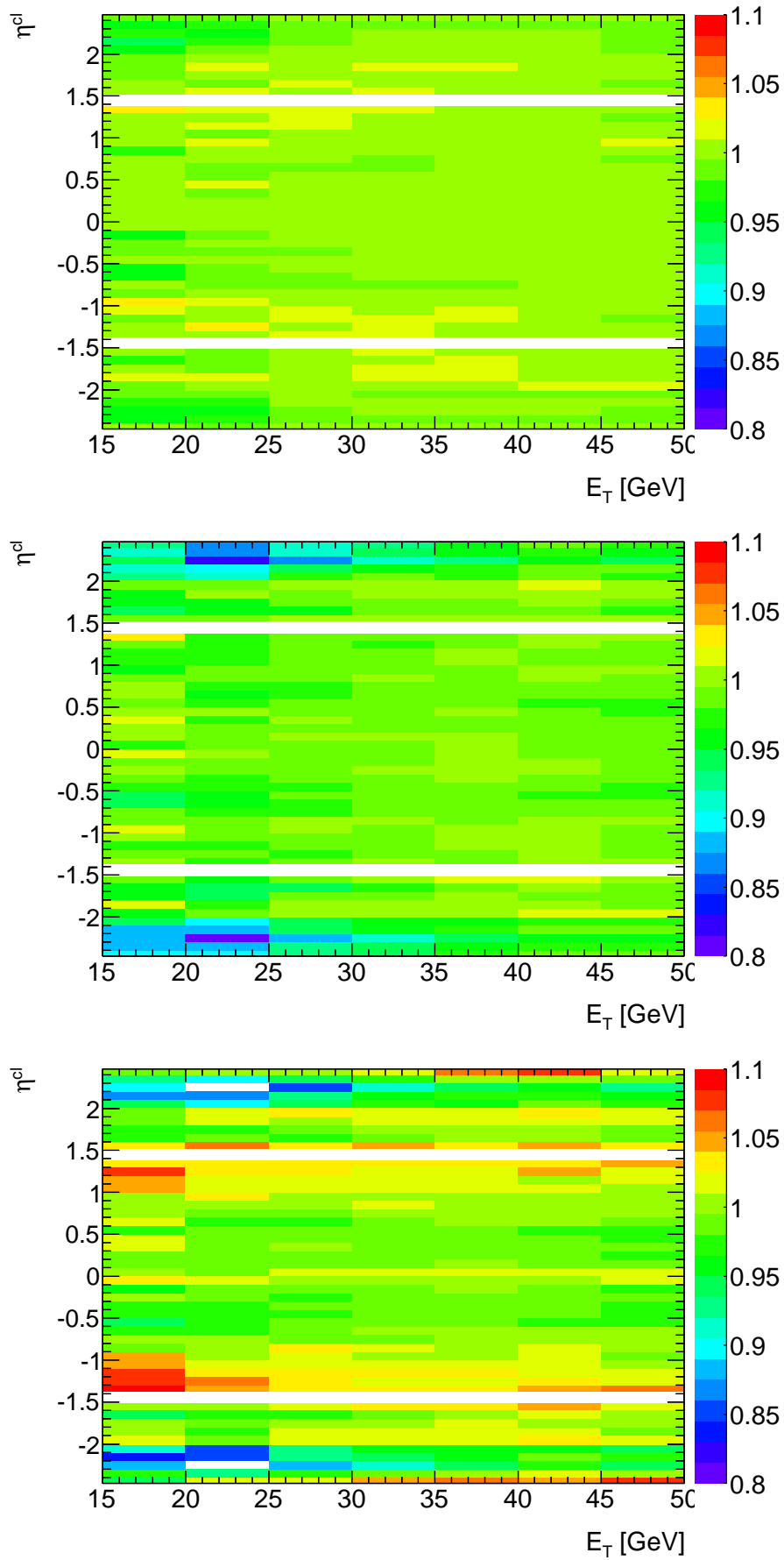


Figure 9.6: Scale-factors as a function of  $E_T$  and  $\eta$  for the fine granularity for LoosePP (top), MediumPP (middle) and TightPP (bottom). To allow for comparison, the colour scale is chosen to be the same in the three sub-figures.

	15-20 GeV	20-25 GeV	25-30 GeV	30-35 GeV	35-40 GeV	40-45 GeV	45-50 GeV
[-2.47, -2.37]	0.876 ± 0.045	0.894 ± 0.032	0.936 ± 0.019	0.948 ± 0.010	0.973 ± 0.007	0.988 ± 0.009	0.986 ± 0.019
[-2.37, -2.01]	0.909 ± 0.030	0.868 ± 0.022	0.923 ± 0.014	0.941 ± 0.007	0.955 ± 0.004	0.968 ± 0.005	0.965 ± 0.010
[-2.01, -1.81]	0.984 ± 0.034	0.988 ± 0.023	1.002 ± 0.014	1.001 ± 0.006	1.004 ± 0.004	1.004 ± 0.006	0.994 ± 0.012
[-1.81, -1.52]	0.968 ± 0.032	0.949 ± 0.018	0.973 ± 0.011	0.991 ± 0.006	1.002 ± 0.005	1.001 ± 0.005	0.987 ± 0.008
[-1.37, -1.15]	0.993 ± 0.031	0.981 ± 0.021	0.982 ± 0.011	0.991 ± 0.005	0.996 ± 0.004	0.999 ± 0.004	0.991 ± 0.008
[-1.15, -0.8]	0.989 ± 0.026	0.977 ± 0.017	0.997 ± 0.009	0.995 ± 0.004	0.998 ± 0.003	0.997 ± 0.004	0.994 ± 0.006
[-0.8, -0.6]	0.963 ± 0.025	0.969 ± 0.018	0.976 ± 0.010	0.986 ± 0.006	0.990 ± 0.003	0.992 ± 0.004	0.991 ± 0.006
[-0.6, -0.1]	0.972 ± 0.019	0.978 ± 0.017	0.989 ± 0.008	0.990 ± 0.004	0.995 ± 0.002	0.987 ± 0.003	0.982 ± 0.004
[-0.1, 0]	1.016 ± 0.032	1.000 ± 0.021	0.991 ± 0.010	0.986 ± 0.006	0.995 ± 0.004	0.985 ± 0.005	0.990 ± 0.008
[0, 0.1]	0.975 ± 0.034	0.988 ± 0.022	0.994 ± 0.011	0.988 ± 0.006	0.998 ± 0.004	0.994 ± 0.005	0.987 ± 0.007
[0.1, 0.6]	1.000 ± 0.022	0.985 ± 0.017	0.989 ± 0.008	0.992 ± 0.004	0.993 ± 0.002	0.984 ± 0.003	0.982 ± 0.004
[0.6, 0.8]	1.004 ± 0.031	0.971 ± 0.021	0.974 ± 0.011	0.987 ± 0.006	0.994 ± 0.003	0.994 ± 0.004	0.990 ± 0.006
[0.8, 1.15]	0.972 ± 0.029	0.975 ± 0.017	0.986 ± 0.009	0.992 ± 0.004	0.995 ± 0.003	0.993 ± 0.004	0.994 ± 0.006
[1.15, 1.37]	0.993 ± 0.032	0.970 ± 0.022	0.985 ± 0.012	0.984 ± 0.005	0.993 ± 0.004	1.000 ± 0.004	0.988 ± 0.007
[1.52, 1.81]	0.965 ± 0.027	0.973 ± 0.017	0.981 ± 0.010	0.995 ± 0.006	0.998 ± 0.005	0.998 ± 0.004	0.985 ± 0.008
[1.81, 2.01]	0.974 ± 0.034	0.996 ± 0.018	1.005 ± 0.014	1.002 ± 0.007	1.004 ± 0.004	1.010 ± 0.005	0.998 ± 0.011
[2.01, 2.37]	0.927 ± 0.028	0.876 ± 0.019	0.921 ± 0.014	0.949 ± 0.006	0.959 ± 0.003	0.972 ± 0.004	0.959 ± 0.009
[2.37, 2.47]	0.918 ± 0.041	0.876 ± 0.030	0.920 ± 0.014	0.941 ± 0.007	0.970 ± 0.005	0.989 ± 0.007	0.966 ± 0.012

Table 9.1: MediumPP scale-factors in intermediate  $\eta$  granularity with their total uncertainty, i.e. statistical and systematic uncertainty, where the systematic uncertainty includes the uncertainty from 80 variations, pile-up and charge.

	15-20 GeV	20-25 GeV	25-30 GeV	30-35 GeV	35-40 GeV	40-45 GeV	45-50 GeV
[-2.47, -2.37]	0.911 ± 0.090	0.989 ± 0.049	1.009 ± 0.027	1.032 ± 0.019	1.065 ± 0.015	1.053 ± 0.019	1.050 ± 0.037
[-2.37, -2.01]	0.902 ± 0.046	0.854 ± 0.029	0.919 ± 0.018	0.943 ± 0.009	0.955 ± 0.006	0.972 ± 0.008	0.954 ± 0.015
[-2.01, -1.81]	1.023 ± 0.065	0.987 ± 0.025	1.019 ± 0.017	1.016 ± 0.008	1.016 ± 0.005	1.018 ± 0.007	1.000 ± 0.015
[-1.81, -1.52]	0.977 ± 0.050	0.980 ± 0.022	0.992 ± 0.012	1.006 ± 0.007	1.014 ± 0.006	1.020 ± 0.007	1.001 ± 0.010
[-1.37, -1.15]	1.091 ± 0.041	1.046 ± 0.025	1.031 ± 0.013	1.030 ± 0.007	1.025 ± 0.005	1.033 ± 0.006	1.029 ± 0.012
[-1.15, -0.8]	1.029 ± 0.030	1.012 ± 0.019	1.018 ± 0.010	1.013 ± 0.006	1.010 ± 0.004	1.012 ± 0.005	1.003 ± 0.008
[-0.8, -0.6]	0.981 ± 0.032	0.979 ± 0.021	0.984 ± 0.011	0.995 ± 0.006	0.998 ± 0.004	0.997 ± 0.004	1.002 ± 0.007
[-0.6, -0.1]	0.970 ± 0.021	0.979 ± 0.018	0.984 ± 0.008	0.988 ± 0.004	0.993 ± 0.003	0.985 ± 0.004	0.978 ± 0.005
[-0.1, 0]	1.040 ± 0.042	1.009 ± 0.024	1.003 ± 0.015	1.002 ± 0.008	1.007 ± 0.005	1.006 ± 0.007	1.024 ± 0.012
[0, 0.1]	1.001 ± 0.039	0.995 ± 0.029	1.012 ± 0.015	1.011 ± 0.008	1.024 ± 0.006	1.023 ± 0.007	1.011 ± 0.012
[0.1, 0.6]	0.995 ± 0.022	0.989 ± 0.019	0.987 ± 0.009	0.985 ± 0.004	0.991 ± 0.003	0.981 ± 0.003	0.978 ± 0.005
[0.6, 0.8]	1.007 ± 0.031	0.979 ± 0.023	0.983 ± 0.013	0.994 ± 0.007	1.001 ± 0.004	1.002 ± 0.004	0.993 ± 0.007
[0.8, 1.15]	1.023 ± 0.037	1.013 ± 0.019	1.006 ± 0.009	1.008 ± 0.005	1.009 ± 0.003	1.008 ± 0.004	1.005 ± 0.007
[1.15, 1.37]	1.047 ± 0.044	1.021 ± 0.026	1.035 ± 0.013	1.024 ± 0.007	1.020 ± 0.005	1.031 ± 0.006	1.028 ± 0.010
[1.52, 1.81]	0.986 ± 0.032	1.006 ± 0.024	0.997 ± 0.014	1.011 ± 0.007	1.012 ± 0.006	1.013 ± 0.005	0.998 ± 0.010
[1.81, 2.01]	0.994 ± 0.040	1.017 ± 0.028	1.020 ± 0.019	1.015 ± 0.007	1.016 ± 0.005	1.025 ± 0.006	1.011 ± 0.013
[2.01, 2.37]	0.906 ± 0.040	0.860 ± 0.026	0.913 ± 0.017	0.950 ± 0.008	0.960 ± 0.005	0.973 ± 0.006	0.949 ± 0.013
[2.37, 2.47]	0.971 ± 0.065	0.985 ± 0.056	0.981 ± 0.023	1.021 ± 0.014	1.058 ± 0.012	1.061 ± 0.013	1.015 ± 0.024

Table 9.2: TightPP scale-factors in intermediate  $\eta$  granularity with their total uncertainty, i.e. statistical and systematic uncertainty, where the systematic uncertainty includes the uncertainty from 80 variations, pile-up and charge.

Considering the region of interest to Standard Model analyses – the single electron trigger limits the analyses to an electron transverse energy of  $E_T > 25$  GeV – sub-percent level has indeed been reached for MediumPP scale-factors. For the TightPP identification criterion this precision has been reached in most of the kinematic range. For analyses using the heavy gauge bosons this will definitely result in a sub-percent precision on final results. The use in events with multiple electrons will of course increase this uncertainty.

### 9.4.3 Fine Binning

The rich substructure of the electron efficiencies is only seen in the fine  $\eta$  granularity. It even reveals small variations of the efficiencies and scale-factors that beforehand were not expected to be that large. Of all granularities this one provides the most detailed knowledge of the efficiencies and scale-factors.

This granularity is particularly suitable for differential measurements that can make use of this substructure. Again, tables with scale-factors are presented in Tables 9.3 and 9.4 for MediumPP and TightPP criteria.

The increased total uncertainty w.r.t. the intermediate granularity is a consequence of the smaller statistical precision resulting from the finer granularity. The stochastic nature of the statistical uncertainties can be used to average out the impact of the statistical uncertainties as already discussed in Section 4.2.

The detailed treatment of statistical and systematic uncertainties to get a maximum of precision in a physics analysis is still under discussion. What is needed from the performance side is discussed in Section 9.6.

## 9.5 Systematic Uncertainty from Variations

The systematic uncertainties, that have been estimated by varying cut-flow, isolation threshold, template selection and discriminating variables, are decreasing with the increasing transverse energy of the probes. Appendix A lists all efficiencies on data and Monte-Carlo and scale-factors with the statistical and the systematic uncertainty from the variations. The variations of the different parameters are presented graphically for two specific  $\eta \times E_T$  bins in Fig. 9.7. The efficiency obtained using each of the 80 different configurations are plotted. All histograms within a row are identical in shape and each single plot is coloured for a particular parameter varied.

Especially in the low  $E_T$  bins – here as an example  $-0.80 < \eta < -0.10$  with  $15 < E_T < 20$  GeV is shown – a large amount of background needs to be subtracted. Therefore the systematic uncertainty is particularly large here. The largest contributions to the systematic uncertainty come from the variation of the background template and the discriminating variable. Interesting is that the isolation threshold that determines the normalisation of the background template has a relatively small effect. This is although a considerable amount of signal could be present in the control region as is seen in Fig. 6.1.

In the high  $E_T$  bin of  $35 < E_T < 40$  GeV the single largest contribution to the systematic uncertainty comes from the shape of the background templates. The impact

	15-20 GeV	20-25 GeV	25-30 GeV	30-35 GeV	35-40 GeV	40-45 GeV	45-50 GeV
[-2.47, -2.4]	0.893 ± 0.055	0.893 ± 0.033	0.933 ± 0.020	0.940 ± 0.009	0.968 ± 0.007	0.982 ± 0.009	0.990 ± 0.025
[-2.4, -2.3]	0.889 ± 0.051	0.881 ± 0.031	0.927 ± 0.018	0.945 ± 0.008	0.957 ± 0.006	0.974 ± 0.006	0.974 ± 0.014
[-2.3, -2.2]	0.886 ± 0.044	0.809 ± 0.026	0.887 ± 0.017	0.919 ± 0.008	0.943 ± 0.006	0.959 ± 0.006	0.954 ± 0.013
[-2.2, -2.1]	0.880 ± 0.039	0.875 ± 0.027	0.935 ± 0.016	0.956 ± 0.007	0.968 ± 0.004	0.987 ± 0.005	0.986 ± 0.014
[-2.1, -2.01]	0.946 ± 0.049	0.903 ± 0.029	0.942 ± 0.016	0.955 ± 0.008	0.957 ± 0.005	0.973 ± 0.006	0.968 ± 0.015
[-2.01, -1.9]	0.960 ± 0.040	0.992 ± 0.026	1.000 ± 0.016	1.000 ± 0.007	1.004 ± 0.005	1.013 ± 0.007	1.012 ± 0.017
[-1.9, -1.8]	1.024 ± 0.041	0.975 ± 0.024	0.995 ± 0.014	1.001 ± 0.007	1.003 ± 0.005	1.000 ± 0.006	0.984 ± 0.012
[-1.8, -1.7]	0.955 ± 0.043	0.949 ± 0.024	0.983 ± 0.015	0.994 ± 0.008	1.003 ± 0.006	0.994 ± 0.006	0.982 ± 0.011
[-1.7, -1.6]	0.954 ± 0.039	0.940 ± 0.023	0.947 ± 0.011	0.973 ± 0.008	0.992 ± 0.006	0.995 ± 0.007	0.982 ± 0.011
[-1.6, -1.52]	0.981 ± 0.045	0.959 ± 0.022	0.989 ± 0.014	1.001 ± 0.009	1.011 ± 0.006	1.016 ± 0.007	0.996 ± 0.011
[-1.37, -1.3]	1.007 ± 0.043	0.978 ± 0.027	0.992 ± 0.014	0.996 ± 0.007	0.994 ± 0.005	1.001 ± 0.005	0.999 ± 0.011
[-1.3, -1.2]	0.985 ± 0.039	0.990 ± 0.027	0.970 ± 0.013	0.986 ± 0.007	0.990 ± 0.005	0.995 ± 0.005	0.990 ± 0.008
[-1.2, -1.1]	0.979 ± 0.040	0.963 ± 0.024	0.991 ± 0.013	0.992 ± 0.007	1.003 ± 0.004	0.996 ± 0.005	0.989 ± 0.010
[-1.1, -1]	0.998 ± 0.043	0.983 ± 0.028	0.994 ± 0.013	0.994 ± 0.006	1.002 ± 0.004	0.996 ± 0.005	0.992 ± 0.009
[-1, -0.9]	1.008 ± 0.043	0.985 ± 0.028	1.001 ± 0.011	0.994 ± 0.005	1.002 ± 0.004	1.002 ± 0.005	0.991 ± 0.008
[-0.9, -0.8]	0.986 ± 0.032	0.981 ± 0.019	1.004 ± 0.011	0.999 ± 0.006	0.992 ± 0.004	1.002 ± 0.005	0.997 ± 0.008
[-0.8, -0.7]	0.984 ± 0.033	0.977 ± 0.022	0.977 ± 0.012	0.983 ± 0.007	0.989 ± 0.004	0.992 ± 0.005	0.992 ± 0.009
[-0.7, -0.6]	0.946 ± 0.030	0.964 ± 0.022	0.975 ± 0.012	0.989 ± 0.006	0.991 ± 0.003	0.991 ± 0.004	0.991 ± 0.007
[-0.6, -0.5]	0.937 ± 0.030	0.963 ± 0.020	0.989 ± 0.013	0.983 ± 0.006	0.989 ± 0.003	0.972 ± 0.005	0.974 ± 0.007
[-0.5, -0.4]	0.969 ± 0.031	0.974 ± 0.023	0.979 ± 0.011	0.990 ± 0.006	0.994 ± 0.004	0.982 ± 0.005	0.978 ± 0.008
[-0.4, -0.3]	0.987 ± 0.028	0.974 ± 0.024	0.994 ± 0.011	0.993 ± 0.005	0.995 ± 0.004	0.987 ± 0.004	0.990 ± 0.007
[-0.3, -0.2]	0.995 ± 0.026	0.991 ± 0.019	0.989 ± 0.011	0.995 ± 0.005	0.997 ± 0.004	0.997 ± 0.004	0.982 ± 0.007
[-0.2, -0.1]	0.980 ± 0.031	0.988 ± 0.025	0.994 ± 0.010	0.990 ± 0.005	1.002 ± 0.003	0.996 ± 0.004	0.987 ± 0.007
[-0.1, 0]	1.016 ± 0.032	1.000 ± 0.021	0.991 ± 0.011	0.986 ± 0.006	0.995 ± 0.004	0.985 ± 0.005	0.990 ± 0.008
[0, 0.1]	0.975 ± 0.031	0.988 ± 0.023	0.994 ± 0.011	0.988 ± 0.006	0.998 ± 0.004	0.994 ± 0.005	0.987 ± 0.007
[0.1, 0.2]	1.002 ± 0.035	0.995 ± 0.025	0.996 ± 0.011	0.997 ± 0.006	1.002 ± 0.003	0.990 ± 0.004	0.985 ± 0.007
[0.2, 0.3]	1.002 ± 0.030	0.990 ± 0.019	0.983 ± 0.011	0.991 ± 0.005	0.995 ± 0.004	0.990 ± 0.004	0.986 ± 0.008
[0.3, 0.4]	1.016 ± 0.031	0.980 ± 0.027	0.999 ± 0.012	0.991 ± 0.005	0.993 ± 0.004	0.988 ± 0.004	0.992 ± 0.007
[0.4, 0.5]	1.000 ± 0.037	0.998 ± 0.025	0.985 ± 0.011	0.990 ± 0.006	0.995 ± 0.004	0.982 ± 0.004	0.977 ± 0.008
[0.5, 0.6]	0.986 ± 0.033	0.966 ± 0.021	0.986 ± 0.013	0.989 ± 0.006	0.984 ± 0.003	0.969 ± 0.004	0.970 ± 0.007
[0.6, 0.7]	1.002 ± 0.035	0.965 ± 0.025	0.970 ± 0.013	0.987 ± 0.007	0.994 ± 0.004	0.993 ± 0.004	0.993 ± 0.007
[0.7, 0.8]	1.007 ± 0.036	0.979 ± 0.024	0.978 ± 0.013	0.986 ± 0.007	0.993 ± 0.004	0.995 ± 0.005	0.988 ± 0.009
[0.8, 0.9]	0.986 ± 0.038	0.982 ± 0.018	0.992 ± 0.011	1.001 ± 0.007	0.994 ± 0.004	0.995 ± 0.005	0.987 ± 0.008
[0.9, 1]	0.963 ± 0.039	0.987 ± 0.028	0.992 ± 0.011	0.992 ± 0.006	0.994 ± 0.004	0.999 ± 0.005	1.007 ± 0.008
[1, 1.1]	0.976 ± 0.044	0.966 ± 0.027	0.983 ± 0.013	0.992 ± 0.006	0.999 ± 0.004	0.993 ± 0.005	0.991 ± 0.009
[1.1, 1.2]	0.970 ± 0.040	0.971 ± 0.023	0.991 ± 0.014	0.983 ± 0.007	0.998 ± 0.005	0.991 ± 0.005	0.990 ± 0.011
[1.2, 1.3]	0.983 ± 0.043	0.966 ± 0.026	0.979 ± 0.014	0.979 ± 0.007	0.990 ± 0.005	1.001 ± 0.005	0.981 ± 0.009
[1.3, 1.37]	1.027 ± 0.047	0.978 ± 0.029	0.985 ± 0.014	0.991 ± 0.008	0.990 ± 0.005	0.999 ± 0.006	0.999 ± 0.010
[1.52, 1.6]	0.990 ± 0.048	0.994 ± 0.024	0.996 ± 0.014	1.005 ± 0.008	1.009 ± 0.006	1.010 ± 0.006	0.999 ± 0.011
[1.6, 1.7]	0.947 ± 0.040	0.956 ± 0.025	0.964 ± 0.012	0.980 ± 0.008	0.993 ± 0.006	0.990 ± 0.005	0.974 ± 0.011
[1.7, 1.8]	0.963 ± 0.040	0.957 ± 0.023	0.984 ± 0.015	0.993 ± 0.007	0.993 ± 0.006	0.997 ± 0.005	0.981 ± 0.012
[1.8, 1.9]	0.950 ± 0.042	1.006 ± 0.021	0.993 ± 0.014	1.005 ± 0.008	1.006 ± 0.004	1.006 ± 0.006	1.004 ± 0.011
[1.9, 2.01]	0.988 ± 0.047	0.987 ± 0.025	1.008 ± 0.018	1.000 ± 0.008	1.001 ± 0.004	1.013 ± 0.006	1.000 ± 0.014
[2.01, 2.1]	0.924 ± 0.041	0.909 ± 0.022	0.966 ± 0.019	0.980 ± 0.006	0.971 ± 0.004	0.984 ± 0.005	0.971 ± 0.013
[2.1, 2.2]	0.911 ± 0.040	0.892 ± 0.025	0.941 ± 0.015	0.964 ± 0.006	0.973 ± 0.004	0.990 ± 0.005	0.983 ± 0.013
[2.2, 2.3]	0.934 ± 0.041	0.822 ± 0.025	0.864 ± 0.015	0.918 ± 0.007	0.934 ± 0.004	0.961 ± 0.005	0.945 ± 0.012
[2.3, 2.4]	0.916 ± 0.050	0.872 ± 0.031	0.914 ± 0.016	0.944 ± 0.008	0.962 ± 0.005	0.972 ± 0.006	0.955 ± 0.013
[2.4, 2.47]	0.930 ± 0.049	0.869 ± 0.031	0.914 ± 0.014	0.932 ± 0.008	0.962 ± 0.006	0.987 ± 0.008	0.971 ± 0.017

Table 9.3: MediumPP scale-factors in fine  $\eta$  granularity with their total uncertainty, i.e. statistical and systematic uncertainty, where the systematic uncertainty includes the uncertainty from 80 variations, pile-up and charge.

	15-20 GeV	20-25 GeV	25-30 GeV	30-35 GeV	35-40 GeV	40-45 GeV	45-50 GeV
[-2.47, -2.4]	0.941 ± 0.084	1.013 ± 0.052	1.015 ± 0.029	1.040 ± 0.019	1.069 ± 0.015	1.047 ± 0.020	1.076 ± 0.045
[-2.4, -2.3]	0.977 ± 0.076	0.931 ± 0.043	0.966 ± 0.024	0.984 ± 0.015	1.002 ± 0.010	1.021 ± 0.013	1.000 ± 0.025
[-2.3, -2.2]	0.878 ± 0.055	0.793 ± 0.035	0.877 ± 0.022	0.917 ± 0.012	0.935 ± 0.008	0.965 ± 0.011	0.944 ± 0.020
[-2.2, -2.1]	0.834 ± 0.045	0.851 ± 0.033	0.920 ± 0.019	0.949 ± 0.011	0.961 ± 0.007	0.984 ± 0.009	0.969 ± 0.021
[-2.1, -2.01]	0.918 ± 0.056	0.858 ± 0.035	0.930 ± 0.021	0.951 ± 0.012	0.953 ± 0.008	0.964 ± 0.010	0.942 ± 0.021
[-2.01, -1.9]	1.018 ± 0.068	0.990 ± 0.031	1.017 ± 0.021	1.016 ± 0.009	1.014 ± 0.006	1.030 ± 0.008	1.021 ± 0.020
[-1.9, -1.8]	1.007 ± 0.064	0.970 ± 0.029	1.014 ± 0.018	1.015 ± 0.009	1.014 ± 0.006	1.015 ± 0.008	0.993 ± 0.015
[-1.8, -1.7]	1.001 ± 0.063	0.979 ± 0.029	0.995 ± 0.019	1.003 ± 0.010	1.012 ± 0.007	1.007 ± 0.008	1.001 ± 0.015
[-1.7, -1.6]	0.946 ± 0.059	0.968 ± 0.029	0.965 ± 0.014	0.983 ± 0.009	1.000 ± 0.007	1.010 ± 0.009	0.996 ± 0.014
[-1.6, -1.52]	0.999 ± 0.068	1.000 ± 0.031	1.016 ± 0.016	1.031 ± 0.010	1.036 ± 0.008	1.048 ± 0.009	1.011 ± 0.013
[-1.37, -1.3]	1.116 ± 0.062	1.047 ± 0.035	1.029 ± 0.018	1.039 ± 0.012	1.031 ± 0.009	1.051 ± 0.010	1.055 ± 0.020
[-1.3, -1.2]	1.082 ± 0.051	1.067 ± 0.034	1.033 ± 0.018	1.022 ± 0.010	1.016 ± 0.007	1.029 ± 0.008	1.023 ± 0.016
[-1.2, -1.1]	1.079 ± 0.055	1.029 ± 0.030	1.028 ± 0.016	1.026 ± 0.010	1.025 ± 0.007	1.014 ± 0.008	1.018 ± 0.015
[-1.1, -1]	1.046 ± 0.049	1.019 ± 0.031	1.013 ± 0.015	1.022 ± 0.009	1.021 ± 0.006	1.015 ± 0.008	1.002 ± 0.014
[-1, -0.9]	1.047 ± 0.050	1.003 ± 0.032	1.016 ± 0.015	1.004 ± 0.008	1.008 ± 0.006	1.011 ± 0.007	0.993 ± 0.012
[-0.9, -0.8]	0.990 ± 0.037	1.005 ± 0.022	1.026 ± 0.014	1.014 ± 0.009	1.004 ± 0.006	1.014 ± 0.008	1.001 ± 0.012
[-0.8, -0.7]	0.994 ± 0.039	0.998 ± 0.025	0.985 ± 0.013	0.991 ± 0.008	0.997 ± 0.005	1.000 ± 0.006	1.009 ± 0.011
[-0.7, -0.6]	0.969 ± 0.038	0.966 ± 0.024	0.982 ± 0.013	0.997 ± 0.007	1.000 ± 0.004	0.996 ± 0.005	0.995 ± 0.009
[-0.6, -0.5]	0.940 ± 0.034	0.975 ± 0.022	0.987 ± 0.014	0.988 ± 0.007	0.992 ± 0.004	0.976 ± 0.006	0.979 ± 0.009
[-0.5, -0.4]	0.975 ± 0.035	0.971 ± 0.024	0.979 ± 0.012	0.993 ± 0.007	0.991 ± 0.004	0.980 ± 0.005	0.973 ± 0.009
[-0.4, -0.3]	0.978 ± 0.032	0.976 ± 0.026	0.987 ± 0.012	0.988 ± 0.006	0.994 ± 0.004	0.985 ± 0.006	0.978 ± 0.009
[-0.3, -0.2]	1.002 ± 0.031	0.991 ± 0.020	0.980 ± 0.011	0.990 ± 0.006	0.991 ± 0.004	0.993 ± 0.006	0.984 ± 0.009
[-0.2, -0.1]	0.957 ± 0.035	0.984 ± 0.027	0.991 ± 0.011	0.983 ± 0.006	0.998 ± 0.004	0.994 ± 0.006	0.978 ± 0.008
[-0.1, 0]	1.040 ± 0.039	1.009 ± 0.024	1.003 ± 0.015	1.002 ± 0.008	1.007 ± 0.005	1.006 ± 0.007	1.024 ± 0.012
[0, 0.1]	1.001 ± 0.043	0.995 ± 0.031	1.012 ± 0.016	1.011 ± 0.008	1.024 ± 0.006	1.023 ± 0.007	1.011 ± 0.012
[0.1, 0.2]	0.982 ± 0.040	0.993 ± 0.029	0.988 ± 0.014	0.985 ± 0.006	0.996 ± 0.004	0.981 ± 0.005	0.983 ± 0.010
[0.2, 0.3]	0.983 ± 0.035	0.988 ± 0.025	0.982 ± 0.014	0.982 ± 0.006	0.987 ± 0.004	0.983 ± 0.005	0.974 ± 0.009
[0.3, 0.4]	1.023 ± 0.039	0.991 ± 0.032	0.995 ± 0.015	0.985 ± 0.006	0.988 ± 0.004	0.982 ± 0.005	0.983 ± 0.009
[0.4, 0.5]	1.014 ± 0.043	0.992 ± 0.030	0.984 ± 0.014	0.990 ± 0.007	0.994 ± 0.005	0.982 ± 0.005	0.978 ± 0.010
[0.5, 0.6]	0.978 ± 0.038	0.985 ± 0.027	0.987 ± 0.016	0.985 ± 0.008	0.990 ± 0.004	0.977 ± 0.006	0.974 ± 0.009
[0.6, 0.7]	1.010 ± 0.041	0.971 ± 0.029	0.977 ± 0.016	0.994 ± 0.008	1.002 ± 0.005	1.002 ± 0.005	0.991 ± 0.009
[0.7, 0.8]	1.010 ± 0.043	0.990 ± 0.031	0.991 ± 0.017	0.995 ± 0.008	0.999 ± 0.005	1.002 ± 0.006	0.995 ± 0.010
[0.8, 0.9]	1.004 ± 0.044	0.997 ± 0.022	1.002 ± 0.013	1.020 ± 0.008	1.006 ± 0.005	1.009 ± 0.006	0.998 ± 0.010
[0.9, 1]	1.003 ± 0.046	1.027 ± 0.032	1.009 ± 0.013	0.997 ± 0.007	1.005 ± 0.005	1.003 ± 0.006	1.005 ± 0.010
[1, 1.1]	1.044 ± 0.055	1.018 ± 0.033	1.013 ± 0.015	1.010 ± 0.008	1.012 ± 0.005	1.017 ± 0.007	1.005 ± 0.012
[1.1, 1.2]	1.043 ± 0.051	1.015 ± 0.028	1.023 ± 0.016	1.015 ± 0.008	1.024 ± 0.006	1.006 ± 0.007	1.024 ± 0.014
[1.2, 1.3]	1.076 ± 0.057	1.027 ± 0.032	1.036 ± 0.017	1.023 ± 0.009	1.013 ± 0.006	1.041 ± 0.008	1.021 ± 0.013
[1.3, 1.37]	1.038 ± 0.060	1.027 ± 0.037	1.036 ± 0.020	1.030 ± 0.010	1.026 ± 0.007	1.034 ± 0.008	1.045 ± 0.016
[1.52, 1.6]	1.025 ± 0.054	1.062 ± 0.029	1.028 ± 0.017	1.040 ± 0.010	1.035 ± 0.008	1.040 ± 0.009	1.032 ± 0.014
[1.6, 1.7]	0.971 ± 0.050	0.979 ± 0.029	0.976 ± 0.015	0.990 ± 0.010	1.008 ± 0.008	1.004 ± 0.008	0.981 ± 0.014
[1.7, 1.8]	0.968 ± 0.048	0.968 ± 0.028	0.992 ± 0.019	0.996 ± 0.009	0.999 ± 0.008	1.005 ± 0.007	0.984 ± 0.016
[1.8, 1.9]	0.993 ± 0.052	1.021 ± 0.027	1.000 ± 0.017	1.020 ± 0.009	1.019 ± 0.006	1.020 ± 0.008	1.015 ± 0.015
[1.9, 2.01]	0.987 ± 0.050	1.015 ± 0.031	1.028 ± 0.021	1.013 ± 0.009	1.011 ± 0.007	1.030 ± 0.009	1.018 ± 0.018
[2.01, 2.1]	0.935 ± 0.053	0.899 ± 0.028	0.947 ± 0.022	0.973 ± 0.009	0.964 ± 0.006	0.988 ± 0.008	0.968 ± 0.017
[2.1, 2.2]	0.873 ± 0.051	0.873 ± 0.034	0.922 ± 0.017	0.960 ± 0.009	0.966 ± 0.006	0.974 ± 0.007	0.954 ± 0.016
[2.2, 2.3]	0.892 ± 0.058	0.785 ± 0.034	0.847 ± 0.020	0.919 ± 0.010	0.936 ± 0.007	0.962 ± 0.008	0.932 ± 0.016
[2.3, 2.4]	0.923 ± 0.071	0.897 ± 0.051	0.946 ± 0.024	0.972 ± 0.012	1.001 ± 0.009	1.003 ± 0.010	0.987 ± 0.023
[2.4, 2.47]	0.990 ± 0.079	1.002 ± 0.055	0.997 ± 0.025	1.023 ± 0.014	1.062 ± 0.013	1.072 ± 0.015	1.013 ± 0.029

Table 9.4: TightPP scale-factors in fine  $\eta$  granularity with their total uncertainty, i.e. statistical and systematic uncertainty, where the systematic uncertainty includes the uncertainty from 80 variations, pile-up and charge.

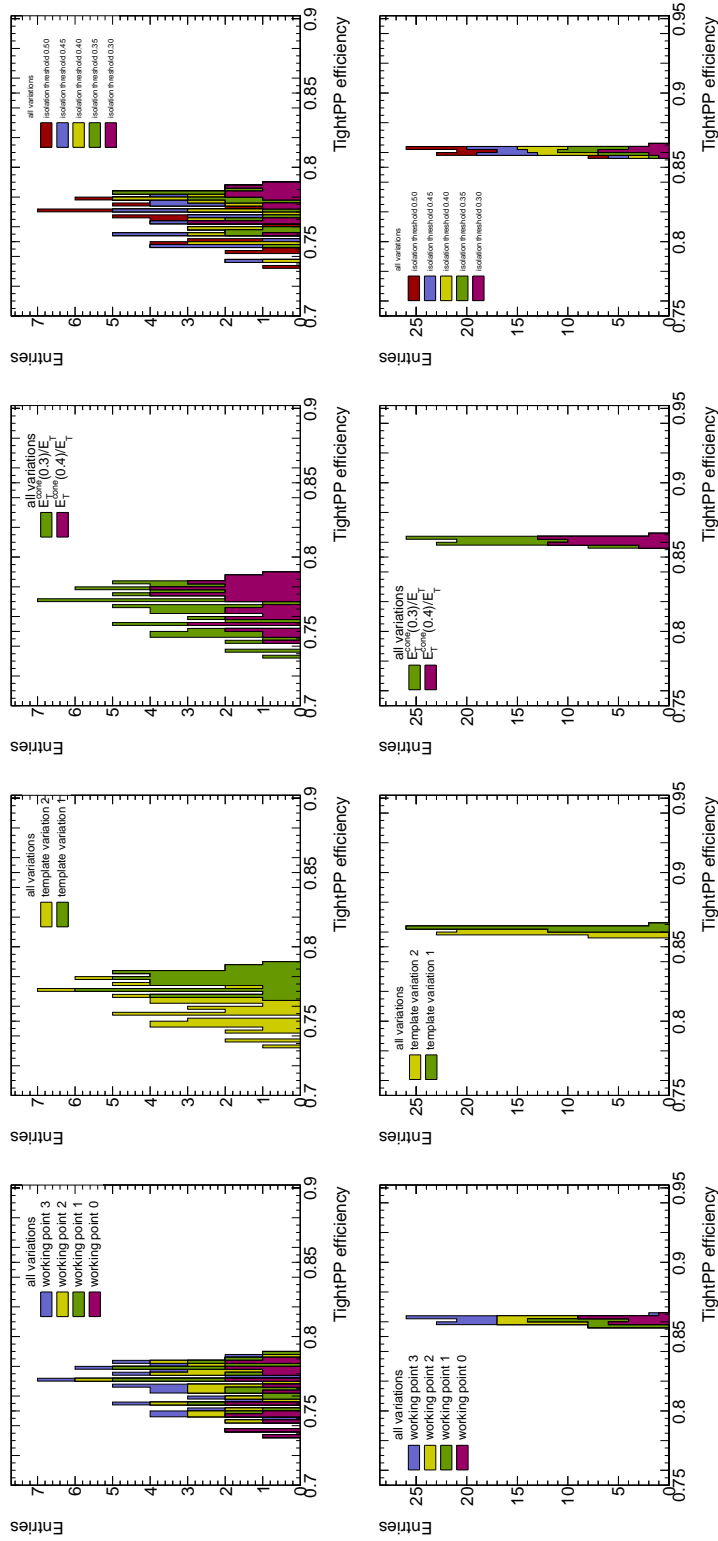


Figure 9.7: Distributions of the efficiency values obtained for the 80 different systematic variations for two selected  $\eta \times E_T$  bins. From left to right: working points, templates, discriminating variables and isolation thresholds. The different  $\eta \times E_T$  bins are:

$-0.80 < \eta < -0.10$  with  $15 < E_T < 20$  GeV (top),

$-0.80 < \eta < -0.10$  with  $35 < E_T < 40$  GeV (bottom).

of the systematic variations of the cut-flow, discriminating variable and the isolation threshold is only minor.

## 9.6 Systematic Correlations Between the Different Bins

The precision of the measurement has been shown to be limited by the prerequisite of providing portability to other physics process. Neighbouring bins are supposed to overlap within their uncertainty. In order to reach a maximum of precision, scale-factors are provided in a very fine granularity in  $\eta$  which leads to higher uncertainties. Still, this fine granularity can provide a very high precision if the uncertainties of the scale-factors are treated accurately.

The different treatment of statistical and systematic uncertainties has already been mentioned in Section 4.2. Improvement on the systematic uncertainties can be reached by considering the systematic correlations between scale-factors in different bins. Therefore, the correlation  $\rho_{x,y}$  between the  $\eta \times E_T$  bins  $x$  and  $y$  is calculated with

$$\rho_{x,y} = \frac{\sum_{i=1}^{80} (\varepsilon_i(x) - \bar{\varepsilon}(x)) (\varepsilon_i(y) - \bar{\varepsilon}(y))}{\sqrt{\sum_{i=1}^{80} (\varepsilon_i(x) - \bar{\varepsilon}(x))^2} \sqrt{\sum_{i=1}^{80} (\varepsilon_i(y) - \bar{\varepsilon}(y))^2}} \quad (9.2)$$

where the sums run over the 80 systematic variations  $i$ . A matrix of all correlations is shown for TightPP scale-factors in Fig. 9.8. The correlation is positive over a large range with a few exceptions in the end-caps, especially in the very low  $E_T$  region.

In addition, the data efficiencies in positive and negative  $\eta$  hemispheres are *statistically* correlated, since they use identical templates. The same applies for the end-cap bins, where one template is used repeatedly. Especially in the lowest  $E_T$  bin, the statistical uncertainty on the background templates has a large contribution to the total statistical uncertainty.

However, there are no plans to provide a matrix of the statistical correlations to the physics analyses. The correlation is always positive. The typical treatment of statistical uncertainties in physics analyses therefore underestimates the uncertainty. It assumes no statistical correlation. The statistical correlation coefficients are found to be of the order of 0.05 and rarely exceeding this value. A faulty estimation of the uncertainties is therefore acceptable. Nevertheless, this is a point where further improvements could be made.

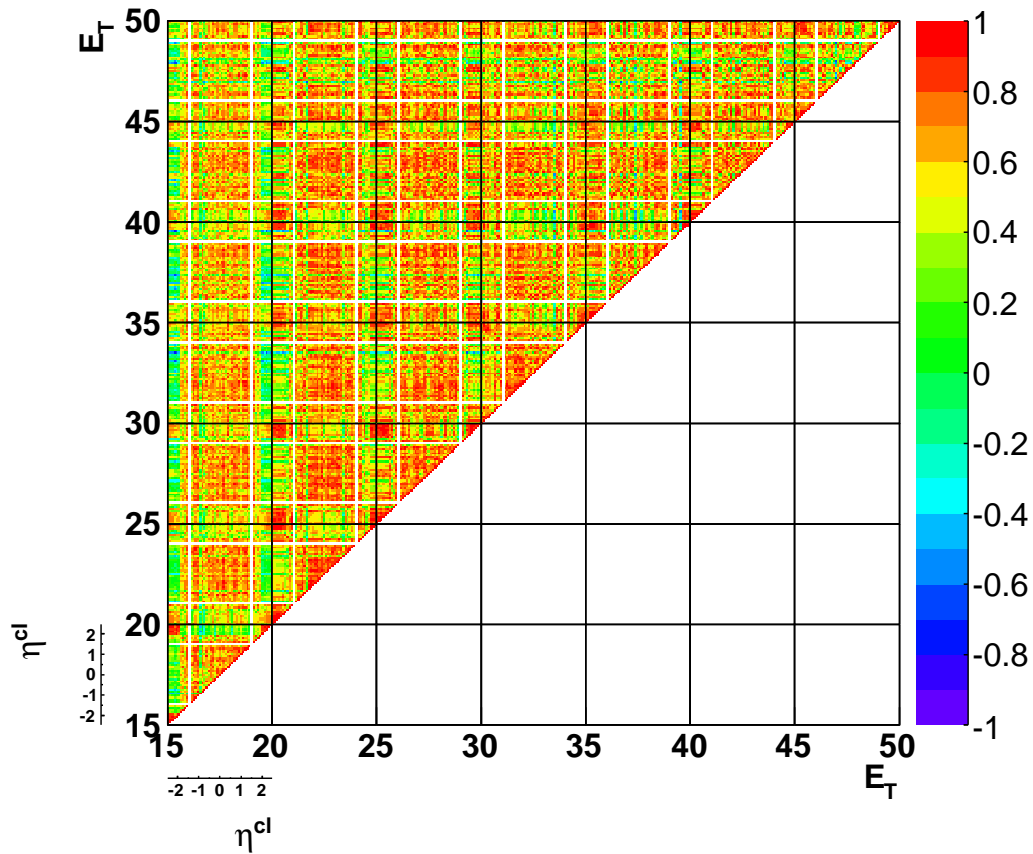


Figure 9.8: Correlation coefficients between all bins for TightPP scale-factors in fine  $\eta$  granularity. The large squares separate the different  $E_T$  bins, each square shows the  $\eta$  range from  $-2.47 < \eta < 2.47$ .



---

In this thesis, the efficiency of the electron identification at the ATLAS detector has been measured. With the full dataset recorded in 2011, corresponding to an integrated luminosity of  $4.7 \text{ fb}^{-1}$ , the measurements could – for the first time – be performed double-differentially in  $E_T$  and  $\eta$ . A tag-and-probe technique was used to obtain a sample of electrons from the decay of  $W$  bosons. Together with detailed studies on Monte-Carlo and a cut optimisation, the amount of data allowed for a finer binning than before. The requirement that the efficiencies should be applicable to other physics processes, necessitates the differential measurement and the finer binning.

The efficiencies are obtained for data and Monte-Carlo. Scale-factors are calculated and provided to analysis groups. The fact that the scale-factors are very close to unity is evidence of the outstanding simulation and excellent understanding of the detector in the identification related variables.

As statistical uncertainties decreased, systematic effects became dominant. To avoid biases, the analysis was critically reassessed. Improvements have been made in the estimation of background, in the estimation of the systematic uncertainty and in particular in the matching of the simulation to conditions in data. Residual effects have been identified, estimated and a systematic uncertainty has been added to account for the effects. Most notably, the measurement was found to be sensitive to effects from pileup and the modelling of the  $W$  charge asymmetry and charge misidentification. These effects were studied for the first time in detail in this thesis.

The challenge of achieving sub-percent precision, needed for Standard Model precision analyses, has been mastered. The efficiency values and scale-factors are provided in a fine binning in  $E_T$  and  $\eta$ , together with the information about the correlations between different bins, will provide ultimate precision. This fine binning unveiled a rich substructure of the efficiencies in the different detector regions.

The results of this thesis have already contributed significantly to several Standard Model analyses and provided an important ingredient to reduce systematic uncertainties in precision measurements of the ATLAS collaboration. The methods developed within this thesis will also constitute the basis for updated future measurements with even higher precision.



# A Tables of Efficiencies and Scalefactors

	15-20 GeV	20-25 GeV	25-30 GeV	30-35 GeV	35-40 GeV	40-45 GeV	45-50 GeV
$[-2.47, -2.01]$	$5589 \pm 98$	$20162 \pm 185$	$55506 \pm 295$	$118603 \pm 409$	$176277 \pm 466$	$92701 \pm 388$	$27686 \pm 260$
$[-2.01, -1.52]$	$6478 \pm 104$	$22725 \pm 196$	$59266 \pm 300$	$120885 \pm 402$	$164005 \pm 448$	$90281 \pm 385$	$28715 \pm 253$
$[-1.37, -0.8]$	$7159 \pm 102$	$21074 \pm 186$	$56687 \pm 284$	$126731 \pm 395$	$195436 \pm 469$	$115135 \pm 377$	$36251 \pm 243$
$[-0.8, -0.1]$	$10576 \pm 124$	$33466 \pm 236$	$86782 \pm 355$	$187917 \pm 480$	$292870 \pm 578$	$171502 \pm 462$	$52663 \pm 299$
$[-0.1, 0.1]$	$2928 \pm 67$	$8904 \pm 122$	$23297 \pm 182$	$50582 \pm 242$	$78215 \pm 299$	$44985 \pm 235$	$13921 \pm 141$
$[0.1, 0.8]$	$10461 \pm 125$	$33042 \pm 237$	$87005 \pm 358$	$187373 \pm 483$	$292334 \pm 578$	$170706 \pm 461$	$52781 \pm 299$
$[0.8, 1.37]$	$7421 \pm 104$	$21794 \pm 190$	$58980 \pm 288$	$130071 \pm 401$	$197680 \pm 473$	$115705 \pm 383$	$36447 \pm 255$
$[1.52, 2.01]$	$6341 \pm 101$	$21537 \pm 196$	$57240 \pm 299$	$117604 \pm 405$	$161728 \pm 440$	$87301 \pm 381$	$27910 \pm 262$
$[2.01, 2.47]$	$5525 \pm 94$	$19772 \pm 180$	$53803 \pm 283$	$116312 \pm 394$	$173010 \pm 453$	$91409 \pm 369$	$27571 \pm 245$

Table A.1: Number of background subtracted signal events on container level for one specific setting. The uncertainties are statistical only.

	15-20 GeV	20-25 GeV	25-30 GeV	30-35 GeV	35-40 GeV	40-45 GeV	45-50 GeV
$[-2.47, -2.01]$	$1140 \pm 54$	$3157 \pm 105$	$4753 \pm 164$	$4890 \pm 209$	$3815 \pm 194$	$3182 \pm 235$	$2243 \pm 194$
$[-2.01, -1.52]$	$1175 \pm 55$	$3379 \pm 111$	$4675 \pm 161$	$4410 \pm 191$	$3540 \pm 182$	$3182 \pm 234$	$2069 \pm 183$
$[-1.37, -0.8]$	$1340 \pm 44$	$3970 \pm 97$	$5374 \pm 136$	$5115 \pm 154$	$3985 \pm 142$	$3471 \pm 153$	$2638 \pm 143$
$[-0.8, -0.1]$	$2069 \pm 53$	$6662 \pm 124$	$8757 \pm 174$	$7728 \pm 186$	$6413 \pm 186$	$5547 \pm 190$	$4408 \pm 180$
$[-0.1, 0.1]$	$604 \pm 30$	$1719 \pm 65$	$2147 \pm 88$	$1651 \pm 79$	$1591 \pm 97$	$1304 \pm 95$	$843 \pm 71$
$[0.1, 0.8]$	$2183 \pm 55$	$6901 \pm 128$	$9123 \pm 180$	$8159 \pm 194$	$6572 \pm 189$	$5525 \pm 189$	$4378 \pm 179$
$[0.8, 1.37]$	$1369 \pm 44$	$4150 \pm 101$	$5427 \pm 137$	$5332 \pm 159$	$4189 \pm 148$	$3873 \pm 166$	$3092 \pm 160$
$[1.52, 2.01]$	$1106 \pm 52$	$3533 \pm 116$	$4817 \pm 165$	$4757 \pm 204$	$3247 \pm 170$	$3175 \pm 234$	$2263 \pm 196$
$[2.01, 2.47]$	$1006 \pm 48$	$2935 \pm 99$	$4206 \pm 148$	$4265 \pm 187$	$3247 \pm 170$	$2688 \pm 205$	$1962 \pm 174$

Table A.2: Number of background events in the signal region on container level in the signal region for one specific setting. The uncertainties are statistical only.

	15-20 GeV	20-25 GeV	25-30 GeV	30-35 GeV	35-40 GeV	40-45 GeV	45-50 GeV
$[-2.47, -2.01]$	4.9	6.4	11.7	24.3	46.2	29.1	12.3
$[-2.01, -1.52]$	5.5	6.7	12.7	27.4	46.3	28.4	13.9
$[-1.37, -0.8]$	5.3	5.3	10.5	24.8	49.0	33.2	13.7
$[-0.8, -0.1]$	5.1	5.0	9.9	24.3	45.7	30.9	11.9
$[-0.1, 0.1]$	4.8	5.2	10.9	30.6	49.2	34.5	16.5
$[0.1, 0.8]$	4.8	4.8	9.5	23.0	44.5	30.9	12.1
$[0.8, 1.37]$	5.4	5.3	10.9	24.4	47.2	29.9	11.8
$[1.52, 2.01]$	5.7	6.1	11.9	24.7	49.8	27.5	12.3
$[2.01, 2.47]$	5.5	6.7	12.8	27.2	53.3	34.0	14.1

Table A.3: Signal-to-background ratio in the signal region on container level for one specific setting.

	15-20 GeV	20-25 GeV	25-30 GeV	30-35 GeV	35-40 GeV	40-45 GeV	45-50 GeV
[-2.47, -2.01]	0.975 ± 0.012 ± 0.012	0.976 ± 0.006 ± 0.008	0.993 ± 0.003 ± 0.006	0.995 ± 0.002 ± 0.003	0.996 ± 0.001 ± 0.002	0.993 ± 0.001 ± 0.002	0.988 ± 0.003 ± 0.005
[-2.01, -1.52]	0.998 ± 0.012 ± 0.010	0.999 ± 0.006 ± 0.008	1.005 ± 0.003 ± 0.006	1.009 ± 0.002 ± 0.003	1.009 ± 0.001 ± 0.002	1.007 ± 0.001 ± 0.002	1.002 ± 0.003 ± 0.005
[-1.37, -0.8]	1.006 ± 0.009 ± 0.019	1.007 ± 0.006 ± 0.013	1.009 ± 0.003 ± 0.007	1.009 ± 0.002 ± 0.003	1.006 ± 0.001 ± 0.002	1.005 ± 0.001 ± 0.002	1.000 ± 0.002 ± 0.004
[-0.8, -0.1]	0.980 ± 0.007 ± 0.013	0.996 ± 0.004 ± 0.012	0.996 ± 0.002 ± 0.006	1.000 ± 0.001 ± 0.003	1.002 ± 0.001 ± 0.002	1.000 ± 0.001 ± 0.002	0.999 ± 0.002 ± 0.003
[-0.1, 0.1]	0.999 ± 0.014 ± 0.014	1.003 ± 0.009 ± 0.010	1.002 ± 0.004 ± 0.005	0.998 ± 0.002 ± 0.004	1.002 ± 0.001 ± 0.002	1.003 ± 0.002 ± 0.002	1.001 ± 0.003 ± 0.002
[0.1, 0.8]	0.998 ± 0.008 ± 0.015	1.000 ± 0.005 ± 0.013	1.001 ± 0.002 ± 0.007	0.998 ± 0.001 ± 0.003	1.001 ± 0.001 ± 0.002	1.000 ± 0.001 ± 0.002	1.000 ± 0.002 ± 0.002
[0.8, 1.37]	0.995 ± 0.009 ± 0.020	1.004 ± 0.006 ± 0.013	1.006 ± 0.003 ± 0.007	1.006 ± 0.002 ± 0.003	1.004 ± 0.001 ± 0.002	1.004 ± 0.001 ± 0.002	1.002 ± 0.002 ± 0.005
[1.52, 2.01]	0.992 ± 0.011 ± 0.013	1.004 ± 0.007 ± 0.007	1.008 ± 0.004 ± 0.007	1.009 ± 0.002 ± 0.003	1.008 ± 0.001 ± 0.002	1.007 ± 0.001 ± 0.002	0.999 ± 0.003 ± 0.005
[2.01, 2.47]	0.965 ± 0.011 ± 0.012	0.975 ± 0.006 ± 0.008	0.989 ± 0.003 ± 0.006	0.996 ± 0.002 ± 0.003	0.999 ± 0.001 ± 0.002	0.996 ± 0.001 ± 0.002	0.987 ± 0.003 ± 0.005

Table A.4: LoosePP scale-factors in coarse  $\eta$  granularity with their statistical and systematic uncertainties from 80 variations.

	15-20 GeV	20-25 GeV	25-30 GeV	30-35 GeV	35-40 GeV	40-45 GeV	45-50 GeV
[-2.47, -2.01]	0.954 ± 0.013 ± 0.012	0.953 ± 0.006 ± 0.008	0.974 ± 0.003 ± 0.006	0.975 ± 0.002 ± 0.003	0.979 ± 0.001 ± 0.002	0.979 ± 0.001 ± 0.002	0.974 ± 0.003 ± 0.005
[-2.01, -1.52]	0.948 ± 0.011 ± 0.010	0.949 ± 0.006 ± 0.007	0.963 ± 0.003 ± 0.006	0.973 ± 0.002 ± 0.003	0.981 ± 0.001 ± 0.002	0.984 ± 0.001 ± 0.002	0.980 ± 0.003 ± 0.005
[-1.37, -0.8]	0.953 ± 0.009 ± 0.018	0.947 ± 0.006 ± 0.012	0.964 ± 0.003 ± 0.006	0.970 ± 0.001 ± 0.003	0.979 ± 0.001 ± 0.002	0.985 ± 0.001 ± 0.002	0.983 ± 0.002 ± 0.004
[-0.8, -0.1]	0.940 ± 0.008 ± 0.013	0.957 ± 0.005 ± 0.012	0.966 ± 0.002 ± 0.006	0.970 ± 0.001 ± 0.003	0.977 ± 0.001 ± 0.002	0.980 ± 0.001 ± 0.002	0.980 ± 0.002 ± 0.003
[-0.1, 0.1]	0.962 ± 0.014 ± 0.013	0.966 ± 0.009 ± 0.010	0.972 ± 0.005 ± 0.005	0.969 ± 0.002 ± 0.004	0.981 ± 0.001 ± 0.002	0.982 ± 0.001 ± 0.002	0.979 ± 0.003 ± 0.002
[0.1, 0.8]	0.958 ± 0.008 ± 0.014	0.961 ± 0.005 ± 0.013	0.971 ± 0.003 ± 0.006	0.971 ± 0.002 ± 0.003	0.979 ± 0.001 ± 0.002	0.980 ± 0.001 ± 0.002	0.982 ± 0.002 ± 0.002
[0.8, 1.37]	0.936 ± 0.009 ± 0.019	0.946 ± 0.006 ± 0.013	0.959 ± 0.003 ± 0.007	0.968 ± 0.001 ± 0.003	0.978 ± 0.001 ± 0.002	0.984 ± 0.001 ± 0.002	0.985 ± 0.002 ± 0.005
[1.52, 2.01]	0.950 ± 0.011 ± 0.013	0.950 ± 0.007 ± 0.007	0.968 ± 0.004 ± 0.006	0.974 ± 0.002 ± 0.003	0.980 ± 0.001 ± 0.002	0.984 ± 0.001 ± 0.002	0.980 ± 0.003 ± 0.005
[2.01, 2.47]	0.946 ± 0.011 ± 0.013	0.954 ± 0.006 ± 0.008	0.971 ± 0.003 ± 0.006	0.976 ± 0.002 ± 0.003	0.982 ± 0.001 ± 0.002	0.981 ± 0.001 ± 0.002	0.971 ± 0.003 ± 0.005

Table A.5: LoosePP efficiencies in coarse  $\eta$  granularity with their statistical and systematic uncertainties from 80 variations.

	15-20 GeV	20-25 GeV	25-30 GeV	30-35 GeV	35-40 GeV	40-45 GeV	45-50 GeV
[-2.47, -2.01]	0.978 ± 0.003 ± 0.001	0.977 ± 0.001 ± 0.001	0.981 ± 0.001 ± 0.000	0.980 ± 0.001 ± 0.000	0.984 ± 0.000 ± 0.000	0.985 ± 0.000 ± 0.000	0.986 ± 0.001 ± 0.000
[-2.01, -1.52]	0.950 ± 0.003 ± 0.001	0.950 ± 0.002 ± 0.000	0.959 ± 0.001 ± 0.000	0.964 ± 0.001 ± 0.001	0.972 ± 0.000 ± 0.000	0.977 ± 0.001 ± 0.000	0.978 ± 0.001 ± 0.000
[-1.37, -0.8]	0.947 ± 0.003 ± 0.002	0.940 ± 0.002 ± 0.001	0.955 ± 0.001 ± 0.001	0.962 ± 0.001 ± 0.001	0.974 ± 0.000 ± 0.000	0.980 ± 0.000 ± 0.000	0.983 ± 0.001 ± 0.000
[-0.8, -0.1]	0.959 ± 0.002 ± 0.002	0.961 ± 0.001 ± 0.000	0.970 ± 0.001 ± 0.000	0.971 ± 0.000 ± 0.001	0.978 ± 0.000 ± 0.000	0.980 ± 0.000 ± 0.000	0.981 ± 0.001 ± 0.000
[-0.1, 0.1]	0.962 ± 0.004 ± 0.003	0.962 ± 0.002 ± 0.001	0.970 ± 0.001 ± 0.001	0.971 ± 0.001 ± 0.000	0.979 ± 0.001 ± 0.000	0.979 ± 0.001 ± 0.000	0.979 ± 0.001 ± 0.000
[0.1, 0.8]	0.959 ± 0.002 ± 0.001	0.961 ± 0.001 ± 0.000	0.970 ± 0.001 ± 0.001	0.972 ± 0.000 ± 0.001	0.978 ± 0.000 ± 0.001	0.980 ± 0.000 ± 0.000	0.982 ± 0.001 ± 0.000
[0.8, 1.37]	0.940 ± 0.003 ± 0.001	0.942 ± 0.002 ± 0.001	0.953 ± 0.001 ± 0.001	0.965 ± 0.001 ± 0.001	0.973 ± 0.000 ± 0.001	0.979 ± 0.001 ± 0.000	0.982 ± 0.001 ± 0.000
[1.52, 2.01]	0.957 ± 0.003 ± 0.001	0.947 ± 0.002 ± 0.001	0.960 ± 0.001 ± 0.001	0.962 ± 0.001 ± 0.000	0.972 ± 0.000 ± 0.000	0.978 ± 0.001 ± 0.000	0.980 ± 0.001 ± 0.000
[2.01, 2.47]	0.980 ± 0.002 ± 0.001	0.978 ± 0.001 ± 0.001	0.981 ± 0.001 ± 0.000	0.980 ± 0.001 ± 0.000	0.983 ± 0.000 ± 0.000	0.985 ± 0.000 ± 0.000	0.984 ± 0.001 ± 0.000

Table A.6: LoosePP Monte-Carlo efficiencies in coarse  $\eta$  granularity with their statistical and systematic uncertainties from 80 variations.

	15-20 GeV	20-25 GeV	25-30 GeV	30-35 GeV	35-40 GeV	40-45 GeV	45-50 GeV
[-2.47, -2.01]	0.901 ± 0.016 ± 0.021	0.869 ± 0.008 ± 0.014	0.920 ± 0.004 ± 0.009	0.942 ± 0.003 ± 0.004	0.960 ± 0.002 ± 0.002	0.972 ± 0.002 ± 0.003	0.968 ± 0.004 ± 0.007
[-2.01, -1.52]	0.973 ± 0.015 ± 0.017	0.964 ± 0.008 ± 0.013	0.984 ± 0.004 ± 0.009	0.995 ± 0.002 ± 0.004	1.002 ± 0.002 ± 0.003	1.003 ± 0.002 ± 0.004	0.989 ± 0.004 ± 0.007
[-1.37, -0.8]	0.991 ± 0.011 ± 0.022	0.978 ± 0.007 ± 0.014	0.990 ± 0.004 ± 0.008	0.993 ± 0.002 ± 0.003	0.997 ± 0.001 ± 0.002	0.998 ± 0.001 ± 0.002	0.992 ± 0.003 ± 0.006
[-0.8, -0.1]	0.970 ± 0.009 ± 0.014	0.975 ± 0.006 ± 0.014	0.985 ± 0.003 ± 0.007	0.989 ± 0.002 ± 0.004	0.994 ± 0.001 ± 0.002	0.988 ± 0.001 ± 0.002	0.985 ± 0.002 ± 0.003
[-0.1, 0.1]	0.995 ± 0.017 ± 0.017	0.994 ± 0.011 ± 0.012	0.993 ± 0.006 ± 0.006	0.987 ± 0.003 ± 0.004	0.996 ± 0.002 ± 0.002	0.989 ± 0.002 ± 0.003	0.989 ± 0.005 ± 0.003
[0.1, 0.8]	1.001 ± 0.009 ± 0.017	0.981 ± 0.006 ± 0.015	0.985 ± 0.003 ± 0.007	0.989 ± 0.002 ± 0.004	0.994 ± 0.001 ± 0.002	0.987 ± 0.001 ± 0.002	0.984 ± 0.002 ± 0.003
[0.8, 1.37]	0.980 ± 0.012 ± 0.024	0.973 ± 0.007 ± 0.015	0.986 ± 0.004 ± 0.008	0.989 ± 0.002 ± 0.003	0.994 ± 0.001 ± 0.002	0.996 ± 0.001 ± 0.002	0.991 ± 0.003 ± 0.005
[1.52, 2.01]	0.968 ± 0.014 ± 0.019	0.983 ± 0.008 ± 0.011	0.990 ± 0.004 ± 0.009	0.998 ± 0.002 ± 0.004	1.000 ± 0.002 ± 0.003	1.003 ± 0.002 ± 0.003	0.990 ± 0.004 ± 0.006
[2.01, 2.47]	0.924 ± 0.015 ± 0.019	0.872 ± 0.008 ± 0.014	0.916 ± 0.004 ± 0.009	0.947 ± 0.002 ± 0.004	0.962 ± 0.002 ± 0.002	0.975 ± 0.002 ± 0.003	0.959 ± 0.004 ± 0.007

Table A.7: MediumPP scale-factors in coarse  $\eta$  granularity with their statistical and systematic uncertainties from 80 variations.

	15-20 GeV	20-25 GeV	25-30 GeV	30-35 GeV	35-40 GeV	40-45 GeV	45-50 GeV
[-2.47, -2.01]	0.739 ± 0.013 ± 0.019	0.699 ± 0.006 ± 0.012	0.779 ± 0.004 ± 0.008	0.827 ± 0.002 ± 0.004	0.866 ± 0.001 ± 0.002	0.900 ± 0.002 ± 0.003	0.904 ± 0.004 ± 0.007
[-2.01, -1.52]	0.800 ± 0.012 ± 0.015	0.788 ± 0.006 ± 0.011	0.838 ± 0.004 ± 0.007	0.866 ± 0.002 ± 0.004	0.900 ± 0.001 ± 0.002	0.925 ± 0.002 ± 0.003	0.921 ± 0.003 ± 0.007
[-1.37, -0.8]	0.843 ± 0.009 ± 0.020	0.826 ± 0.006 ± 0.013	0.873 ± 0.003 ± 0.007	0.892 ± 0.002 ± 0.003	0.920 ± 0.001 ± 0.002	0.934 ± 0.001 ± 0.002	0.934 ± 0.002 ± 0.005
[-0.8, -0.1]	0.856 ± 0.008 ± 0.014	0.831 ± 0.005 ± 0.012	0.879 ± 0.003 ± 0.006	0.905 ± 0.001 ± 0.003	0.926 ± 0.001 ± 0.002	0.920 ± 0.001 ± 0.002	0.922 ± 0.002 ± 0.003
[-0.1, 0.1]	0.873 ± 0.015 ± 0.014	0.837 ± 0.009 ± 0.010	0.878 ± 0.005 ± 0.005	0.893 ± 0.002 ± 0.004	0.920 ± 0.002 ± 0.002	0.914 ± 0.002 ± 0.003	0.915 ± 0.004 ± 0.003
[0.1, 0.8]	0.879 ± 0.008 ± 0.016	0.833 ± 0.005 ± 0.013	0.882 ± 0.003 ± 0.007	0.906 ± 0.001 ± 0.004	0.926 ± 0.001 ± 0.002	0.917 ± 0.001 ± 0.002	0.921 ± 0.002 ± 0.003
[0.8, 1.37]	0.821 ± 0.009 ± 0.022	0.823 ± 0.006 ± 0.014	0.868 ± 0.003 ± 0.008	0.890 ± 0.002 ± 0.004	0.918 ± 0.001 ± 0.002	0.933 ± 0.001 ± 0.003	0.936 ± 0.002 ± 0.005
[1.52, 2.01]	0.808 ± 0.011 ± 0.018	0.802 ± 0.007 ± 0.009	0.847 ± 0.004 ± 0.008	0.874 ± 0.002 ± 0.004	0.903 ± 0.001 ± 0.002	0.927 ± 0.002 ± 0.003	0.921 ± 0.003 ± 0.006
[2.01, 2.47]	0.761 ± 0.012 ± 0.018	0.706 ± 0.006 ± 0.012	0.781 ± 0.003 ± 0.007	0.834 ± 0.002 ± 0.004	0.870 ± 0.001 ± 0.002	0.904 ± 0.002 ± 0.003	0.898 ± 0.003 ± 0.007

Table A.8: MediumPP efficiencies in coarse  $\eta$  granularity with their statistical and systematic uncertainties from 80 variations.

	15-20 GeV	20-25 GeV	25-30 GeV	30-35 GeV	35-40 GeV	40-45 GeV	45-50 GeV
[-2.47, -2.01]	0.820 ± 0.007 ± 0.002	0.804 ± 0.004 ± 0.003	0.846 ± 0.002 ± 0.003	0.877 ± 0.001 ± 0.002	0.902 ± 0.001 ± 0.001	0.926 ± 0.001 ± 0.000	0.933 ± 0.002 ± 0.001
[-2.01, -1.52]	0.821 ± 0.006 ± 0.002	0.816 ± 0.003 ± 0.001	0.851 ± 0.002 ± 0.002	0.870 ± 0.001 ± 0.001	0.897 ± 0.001 ± 0.001	0.922 ± 0.001 ± 0.001	0.931 ± 0.002 ± 0.001
[-1.37, -0.8]	0.849 ± 0.005 ± 0.002	0.844 ± 0.003 ± 0.002	0.881 ± 0.002 ± 0.003	0.899 ± 0.001 ± 0.001	0.923 ± 0.001 ± 0.001	0.935 ± 0.001 ± 0.001	0.942 ± 0.001 ± 0.001
[-0.8, -0.1]	0.882 ± 0.004 ± 0.002	0.852 ± 0.002 ± 0.002	0.892 ± 0.001 ± 0.001	0.915 ± 0.001 ± 0.001	0.932 ± 0.001 ± 0.001	0.931 ± 0.001 ± 0.001	0.937 ± 0.001 ± 0.001
[-0.1, 0.1]	0.876 ± 0.007 ± 0.003	0.842 ± 0.004 ± 0.004	0.884 ± 0.002 ± 0.002	0.904 ± 0.002 ± 0.001	0.924 ± 0.001 ± 0.001	0.924 ± 0.001 ± 0.001	0.925 ± 0.003 ± 0.001
[0.1, 0.8]	0.878 ± 0.004 ± 0.002	0.849 ± 0.002 ± 0.002	0.895 ± 0.001 ± 0.001	0.915 ± 0.001 ± 0.002	0.932 ± 0.001 ± 0.001	0.929 ± 0.001 ± 0.001	0.936 ± 0.001 ± 0.001
[0.8, 1.37]	0.838 ± 0.005 ± 0.002	0.845 ± 0.003 ± 0.002	0.880 ± 0.002 ± 0.002	0.900 ± 0.001 ± 0.002	0.924 ± 0.001 ± 0.001	0.937 ± 0.001 ± 0.001	0.944 ± 0.001 ± 0.001
[1.52, 2.01]	0.833 ± 0.006 ± 0.003	0.816 ± 0.003 ± 0.001	0.855 ± 0.002 ± 0.001	0.876 ± 0.001 ± 0.001	0.903 ± 0.001 ± 0.001	0.925 ± 0.001 ± 0.000	0.931 ± 0.002 ± 0.001
[2.01, 2.47]	0.823 ± 0.007 ± 0.002	0.809 ± 0.004 ± 0.004	0.852 ± 0.002 ± 0.003	0.880 ± 0.001 ± 0.002	0.905 ± 0.001 ± 0.001	0.927 ± 0.001 ± 0.001	0.936 ± 0.002 ± 0.000

Table A.9: MediumPP Monte-Carlo efficiencies in coarse  $\eta$  granularity with their statistical and systematic uncertainties from 80 variations.

	15-20 GeV	20-25 GeV	25-30 GeV	30-35 GeV	35-40 GeV	40-45 GeV	45-50 GeV
[-2.47, -2.01]	0.899 ± 0.020 ± 0.027	0.869 ± 0.010 ± 0.019	0.926 ± 0.006 ± 0.011	0.956 ± 0.004 ± 0.005	0.974 ± 0.003 ± 0.003	0.986 ± 0.003 ± 0.004	0.971 ± 0.006 ± 0.010
[-2.01, -1.52]	0.983 ± 0.019 ± 0.019	0.982 ± 0.010 ± 0.016	1.002 ± 0.006 ± 0.010	1.010 ± 0.003 ± 0.005	1.014 ± 0.003 ± 0.003	1.019 ± 0.003 ± 0.004	1.000 ± 0.005 ± 0.007
[-1.37, -0.8]	1.051 ± 0.016 ± 0.023	1.023 ± 0.009 ± 0.015	1.022 ± 0.005 ± 0.009	1.019 ± 0.003 ± 0.003	1.015 ± 0.002 ± 0.002	1.019 ± 0.002 ± 0.003	1.011 ± 0.004 ± 0.006
[-0.8, -0.1]	0.973 ± 0.011 ± 0.015	0.979 ± 0.006 ± 0.015	0.984 ± 0.003 ± 0.007	0.990 ± 0.001 ± 0.002	0.994 ± 0.001 ± 0.002	0.989 ± 0.002 ± 0.002	0.985 ± 0.003 ± 0.003
[-0.1, 0.1]	1.021 ± 0.024 ± 0.018	1.002 ± 0.014 ± 0.012	1.007 ± 0.008 ± 0.007	1.006 ± 0.004 ± 0.004	1.015 ± 0.003 ± 0.002	1.014 ± 0.004 ± 0.003	1.017 ± 0.008 ± 0.005
[0.1, 0.8]	0.998 ± 0.011 ± 0.017	0.986 ± 0.007 ± 0.015	0.986 ± 0.003 ± 0.007	0.988 ± 0.002 ± 0.004	0.994 ± 0.001 ± 0.002	0.987 ± 0.002 ± 0.002	0.982 ± 0.003 ± 0.003
[0.8, 1.37]	1.030 ± 0.016 ± 0.027	1.016 ± 0.009 ± 0.016	1.016 ± 0.005 ± 0.008	1.013 ± 0.003 ± 0.004	1.013 ± 0.002 ± 0.003	1.016 ± 0.002 ± 0.003	1.013 ± 0.004 ± 0.006
[1.52, 2.01]	0.989 ± 0.019 ± 0.020	1.010 ± 0.010 ± 0.012	1.005 ± 0.006 ± 0.010	1.012 ± 0.003 ± 0.005	1.012 ± 0.003 ± 0.003	1.018 ± 0.003 ± 0.003	1.003 ± 0.005 ± 0.008
[2.01, 2.47]	0.911 ± 0.020 ± 0.029	0.874 ± 0.010 ± 0.022	0.917 ± 0.006 ± 0.011	0.960 ± 0.004 ± 0.006	0.978 ± 0.003 ± 0.004	0.989 ± 0.003 ± 0.004	0.959 ± 0.006 ± 0.009

Table A.10: TightPP scale-factors in coarse  $\eta$  granularity with their statistical and systematic uncertainties from 80 variations.

	15-20 GeV	20-25 GeV	25-30 GeV	30-35 GeV	35-40 GeV	40-45 GeV	45-50 GeV
[-2.47, -2.01]	0.569 ± 0.011 ± 0.018	0.561 ± 0.006 ± 0.013	0.632 ± 0.003 ± 0.007	0.678 ± 0.002 ± 0.003	0.721 ± 0.002 ± 0.002	0.769 ± 0.002 ± 0.003	0.763 ± 0.004 ± 0.008
[-2.01, -1.52]	0.627 ± 0.010 ± 0.015	0.650 ± 0.006 ± 0.012	0.690 ± 0.003 ± 0.006	0.729 ± 0.002 ± 0.003	0.763 ± 0.002 ± 0.002	0.809 ± 0.002 ± 0.003	0.805 ± 0.004 ± 0.006
[-1.37, -0.8]	0.722 ± 0.009 ± 0.019	0.721 ± 0.006 ± 0.013	0.756 ± 0.003 ± 0.006	0.792 ± 0.002 ± 0.003	0.819 ± 0.001 ± 0.003	0.839 ± 0.001 ± 0.003	0.839 ± 0.003 ± 0.005
[-0.8, -0.1]	0.766 ± 0.008 ± 0.014	0.756 ± 0.004 ± 0.011	0.800 ± 0.003 ± 0.006	0.837 ± 0.001 ± 0.004	0.861 ± 0.001 ± 0.002	0.859 ± 0.001 ± 0.002	0.861 ± 0.002 ± 0.003
[-0.1, 0.1]	0.721 ± 0.014 ± 0.013	0.705 ± 0.009 ± 0.008	0.745 ± 0.005 ± 0.004	0.767 ± 0.003 ± 0.003	0.796 ± 0.002 ± 0.002	0.798 ± 0.002 ± 0.002	0.796 ± 0.004 ± 0.003
[0.1, 0.8]	0.784 ± 0.008 ± 0.015	0.761 ± 0.005 ± 0.012	0.806 ± 0.003 ± 0.006	0.837 ± 0.001 ± 0.004	0.861 ± 0.001 ± 0.002	0.857 ± 0.001 ± 0.002	0.859 ± 0.002 ± 0.003
[0.8, 1.37]	0.700 ± 0.009 ± 0.021	0.714 ± 0.006 ± 0.013	0.754 ± 0.003 ± 0.007	0.790 ± 0.002 ± 0.004	0.819 ± 0.001 ± 0.003	0.840 ± 0.001 ± 0.003	0.841 ± 0.003 ± 0.005
[1.52, 2.01]	0.629 ± 0.010 ± 0.017	0.663 ± 0.006 ± 0.008	0.699 ± 0.004 ± 0.007	0.736 ± 0.002 ± 0.003	0.766 ± 0.001 ± 0.002	0.810 ± 0.002 ± 0.003	0.809 ± 0.004 ± 0.007
[2.01, 2.47]	0.579 ± 0.011 ± 0.019	0.567 ± 0.006 ± 0.013	0.631 ± 0.003 ± 0.007	0.682 ± 0.002 ± 0.003	0.723 ± 0.001 ± 0.002	0.771 ± 0.002 ± 0.003	0.758 ± 0.004 ± 0.007

Table A.11: TightPP efficiencies in coarse  $\eta$  granularity with their statistical and systematic uncertainties from 80 variations.

	15-20 GeV	20-25 GeV	25-30 GeV	30-35 GeV	35-40 GeV	40-45 GeV	45-50 GeV
[-2.47, -2.01]	0.632 ± 0.008 ± 0.002	0.645 ± 0.004 ± 0.002	0.683 ± 0.003 ± 0.003	0.708 ± 0.002 ± 0.002	0.740 ± 0.001 ± 0.001	0.780 ± 0.002 ± 0.001	0.786 ± 0.003 ± 0.001
[-2.01, -1.52]	0.631 ± 0.007 ± 0.002	0.661 ± 0.004 ± 0.001	0.688 ± 0.002 ± 0.002	0.722 ± 0.002 ± 0.001	0.752 ± 0.001 ± 0.001	0.794 ± 0.002 ± 0.001	0.805 ± 0.003 ± 0.001
[-1.37, -0.8]	0.686 ± 0.006 ± 0.004	0.703 ± 0.004 ± 0.003	0.739 ± 0.002 ± 0.003	0.777 ± 0.001 ± 0.002	0.807 ± 0.001 ± 0.002	0.823 ± 0.001 ± 0.001	0.829 ± 0.002 ± 0.002
[-0.8, -0.1]	0.787 ± 0.005 ± 0.002	0.772 ± 0.003 ± 0.002	0.813 ± 0.002 ± 0.002	0.845 ± 0.001 ± 0.002	0.866 ± 0.001 ± 0.001	0.868 ± 0.001 ± 0.001	0.874 ± 0.002 ± 0.001
[-0.1, 0.1]	0.706 ± 0.010 ± 0.002	0.704 ± 0.006 ± 0.001	0.739 ± 0.003 ± 0.003	0.762 ± 0.002 ± 0.000	0.784 ± 0.002 ± 0.000	0.787 ± 0.002 ± 0.001	0.783 ± 0.004 ± 0.001
[0.1, 0.8]	0.784 ± 0.005 ± 0.002	0.772 ± 0.003 ± 0.001	0.817 ± 0.002 ± 0.001	0.847 ± 0.001 ± 0.002	0.867 ± 0.001 ± 0.001	0.868 ± 0.001 ± 0.001	0.874 ± 0.002 ± 0.001
[0.8, 1.37]	0.680 ± 0.007 ± 0.002	0.702 ± 0.004 ± 0.002	0.742 ± 0.002 ± 0.001	0.779 ± 0.001 ± 0.002	0.809 ± 0.001 ± 0.002	0.826 ± 0.001 ± 0.001	0.830 ± 0.002 ± 0.001
[1.52, 2.01]	0.635 ± 0.007 ± 0.004	0.656 ± 0.004 ± 0.002	0.695 ± 0.002 ± 0.001	0.727 ± 0.002 ± 0.001	0.757 ± 0.001 ± 0.000	0.796 ± 0.002 ± 0.000	0.806 ± 0.003 ± 0.001
[2.01, 2.47]	0.635 ± 0.008 ± 0.001	0.648 ± 0.004 ± 0.004	0.687 ± 0.003 ± 0.002	0.711 ± 0.002 ± 0.002	0.739 ± 0.001 ± 0.001	0.779 ± 0.002 ± 0.000	0.790 ± 0.003 ± 0.001

Table A.12: TightPP Monte-Carlo efficiencies in coarse  $\eta$  granularity with their statistical and systematic uncertainties from 80 variations.

	15-20 GeV	20-25 GeV	25-30 GeV	30-35 GeV	35-40 GeV	40-45 GeV	45-50 GeV
[-2.47, -2.37]	1.002 ± 0.021 ± 0.009	0.993 ± 0.010 ± 0.007	1.003 ± 0.006 ± 0.006	0.995 ± 0.003 ± 0.003	0.997 ± 0.002 ± 0.002	0.998 ± 0.002 ± 0.002	0.999 ± 0.006 ± 0.006
[-2.37, -2.01]	0.970 ± 0.018 ± 0.013	0.974 ± 0.008 ± 0.011	0.995 ± 0.005 ± 0.008	0.995 ± 0.002 ± 0.004	0.995 ± 0.001 ± 0.002	0.992 ± 0.002 ± 0.002	0.987 ± 0.004 ± 0.006
[-2.01, -1.81]	1.003 ± 0.018 ± 0.010	1.013 ± 0.010 ± 0.009	1.008 ± 0.005 ± 0.006	1.008 ± 0.003 ± 0.003	1.007 ± 0.002 ± 0.002	1.007 ± 0.002 ± 0.002	1.005 ± 0.005 ± 0.006
[-1.81, -1.52]	0.995 ± 0.015 ± 0.014	0.989 ± 0.008 ± 0.008	1.002 ± 0.004 ± 0.006	1.010 ± 0.002 ± 0.003	1.010 ± 0.002 ± 0.002	1.008 ± 0.002 ± 0.002	1.000 ± 0.003 ± 0.005
[-1.37, -1.15]	1.007 ± 0.015 ± 0.020	1.016 ± 0.010 ± 0.014	1.010 ± 0.005 ± 0.008	1.012 ± 0.002 ± 0.003	1.007 ± 0.001 ± 0.002	1.007 ± 0.001 ± 0.002	1.000 ± 0.003 ± 0.005
[-1.15, -0.8]	1.004 ± 0.012 ± 0.019	1.002 ± 0.007 ± 0.012	1.009 ± 0.004 ± 0.006	1.007 ± 0.002 ± 0.003	1.006 ± 0.001 ± 0.002	1.004 ± 0.001 ± 0.002	1.001 ± 0.003 ± 0.004
[-0.8, -0.6]	0.978 ± 0.015 ± 0.015	0.990 ± 0.009 ± 0.013	0.991 ± 0.004 ± 0.007	0.995 ± 0.002 ± 0.005	0.994 ± 0.002 ± 0.002	0.997 ± 0.002 ± 0.002	0.998 ± 0.003 ± 0.004
[-0.6, -0.1]	0.981 ± 0.009 ± 0.013	0.998 ± 0.005 ± 0.013	0.998 ± 0.003 ± 0.006	1.001 ± 0.001 ± 0.003	1.001 ± 0.001 ± 0.002	1.001 ± 0.001 ± 0.002	0.999 ± 0.002 ± 0.002
[-0.1, 0]	1.002 ± 0.020 ± 0.014	1.005 ± 0.012 ± 0.011	1.003 ± 0.006 ± 0.005	0.997 ± 0.003 ± 0.004	1.001 ± 0.002 ± 0.002	1.001 ± 0.002 ± 0.002	1.003 ± 0.004 ± 0.003
[0, 0.1]	0.995 ± 0.020 ± 0.014	1.001 ± 0.013 ± 0.011	1.000 ± 0.006 ± 0.005	0.999 ± 0.003 ± 0.004	1.004 ± 0.002 ± 0.003	1.004 ± 0.002 ± 0.003	0.998 ± 0.005 ± 0.002
[0.1, 0.6]	0.998 ± 0.009 ± 0.015	1.003 ± 0.005 ± 0.013	1.004 ± 0.003 ± 0.006	1.001 ± 0.001 ± 0.003	1.001 ± 0.001 ± 0.002	1.001 ± 0.001 ± 0.002	1.002 ± 0.002 ± 0.002
[0.6, 0.8]	0.999 ± 0.016 ± 0.017	0.992 ± 0.009 ± 0.014	0.993 ± 0.005 ± 0.008	0.992 ± 0.002 ± 0.005	0.999 ± 0.002 ± 0.002	0.999 ± 0.002 ± 0.002	0.997 ± 0.003 ± 0.004
[0.8, 1.15]	0.988 ± 0.012 ± 0.020	1.004 ± 0.007 ± 0.012	1.002 ± 0.004 ± 0.006	1.006 ± 0.002 ± 0.003	1.004 ± 0.001 ± 0.002	1.003 ± 0.001 ± 0.002	1.006 ± 0.003 ± 0.004
[1.15, 1.37]	1.007 ± 0.015 ± 0.021	1.004 ± 0.010 ± 0.014	1.013 ± 0.005 ± 0.008	1.008 ± 0.002 ± 0.004	1.005 ± 0.002 ± 0.002	1.007 ± 0.002 ± 0.003	0.998 ± 0.003 ± 0.005
[1.37, 1.81]	0.996 ± 0.014 ± 0.014	1.001 ± 0.008 ± 0.008	1.008 ± 0.004 ± 0.006	1.010 ± 0.002 ± 0.003	1.008 ± 0.002 ± 0.002	1.007 ± 0.002 ± 0.002	0.998 ± 0.004 ± 0.004
[1.81, 2.01]	0.986 ± 0.019 ± 0.015	1.007 ± 0.011 ± 0.006	1.009 ± 0.006 ± 0.008	1.008 ± 0.003 ± 0.004	1.009 ± 0.002 ± 0.002	1.007 ± 0.002 ± 0.002	1.002 ± 0.005 ± 0.006
[2.01, 2.37]	0.959 ± 0.015 ± 0.014	0.973 ± 0.008 ± 0.010	0.991 ± 0.005 ± 0.008	0.996 ± 0.002 ± 0.003	0.998 ± 0.001 ± 0.002	0.996 ± 0.002 ± 0.002	0.987 ± 0.004 ± 0.006
[2.37, 2.47]	0.991 ± 0.018 ± 0.010	0.993 ± 0.010 ± 0.008	1.000 ± 0.006 ± 0.005	0.995 ± 0.003 ± 0.003	0.998 ± 0.002 ± 0.002	0.998 ± 0.002 ± 0.002	0.992 ± 0.005 ± 0.005

Table A.13: LoosePP scale-factors in intermediate  $\eta$  granularity with their statistical and systematic uncertainties from 80 variations.

	15-20 GeV	20-25 GeV	25-30 GeV	30-35 GeV	35-40 GeV	40-45 GeV	45-50 GeV
[-2.47, -2.37]	0.996 ± 0.022 ± 0.010	0.978 ± 0.010 ± 0.007	0.993 ± 0.006 ± 0.006	0.987 ± 0.003 ± 0.003	0.990 ± 0.002 ± 0.002	0.992 ± 0.002 ± 0.002	0.994 ± 0.006 ± 0.006
[-2.37, -2.01]	0.945 ± 0.019 ± 0.013	0.950 ± 0.009 ± 0.010	0.974 ± 0.005 ± 0.008	0.972 ± 0.003 ± 0.003	0.976 ± 0.001 ± 0.002	0.976 ± 0.002 ± 0.002	0.971 ± 0.005 ± 0.006
[-2.01, -1.81]	0.946 ± 0.018 ± 0.008	0.967 ± 0.010 ± 0.008	0.970 ± 0.005 ± 0.006	0.970 ± 0.003 ± 0.003	0.979 ± 0.002 ± 0.002	0.982 ± 0.002 ± 0.002	0.981 ± 0.005 ± 0.006
[-1.81, -1.52]	0.950 ± 0.015 ± 0.013	0.936 ± 0.008 ± 0.008	0.959 ± 0.004 ± 0.006	0.975 ± 0.002 ± 0.003	0.983 ± 0.002 ± 0.002	0.986 ± 0.002 ± 0.002	0.980 ± 0.004 ± 0.004
[-1.37, -1.15]	0.957 ± 0.014 ± 0.019	0.949 ± 0.009 ± 0.013	0.960 ± 0.005 ± 0.008	0.969 ± 0.002 ± 0.003	0.978 ± 0.001 ± 0.002	0.986 ± 0.001 ± 0.002	0.982 ± 0.003 ± 0.004
[-1.15, -0.8]	0.949 ± 0.011 ± 0.018	0.946 ± 0.007 ± 0.012	0.967 ± 0.004 ± 0.005	0.972 ± 0.002 ± 0.003	0.980 ± 0.001 ± 0.002	0.984 ± 0.001 ± 0.002	0.985 ± 0.003 ± 0.004
[-0.8, -0.6]	0.927 ± 0.015 ± 0.015	0.944 ± 0.009 ± 0.012	0.954 ± 0.005 ± 0.007	0.960 ± 0.002 ± 0.005	0.970 ± 0.002 ± 0.002	0.977 ± 0.001 ± 0.002	0.979 ± 0.004 ± 0.004
[-0.6, -0.1]	0.944 ± 0.009 ± 0.013	0.962 ± 0.005 ± 0.012	0.971 ± 0.003 ± 0.006	0.974 ± 0.001 ± 0.003	0.980 ± 0.001 ± 0.002	0.981 ± 0.001 ± 0.002	0.981 ± 0.002 ± 0.002
[-0.1, 0]	0.960 ± 0.020 ± 0.013	0.967 ± 0.012 ± 0.011	0.974 ± 0.007 ± 0.005	0.968 ± 0.003 ± 0.004	0.979 ± 0.002 ± 0.002	0.982 ± 0.002 ± 0.002	0.983 ± 0.004 ± 0.003
[0, 0.1]	0.964 ± 0.021 ± 0.013	0.964 ± 0.013 ± 0.011	0.970 ± 0.006 ± 0.005	0.970 ± 0.003 ± 0.004	0.983 ± 0.002 ± 0.002	0.982 ± 0.002 ± 0.002	0.975 ± 0.005 ± 0.002
[0.1, 0.6]	0.963 ± 0.009 ± 0.014	0.966 ± 0.006 ± 0.013	0.976 ± 0.003 ± 0.006	0.975 ± 0.001 ± 0.003	0.980 ± 0.001 ± 0.002	0.980 ± 0.001 ± 0.002	0.983 ± 0.002 ± 0.002
[0.6, 0.8]	0.945 ± 0.015 ± 0.016	0.947 ± 0.010 ± 0.013	0.958 ± 0.005 ± 0.008	0.961 ± 0.002 ± 0.005	0.975 ± 0.002 ± 0.002	0.979 ± 0.002 ± 0.002	0.979 ± 0.004 ± 0.004
[0.8, 1.15]	0.927 ± 0.011 ± 0.019	0.949 ± 0.007 ± 0.012	0.960 ± 0.004 ± 0.006	0.972 ± 0.002 ± 0.003	0.980 ± 0.001 ± 0.002	0.984 ± 0.001 ± 0.002	0.988 ± 0.003 ± 0.004
[1.15, 1.37]	0.950 ± 0.014 ± 0.021	0.942 ± 0.009 ± 0.014	0.958 ± 0.005 ± 0.008	0.963 ± 0.002 ± 0.004	0.975 ± 0.001 ± 0.002	0.984 ± 0.001 ± 0.002	0.980 ± 0.003 ± 0.005
[1.37, 1.81]	0.955 ± 0.014 ± 0.014	0.942 ± 0.008 ± 0.007	0.964 ± 0.005 ± 0.005	0.975 ± 0.003 ± 0.003	0.981 ± 0.002 ± 0.002	0.986 ± 0.002 ± 0.002	0.980 ± 0.004 ± 0.004
[1.81, 2.01]	0.944 ± 0.019 ± 0.014	0.962 ± 0.011 ± 0.006	0.974 ± 0.006 ± 0.008	0.972 ± 0.003 ± 0.004	0.979 ± 0.002 ± 0.002	0.983 ± 0.002 ± 0.002	0.980 ± 0.005 ± 0.005
[2.01, 2.37]	0.937 ± 0.016 ± 0.014	0.950 ± 0.009 ± 0.010	0.971 ± 0.005 ± 0.008	0.973 ± 0.002 ± 0.003	0.979 ± 0.001 ± 0.002	0.979 ± 0.002 ± 0.002	0.968 ± 0.004 ± 0.006
[2.37, 2.47]	0.987 ± 0.019 ± 0.010	0.982 ± 0.010 ± 0.008	0.991 ± 0.006 ± 0.005	0.987 ± 0.003 ± 0.003	0.992 ± 0.002 ± 0.002	0.993 ± 0.002 ± 0.002	0.989 ± 0.005 ± 0.005

Table A.14: LoosePP efficiencies in intermediate  $\eta$  granularity with their statistical and systematic uncertainties from 80 variations.

	15-20 GeV	20-25 GeV	25-30 GeV	30-35 GeV	35-40 GeV	40-45 GeV	45-50 GeV
[-2.47, -2.37]	0.994 ± 0.003 ± 0.001	0.985 ± 0.003 ± 0.001	0.990 ± 0.001 ± 0.000	0.991 ± 0.001 ± 0.000	0.993 ± 0.001 ± 0.000	0.994 ± 0.001 ± 0.000	0.995 ± 0.001 ± 0.000
[-2.37, -2.01]	0.975 ± 0.003 ± 0.001	0.975 ± 0.002 ± 0.001	0.979 ± 0.001 ± 0.000	0.977 ± 0.001 ± 0.001	0.981 ± 0.000 ± 0.000	0.983 ± 0.001 ± 0.000	0.984 ± 0.001 ± 0.000
[-2.01, -1.81]	0.943 ± 0.006 ± 0.002	0.955 ± 0.003 ± 0.001	0.963 ± 0.002 ± 0.000	0.963 ± 0.001 ± 0.001	0.972 ± 0.001 ± 0.001	0.975 ± 0.001 ± 0.000	0.976 ± 0.002 ± 0.001
[-1.81, -1.52]	0.955 ± 0.004 ± 0.001	0.946 ± 0.002 ± 0.001	0.957 ± 0.001 ± 0.001	0.965 ± 0.001 ± 0.001	0.973 ± 0.001 ± 0.000	0.978 ± 0.001 ± 0.000	0.980 ± 0.001 ± 0.000
[-1.37, -1.15]	0.950 ± 0.005 ± 0.001	0.934 ± 0.003 ± 0.002	0.951 ± 0.002 ± 0.001	0.957 ± 0.001 ± 0.001	0.972 ± 0.001 ± 0.001	0.980 ± 0.001 ± 0.000	0.982 ± 0.001 ± 0.001
[-1.15, -0.8]	0.945 ± 0.004 ± 0.002	0.944 ± 0.002 ± 0.001	0.958 ± 0.001 ± 0.001	0.965 ± 0.001 ± 0.001	0.975 ± 0.001 ± 0.000	0.980 ± 0.001 ± 0.000	0.984 ± 0.001 ± 0.000
[-0.8, -0.6]	0.948 ± 0.005 ± 0.002	0.952 ± 0.003 ± 0.001	0.962 ± 0.001 ± 0.000	0.965 ± 0.001 ± 0.001	0.976 ± 0.001 ± 0.000	0.980 ± 0.001 ± 0.000	0.980 ± 0.001 ± 0.000
[-0.6, -0.1]	0.963 ± 0.003 ± 0.002	0.965 ± 0.001 ± 0.000	0.972 ± 0.001 ± 0.000	0.973 ± 0.001 ± 0.001	0.979 ± 0.000 ± 0.000	0.980 ± 0.000 ± 0.000	0.982 ± 0.001 ± 0.000
[-0.1, 0]	0.957 ± 0.006 ± 0.004	0.961 ± 0.003 ± 0.002	0.971 ± 0.002 ± 0.000	0.971 ± 0.001 ± 0.001	0.978 ± 0.001 ± 0.000	0.980 ± 0.001 ± 0.000	0.980 ± 0.002 ± 0.000
[0, 0.1]	0.968 ± 0.005 ± 0.002	0.963 ± 0.003 ± 0.001	0.970 ± 0.002 ± 0.001	0.971 ± 0.001 ± 0.000	0.979 ± 0.001 ± 0.000	0.977 ± 0.001 ± 0.001	0.977 ± 0.002 ± 0.001
[0.1, 0.6]	0.964 ± 0.003 ± 0.001	0.964 ± 0.001 ± 0.000	0.972 ± 0.001 ± 0.001	0.974 ± 0.001 ± 0.001	0.979 ± 0.000 ± 0.001	0.979 ± 0.000 ± 0.000	0.982 ± 0.001 ± 0.000
[0.6, 0.8]	0.946 ± 0.005 ± 0.002	0.954 ± 0.003 ± 0.001	0.964 ± 0.001 ± 0.000	0.968 ± 0.001 ± 0.001	0.976 ± 0.001 ± 0.001	0.980 ± 0.001 ± 0.000	0.982 ± 0.001 ± 0.001
[0.8, 1.15]	0.938 ± 0.004 ± 0.001	0.945 ± 0.002 ± 0.001	0.958 ± 0.001 ± 0.001	0.965 ± 0.001 ± 0.001	0.975 ± 0.001 ± 0.000	0.981 ± 0.001 ± 0.000	0.982 ± 0.001 ± 0.000
[1.15, 1.37]	0.944 ± 0.005 ± 0.002	0.938 ± 0.003 ± 0.001	0.946 ± 0.002 ± 0.001	0.955 ± 0.001 ± 0.001	0.970 ± 0.001 ± 0.001	0.977 ± 0.001 ± 0.001	0.982 ± 0.001 ± 0.000
[1.37, 1.81]	0.958 ± 0.004 ± 0.001	0.941 ± 0.002 ± 0.001	0.956 ± 0.001 ± 0.001	0.966 ± 0.001 ± 0.000	0.974 ± 0.001 ± 0.000	0.979 ± 0.001 ± 0.000	0.982 ± 0.001 ± 0.000
[1.81, 2.01]	0.957 ± 0.005 ± 0.002	0.955 ± 0.003 ± 0.001	0.965 ± 0.001 ± 0.000	0.964 ± 0.001 ± 0.000	0.971 ± 0.001 ± 0.000	0.976 ± 0.001 ± 0.000	0.979 ± 0.002 ± 0.000
[2.01, 2.37]	0.977 ± 0.003 ± 0.001	0.976 ± 0.002 ± 0.001	0.979 ± 0.001 ± 0.000	0.977 ± 0.001 ± 0.000	0.981 ± 0.000 ± 0.000	0.983 ± 0.001 ± 0.000	0.981 ± 0.001 ± 0.000
[2.37, 2.47]	0.996 ± 0.002 ± 0.001	0.990 ± 0.002 ± 0.001	0.991 ± 0.001 ± 0.000	0.992 ± 0.001 ± 0.000	0.993 ± 0.001 ± 0.000	0.996 ± 0.001 ± 0.000	0.996 ± 0.001 ± 0.001

Table A.15: LoosePP Monte-Carlo efficiencies in intermediate  $\eta$  granularity with their statistical and systematic uncertainties from 80 variations.

	15-20 GeV	20-25 GeV	25-30 GeV	30-35 GeV	35-40 GeV	40-45 GeV	45-50 GeV
[-2.47, -2.37]	0.876 ± 0.037 ± 0.024	0.894 ± 0.018 ± 0.018	0.936 ± 0.010 ± 0.011	0.948 ± 0.005 ± 0.005	0.973 ± 0.004 ± 0.004	0.988 ± 0.005 ± 0.004	0.986 ± 0.010 ± 0.011
[-2.37, -2.01]	0.909 ± 0.021 ± 0.021	0.868 ± 0.010 ± 0.016	0.923 ± 0.006 ± 0.011	0.941 ± 0.003 ± 0.005	0.955 ± 0.002 ± 0.002	0.968 ± 0.002 ± 0.003	0.965 ± 0.005 ± 0.007
[-2.01, -1.81]	0.984 ± 0.024 ± 0.015	0.988 ± 0.013 ± 0.015	1.002 ± 0.007 ± 0.010	1.001 ± 0.004 ± 0.004	1.004 ± 0.003 ± 0.002	1.004 ± 0.003 ± 0.004	0.994 ± 0.006 ± 0.009
[-1.81, -1.52]	0.968 ± 0.019 ± 0.021	0.949 ± 0.010 ± 0.012	0.973 ± 0.005 ± 0.009	0.991 ± 0.003 ± 0.005	1.002 ± 0.002 ± 0.003	1.001 ± 0.002 ± 0.003	0.987 ± 0.004 ± 0.006
[-1.37, -1.15]	0.993 ± 0.019 ± 0.024	0.981 ± 0.012 ± 0.016	0.982 ± 0.006 ± 0.009	0.991 ± 0.003 ± 0.004	0.996 ± 0.002 ± 0.003	0.999 ± 0.002 ± 0.003	0.991 ± 0.004 ± 0.006
[-1.15, -0.8]	0.989 ± 0.014 ± 0.021	0.977 ± 0.009 ± 0.014	0.997 ± 0.005 ± 0.007	0.995 ± 0.003 ± 0.003	0.998 ± 0.002 ± 0.002	0.997 ± 0.002 ± 0.003	0.994 ± 0.004 ± 0.005
[-0.8, -0.6]	0.963 ± 0.018 ± 0.016	0.969 ± 0.011 ± 0.014	0.976 ± 0.006 ± 0.008	0.986 ± 0.003 ± 0.005	0.990 ± 0.002 ± 0.002	0.992 ± 0.002 ± 0.002	0.991 ± 0.004 ± 0.004
[-0.6, -0.1]	0.972 ± 0.010 ± 0.014	0.978 ± 0.006 ± 0.014	0.989 ± 0.003 ± 0.006	0.990 ± 0.002 ± 0.003	0.995 ± 0.001 ± 0.002	0.987 ± 0.001 ± 0.002	0.982 ± 0.003 ± 0.003
[-0.1, 0]	1.016 ± 0.025 ± 0.019	1.000 ± 0.015 ± 0.013	0.991 ± 0.008 ± 0.006	0.986 ± 0.004 ± 0.004	0.995 ± 0.003 ± 0.002	0.985 ± 0.003 ± 0.003	0.990 ± 0.007 ± 0.004
[0, 0.1]	0.975 ± 0.024 ± 0.016	0.988 ± 0.016 ± 0.013	0.994 ± 0.008 ± 0.006	0.988 ± 0.004 ± 0.004	0.998 ± 0.003 ± 0.003	0.994 ± 0.004 ± 0.003	0.987 ± 0.007 ± 0.003
[0.1, 0.6]	1.000 ± 0.011 ± 0.017	0.985 ± 0.007 ± 0.015	0.989 ± 0.003 ± 0.007	0.992 ± 0.002 ± 0.003	0.993 ± 0.001 ± 0.002	0.984 ± 0.002 ± 0.002	0.982 ± 0.003 ± 0.003
[0.6, 0.8]	1.004 ± 0.019 ± 0.019	0.971 ± 0.011 ± 0.016	0.974 ± 0.006 ± 0.009	0.987 ± 0.003 ± 0.005	0.994 ± 0.002 ± 0.003	0.994 ± 0.002 ± 0.002	0.990 ± 0.004 ± 0.004
[0.8, 1.15]	0.972 ± 0.015 ± 0.025	0.975 ± 0.009 ± 0.013	0.986 ± 0.005 ± 0.007	0.992 ± 0.003 ± 0.003	0.995 ± 0.002 ± 0.002	0.993 ± 0.002 ± 0.003	0.994 ± 0.004 ± 0.005
[1.15, 1.37]	0.993 ± 0.019 ± 0.025	0.970 ± 0.012 ± 0.017	0.985 ± 0.006 ± 0.010	0.984 ± 0.003 ± 0.004	0.993 ± 0.002 ± 0.003	1.000 ± 0.002 ± 0.003	0.988 ± 0.004 ± 0.006
[1.52, 1.81]	0.965 ± 0.018 ± 0.019	0.973 ± 0.010 ± 0.012	0.981 ± 0.005 ± 0.008	0.995 ± 0.003 ± 0.004	0.998 ± 0.002 ± 0.004	0.998 ± 0.002 ± 0.003	0.985 ± 0.005 ± 0.006
[1.81, 2.01]	0.974 ± 0.024 ± 0.023	0.996 ± 0.014 ± 0.009	1.005 ± 0.007 ± 0.011	1.002 ± 0.004 ± 0.005	1.004 ± 0.003 ± 0.002	1.010 ± 0.003 ± 0.003	0.998 ± 0.006 ± 0.007
[2.01, 2.37]	0.927 ± 0.019 ± 0.020	0.876 ± 0.010 ± 0.014	0.921 ± 0.006 ± 0.012	0.949 ± 0.003 ± 0.005	0.959 ± 0.002 ± 0.002	0.972 ± 0.002 ± 0.003	0.959 ± 0.005 ± 0.007
[2.37, 2.47]	0.918 ± 0.035 ± 0.019	0.876 ± 0.018 ± 0.021	0.920 ± 0.010 ± 0.009	0.941 ± 0.005 ± 0.005	0.970 ± 0.004 ± 0.003	0.989 ± 0.005 ± 0.004	0.966 ± 0.009 ± 0.009

Table A.16: MediumPP scale-factors in intermediate  $\eta$  granularity with their statistical and systematic uncertainties from 80 variations.

	15-20 GeV	20-25 GeV	25-30 GeV	30-35 GeV	35-40 GeV	40-45 GeV	45-50 GeV
[-2.47, -2.37]	0.672 ± 0.025 ± 0.018	0.690 ± 0.012 ± 0.015	0.775 ± 0.008 ± 0.009	0.814 ± 0.004 ± 0.004	0.853 ± 0.003 ± 0.003	0.891 ± 0.004 ± 0.004	0.897 ± 0.008 ± 0.010
[-2.37, -2.01]	0.756 ± 0.018 ± 0.019	0.705 ± 0.009 ± 0.014	0.786 ± 0.005 ± 0.009	0.830 ± 0.003 ± 0.004	0.868 ± 0.002 ± 0.002	0.902 ± 0.002 ± 0.003	0.906 ± 0.005 ± 0.007
[-2.01, -1.81]	0.782 ± 0.018 ± 0.012	0.796 ± 0.010 ± 0.013	0.840 ± 0.006 ± 0.008	0.860 ± 0.003 ± 0.004	0.893 ± 0.002 ± 0.002	0.915 ± 0.003 ± 0.003	0.911 ± 0.006 ± 0.008
[-1.81, -1.52]	0.812 ± 0.015 ± 0.019	0.783 ± 0.008 ± 0.011	0.836 ± 0.004 ± 0.007	0.870 ± 0.003 ± 0.004	0.904 ± 0.002 ± 0.002	0.932 ± 0.002 ± 0.003	0.927 ± 0.004 ± 0.006
[-1.37, -1.15]	0.842 ± 0.015 ± 0.022	0.816 ± 0.009 ± 0.014	0.860 ± 0.005 ± 0.009	0.882 ± 0.003 ± 0.004	0.915 ± 0.002 ± 0.003	0.936 ± 0.002 ± 0.003	0.934 ± 0.003 ± 0.005
[-1.15, -0.8]	0.842 ± 0.012 ± 0.019	0.833 ± 0.007 ± 0.013	0.882 ± 0.004 ± 0.005	0.900 ± 0.002 ± 0.003	0.923 ± 0.001 ± 0.002	0.932 ± 0.001 ± 0.002	0.936 ± 0.003 ± 0.004
[-0.8, -0.6]	0.832 ± 0.015 ± 0.016	0.817 ± 0.009 ± 0.012	0.862 ± 0.005 ± 0.007	0.899 ± 0.003 ± 0.005	0.923 ± 0.002 ± 0.002	0.933 ± 0.002 ± 0.002	0.937 ± 0.004 ± 0.004
[-0.6, -0.1]	0.866 ± 0.009 ± 0.014	0.837 ± 0.005 ± 0.012	0.885 ± 0.003 ± 0.006	0.908 ± 0.002 ± 0.003	0.928 ± 0.001 ± 0.002	0.915 ± 0.001 ± 0.002	0.916 ± 0.002 ± 0.003
[-0.1, 0]	0.882 ± 0.020 ± 0.015	0.840 ± 0.012 ± 0.011	0.879 ± 0.007 ± 0.005	0.895 ± 0.003 ± 0.004	0.920 ± 0.002 ± 0.002	0.914 ± 0.003 ± 0.003	0.920 ± 0.005 ± 0.003
[0, 0.1]	0.863 ± 0.021 ± 0.014	0.834 ± 0.013 ± 0.011	0.877 ± 0.007 ± 0.005	0.891 ± 0.003 ± 0.004	0.921 ± 0.002 ± 0.003	0.914 ± 0.003 ± 0.003	0.910 ± 0.006 ± 0.002
[0.1, 0.6]	0.887 ± 0.009 ± 0.015	0.839 ± 0.006 ± 0.013	0.888 ± 0.003 ± 0.006	0.909 ± 0.002 ± 0.003	0.926 ± 0.001 ± 0.002	0.909 ± 0.001 ± 0.002	0.914 ± 0.002 ± 0.003
[0.6, 0.8]	0.860 ± 0.016 ± 0.018	0.819 ± 0.009 ± 0.013	0.865 ± 0.005 ± 0.008	0.901 ± 0.003 ± 0.005	0.928 ± 0.002 ± 0.002	0.936 ± 0.002 ± 0.002	0.939 ± 0.004 ± 0.004
[0.8, 1.15]	0.815 ± 0.011 ± 0.022	0.830 ± 0.007 ± 0.013	0.876 ± 0.004 ± 0.007	0.899 ± 0.002 ± 0.003	0.923 ± 0.001 ± 0.002	0.931 ± 0.001 ± 0.003	0.937 ± 0.003 ± 0.005
[1.15, 1.37]	0.831 ± 0.015 ± 0.023	0.812 ± 0.009 ± 0.016	0.855 ± 0.005 ± 0.009	0.875 ± 0.003 ± 0.004	0.911 ± 0.002 ± 0.003	0.935 ± 0.002 ± 0.003	0.935 ± 0.003 ± 0.006
[1.52, 1.81]	0.814 ± 0.015 ± 0.019	0.797 ± 0.008 ± 0.010	0.847 ± 0.005 ± 0.007	0.877 ± 0.003 ± 0.004	0.907 ± 0.002 ± 0.003	0.934 ± 0.002 ± 0.003	0.927 ± 0.004 ± 0.006
[1.81, 2.01]	0.799 ± 0.019 ± 0.020	0.810 ± 0.011 ± 0.008	0.848 ± 0.006 ± 0.010	0.870 ± 0.003 ± 0.004	0.897 ± 0.002 ± 0.002	0.918 ± 0.003 ± 0.003	0.912 ± 0.006 ± 0.007
[2.01, 2.37]	0.771 ± 0.016 ± 0.018	0.711 ± 0.008 ± 0.012	0.788 ± 0.005 ± 0.009	0.838 ± 0.002 ± 0.004	0.872 ± 0.002 ± 0.002	0.906 ± 0.002 ± 0.003	0.900 ± 0.005 ± 0.007
[2.37, 2.47]	0.721 ± 0.025 ± 0.016	0.698 ± 0.013 ± 0.017	0.771 ± 0.007 ± 0.008	0.819 ± 0.004 ± 0.004	0.861 ± 0.003 ± 0.003	0.897 ± 0.004 ± 0.004	0.894 ± 0.008 ± 0.008

Table A.17: MediumPP efficiencies in intermediate  $\eta$  granularity with their statistical and systematic uncertainties from 80 variations.

	15-20 GeV	20-25 GeV	25-30 GeV	30-35 GeV	35-40 GeV	40-45 GeV	45-50 GeV
[-2.47, -2.37]	0.766 ± 0.018 ± 0.004	0.771 ± 0.009 ± 0.005	0.828 ± 0.005 ± 0.004	0.858 ± 0.003 ± 0.002	0.877 ± 0.002 ± 0.001	0.902 ± 0.003 ± 0.001	0.910 ± 0.005 ± 0.001
[-2.37, -2.01]	0.832 ± 0.007 ± 0.003	0.811 ± 0.004 ± 0.003	0.850 ± 0.002 ± 0.002	0.882 ± 0.001 ± 0.002	0.908 ± 0.001 ± 0.001	0.932 ± 0.001 ± 0.001	0.939 ± 0.002 ± 0.001
[-2.01, -1.81]	0.795 ± 0.010 ± 0.001	0.804 ± 0.005 ± 0.002	0.838 ± 0.003 ± 0.002	0.859 ± 0.002 ± 0.001	0.890 ± 0.001 ± 0.001	0.910 ± 0.002 ± 0.001	0.917 ± 0.003 ± 0.002
[-1.81, -1.52]	0.838 ± 0.007 ± 0.003	0.824 ± 0.004 ± 0.002	0.858 ± 0.002 ± 0.002	0.878 ± 0.001 ± 0.002	0.903 ± 0.001 ± 0.001	0.930 ± 0.001 ± 0.001	0.940 ± 0.002 ± 0.000
[-1.37, -1.15]	0.846 ± 0.008 ± 0.002	0.831 ± 0.005 ± 0.003	0.875 ± 0.003 ± 0.002	0.889 ± 0.002 ± 0.002	0.919 ± 0.001 ± 0.001	0.937 ± 0.001 ± 0.001	0.942 ± 0.002 ± 0.002
[-1.15, -0.8]	0.851 ± 0.006 ± 0.002	0.851 ± 0.004 ± 0.002	0.884 ± 0.002 ± 0.003	0.904 ± 0.001 ± 0.001	0.925 ± 0.001 ± 0.001	0.935 ± 0.001 ± 0.001	0.942 ± 0.002 ± 0.001
[-0.8, -0.6]	0.863 ± 0.008 ± 0.006	0.843 ± 0.004 ± 0.002	0.883 ± 0.002 ± 0.001	0.911 ± 0.001 ± 0.001	0.932 ± 0.001 ± 0.001	0.941 ± 0.001 ± 0.000	0.945 ± 0.002 ± 0.001
[-0.6, -0.1]	0.890 ± 0.004 ± 0.001	0.855 ± 0.003 ± 0.002	0.895 ± 0.001 ± 0.001	0.916 ± 0.001 ± 0.001	0.932 ± 0.001 ± 0.001	0.927 ± 0.001 ± 0.001	0.933 ± 0.002 ± 0.001
[-0.1, 0]	0.868 ± 0.010 ± 0.004	0.839 ± 0.006 ± 0.004	0.887 ± 0.003 ± 0.002	0.907 ± 0.002 ± 0.001	0.925 ± 0.002 ± 0.001	0.928 ± 0.002 ± 0.000	0.929 ± 0.004 ± 0.001
[0, 0.1]	0.885 ± 0.010 ± 0.002	0.844 ± 0.006 ± 0.004	0.882 ± 0.004 ± 0.002	0.902 ± 0.002 ± 0.000	0.923 ± 0.002 ± 0.001	0.920 ± 0.002 ± 0.001	0.922 ± 0.004 ± 0.001
[0.1, 0.6]	0.886 ± 0.004 ± 0.002	0.852 ± 0.003 ± 0.002	0.898 ± 0.001 ± 0.001	0.916 ± 0.001 ± 0.001	0.932 ± 0.001 ± 0.001	0.924 ± 0.001 ± 0.001	0.931 ± 0.002 ± 0.001
[0.6, 0.8]	0.856 ± 0.008 ± 0.004	0.843 ± 0.005 ± 0.002	0.889 ± 0.002 ± 0.002	0.913 ± 0.001 ± 0.002	0.933 ± 0.001 ± 0.001	0.942 ± 0.001 ± 0.001	0.948 ± 0.002 ± 0.001
[0.8, 1.15]	0.839 ± 0.007 ± 0.003	0.851 ± 0.004 ± 0.002	0.888 ± 0.002 ± 0.001	0.906 ± 0.001 ± 0.001	0.927 ± 0.001 ± 0.001	0.937 ± 0.001 ± 0.001	0.943 ± 0.002 ± 0.000
[1.15, 1.37]	0.836 ± 0.009 ± 0.003	0.836 ± 0.005 ± 0.001	0.867 ± 0.003 ± 0.002	0.889 ± 0.002 ± 0.002	0.917 ± 0.001 ± 0.002	0.936 ± 0.001 ± 0.001	0.946 ± 0.002 ± 0.001
[1.52, 1.81]	0.842 ± 0.007 ± 0.003	0.818 ± 0.004 ± 0.002	0.862 ± 0.002 ± 0.002	0.881 ± 0.001 ± 0.001	0.910 ± 0.001 ± 0.001	0.935 ± 0.001 ± 0.000	0.942 ± 0.002 ± 0.001
[1.81, 2.01]	0.819 ± 0.009 ± 0.002	0.812 ± 0.005 ± 0.001	0.844 ± 0.003 ± 0.001	0.868 ± 0.002 ± 0.002	0.893 ± 0.001 ± 0.000	0.910 ± 0.002 ± 0.000	0.914 ± 0.003 ± 0.001
[2.01, 2.37]	0.830 ± 0.007 ± 0.002	0.812 ± 0.004 ± 0.004	0.856 ± 0.002 ± 0.003	0.882 ± 0.001 ± 0.002	0.909 ± 0.001 ± 0.001	0.932 ± 0.001 ± 0.001	0.938 ± 0.002 ± 0.001
[2.37, 2.47]	0.784 ± 0.017 ± 0.002	0.796 ± 0.009 ± 0.005	0.838 ± 0.005 ± 0.001	0.870 ± 0.003 ± 0.002	0.887 ± 0.002 ± 0.000	0.906 ± 0.003 ± 0.001	0.925 ± 0.005 ± 0.001

Table A.18: MediumPP Monte-Carlo efficiencies in intermediate  $\eta$  granularity with their statistical and systematic uncertainties from 80 variations.

	15-20 GeV	20-25 GeV	25-30 GeV	30-35 GeV	35-40 GeV	40-45 GeV	45-50 GeV
[-2.47, -2.37]	0.911 ± 0.056 ± 0.038	0.989 ± 0.030 ± 0.021	1.009 ± 0.016 ± 0.012	1.032 ± 0.010 ± 0.006	1.065 ± 0.008 ± 0.004	1.053 ± 0.009 ± 0.006	1.050 ± 0.018 ± 0.016
[-2.37, -2.01]	0.902 ± 0.024 ± 0.028	0.854 ± 0.012 ± 0.022	0.919 ± 0.007 ± 0.014	0.943 ± 0.004 ± 0.006	0.955 ± 0.003 ± 0.003	0.972 ± 0.003 ± 0.005	0.954 ± 0.007 ± 0.009
[-2.01, -1.81]	1.023 ± 0.033 ± 0.020	0.987 ± 0.017 ± 0.017	1.019 ± 0.010 ± 0.013	1.016 ± 0.005 ± 0.004	1.016 ± 0.004 ± 0.003	1.018 ± 0.005 ± 0.004	1.000 ± 0.009 ± 0.010
[-1.81, -1.52]	0.977 ± 0.024 ± 0.021	0.980 ± 0.012 ± 0.016	0.992 ± 0.007 ± 0.009	1.006 ± 0.004 ± 0.005	1.014 ± 0.003 ± 0.004	1.020 ± 0.004 ± 0.005	1.001 ± 0.007 ± 0.006
[-1.37, -1.15]	1.091 ± 0.028 ± 0.028	1.046 ± 0.016 ± 0.017	1.031 ± 0.008 ± 0.010	1.030 ± 0.005 ± 0.004	1.025 ± 0.003 ± 0.003	1.033 ± 0.004 ± 0.003	1.029 ± 0.007 ± 0.008
[-1.15, -0.8]	1.029 ± 0.019 ± 0.022	1.012 ± 0.011 ± 0.014	1.018 ± 0.006 ± 0.008	1.013 ± 0.003 ± 0.003	1.010 ± 0.002 ± 0.002	1.012 ± 0.003 ± 0.003	1.003 ± 0.005 ± 0.005
[-0.8, -0.6]	0.981 ± 0.021 ± 0.020	0.979 ± 0.012 ± 0.015	0.984 ± 0.007 ± 0.008	0.995 ± 0.004 ± 0.005	0.998 ± 0.003 ± 0.002	0.997 ± 0.003 ± 0.002	1.002 ± 0.006 ± 0.004
[-0.6, -0.1]	0.970 ± 0.012 ± 0.015	0.979 ± 0.007 ± 0.015	0.984 ± 0.004 ± 0.007	0.988 ± 0.002 ± 0.003	0.993 ± 0.002 ± 0.002	0.985 ± 0.002 ± 0.003	0.978 ± 0.004 ± 0.003
[-0.1, 0]	1.040 ± 0.034 ± 0.019	1.009 ± 0.019 ± 0.012	1.003 ± 0.011 ± 0.009	1.002 ± 0.006 ± 0.005	1.007 ± 0.004 ± 0.002	1.006 ± 0.006 ± 0.003	1.024 ± 0.011 ± 0.006
[0, 0.1]	1.001 ± 0.033 ± 0.020	0.995 ± 0.020 ± 0.014	1.012 ± 0.011 ± 0.006	1.011 ± 0.006 ± 0.005	1.024 ± 0.005 ± 0.003	1.023 ± 0.006 ± 0.003	1.011 ± 0.011 ± 0.004
[0.1, 0.6]	0.995 ± 0.013 ± 0.017	0.989 ± 0.008 ± 0.015	0.987 ± 0.004 ± 0.007	0.985 ± 0.002 ± 0.003	0.991 ± 0.002 ± 0.002	0.981 ± 0.002 ± 0.002	0.978 ± 0.004 ± 0.003
[0.6, 0.8]	1.007 ± 0.022 ± 0.020	0.979 ± 0.013 ± 0.016	0.983 ± 0.007 ± 0.010	0.994 ± 0.004 ± 0.005	1.001 ± 0.003 ± 0.002	1.002 ± 0.003 ± 0.003	0.993 ± 0.006 ± 0.004
[0.8, 1.15]	1.023 ± 0.019 ± 0.028	1.013 ± 0.011 ± 0.014	1.006 ± 0.006 ± 0.007	1.008 ± 0.003 ± 0.003	1.009 ± 0.002 ± 0.002	1.008 ± 0.003 ± 0.003	1.005 ± 0.005 ± 0.005
[1.15, 1.37]	1.047 ± 0.028 ± 0.027	1.021 ± 0.016 ± 0.019	1.035 ± 0.009 ± 0.010	1.024 ± 0.005 ± 0.004	1.020 ± 0.003 ± 0.003	1.031 ± 0.004 ± 0.003	1.028 ± 0.007 ± 0.006
[1.37, 1.52]	0.986 ± 0.024 ± 0.021	1.006 ± 0.013 ± 0.013	0.997 ± 0.007 ± 0.010	1.011 ± 0.004 ± 0.005	1.012 ± 0.003 ± 0.005	1.013 ± 0.004 ± 0.003	0.998 ± 0.007 ± 0.008
[1.52, 2.01]	0.994 ± 0.032 ± 0.022	1.017 ± 0.017 ± 0.011	1.020 ± 0.010 ± 0.012	1.015 ± 0.005 ± 0.005	1.016 ± 0.004 ± 0.003	1.025 ± 0.005 ± 0.003	1.011 ± 0.009 ± 0.009
[2.01, 2.37]	0.906 ± 0.024 ± 0.031	0.860 ± 0.012 ± 0.021	0.913 ± 0.007 ± 0.014	0.950 ± 0.004 ± 0.006	0.960 ± 0.003 ± 0.004	0.973 ± 0.003 ± 0.004	0.949 ± 0.007 ± 0.010
[2.37, 2.47]	0.971 ± 0.055 ± 0.034	0.985 ± 0.030 ± 0.040	0.981 ± 0.016 ± 0.011	1.021 ± 0.010 ± 0.007	1.058 ± 0.007 ± 0.007	1.061 ± 0.009 ± 0.006	1.015 ± 0.017 ± 0.011

Table A.19: TightPP scale-factors in intermediate  $\eta$  granularity with their statistical and systematic uncertainties from 80 variations.

	15-20 GeV	20-25 GeV	25-30 GeV	30-35 GeV	35-40 GeV	40-45 GeV	45-50 GeV
[-2.47, -2.37]	0.459 ± 0.022 ± 0.017	0.518 ± 0.011 ± 0.012	0.579 ± 0.007 ± 0.007	0.617 ± 0.004 ± 0.003	0.660 ± 0.003 ± 0.003	0.704 ± 0.004 ± 0.004	0.705 ± 0.009 ± 0.011
[-2.37, -2.01]	0.595 ± 0.016 ± 0.019	0.575 ± 0.008 ± 0.015	0.651 ± 0.005 ± 0.009	0.693 ± 0.003 ± 0.004	0.734 ± 0.002 ± 0.002	0.784 ± 0.002 ± 0.004	0.777 ± 0.005 ± 0.008
[-2.01, -1.81]	0.623 ± 0.016 ± 0.012	0.633 ± 0.009 ± 0.013	0.673 ± 0.005 ± 0.007	0.712 ± 0.003 ± 0.003	0.748 ± 0.002 ± 0.002	0.795 ± 0.003 ± 0.003	0.788 ± 0.006 ± 0.007
[-1.81, -1.52]	0.630 ± 0.014 ± 0.018	0.661 ± 0.007 ± 0.012	0.701 ± 0.004 ± 0.006	0.741 ± 0.003 ± 0.003	0.774 ± 0.002 ± 0.002	0.819 ± 0.002 ± 0.003	0.817 ± 0.005 ± 0.006
[-1.37, -1.15]	0.702 ± 0.015 ± 0.022	0.698 ± 0.009 ± 0.014	0.731 ± 0.005 ± 0.008	0.768 ± 0.003 ± 0.004	0.802 ± 0.002 ± 0.003	0.828 ± 0.002 ± 0.003	0.826 ± 0.004 ± 0.004
[-1.15, -0.8]	0.734 ± 0.011 ± 0.018	0.736 ± 0.007 ± 0.012	0.772 ± 0.004 ± 0.005	0.806 ± 0.002 ± 0.003	0.830 ± 0.002 ± 0.003	0.845 ± 0.002 ± 0.002	0.848 ± 0.003 ± 0.004
[-0.8, -0.6]	0.752 ± 0.015 ± 0.018	0.745 ± 0.009 ± 0.012	0.784 ± 0.005 ± 0.007	0.831 ± 0.003 ± 0.004	0.857 ± 0.002 ± 0.002	0.870 ± 0.002 ± 0.002	0.876 ± 0.004 ± 0.004
[-0.6, -0.1]	0.772 ± 0.009 ± 0.013	0.761 ± 0.005 ± 0.011	0.806 ± 0.003 ± 0.006	0.839 ± 0.002 ± 0.003	0.862 ± 0.001 ± 0.002	0.854 ± 0.001 ± 0.002	0.855 ± 0.003 ± 0.003
[-0.1, 0]	0.729 ± 0.019 ± 0.015	0.711 ± 0.012 ± 0.009	0.746 ± 0.007 ± 0.005	0.771 ± 0.004 ± 0.003	0.795 ± 0.003 ± 0.002	0.798 ± 0.003 ± 0.002	0.802 ± 0.006 ± 0.004
[0, 0.1]	0.712 ± 0.020 ± 0.013	0.700 ± 0.013 ± 0.010	0.744 ± 0.007 ± 0.005	0.764 ± 0.004 ± 0.003	0.797 ± 0.003 ± 0.002	0.798 ± 0.003 ± 0.002	0.791 ± 0.006 ± 0.002
[0.1, 0.6]	0.791 ± 0.009 ± 0.015	0.767 ± 0.005 ± 0.012	0.812 ± 0.003 ± 0.006	0.838 ± 0.002 ± 0.003	0.861 ± 0.001 ± 0.002	0.850 ± 0.001 ± 0.002	0.853 ± 0.003 ± 0.003
[0.6, 0.8]	0.767 ± 0.015 ± 0.017	0.746 ± 0.009 ± 0.012	0.792 ± 0.005 ± 0.007	0.833 ± 0.003 ± 0.005	0.863 ± 0.002 ± 0.002	0.875 ± 0.002 ± 0.002	0.875 ± 0.004 ± 0.004
[0.8, 1.15]	0.716 ± 0.011 ± 0.022	0.733 ± 0.007 ± 0.012	0.772 ± 0.004 ± 0.006	0.806 ± 0.002 ± 0.003	0.833 ± 0.002 ± 0.002	0.847 ± 0.002 ± 0.003	0.851 ± 0.004 ± 0.005
[1.15, 1.37]	0.676 ± 0.014 ± 0.021	0.682 ± 0.009 ± 0.015	0.727 ± 0.005 ± 0.008	0.764 ± 0.003 ± 0.004	0.797 ± 0.002 ± 0.003	0.828 ± 0.002 ± 0.003	0.826 ± 0.004 ± 0.006
[1.37, 1.52]	0.636 ± 0.013 ± 0.018	0.672 ± 0.008 ± 0.010	0.712 ± 0.005 ± 0.006	0.748 ± 0.003 ± 0.003	0.779 ± 0.002 ± 0.002	0.820 ± 0.002 ± 0.002	0.820 ± 0.005 ± 0.006
[1.52, 2.01]	0.618 ± 0.017 ± 0.017	0.651 ± 0.010 ± 0.007	0.679 ± 0.006 ± 0.009	0.718 ± 0.003 ± 0.004	0.750 ± 0.002 ± 0.002	0.797 ± 0.003 ± 0.003	0.792 ± 0.006 ± 0.007
[2.01, 2.37]	0.596 ± 0.014 ± 0.021	0.581 ± 0.007 ± 0.014	0.649 ± 0.005 ± 0.009	0.699 ± 0.002 ± 0.004	0.737 ± 0.002 ± 0.002	0.783 ± 0.002 ± 0.004	0.772 ± 0.005 ± 0.008
[2.37, 2.47]	0.511 ± 0.022 ± 0.017	0.523 ± 0.012 ± 0.016	0.578 ± 0.007 ± 0.007	0.618 ± 0.004 ± 0.004	0.661 ± 0.003 ± 0.003	0.713 ± 0.004 ± 0.004	0.700 ± 0.008 ± 0.008

Table A.20: TightPP efficiencies in intermediate  $\eta$  granularity with their statistical and systematic uncertainties from 80 variations.

	15-20 GeV	20-25 GeV	25-30 GeV	30-35 GeV	35-40 GeV	40-45 GeV	45-50 GeV
[-2.47, -2.37]	0.501 ± 0.021 ± 0.003	0.522 ± 0.011 ± 0.000	0.573 ± 0.006 ± 0.002	0.598 ± 0.004 ± 0.002	0.619 ± 0.003 ± 0.000	0.669 ± 0.004 ± 0.000	0.671 ± 0.008 ± 0.001
[-2.37, -2.01]	0.659 ± 0.009 ± 0.003	0.673 ± 0.005 ± 0.002	0.708 ± 0.003 ± 0.003	0.735 ± 0.002 ± 0.003	0.769 ± 0.001 ± 0.001	0.806 ± 0.002 ± 0.001	0.814 ± 0.003 ± 0.001
[-2.01, -1.81]	0.611 ± 0.012 ± 0.003	0.641 ± 0.006 ± 0.003	0.660 ± 0.004 ± 0.003	0.701 ± 0.003 ± 0.001	0.736 ± 0.002 ± 0.001	0.781 ± 0.003 ± 0.001	0.788 ± 0.005 ± 0.002
[-1.81, -1.52]	0.644 ± 0.009 ± 0.004	0.673 ± 0.005 ± 0.001	0.706 ± 0.003 ± 0.002	0.736 ± 0.002 ± 0.002	0.764 ± 0.002 ± 0.002	0.803 ± 0.002 ± 0.001	0.816 ± 0.004 ± 0.001
[-1.37, -1.15]	0.643 ± 0.011 ± 0.004	0.666 ± 0.006 ± 0.003	0.709 ± 0.004 ± 0.002	0.746 ± 0.002 ± 0.003	0.783 ± 0.002 ± 0.001	0.801 ± 0.002 ± 0.001	0.802 ± 0.004 ± 0.002
[-1.15, -0.8]	0.712 ± 0.008 ± 0.005	0.726 ± 0.004 ± 0.002	0.758 ± 0.003 ± 0.004	0.796 ± 0.002 ± 0.001	0.821 ± 0.001 ± 0.002	0.835 ± 0.002 ± 0.001	0.845 ± 0.003 ± 0.001
[-0.8, -0.6]	0.764 ± 0.009 ± 0.005	0.760 ± 0.005 ± 0.002	0.797 ± 0.003 ± 0.001	0.835 ± 0.002 ± 0.001	0.859 ± 0.001 ± 0.001	0.873 ± 0.002 ± 0.001	0.874 ± 0.003 ± 0.001
[-0.6, -0.1]	0.795 ± 0.005 ± 0.001	0.777 ± 0.003 ± 0.003	0.818 ± 0.002 ± 0.002	0.849 ± 0.001 ± 0.002	0.868 ± 0.001 ± 0.001	0.867 ± 0.001 ± 0.002	0.874 ± 0.002 ± 0.001
[-0.1, 0]	0.701 ± 0.014 ± 0.004	0.704 ± 0.008 ± 0.001	0.743 ± 0.005 ± 0.005	0.769 ± 0.003 ± 0.001	0.790 ± 0.002 ± 0.000	0.793 ± 0.003 ± 0.001	0.783 ± 0.006 ± 0.001
[0, 0.1]	0.711 ± 0.015 ± 0.003	0.704 ± 0.008 ± 0.002	0.735 ± 0.005 ± 0.002	0.756 ± 0.003 ± 0.001	0.778 ± 0.003 ± 0.001	0.780 ± 0.003 ± 0.001	0.782 ± 0.006 ± 0.001
[0.1, 0.6]	0.794 ± 0.006 ± 0.002	0.776 ± 0.003 ± 0.001	0.822 ± 0.002 ± 0.001	0.851 ± 0.001 ± 0.001	0.869 ± 0.001 ± 0.002	0.866 ± 0.001 ± 0.001	0.872 ± 0.002 ± 0.001
[0.6, 0.8]	0.761 ± 0.010 ± 0.003	0.762 ± 0.005 ± 0.002	0.805 ± 0.003 ± 0.002	0.838 ± 0.002 ± 0.003	0.862 ± 0.001 ± 0.001	0.873 ± 0.002 ± 0.002	0.881 ± 0.003 ± 0.001
[0.8, 1.15]	0.700 ± 0.008 ± 0.001	0.723 ± 0.005 ± 0.002	0.766 ± 0.003 ± 0.001	0.799 ± 0.002 ± 0.002	0.825 ± 0.001 ± 0.002	0.840 ± 0.002 ± 0.001	0.846 ± 0.003 ± 0.001
[1.15, 1.37]	0.647 ± 0.011 ± 0.005	0.667 ± 0.006 ± 0.002	0.702 ± 0.004 ± 0.001	0.746 ± 0.002 ± 0.002	0.782 ± 0.002 ± 0.003	0.803 ± 0.002 ± 0.002	0.803 ± 0.004 ± 0.001
[1.37, 1.52]	0.644 ± 0.009 ± 0.004	0.667 ± 0.005 ± 0.002	0.714 ± 0.003 ± 0.002	0.740 ± 0.002 ± 0.001	0.770 ± 0.002 ± 0.002	0.809 ± 0.002 ± 0.001	0.821 ± 0.003 ± 0.001
[1.52, 2.01]	0.621 ± 0.012 ± 0.004	0.639 ± 0.006 ± 0.001	0.665 ± 0.004 ± 0.001	0.708 ± 0.002 ± 0.002	0.739 ± 0.002 ± 0.001	0.777 ± 0.003 ± 0.000	0.783 ± 0.005 ± 0.001
[2.01, 2.37]	0.657 ± 0.009 ± 0.001	0.674 ± 0.005 ± 0.004	0.710 ± 0.003 ± 0.003	0.735 ± 0.002 ± 0.002	0.767 ± 0.001 ± 0.001	0.805 ± 0.002 ± 0.000	0.813 ± 0.003 ± 0.001
[2.37, 2.47]	0.524 ± 0.021 ± 0.003	0.531 ± 0.011 ± 0.009	0.589 ± 0.006 ± 0.001	0.605 ± 0.004 ± 0.002	0.625 ± 0.003 ± 0.003	0.672 ± 0.004 ± 0.001	0.689 ± 0.008 ± 0.003

Table A.21: TightPP Monte-Carlo efficiencies in intermediate  $\eta$  granularity with their statistical and systematic uncertainties from 80 variations.

	15-20 GeV	20-25 GeV	25-30 GeV	30-35 GeV	35-40 GeV	40-45 GeV	45-50 GeV
[-2.47, -2.4]	1.005 ± 0.028 ± 0.012	0.995 ± 0.012 ± 0.007	1.002 ± 0.008 ± 0.006	0.997 ± 0.004 ± 0.003	0.996 ± 0.002 ± 0.003	1.000 ± 0.004 ± 0.002	1.002 ± 0.010 ± 0.009
[-2.4, -2.3]	0.955 ± 0.026 ± 0.013	0.979 ± 0.013 ± 0.015	0.992 ± 0.007 ± 0.009	0.990 ± 0.004 ± 0.003	0.993 ± 0.002 ± 0.002	0.994 ± 0.003 ± 0.002	0.993 ± 0.007 ± 0.007
[-2.3, -2.2]	0.956 ± 0.025 ± 0.013	0.958 ± 0.012 ± 0.011	0.986 ± 0.007 ± 0.009	0.998 ± 0.004 ± 0.003	0.995 ± 0.002 ± 0.002	0.998 ± 0.003 ± 0.002	0.993 ± 0.007 ± 0.007
[-2.2, -2.1]	0.976 ± 0.025 ± 0.016	0.973 ± 0.012 ± 0.012	0.995 ± 0.007 ± 0.009	1.000 ± 0.004 ± 0.003	0.998 ± 0.002 ± 0.002	1.000 ± 0.003 ± 0.001	0.997 ± 0.007 ± 0.008
[-2.1, -2.01]	0.983 ± 0.029 ± 0.018	0.982 ± 0.012 ± 0.010	1.003 ± 0.007 ± 0.005	0.992 ± 0.004 ± 0.003	0.989 ± 0.002 ± 0.002	0.985 ± 0.003 ± 0.002	0.981 ± 0.007 ± 0.007
[-2.01, -1.9]	0.990 ± 0.025 ± 0.014	1.005 ± 0.014 ± 0.011	1.006 ± 0.007 ± 0.007	1.005 ± 0.004 ± 0.003	1.004 ± 0.002 ± 0.003	1.011 ± 0.003 ± 0.001	1.011 ± 0.008 ± 0.009
[-1.9, -1.8]	1.022 ± 0.026 ± 0.013	1.015 ± 0.014 ± 0.012	1.005 ± 0.007 ± 0.007	1.012 ± 0.003 ± 0.004	1.010 ± 0.003 ± 0.002	1.009 ± 0.003 ± 0.003	1.004 ± 0.006 ± 0.005
[-1.8, -1.7]	1.008 ± 0.027 ± 0.019	0.994 ± 0.016 ± 0.008	1.007 ± 0.008 ± 0.006	1.011 ± 0.004 ± 0.003	1.013 ± 0.003 ± 0.002	1.006 ± 0.003 ± 0.003	1.000 ± 0.006 ± 0.007
[-1.7, -1.6]	0.968 ± 0.026 ± 0.011	0.992 ± 0.013 ± 0.010	1.000 ± 0.007 ± 0.004	1.007 ± 0.004 ± 0.003	1.010 ± 0.003 ± 0.003	1.004 ± 0.003 ± 0.003	1.000 ± 0.006 ± 0.006
[-1.6, -1.52]	1.003 ± 0.025 ± 0.021	0.987 ± 0.011 ± 0.011	1.004 ± 0.007 ± 0.008	1.011 ± 0.004 ± 0.004	1.007 ± 0.003 ± 0.003	1.007 ± 0.004 ± 0.003	0.999 ± 0.007 ± 0.004
[-1.52, -1.3]	1.000 ± 0.025 ± 0.017	1.006 ± 0.018 ± 0.015	1.018 ± 0.008 ± 0.007	1.011 ± 0.004 ± 0.003	1.006 ± 0.003 ± 0.003	1.010 ± 0.003 ± 0.002	1.007 ± 0.005 ± 0.005
[-1.3, -1.2]	1.010 ± 0.022 ± 0.023	1.031 ± 0.015 ± 0.017	1.004 ± 0.007 ± 0.009	1.013 ± 0.004 ± 0.003	1.005 ± 0.002 ± 0.002	1.004 ± 0.002 ± 0.002	1.001 ± 0.004 ± 0.004
[-1.2, -1.1]	0.990 ± 0.021 ± 0.023	0.996 ± 0.013 ± 0.014	1.013 ± 0.007 ± 0.008	1.014 ± 0.004 ± 0.004	1.010 ± 0.002 ± 0.002	1.007 ± 0.002 ± 0.002	0.993 ± 0.004 ± 0.007
[-1.1, -1]	1.024 ± 0.023 ± 0.027	1.004 ± 0.014 ± 0.018	1.012 ± 0.007 ± 0.008	1.007 ± 0.004 ± 0.003	1.011 ± 0.002 ± 0.002	1.004 ± 0.002 ± 0.002	1.002 ± 0.005 ± 0.005
[-1, -0.9]	1.029 ± 0.026 ± 0.028	1.012 ± 0.015 ± 0.019	1.007 ± 0.007 ± 0.007	1.008 ± 0.004 ± 0.002	1.006 ± 0.002 ± 0.003	1.005 ± 0.002 ± 0.002	1.000 ± 0.005 ± 0.004
[-0.9, -0.8]	0.989 ± 0.020 ± 0.016	1.002 ± 0.014 ± 0.005	1.009 ± 0.008 ± 0.005	1.003 ± 0.004 ± 0.004	0.999 ± 0.002 ± 0.002	1.002 ± 0.002 ± 0.003	1.002 ± 0.005 ± 0.003
[-0.8, -0.7]	0.995 ± 0.022 ± 0.016	0.992 ± 0.012 ± 0.012	0.993 ± 0.007 ± 0.007	0.992 ± 0.004 ± 0.005	0.992 ± 0.002 ± 0.002	0.996 ± 0.002 ± 0.002	1.000 ± 0.005 ± 0.005
[-0.7, -0.6]	0.963 ± 0.020 ± 0.016	0.989 ± 0.012 ± 0.014	0.990 ± 0.006 ± 0.009	0.988 ± 0.003 ± 0.005	0.996 ± 0.002 ± 0.002	0.998 ± 0.002 ± 0.002	0.996 ± 0.005 ± 0.004
[-0.6, -0.5]	0.959 ± 0.020 ± 0.016	0.994 ± 0.011 ± 0.011	1.000 ± 0.006 ± 0.009	0.999 ± 0.003 ± 0.004	1.001 ± 0.002 ± 0.001	1.000 ± 0.002 ± 0.003	1.000 ± 0.005 ± 0.003
[-0.5, -0.4]	1.003 ± 0.022 ± 0.016	1.002 ± 0.012 ± 0.015	0.996 ± 0.006 ± 0.006	1.001 ± 0.003 ± 0.004	1.001 ± 0.002 ± 0.002	0.999 ± 0.002 ± 0.002	1.000 ± 0.005 ± 0.004
[-0.4, -0.3]	0.992 ± 0.019 ± 0.014	0.994 ± 0.011 ± 0.017	0.995 ± 0.006 ± 0.006	1.005 ± 0.003 ± 0.003	1.002 ± 0.002 ± 0.002	0.998 ± 0.002 ± 0.002	1.003 ± 0.005 ± 0.003
[-0.3, -0.2]	0.988 ± 0.018 ± 0.014	1.005 ± 0.011 ± 0.008	1.001 ± 0.006 ± 0.006	1.003 ± 0.003 ± 0.003	1.000 ± 0.002 ± 0.002	1.003 ± 0.002 ± 0.002	0.996 ± 0.004 ± 0.004
[-0.2, -0.1]	0.964 ± 0.018 ± 0.017	0.993 ± 0.012 ± 0.016	1.000 ± 0.006 ± 0.006	0.999 ± 0.003 ± 0.003	1.002 ± 0.002 ± 0.001	1.004 ± 0.002 ± 0.002	0.999 ± 0.004 ± 0.003
[-0.1, 0]	1.002 ± 0.020 ± 0.014	1.005 ± 0.012 ± 0.011	1.003 ± 0.006 ± 0.005	0.997 ± 0.003 ± 0.004	1.001 ± 0.002 ± 0.002	1.001 ± 0.002 ± 0.002	1.003 ± 0.004 ± 0.003
[0, 0.1]	0.995 ± 0.020 ± 0.014	1.001 ± 0.013 ± 0.011	1.000 ± 0.006 ± 0.005	0.999 ± 0.003 ± 0.004	1.004 ± 0.002 ± 0.003	1.004 ± 0.002 ± 0.003	0.998 ± 0.005 ± 0.002
[0.1, 0.2]	1.001 ± 0.020 ± 0.020	1.005 ± 0.011 ± 0.016	1.005 ± 0.006 ± 0.006	1.003 ± 0.003 ± 0.003	1.006 ± 0.002 ± 0.001	1.001 ± 0.002 ± 0.001	1.000 ± 0.004 ± 0.004
[0.2, 0.3]	0.999 ± 0.019 ± 0.012	1.009 ± 0.012 ± 0.008	1.001 ± 0.006 ± 0.006	1.000 ± 0.003 ± 0.003	1.001 ± 0.002 ± 0.002	1.002 ± 0.002 ± 0.002	0.998 ± 0.004 ± 0.004
[0.3, 0.4]	0.996 ± 0.019 ± 0.013	0.992 ± 0.012 ± 0.018	1.008 ± 0.007 ± 0.007	0.999 ± 0.003 ± 0.003	0.998 ± 0.002 ± 0.002	1.001 ± 0.002 ± 0.002	1.009 ± 0.005 ± 0.002
[0.4, 0.5]	1.001 ± 0.022 ± 0.021	1.016 ± 0.013 ± 0.016	1.002 ± 0.007 ± 0.006	1.001 ± 0.003 ± 0.003	1.003 ± 0.002 ± 0.003	0.999 ± 0.002 ± 0.002	1.002 ± 0.005 ± 0.004
[0.5, 0.6]	0.997 ± 0.021 ± 0.017	0.993 ± 0.012 ± 0.012	1.005 ± 0.007 ± 0.009	1.000 ± 0.003 ± 0.004	0.999 ± 0.002 ± 0.002	1.001 ± 0.002 ± 0.002	1.001 ± 0.005 ± 0.004
[0.6, 0.7]	1.002 ± 0.023 ± 0.018	0.983 ± 0.013 ± 0.016	0.990 ± 0.006 ± 0.009	0.993 ± 0.003 ± 0.005	1.001 ± 0.002 ± 0.002	1.001 ± 0.002 ± 0.002	0.999 ± 0.005 ± 0.003
[0.7, 0.8]	0.996 ± 0.021 ± 0.018	1.002 ± 0.013 ± 0.013	0.997 ± 0.007 ± 0.007	0.992 ± 0.004 ± 0.005	0.997 ± 0.002 ± 0.003	0.997 ± 0.002 ± 0.003	0.995 ± 0.005 ± 0.005
[0.8, 0.9]	0.965 ± 0.021 ± 0.019	1.005 ± 0.014 ± 0.005	1.001 ± 0.008 ± 0.005	1.007 ± 0.004 ± 0.005	1.001 ± 0.002 ± 0.002	1.000 ± 0.002 ± 0.002	0.998 ± 0.005 ± 0.003
[0.9, 1]	0.998 ± 0.023 ± 0.018	1.013 ± 0.015 ± 0.018	1.001 ± 0.007 ± 0.006	1.005 ± 0.004 ± 0.003	1.002 ± 0.002 ± 0.002	1.006 ± 0.002 ± 0.003	1.010 ± 0.005 ± 0.004
[1, 1.1]	1.000 ± 0.023 ± 0.025	0.993 ± 0.014 ± 0.018	1.004 ± 0.007 ± 0.007	1.009 ± 0.004 ± 0.003	1.008 ± 0.002 ± 0.002	1.004 ± 0.002 ± 0.003	1.008 ± 0.005 ± 0.005
[1.1, 1.2]	0.999 ± 0.021 ± 0.024	1.010 ± 0.014 ± 0.013	1.011 ± 0.007 ± 0.008	1.007 ± 0.004 ± 0.004	1.009 ± 0.002 ± 0.003	1.006 ± 0.002 ± 0.002	1.000 ± 0.005 ± 0.007
[1.2, 1.3]	0.995 ± 0.022 ± 0.023	0.999 ± 0.014 ± 0.014	1.013 ± 0.007 ± 0.009	1.005 ± 0.004 ± 0.004	1.004 ± 0.002 ± 0.003	1.006 ± 0.002 ± 0.003	0.994 ± 0.004 ± 0.005
[1.3, 1.37]	1.035 ± 0.028 ± 0.020	1.022 ± 0.019 ± 0.017	1.015 ± 0.009 ± 0.008	1.013 ± 0.005 ± 0.003	1.006 ± 0.003 ± 0.003	1.008 ± 0.003 ± 0.003	1.009 ± 0.006 ± 0.005
[1.52, 1.6]	0.997 ± 0.025 ± 0.020	1.014 ± 0.013 ± 0.009	1.009 ± 0.007 ± 0.008	1.011 ± 0.004 ± 0.004	1.007 ± 0.003 ± 0.003	1.008 ± 0.003 ± 0.003	1.002 ± 0.008 ± 0.005
[1.6, 1.7]	1.008 ± 0.026 ± 0.012	0.989 ± 0.014 ± 0.011	1.013 ± 0.008 ± 0.004	1.008 ± 0.004 ± 0.004	1.007 ± 0.003 ± 0.003	1.004 ± 0.003 ± 0.002	0.986 ± 0.006 ± 0.006
[1.7, 1.8]	0.986 ± 0.023 ± 0.015	0.997 ± 0.016 ± 0.008	1.007 ± 0.008 ± 0.006	1.010 ± 0.004 ± 0.003	1.009 ± 0.003 ± 0.003	1.008 ± 0.003 ± 0.002	1.001 ± 0.006 ± 0.006
[1.8, 1.9]	0.985 ± 0.026 ± 0.014	1.011 ± 0.014 ± 0.006	1.005 ± 0.007 ± 0.008	1.010 ± 0.004 ± 0.004	1.011 ± 0.002 ± 0.002	1.006 ± 0.003 ± 0.003	1.007 ± 0.006 ± 0.004
[1.9, 2.01]	0.989 ± 0.025 ± 0.019	1.002 ± 0.016 ± 0.010	1.009 ± 0.009 ± 0.009	1.007 ± 0.004 ± 0.004	1.007 ± 0.002 ± 0.002	1.009 ± 0.004 ± 0.002	1.004 ± 0.008 ± 0.008
[2.01, 2.1]	0.962 ± 0.023 ± 0.017	0.980 ± 0.012 ± 0.008	0.997 ± 0.007 ± 0.010	1.000 ± 0.003 ± 0.003	0.999 ± 0.002 ± 0.002	0.998 ± 0.003 ± 0.001	0.990 ± 0.007 ± 0.006
[2.1, 2.2]	0.949 ± 0.023 ± 0.016	0.978 ± 0.012 ± 0.011	0.991 ± 0.006 ± 0.008	0.998 ± 0.003 ± 0.003	0.999 ± 0.002 ± 0.002	1.002 ± 0.003 ± 0.002	0.993 ± 0.007 ± 0.007
[2.2, 2.3]	0.969 ± 0.023 ± 0.020	0.961 ± 0.012 ± 0.013	0.985 ± 0.006 ± 0.010	0.997 ± 0.003 ± 0.003	0.998 ± 0.002 ± 0.002	1.000 ± 0.003 ± 0.001	0.994 ± 0.007 ± 0.007
[2.3, 2.4]	0.951 ± 0.025 ± 0.023	0.968 ± 0.012 ± 0.014	0.991 ± 0.008 ± 0.007	0.987 ± 0.003 ± 0.003	0.993 ± 0.002 ± 0.002	0.993 ± 0.003 ± 0.001	0.981 ± 0.007 ± 0.007
[2.4, 2.47]	0.986 ± 0.022 ± 0.010	0.993 ± 0.013 ± 0.009	0.997 ± 0.006 ± 0.004	0.998 ± 0.004 ± 0.003	0.996 ± 0.002 ± 0.002	0.999 ± 0.004 ± 0.002	1.001 ± 0.009 ± 0.008

Table A.22: LoosePP scale-factors in fine  $\eta$  granularity with their statistical and systematic uncertainties from 80 variations.

	15-20 GeV	20-25 GeV	25-30 GeV	30-35 GeV	35-40 GeV	40-45 GeV	45-50 GeV
[-2.47, -2.4]	0.999 ± 0.029 ± 0.012	0.982 ± 0.013 ± 0.008	0.991 ± 0.008 ± 0.005	0.988 ± 0.004 ± 0.003	0.989 ± 0.002 ± 0.003	0.993 ± 0.004 ± 0.002	1.000 ± 0.011 ± 0.010
[-2.4, -2.3]	0.925 ± 0.026 ± 0.018	0.952 ± 0.014 ± 0.013	0.973 ± 0.007 ± 0.009	0.969 ± 0.004 ± 0.003	0.975 ± 0.002 ± 0.002	0.979 ± 0.003 ± 0.001	0.978 ± 0.008 ± 0.007
[-2.3, -2.2]	0.945 ± 0.027 ± 0.024	0.942 ± 0.013 ± 0.011	0.972 ± 0.007 ± 0.008	0.981 ± 0.004 ± 0.003	0.982 ± 0.002 ± 0.002	0.988 ± 0.003 ± 0.001	0.984 ± 0.007 ± 0.007
[-2.2, -2.1]	0.960 ± 0.027 ± 0.015	0.949 ± 0.012 ± 0.012	0.978 ± 0.007 ± 0.008	0.984 ± 0.004 ± 0.003	0.984 ± 0.002 ± 0.002	0.987 ± 0.003 ± 0.001	0.988 ± 0.008 ± 0.008
[-2.1, -2.01]	0.946 ± 0.028 ± 0.019	0.954 ± 0.013 ± 0.009	0.974 ± 0.007 ± 0.005	0.960 ± 0.004 ± 0.003	0.963 ± 0.002 ± 0.002	0.959 ± 0.003 ± 0.002	0.954 ± 0.008 ± 0.007
[-2.01, -1.9]	0.931 ± 0.025 ± 0.011	0.968 ± 0.014 ± 0.010	0.972 ± 0.007 ± 0.007	0.970 ± 0.004 ± 0.003	0.978 ± 0.002 ± 0.002	0.987 ± 0.003 ± 0.001	0.987 ± 0.008 ± 0.008
[-1.9, -1.8]	0.963 ± 0.025 ± 0.011	0.963 ± 0.014 ± 0.011	0.965 ± 0.008 ± 0.007	0.972 ± 0.003 ± 0.004	0.979 ± 0.003 ± 0.003	0.980 ± 0.003 ± 0.003	0.979 ± 0.006 ± 0.005
[-1.8, -1.7]	0.969 ± 0.028 ± 0.017	0.950 ± 0.017 ± 0.008	0.968 ± 0.008 ± 0.006	0.978 ± 0.004 ± 0.003	0.987 ± 0.003 ± 0.002	0.987 ± 0.003 ± 0.003	0.981 ± 0.006 ± 0.006
[-1.7, -1.6]	0.927 ± 0.026 ± 0.011	0.927 ± 0.013 ± 0.010	0.954 ± 0.007 ± 0.004	0.970 ± 0.004 ± 0.003	0.982 ± 0.003 ± 0.002	0.983 ± 0.003 ± 0.003	0.978 ± 0.006 ± 0.006
[-1.6, -1.52]	0.950 ± 0.025 ± 0.020	0.933 ± 0.011 ± 0.010	0.955 ± 0.007 ± 0.007	0.974 ± 0.004 ± 0.004	0.981 ± 0.003 ± 0.002	0.985 ± 0.004 ± 0.003	0.980 ± 0.007 ± 0.004
[-1.37, -1.3]	0.951 ± 0.024 ± 0.017	0.946 ± 0.017 ± 0.013	0.967 ± 0.008 ± 0.007	0.970 ± 0.004 ± 0.003	0.978 ± 0.003 ± 0.003	0.990 ± 0.002 ± 0.002	0.982 ± 0.005 ± 0.005
[-1.3, -1.2]	0.959 ± 0.021 ± 0.022	0.957 ± 0.014 ± 0.015	0.954 ± 0.007 ± 0.009	0.969 ± 0.003 ± 0.003	0.977 ± 0.002 ± 0.002	0.985 ± 0.002 ± 0.002	0.982 ± 0.004 ± 0.004
[-1.2, -1.1]	0.937 ± 0.020 ± 0.022	0.928 ± 0.012 ± 0.014	0.963 ± 0.007 ± 0.008	0.968 ± 0.003 ± 0.004	0.978 ± 0.002 ± 0.003	0.982 ± 0.002 ± 0.002	0.977 ± 0.004 ± 0.007
[-1.1, -1]	0.963 ± 0.023 ± 0.026	0.945 ± 0.014 ± 0.017	0.968 ± 0.007 ± 0.007	0.971 ± 0.004 ± 0.003	0.983 ± 0.002 ± 0.002	0.984 ± 0.002 ± 0.002	0.984 ± 0.005 ± 0.005
[-1, -0.9]	0.977 ± 0.026 ± 0.023	0.958 ± 0.016 ± 0.018	0.968 ± 0.007 ± 0.006	0.977 ± 0.004 ± 0.002	0.984 ± 0.003 ± 0.002	0.989 ± 0.002 ± 0.002	0.988 ± 0.005 ± 0.004
[-0.9, -0.8]	0.937 ± 0.019 ± 0.016	0.937 ± 0.014 ± 0.006	0.972 ± 0.009 ± 0.005	0.970 ± 0.004 ± 0.004	0.976 ± 0.002 ± 0.002	0.982 ± 0.002 ± 0.003	0.985 ± 0.005 ± 0.003
[-0.8, -0.7]	0.932 ± 0.021 ± 0.015	0.934 ± 0.012 ± 0.011	0.952 ± 0.007 ± 0.007	0.951 ± 0.003 ± 0.005	0.964 ± 0.002 ± 0.003	0.973 ± 0.002 ± 0.002	0.977 ± 0.005 ± 0.005
[-0.7, -0.6]	0.923 ± 0.021 ± 0.016	0.953 ± 0.013 ± 0.014	0.956 ± 0.006 ± 0.008	0.968 ± 0.003 ± 0.005	0.975 ± 0.002 ± 0.002	0.981 ± 0.002 ± 0.002	0.980 ± 0.005 ± 0.003
[-0.6, -0.5]	0.926 ± 0.021 ± 0.016	0.962 ± 0.011 ± 0.011	0.976 ± 0.007 ± 0.009	0.973 ± 0.003 ± 0.004	0.980 ± 0.002 ± 0.001	0.981 ± 0.002 ± 0.002	0.982 ± 0.005 ± 0.002
[-0.5, -0.4]	0.963 ± 0.022 ± 0.015	0.969 ± 0.012 ± 0.014	0.968 ± 0.006 ± 0.006	0.974 ± 0.003 ± 0.004	0.979 ± 0.002 ± 0.002	0.980 ± 0.002 ± 0.002	0.980 ± 0.005 ± 0.004
[-0.4, -0.3]	0.949 ± 0.019 ± 0.013	0.958 ± 0.012 ± 0.016	0.968 ± 0.007 ± 0.005	0.977 ± 0.004 ± 0.002	0.981 ± 0.002 ± 0.002	0.978 ± 0.002 ± 0.002	0.986 ± 0.005 ± 0.003
[-0.3, -0.2]	0.957 ± 0.018 ± 0.013	0.970 ± 0.012 ± 0.008	0.975 ± 0.006 ± 0.006	0.978 ± 0.003 ± 0.003	0.980 ± 0.002 ± 0.002	0.983 ± 0.002 ± 0.002	0.976 ± 0.004 ± 0.004
[-0.2, -0.1]	0.930 ± 0.018 ± 0.017	0.954 ± 0.012 ± 0.015	0.967 ± 0.006 ± 0.005	0.970 ± 0.003 ± 0.003	0.981 ± 0.002 ± 0.001	0.982 ± 0.002 ± 0.001	0.983 ± 0.004 ± 0.003
[-0.1, 0]	0.960 ± 0.020 ± 0.013	0.967 ± 0.012 ± 0.011	0.974 ± 0.007 ± 0.005	0.968 ± 0.003 ± 0.004	0.979 ± 0.002 ± 0.002	0.982 ± 0.002 ± 0.002	0.983 ± 0.004 ± 0.003
[0, 0.1]	0.964 ± 0.021 ± 0.013	0.964 ± 0.013 ± 0.011	0.970 ± 0.006 ± 0.005	0.970 ± 0.003 ± 0.004	0.983 ± 0.002 ± 0.002	0.982 ± 0.002 ± 0.002	0.975 ± 0.005 ± 0.002
[0.1, 0.2]	0.968 ± 0.021 ± 0.020	0.971 ± 0.012 ± 0.015	0.976 ± 0.006 ± 0.005	0.975 ± 0.003 ± 0.003	0.984 ± 0.002 ± 0.001	0.980 ± 0.002 ± 0.001	0.981 ± 0.004 ± 0.004
[0.2, 0.3]	0.961 ± 0.019 ± 0.011	0.967 ± 0.012 ± 0.007	0.973 ± 0.006 ± 0.006	0.973 ± 0.003 ± 0.003	0.979 ± 0.002 ± 0.002	0.982 ± 0.002 ± 0.002	0.981 ± 0.004 ± 0.004
[0.3, 0.4]	0.956 ± 0.019 ± 0.013	0.961 ± 0.012 ± 0.018	0.981 ± 0.007 ± 0.006	0.973 ± 0.003 ± 0.002	0.978 ± 0.002 ± 0.002	0.979 ± 0.002 ± 0.002	0.989 ± 0.005 ± 0.002
[0.4, 0.5]	0.966 ± 0.023 ± 0.020	0.976 ± 0.013 ± 0.016	0.973 ± 0.006 ± 0.006	0.975 ± 0.003 ± 0.004	0.982 ± 0.002 ± 0.002	0.980 ± 0.002 ± 0.002	0.983 ± 0.005 ± 0.004
[0.5, 0.6]	0.966 ± 0.023 ± 0.017	0.958 ± 0.012 ± 0.012	0.980 ± 0.007 ± 0.009	0.976 ± 0.003 ± 0.004	0.979 ± 0.002 ± 0.001	0.981 ± 0.002 ± 0.002	0.984 ± 0.005 ± 0.003
[0.6, 0.7]	0.954 ± 0.023 ± 0.017	0.948 ± 0.014 ± 0.015	0.960 ± 0.007 ± 0.009	0.966 ± 0.003 ± 0.005	0.979 ± 0.002 ± 0.002	0.982 ± 0.002 ± 0.002	0.982 ± 0.005 ± 0.003
[0.7, 0.8]	0.936 ± 0.020 ± 0.017	0.946 ± 0.014 ± 0.013	0.956 ± 0.007 ± 0.007	0.955 ± 0.004 ± 0.005	0.970 ± 0.002 ± 0.002	0.976 ± 0.002 ± 0.003	0.976 ± 0.005 ± 0.005
[0.8, 0.9]	0.909 ± 0.020 ± 0.018	0.957 ± 0.015 ± 0.005	0.965 ± 0.008 ± 0.005	0.976 ± 0.004 ± 0.005	0.979 ± 0.002 ± 0.002	0.982 ± 0.002 ± 0.002	0.983 ± 0.005 ± 0.003
[0.9, 1]	0.946 ± 0.023 ± 0.016	0.959 ± 0.016 ± 0.018	0.964 ± 0.007 ± 0.005	0.973 ± 0.004 ± 0.003	0.979 ± 0.003 ± 0.003	0.989 ± 0.002 ± 0.003	0.994 ± 0.006 ± 0.004
[1, 1.1]	0.934 ± 0.022 ± 0.025	0.942 ± 0.014 ± 0.018	0.959 ± 0.007 ± 0.007	0.973 ± 0.004 ± 0.003	0.982 ± 0.002 ± 0.002	0.984 ± 0.002 ± 0.002	0.990 ± 0.005 ± 0.005
[1.1, 1.2]	0.933 ± 0.020 ± 0.023	0.937 ± 0.013 ± 0.014	0.955 ± 0.007 ± 0.008	0.964 ± 0.003 ± 0.004	0.979 ± 0.002 ± 0.003	0.984 ± 0.002 ± 0.002	0.981 ± 0.005 ± 0.007
[1.2, 1.3]	0.936 ± 0.021 ± 0.022	0.937 ± 0.014 ± 0.014	0.958 ± 0.007 ± 0.009	0.960 ± 0.003 ± 0.004	0.973 ± 0.002 ± 0.003	0.983 ± 0.002 ± 0.003	0.978 ± 0.004 ± 0.004
[1.3, 1.37]	0.977 ± 0.026 ± 0.020	0.959 ± 0.018 ± 0.014	0.959 ± 0.008 ± 0.008	0.965 ± 0.004 ± 0.003	0.977 ± 0.003 ± 0.003	0.983 ± 0.002 ± 0.002	0.986 ± 0.005 ± 0.005
[1.52, 1.6]	0.957 ± 0.026 ± 0.019	0.953 ± 0.013 ± 0.009	0.962 ± 0.007 ± 0.007	0.977 ± 0.005 ± 0.004	0.981 ± 0.003 ± 0.003	0.989 ± 0.003 ± 0.003	0.986 ± 0.005 ± 0.005
[1.6, 1.7]	0.964 ± 0.026 ± 0.013	0.924 ± 0.014 ± 0.010	0.965 ± 0.008 ± 0.004	0.972 ± 0.005 ± 0.004	0.982 ± 0.004 ± 0.002	0.983 ± 0.003 ± 0.002	0.970 ± 0.006 ± 0.006
[1.7, 1.8]	0.942 ± 0.023 ± 0.015	0.943 ± 0.016 ± 0.007	0.968 ± 0.009 ± 0.006	0.975 ± 0.004 ± 0.003	0.981 ± 0.003 ± 0.002	0.987 ± 0.003 ± 0.002	0.981 ± 0.006 ± 0.006
[1.8, 1.9]	0.946 ± 0.027 ± 0.014	0.962 ± 0.014 ± 0.006	0.968 ± 0.007 ± 0.008	0.971 ± 0.004 ± 0.004	0.979 ± 0.002 ± 0.002	0.980 ± 0.003 ± 0.003	0.983 ± 0.006 ± 0.004
[1.9, 2.01]	0.945 ± 0.026 ± 0.018	0.962 ± 0.016 ± 0.008	0.977 ± 0.009 ± 0.009	0.974 ± 0.005 ± 0.004	0.979 ± 0.002 ± 0.002	0.986 ± 0.004 ± 0.001	0.983 ± 0.008 ± 0.008
[2.01, 2.1]	0.925 ± 0.023 ± 0.016	0.950 ± 0.012 ± 0.009	0.968 ± 0.007 ± 0.009	0.966 ± 0.003 ± 0.003	0.973 ± 0.002 ± 0.002	0.970 ± 0.003 ± 0.001	0.964 ± 0.007 ± 0.006
[2.1, 2.2]	0.933 ± 0.024 ± 0.018	0.956 ± 0.012 ± 0.010	0.975 ± 0.007 ± 0.007	0.981 ± 0.004 ± 0.003	0.982 ± 0.002 ± 0.002	0.988 ± 0.003 ± 0.002	0.979 ± 0.008 ± 0.007
[2.2, 2.3]	0.951 ± 0.024 ± 0.020	0.944 ± 0.013 ± 0.012	0.968 ± 0.007 ± 0.010	0.979 ± 0.004 ± 0.003	0.983 ± 0.002 ± 0.002	0.989 ± 0.003 ± 0.002	0.979 ± 0.007 ± 0.007
[2.3, 2.4]	0.938 ± 0.027 ± 0.023	0.947 ± 0.012 ± 0.013	0.973 ± 0.008 ± 0.007	0.967 ± 0.004 ± 0.003	0.976 ± 0.002 ± 0.002	0.979 ± 0.003 ± 0.001	0.969 ± 0.008 ± 0.007
[2.4, 2.47]	0.981 ± 0.023 ± 0.010	0.982 ± 0.013 ± 0.009	0.989 ± 0.007 ± 0.005	0.991 ± 0.004 ± 0.003	0.990 ± 0.002 ± 0.002	0.995 ± 0.004 ± 0.002	0.997 ± 0.009 ± 0.008

Table A.23: LoosePP efficiencies in fine  $\eta$  granularity with their statistical and systematic uncertainties from 80 variations.

	15-20 GeV	20-25 GeV	25-30 GeV	30-35 GeV	35-40 GeV	40-45 GeV	45-50 GeV
[-2.47, -2.4]	0.994 ± 0.003 ± 0.000	0.987 ± 0.003 ± 0.001	0.989 ± 0.002 ± 0.001	0.991 ± 0.001 ± 0.000	0.993 ± 0.001 ± 0.000	0.994 ± 0.001 ± 0.000	0.998 ± 0.001 ± 0.000
[-2.4, -2.3]	0.969 ± 0.007 ± 0.002	0.972 ± 0.003 ± 0.002	0.981 ± 0.002 ± 0.001	0.979 ± 0.001 ± 0.000	0.982 ± 0.001 ± 0.000	0.985 ± 0.001 ± 0.000	0.984 ± 0.002 ± 0.000
[-2.3, -2.2]	0.989 ± 0.004 ± 0.001	0.983 ± 0.002 ± 0.000	0.985 ± 0.001 ± 0.001	0.984 ± 0.001 ± 0.001	0.986 ± 0.001 ± 0.000	0.990 ± 0.001 ± 0.000	0.990 ± 0.002 ± 0.000
[-2.2, -2.1]	0.984 ± 0.005 ± 0.002	0.975 ± 0.003 ± 0.001	0.983 ± 0.001 ± 0.001	0.982 ± 0.001 ± 0.001	0.986 ± 0.001 ± 0.000	0.987 ± 0.001 ± 0.000	0.990 ± 0.002 ± 0.000
[-2.1, -2.01]	0.963 ± 0.007 ± 0.002	0.971 ± 0.003 ± 0.001	0.971 ± 0.002 ± 0.000	0.968 ± 0.001 ± 0.000	0.974 ± 0.001 ± 0.000	0.974 ± 0.001 ± 0.001	0.972 ± 0.003 ± 0.000
[-2.01, -1.9]	0.941 ± 0.008 ± 0.001	0.963 ± 0.003 ± 0.001	0.966 ± 0.002 ± 0.000	0.965 ± 0.001 ± 0.001	0.974 ± 0.001 ± 0.000	0.976 ± 0.001 ± 0.000	0.976 ± 0.002 ± 0.001
[-1.9, -1.8]	0.942 ± 0.008 ± 0.001	0.948 ± 0.004 ± 0.001	0.960 ± 0.002 ± 0.000	0.960 ± 0.002 ± 0.000	0.969 ± 0.001 ± 0.001	0.974 ± 0.001 ± 0.001	0.975 ± 0.002 ± 0.001
[-1.8, -1.7]	0.962 ± 0.007 ± 0.002	0.955 ± 0.004 ± 0.001	0.962 ± 0.002 ± 0.001	0.968 ± 0.001 ± 0.000	0.974 ± 0.001 ± 0.000	0.979 ± 0.001 ± 0.000	0.980 ± 0.002 ± 0.001
[-1.7, -1.6]	0.957 ± 0.007 ± 0.001	0.935 ± 0.005 ± 0.001	0.954 ± 0.002 ± 0.001	0.963 ± 0.002 ± 0.001	0.972 ± 0.001 ± 0.001	0.979 ± 0.001 ± 0.000	0.977 ± 0.003 ± 0.000
[-1.6, -1.52]	0.949 ± 0.007 ± 0.004	0.945 ± 0.004 ± 0.000	0.952 ± 0.002 ± 0.001	0.964 ± 0.002 ± 0.001	0.974 ± 0.001 ± 0.001	0.979 ± 0.001 ± 0.000	0.981 ± 0.002 ± 0.000
[-1.37, -1.3]	0.950 ± 0.009 ± 0.003	0.941 ± 0.006 ± 0.001	0.950 ± 0.003 ± 0.001	0.960 ± 0.002 ± 0.001	0.972 ± 0.001 ± 0.001	0.980 ± 0.001 ± 0.001	0.982 ± 0.002 ± 0.001
[-1.3, -1.2]	0.950 ± 0.007 ± 0.002	0.928 ± 0.005 ± 0.003	0.949 ± 0.003 ± 0.001	0.956 ± 0.002 ± 0.001	0.972 ± 0.001 ± 0.001	0.980 ± 0.001 ± 0.000	0.980 ± 0.002 ± 0.001
[-1.2, -1.1]	0.948 ± 0.007 ± 0.001	0.931 ± 0.005 ± 0.003	0.950 ± 0.003 ± 0.001	0.955 ± 0.002 ± 0.001	0.969 ± 0.001 ± 0.000	0.976 ± 0.001 ± 0.000	0.983 ± 0.002 ± 0.001
[-1.1, -1]	0.940 ± 0.007 ± 0.002	0.941 ± 0.004 ± 0.002	0.956 ± 0.002 ± 0.001	0.963 ± 0.001 ± 0.001	0.973 ± 0.001 ± 0.000	0.980 ± 0.001 ± 0.000	0.981 ± 0.002 ± 0.000
[-1, -0.9]	0.948 ± 0.007 ± 0.005	0.947 ± 0.004 ± 0.001	0.961 ± 0.002 ± 0.001	0.969 ± 0.001 ± 0.001	0.977 ± 0.001 ± 0.001	0.983 ± 0.001 ± 0.000	0.988 ± 0.002 ± 0.000
[-0.9, -0.8]	0.946 ± 0.007 ± 0.001	0.955 ± 0.004 ± 0.001	0.962 ± 0.002 ± 0.001	0.967 ± 0.001 ± 0.001	0.976 ± 0.001 ± 0.000	0.980 ± 0.001 ± 0.000	0.983 ± 0.002 ± 0.000
[-0.8, -0.7]	0.936 ± 0.008 ± 0.002	0.941 ± 0.004 ± 0.001	0.959 ± 0.002 ± 0.000	0.959 ± 0.002 ± 0.001	0.972 ± 0.001 ± 0.000	0.976 ± 0.001 ± 0.000	0.977 ± 0.002 ± 0.000
[-0.7, -0.6]	0.958 ± 0.006 ± 0.003	0.963 ± 0.003 ± 0.001	0.966 ± 0.002 ± 0.001	0.970 ± 0.001 ± 0.001	0.980 ± 0.001 ± 0.000	0.983 ± 0.001 ± 0.000	0.984 ± 0.002 ± 0.001
[-0.6, -0.5]	0.966 ± 0.006 ± 0.003	0.968 ± 0.003 ± 0.001	0.976 ± 0.002 ± 0.001	0.974 ± 0.001 ± 0.001	0.979 ± 0.001 ± 0.000	0.981 ± 0.001 ± 0.000	0.982 ± 0.002 ± 0.001
[-0.5, -0.4]	0.959 ± 0.006 ± 0.002	0.966 ± 0.003 ± 0.001	0.972 ± 0.002 ± 0.000	0.973 ± 0.001 ± 0.001	0.979 ± 0.001 ± 0.000	0.981 ± 0.001 ± 0.000	0.980 ± 0.002 ± 0.001
[-0.4, -0.3]	0.956 ± 0.006 ± 0.003	0.964 ± 0.003 ± 0.001	0.973 ± 0.002 ± 0.001	0.972 ± 0.001 ± 0.001	0.979 ± 0.001 ± 0.000	0.980 ± 0.001 ± 0.000	0.983 ± 0.002 ± 0.000
[-0.3, -0.2]	0.969 ± 0.005 ± 0.001	0.964 ± 0.003 ± 0.001	0.973 ± 0.002 ± 0.001	0.974 ± 0.001 ± 0.001	0.980 ± 0.001 ± 0.000	0.980 ± 0.001 ± 0.000	0.979 ± 0.002 ± 0.001
[-0.2, -0.1]	0.964 ± 0.006 ± 0.004	0.961 ± 0.003 ± 0.001	0.967 ± 0.002 ± 0.001	0.971 ± 0.001 ± 0.001	0.979 ± 0.001 ± 0.000	0.978 ± 0.001 ± 0.001	0.984 ± 0.002 ± 0.000
[-0.1, 0]	0.957 ± 0.006 ± 0.004	0.961 ± 0.003 ± 0.002	0.971 ± 0.002 ± 0.000	0.971 ± 0.001 ± 0.001	0.978 ± 0.001 ± 0.000	0.980 ± 0.001 ± 0.000	0.980 ± 0.002 ± 0.000
[0, 0.1]	0.968 ± 0.005 ± 0.002	0.963 ± 0.003 ± 0.001	0.970 ± 0.002 ± 0.001	0.971 ± 0.001 ± 0.000	0.979 ± 0.001 ± 0.000	0.977 ± 0.001 ± 0.001	0.977 ± 0.002 ± 0.001
[0.1, 0.2]	0.967 ± 0.005 ± 0.001	0.966 ± 0.003 ± 0.001	0.971 ± 0.002 ± 0.002	0.973 ± 0.001 ± 0.000	0.979 ± 0.001 ± 0.001	0.980 ± 0.001 ± 0.001	0.981 ± 0.002 ± 0.000
[0.2, 0.3]	0.961 ± 0.006 ± 0.001	0.959 ± 0.003 ± 0.000	0.972 ± 0.002 ± 0.001	0.973 ± 0.001 ± 0.001	0.978 ± 0.001 ± 0.000	0.980 ± 0.001 ± 0.000	0.983 ± 0.002 ± 0.000
[0.3, 0.4]	0.960 ± 0.006 ± 0.001	0.969 ± 0.003 ± 0.000	0.973 ± 0.002 ± 0.001	0.974 ± 0.001 ± 0.001	0.980 ± 0.001 ± 0.000	0.980 ± 0.001 ± 0.000	0.980 ± 0.002 ± 0.000
[0.4, 0.5]	0.964 ± 0.006 ± 0.001	0.961 ± 0.003 ± 0.001	0.972 ± 0.002 ± 0.000	0.974 ± 0.001 ± 0.001	0.979 ± 0.001 ± 0.001	0.980 ± 0.001 ± 0.000	0.982 ± 0.002 ± 0.001
[0.5, 0.6]	0.970 ± 0.005 ± 0.002	0.964 ± 0.003 ± 0.001	0.975 ± 0.002 ± 0.001	0.976 ± 0.001 ± 0.000	0.980 ± 0.001 ± 0.000	0.980 ± 0.001 ± 0.001	0.983 ± 0.002 ± 0.001
[0.6, 0.7]	0.952 ± 0.007 ± 0.002	0.964 ± 0.003 ± 0.001	0.970 ± 0.002 ± 0.000	0.973 ± 0.001 ± 0.001	0.978 ± 0.001 ± 0.001	0.981 ± 0.001 ± 0.000	0.983 ± 0.002 ± 0.001
[0.7, 0.8]	0.940 ± 0.008 ± 0.003	0.944 ± 0.004 ± 0.002	0.958 ± 0.002 ± 0.001	0.962 ± 0.001 ± 0.001	0.974 ± 0.001 ± 0.001	0.979 ± 0.001 ± 0.001	0.981 ± 0.002 ± 0.001
[0.8, 0.9]	0.942 ± 0.007 ± 0.001	0.952 ± 0.004 ± 0.001	0.964 ± 0.002 ± 0.001	0.969 ± 0.001 ± 0.001	0.978 ± 0.001 ± 0.000	0.982 ± 0.001 ± 0.000	0.985 ± 0.002 ± 0.000
[0.9, 1]	0.948 ± 0.008 ± 0.003	0.946 ± 0.004 ± 0.002	0.962 ± 0.002 ± 0.001	0.968 ± 0.001 ± 0.000	0.976 ± 0.001 ± 0.001	0.983 ± 0.001 ± 0.000	0.984 ± 0.002 ± 0.000
[1, 1.1]	0.935 ± 0.008 ± 0.002	0.949 ± 0.004 ± 0.001	0.956 ± 0.002 ± 0.001	0.964 ± 0.001 ± 0.001	0.975 ± 0.001 ± 0.001	0.980 ± 0.001 ± 0.001	0.982 ± 0.002 ± 0.000
[1.1, 1.2]	0.933 ± 0.008 ± 0.001	0.927 ± 0.005 ± 0.001	0.944 ± 0.003 ± 0.001	0.957 ± 0.002 ± 0.002	0.969 ± 0.001 ± 0.001	0.978 ± 0.001 ± 0.000	0.981 ± 0.002 ± 0.000
[1.2, 1.3]	0.941 ± 0.008 ± 0.002	0.938 ± 0.005 ± 0.001	0.945 ± 0.003 ± 0.000	0.955 ± 0.002 ± 0.001	0.970 ± 0.001 ± 0.001	0.977 ± 0.001 ± 0.000	0.984 ± 0.002 ± 0.000
[1.3, 1.37]	0.944 ± 0.010 ± 0.003	0.938 ± 0.006 ± 0.003	0.945 ± 0.003 ± 0.001	0.953 ± 0.002 ± 0.001	0.971 ± 0.001 ± 0.000	0.976 ± 0.002 ± 0.001	0.978 ± 0.003 ± 0.001
[1.52, 1.6]	0.958 ± 0.007 ± 0.002	0.940 ± 0.004 ± 0.002	0.953 ± 0.002 ± 0.002	0.967 ± 0.001 ± 0.001	0.974 ± 0.001 ± 0.000	0.980 ± 0.001 ± 0.000	0.984 ± 0.002 ± 0.000
[1.6, 1.7]	0.957 ± 0.007 ± 0.002	0.934 ± 0.005 ± 0.002	0.952 ± 0.002 ± 0.001	0.964 ± 0.001 ± 0.001	0.975 ± 0.001 ± 0.000	0.978 ± 0.001 ± 0.000	0.983 ± 0.002 ± 0.001
[1.7, 1.8]	0.956 ± 0.007 ± 0.001	0.947 ± 0.004 ± 0.001	0.961 ± 0.002 ± 0.001	0.966 ± 0.001 ± 0.000	0.973 ± 0.001 ± 0.001	0.979 ± 0.001 ± 0.000	0.980 ± 0.002 ± 0.000
[1.8, 1.9]	0.961 ± 0.007 ± 0.003	0.951 ± 0.004 ± 0.001	0.963 ± 0.002 ± 0.000	0.961 ± 0.001 ± 0.001	0.969 ± 0.001 ± 0.001	0.973 ± 0.001 ± 0.000	0.976 ± 0.002 ± 0.000
[1.9, 2.01]	0.955 ± 0.006 ± 0.001	0.960 ± 0.003 ± 0.001	0.968 ± 0.002 ± 0.001	0.967 ± 0.001 ± 0.000	0.972 ± 0.001 ± 0.001	0.978 ± 0.001 ± 0.000	0.979 ± 0.002 ± 0.000
[2.01, 2.1]	0.961 ± 0.007 ± 0.002	0.969 ± 0.003 ± 0.000	0.971 ± 0.002 ± 0.000	0.966 ± 0.001 ± 0.001	0.974 ± 0.001 ± 0.000	0.972 ± 0.001 ± 0.000	0.974 ± 0.003 ± 0.000
[2.1, 2.2]	0.984 ± 0.005 ± 0.002	0.977 ± 0.003 ± 0.001	0.985 ± 0.001 ± 0.000	0.983 ± 0.001 ± 0.000	0.983 ± 0.001 ± 0.000	0.987 ± 0.001 ± 0.001	0.986 ± 0.002 ± 0.000
[2.2, 2.3]	0.981 ± 0.005 ± 0.002	0.983 ± 0.002 ± 0.002	0.982 ± 0.002 ± 0.001	0.982 ± 0.001 ± 0.000	0.983 ± 0.001 ± 0.000	0.989 ± 0.001 ± 0.000	0.984 ± 0.002 ± 0.001
[2.3, 2.4]	0.987 ± 0.004 ± 0.001	0.979 ± 0.003 ± 0.001	0.982 ± 0.002 ± 0.000	0.980 ± 0.001 ± 0.001	0.983 ± 0.001 ± 0.000	0.986 ± 0.001 ± 0.000	0.987 ± 0.002 ± 0.000
[2.4, 2.47]	0.995 ± 0.003 ± 0.001	0.989 ± 0.003 ± 0.001	0.991 ± 0.001 ± 0.001	0.993 ± 0.001 ± 0.000	0.994 ± 0.001 ± 0.000	0.996 ± 0.001 ± 0.000	0.996 ± 0.001 ± 0.001

Table A.24: LoosePP Monte-Carlo efficiencies in fine  $\eta$  granularity with their statistical and systematic uncertainties from 80 variations.

	15-20 GeV	20-25 GeV	25-30 GeV	30-35 GeV	35-40 GeV	40-45 GeV	45-50 GeV
[-2.47, -2.4]	0.893 ± 0.049 ± 0.025	0.893 ± 0.022 ± 0.017	0.933 ± 0.013 ± 0.012	0.940 ± 0.007 ± 0.004	0.968 ± 0.005 ± 0.005	0.982 ± 0.007 ± 0.005	0.990 ± 0.015 ± 0.018
[-2.4, -2.3]	0.889 ± 0.034 ± 0.037	0.881 ± 0.019 ± 0.020	0.927 ± 0.010 ± 0.012	0.945 ± 0.006 ± 0.005	0.957 ± 0.004 ± 0.004	0.974 ± 0.005 ± 0.003	0.974 ± 0.010 ± 0.009
[-2.3, -2.2]	0.886 ± 0.032 ± 0.029	0.809 ± 0.017 ± 0.016	0.887 ± 0.010 ± 0.012	0.919 ± 0.005 ± 0.005	0.943 ± 0.003 ± 0.004	0.959 ± 0.004 ± 0.003	0.954 ± 0.008 ± 0.008
[-2.2, -2.1]	0.880 ± 0.030 ± 0.024	0.875 ± 0.016 ± 0.018	0.935 ± 0.009 ± 0.012	0.956 ± 0.005 ± 0.004	0.968 ± 0.003 ± 0.002	0.987 ± 0.004 ± 0.002	0.986 ± 0.008 ± 0.010
[-2.1, -2.01]	0.946 ± 0.038 ± 0.031	0.903 ± 0.018 ± 0.018	0.942 ± 0.010 ± 0.010	0.955 ± 0.006 ± 0.004	0.957 ± 0.003 ± 0.003	0.973 ± 0.004 ± 0.003	0.968 ± 0.009 ± 0.010
[-2.01, -1.9]	0.960 ± 0.032 ± 0.021	0.992 ± 0.018 ± 0.018	1.000 ± 0.009 ± 0.013	1.000 ± 0.005 ± 0.005	1.004 ± 0.003 ± 0.003	1.013 ± 0.005 ± 0.004	1.012 ± 0.010 ± 0.013
[-1.9, -1.8]	1.024 ± 0.035 ± 0.018	0.975 ± 0.018 ± 0.014	0.995 ± 0.010 ± 0.010	1.001 ± 0.005 ± 0.005	1.003 ± 0.004 ± 0.003	1.000 ± 0.004 ± 0.004	0.984 ± 0.008 ± 0.007
[-1.8, -1.7]	0.955 ± 0.032 ± 0.027	0.949 ± 0.019 ± 0.014	0.983 ± 0.010 ± 0.011	0.994 ± 0.006 ± 0.005	0.992 ± 0.004 ± 0.003	0.994 ± 0.004 ± 0.003	0.982 ± 0.008 ± 0.007
[-1.7, -1.6]	0.954 ± 0.033 ± 0.018	0.940 ± 0.018 ± 0.013	0.947 ± 0.009 ± 0.005	0.973 ± 0.006 ± 0.005	0.992 ± 0.004 ± 0.003	0.995 ± 0.004 ± 0.004	0.982 ± 0.008 ± 0.007
[-1.6, -1.52]	0.981 ± 0.032 ± 0.029	0.959 ± 0.015 ± 0.015	0.989 ± 0.009 ± 0.011	1.001 ± 0.006 ± 0.006	1.011 ± 0.004 ± 0.004	1.016 ± 0.005 ± 0.004	0.996 ± 0.009 ± 0.006
[-1.52, -1.3]	1.007 ± 0.034 ± 0.024	0.978 ± 0.022 ± 0.014	0.992 ± 0.011 ± 0.008	0.996 ± 0.006 ± 0.003	0.994 ± 0.004 ± 0.003	1.001 ± 0.004 ± 0.002	0.999 ± 0.008 ± 0.008
[-1.3, -1.2]	0.985 ± 0.027 ± 0.028	0.990 ± 0.018 ± 0.019	0.970 ± 0.009 ± 0.010	0.986 ± 0.005 ± 0.004	0.990 ± 0.003 ± 0.003	0.995 ± 0.003 ± 0.003	0.990 ± 0.006 ± 0.006
[-1.2, -1.1]	0.979 ± 0.028 ± 0.028	0.963 ± 0.017 ± 0.015	0.991 ± 0.009 ± 0.009	0.992 ± 0.005 ± 0.004	1.003 ± 0.003 ± 0.003	0.996 ± 0.003 ± 0.003	0.989 ± 0.007 ± 0.008
[-1.1, -1]	0.998 ± 0.028 ± 0.031	0.983 ± 0.017 ± 0.021	0.994 ± 0.009 ± 0.009	0.994 ± 0.005 ± 0.003	1.002 ± 0.003 ± 0.002	0.996 ± 0.003 ± 0.003	0.992 ± 0.007 ± 0.006
[-1, -0.9]	1.008 ± 0.031 ± 0.029	0.985 ± 0.018 ± 0.020	1.001 ± 0.009 ± 0.007	0.994 ± 0.005 ± 0.002	1.002 ± 0.003 ± 0.003	1.002 ± 0.004 ± 0.002	0.991 ± 0.007 ± 0.004
[-0.9, -0.8]	0.986 ± 0.024 ± 0.019	0.981 ± 0.016 ± 0.008	1.004 ± 0.010 ± 0.006	0.999 ± 0.005 ± 0.004	0.992 ± 0.003 ± 0.002	1.002 ± 0.003 ± 0.003	0.997 ± 0.007 ± 0.004
[-0.8, -0.7]	0.984 ± 0.027 ± 0.018	0.977 ± 0.016 ± 0.013	0.977 ± 0.009 ± 0.008	0.983 ± 0.005 ± 0.005	0.989 ± 0.003 ± 0.002	0.992 ± 0.003 ± 0.002	0.992 ± 0.007 ± 0.005
[-0.7, -0.6]	0.946 ± 0.023 ± 0.017	0.964 ± 0.014 ± 0.015	0.975 ± 0.007 ± 0.009	0.989 ± 0.004 ± 0.005	0.991 ± 0.003 ± 0.002	0.991 ± 0.003 ± 0.002	0.991 ± 0.006 ± 0.005
[-0.6, -0.5]	0.937 ± 0.023 ± 0.017	0.963 ± 0.014 ± 0.012	0.989 ± 0.008 ± 0.009	0.983 ± 0.004 ± 0.005	0.989 ± 0.003 ± 0.003	0.972 ± 0.003 ± 0.003	0.974 ± 0.007 ± 0.002
[-0.5, -0.4]	0.969 ± 0.025 ± 0.018	0.974 ± 0.015 ± 0.016	0.979 ± 0.008 ± 0.007	0.990 ± 0.004 ± 0.004	0.994 ± 0.003 ± 0.003	0.982 ± 0.003 ± 0.003	0.978 ± 0.007 ± 0.004
[-0.4, -0.3]	0.987 ± 0.023 ± 0.015	0.974 ± 0.014 ± 0.009	0.994 ± 0.008 ± 0.007	0.983 ± 0.004 ± 0.003	0.995 ± 0.003 ± 0.003	0.987 ± 0.003 ± 0.003	0.990 ± 0.006 ± 0.004
[-0.3, -0.2]	0.995 ± 0.022 ± 0.013	0.991 ± 0.014 ± 0.009	0.989 ± 0.007 ± 0.007	0.995 ± 0.004 ± 0.003	0.997 ± 0.003 ± 0.002	0.997 ± 0.003 ± 0.002	0.982 ± 0.006 ± 0.004
[-0.2, -0.1]	0.980 ± 0.023 ± 0.021	0.988 ± 0.015 ± 0.018	0.994 ± 0.008 ± 0.005	0.990 ± 0.004 ± 0.003	1.002 ± 0.003 ± 0.002	0.996 ± 0.003 ± 0.002	0.987 ± 0.006 ± 0.003
[-0.1, 0]	1.016 ± 0.025 ± 0.019	1.000 ± 0.015 ± 0.013	0.991 ± 0.008 ± 0.006	0.986 ± 0.004 ± 0.004	0.985 ± 0.003 ± 0.003	0.985 ± 0.003 ± 0.003	0.990 ± 0.007 ± 0.004
[0, 0.1]	0.975 ± 0.024 ± 0.016	0.988 ± 0.016 ± 0.013	0.994 ± 0.008 ± 0.006	0.988 ± 0.004 ± 0.004	0.998 ± 0.003 ± 0.003	0.994 ± 0.004 ± 0.003	0.987 ± 0.007 ± 0.003
[0.1, 0.2]	1.002 ± 0.024 ± 0.023	0.995 ± 0.015 ± 0.018	0.996 ± 0.008 ± 0.006	0.997 ± 0.004 ± 0.004	1.002 ± 0.003 ± 0.001	0.990 ± 0.003 ± 0.002	0.985 ± 0.006 ± 0.004
[0.2, 0.3]	1.002 ± 0.023 ± 0.016	0.990 ± 0.015 ± 0.009	0.983 ± 0.008 ± 0.007	0.991 ± 0.004 ± 0.003	0.995 ± 0.003 ± 0.002	0.990 ± 0.003 ± 0.002	0.986 ± 0.006 ± 0.005
[0.3, 0.4]	1.016 ± 0.024 ± 0.017	0.980 ± 0.015 ± 0.021	0.999 ± 0.008 ± 0.007	0.991 ± 0.004 ± 0.003	0.993 ± 0.003 ± 0.003	0.988 ± 0.003 ± 0.002	0.992 ± 0.006 ± 0.002
[0.4, 0.5]	1.000 ± 0.026 ± 0.023	0.968 ± 0.016 ± 0.018	0.985 ± 0.008 ± 0.007	0.990 ± 0.004 ± 0.004	0.995 ± 0.003 ± 0.003	0.982 ± 0.003 ± 0.002	0.977 ± 0.007 ± 0.005
[0.5, 0.6]	0.986 ± 0.024 ± 0.019	0.966 ± 0.015 ± 0.013	0.986 ± 0.008 ± 0.009	0.989 ± 0.004 ± 0.004	0.984 ± 0.003 ± 0.002	0.969 ± 0.004 ± 0.002	0.970 ± 0.007 ± 0.003
[0.6, 0.7]	1.002 ± 0.026 ± 0.020	0.965 ± 0.015 ± 0.018	0.970 ± 0.007 ± 0.010	0.987 ± 0.004 ± 0.005	0.994 ± 0.003 ± 0.002	0.993 ± 0.003 ± 0.002	0.993 ± 0.006 ± 0.004
[0.7, 0.8]	1.007 ± 0.027 ± 0.020	0.979 ± 0.017 ± 0.015	0.978 ± 0.009 ± 0.008	0.986 ± 0.005 ± 0.005	0.993 ± 0.003 ± 0.003	0.995 ± 0.003 ± 0.003	0.988 ± 0.006 ± 0.006
[0.8, 0.9]	0.986 ± 0.027 ± 0.023	0.982 ± 0.016 ± 0.005	0.992 ± 0.009 ± 0.006	1.001 ± 0.005 ± 0.005	0.994 ± 0.003 ± 0.002	0.995 ± 0.003 ± 0.003	0.987 ± 0.007 ± 0.004
[0.9, 1]	0.963 ± 0.028 ± 0.024	0.987 ± 0.018 ± 0.020	0.992 ± 0.008 ± 0.006	0.992 ± 0.005 ± 0.004	0.994 ± 0.003 ± 0.002	0.999 ± 0.004 ± 0.003	1.007 ± 0.007 ± 0.004
[1, 1.1]	0.976 ± 0.028 ± 0.031	0.966 ± 0.017 ± 0.018	0.983 ± 0.009 ± 0.009	0.992 ± 0.005 ± 0.004	0.999 ± 0.003 ± 0.002	0.993 ± 0.003 ± 0.003	0.991 ± 0.007 ± 0.006
[1.1, 1.2]	0.970 ± 0.026 ± 0.028	0.971 ± 0.017 ± 0.015	0.991 ± 0.009 ± 0.010	0.983 ± 0.005 ± 0.004	0.998 ± 0.003 ± 0.003	0.991 ± 0.003 ± 0.003	0.990 ± 0.006 ± 0.008
[1.2, 1.3]	0.983 ± 0.029 ± 0.028	0.966 ± 0.017 ± 0.018	0.979 ± 0.009 ± 0.010	0.979 ± 0.005 ± 0.005	0.990 ± 0.003 ± 0.004	1.001 ± 0.003 ± 0.004	0.981 ± 0.006 ± 0.006
[1.3, 1.37]	1.027 ± 0.037 ± 0.023	0.978 ± 0.022 ± 0.018	0.985 ± 0.011 ± 0.009	0.991 ± 0.006 ± 0.004	0.990 ± 0.004 ± 0.003	1.010 ± 0.005 ± 0.003	0.999 ± 0.008 ± 0.005
[1.52, 1.6]	0.990 ± 0.033 ± 0.030	0.994 ± 0.017 ± 0.016	0.996 ± 0.009 ± 0.010	1.005 ± 0.006 ± 0.005	1.009 ± 0.004 ± 0.005	0.999 ± 0.004 ± 0.003	0.999 ± 0.009 ± 0.005
[1.6, 1.7]	0.947 ± 0.032 ± 0.018	0.956 ± 0.019 ± 0.014	0.964 ± 0.010 ± 0.006	0.980 ± 0.006 ± 0.005	0.993 ± 0.004 ± 0.004	0.990 ± 0.004 ± 0.003	0.974 ± 0.008 ± 0.008
[1.7, 1.8]	0.963 ± 0.029 ± 0.022	0.957 ± 0.019 ± 0.012	0.984 ± 0.010 ± 0.010	0.993 ± 0.006 ± 0.003	0.993 ± 0.004 ± 0.004	0.997 ± 0.004 ± 0.003	0.981 ± 0.007 ± 0.009
[1.8, 1.9]	0.950 ± 0.032 ± 0.021	1.006 ± 0.018 ± 0.009	0.993 ± 0.009 ± 0.011	1.005 ± 0.005 ± 0.006	1.006 ± 0.004 ± 0.002	1.006 ± 0.004 ± 0.004	1.004 ± 0.008 ± 0.007
[1.9, 2.01]	0.988 ± 0.032 ± 0.029	0.987 ± 0.020 ± 0.014	1.008 ± 0.011 ± 0.015	1.000 ± 0.006 ± 0.005	1.001 ± 0.003 ± 0.003	0.984 ± 0.005 ± 0.003	1.000 ± 0.010 ± 0.010
[2.01, 2.1]	0.924 ± 0.032 ± 0.026	0.909 ± 0.017 ± 0.011	0.966 ± 0.010 ± 0.016	0.980 ± 0.005 ± 0.003	0.971 ± 0.003 ± 0.003	0.984 ± 0.004 ± 0.002	0.971 ± 0.009 ± 0.009
[2.1, 2.2]	0.911 ± 0.031 ± 0.025	0.892 ± 0.016 ± 0.017	0.941 ± 0.009 ± 0.011	0.964 ± 0.005 ± 0.003	0.973 ± 0.003 ± 0.003	0.990 ± 0.004 ± 0.002	0.983 ± 0.009 ± 0.009
[2.2, 2.3]	0.934 ± 0.033 ± 0.024	0.822 ± 0.017 ± 0.016	0.864 ± 0.009 ± 0.011	0.918 ± 0.005 ± 0.004	0.934 ± 0.003 ± 0.003	0.961 ± 0.004 ± 0.003	0.945 ± 0.008 ± 0.008
[2.3, 2.4]	0.916 ± 0.035 ± 0.035	0.872 ± 0.018 ± 0.024	0.914 ± 0.010 ± 0.012	0.944 ± 0.005 ± 0.006	0.962 ± 0.003 ± 0.003	0.972 ± 0.005 ± 0.003	0.955 ± 0.009 ± 0.010
[2.4, 2.47]	0.930 ± 0.043 ± 0.021	0.869 ± 0.022 ± 0.018	0.914 ± 0.012 ± 0.007	0.932 ± 0.007 ± 0.005	0.962 ± 0.005 ± 0.003	0.987 ± 0.007 ± 0.003	0.971 ± 0.013 ± 0.011

Table A.25: MediumPP scale-factors in fine  $\eta$  granularity with their statistical and systematic uncertainties from 80 variations.

	15-20 GeV	20-25 GeV	25-30 GeV	30-35 GeV	35-40 GeV	40-45 GeV	45-50 GeV
[-2.47, -2.4]	0.667 ± 0.032 ± 0.018	0.683 ± 0.015 ± 0.015	0.764 ± 0.010 ± 0.009	0.799 ± 0.005 ± 0.004	0.842 ± 0.003 ± 0.003	0.880 ± 0.006 ± 0.004	0.892 ± 0.013 ± 0.015
[-2.4, -2.3]	0.717 ± 0.027 ± 0.029	0.693 ± 0.014 ± 0.016	0.768 ± 0.008 ± 0.011	0.817 ± 0.005 ± 0.004	0.851 ± 0.003 ± 0.003	0.889 ± 0.004 ± 0.003	0.898 ± 0.009 ± 0.008
[-2.3, -2.2]	0.744 ± 0.027 ± 0.025	0.655 ± 0.013 ± 0.013	0.755 ± 0.008 ± 0.010	0.816 ± 0.004 ± 0.004	0.858 ± 0.003 ± 0.003	0.902 ± 0.004 ± 0.003	0.907 ± 0.008 ± 0.007
[-2.2, -2.1]	0.765 ± 0.026 ± 0.021	0.736 ± 0.013 ± 0.016	0.826 ± 0.008 ± 0.010	0.868 ± 0.004 ± 0.004	0.900 ± 0.002 ± 0.002	0.936 ± 0.004 ± 0.002	0.943 ± 0.008 ± 0.009
[-2.1, -2.01]	0.759 ± 0.029 ± 0.026	0.722 ± 0.013 ± 0.013	0.786 ± 0.008 ± 0.007	0.826 ± 0.004 ± 0.005	0.858 ± 0.003 ± 0.002	0.895 ± 0.004 ± 0.002	0.894 ± 0.009 ± 0.008
[-2.01, -1.9]	0.768 ± 0.024 ± 0.017	0.807 ± 0.014 ± 0.014	0.842 ± 0.008 ± 0.010	0.862 ± 0.004 ± 0.004	0.894 ± 0.003 ± 0.003	0.918 ± 0.004 ± 0.002	0.919 ± 0.009 ± 0.011
[-1.9, -1.8]	0.804 ± 0.025 ± 0.013	0.782 ± 0.014 ± 0.013	0.836 ± 0.008 ± 0.008	0.863 ± 0.004 ± 0.004	0.895 ± 0.003 ± 0.002	0.914 ± 0.003 ± 0.004	0.911 ± 0.007 ± 0.006
[-1.8, -1.7]	0.819 ± 0.028 ± 0.022	0.799 ± 0.017 ± 0.010	0.849 ± 0.009 ± 0.008	0.876 ± 0.005 ± 0.004	0.909 ± 0.004 ± 0.002	0.930 ± 0.003 ± 0.003	0.927 ± 0.007 ± 0.008
[-1.7, -1.6]	0.790 ± 0.028 ± 0.016	0.743 ± 0.013 ± 0.012	0.802 ± 0.008 ± 0.005	0.846 ± 0.005 ± 0.003	0.892 ± 0.004 ± 0.002	0.924 ± 0.004 ± 0.003	0.918 ± 0.007 ± 0.007
[-1.6, -1.52]	0.823 ± 0.026 ± 0.025	0.800 ± 0.012 ± 0.014	0.852 ± 0.007 ± 0.009	0.882 ± 0.005 ± 0.005	0.912 ± 0.003 ± 0.003	0.942 ± 0.004 ± 0.003	0.934 ± 0.008 ± 0.005
[-1.37, -1.3]	0.841 ± 0.026 ± 0.025	0.818 ± 0.017 ± 0.012	0.863 ± 0.009 ± 0.007	0.880 ± 0.005 ± 0.004	0.911 ± 0.003 ± 0.003	0.935 ± 0.003 ± 0.003	0.939 ± 0.006 ± 0.006
[-1.3, -1.2]	0.845 ± 0.022 ± 0.025	0.816 ± 0.014 ± 0.017	0.849 ± 0.007 ± 0.010	0.879 ± 0.004 ± 0.004	0.912 ± 0.002 ± 0.003	0.934 ± 0.003 ± 0.003	0.934 ± 0.005 ± 0.005
[-1.2, -1.1]	0.811 ± 0.021 ± 0.024	0.791 ± 0.012 ± 0.014	0.864 ± 0.007 ± 0.008	0.883 ± 0.004 ± 0.004	0.917 ± 0.002 ± 0.003	0.929 ± 0.002 ± 0.003	0.927 ± 0.005 ± 0.007
[-1.1, -1]	0.842 ± 0.023 ± 0.028	0.823 ± 0.014 ± 0.018	0.873 ± 0.008 ± 0.006	0.895 ± 0.004 ± 0.003	0.925 ± 0.003 ± 0.002	0.932 ± 0.003 ± 0.003	0.935 ± 0.006 ± 0.005
[-1, -0.9]	0.865 ± 0.026 ± 0.020	0.848 ± 0.015 ± 0.019	0.891 ± 0.008 ± 0.006	0.908 ± 0.004 ± 0.002	0.928 ± 0.003 ± 0.003	0.940 ± 0.003 ± 0.002	0.938 ± 0.006 ± 0.003
[-0.9, -0.8]	0.860 ± 0.020 ± 0.017	0.866 ± 0.014 ± 0.008	0.902 ± 0.009 ± 0.005	0.908 ± 0.004 ± 0.004	0.923 ± 0.002 ± 0.002	0.934 ± 0.003 ± 0.003	0.939 ± 0.006 ± 0.004
[-0.8, -0.7]	0.819 ± 0.021 ± 0.016	0.778 ± 0.012 ± 0.011	0.835 ± 0.007 ± 0.007	0.876 ± 0.004 ± 0.005	0.905 ± 0.003 ± 0.003	0.920 ± 0.003 ± 0.002	0.926 ± 0.006 ± 0.005
[-0.7, -0.6]	0.844 ± 0.021 ± 0.018	0.855 ± 0.013 ± 0.013	0.887 ± 0.006 ± 0.008	0.920 ± 0.004 ± 0.005	0.939 ± 0.002 ± 0.002	0.946 ± 0.002 ± 0.002	0.948 ± 0.005 ± 0.004
[-0.6, -0.5]	0.844 ± 0.021 ± 0.016	0.837 ± 0.012 ± 0.010	0.893 ± 0.007 ± 0.009	0.909 ± 0.004 ± 0.004	0.925 ± 0.002 ± 0.002	0.900 ± 0.003 ± 0.002	0.906 ± 0.006 ± 0.002
[-0.5, -0.4]	0.868 ± 0.022 ± 0.016	0.841 ± 0.013 ± 0.014	0.881 ± 0.007 ± 0.006	0.908 ± 0.004 ± 0.004	0.927 ± 0.002 ± 0.002	0.911 ± 0.003 ± 0.003	0.906 ± 0.006 ± 0.003
[-0.4, -0.3]	0.873 ± 0.020 ± 0.014	0.826 ± 0.012 ± 0.015	0.888 ± 0.007 ± 0.006	0.908 ± 0.004 ± 0.003	0.929 ± 0.002 ± 0.002	0.918 ± 0.002 ± 0.002	0.927 ± 0.005 ± 0.004
[-0.3, -0.2]	0.890 ± 0.019 ± 0.012	0.845 ± 0.012 ± 0.008	0.886 ± 0.006 ± 0.007	0.911 ± 0.003 ± 0.003	0.927 ± 0.002 ± 0.002	0.924 ± 0.002 ± 0.002	0.919 ± 0.005 ± 0.004
[-0.2, -0.1]	0.855 ± 0.019 ± 0.018	0.835 ± 0.012 ± 0.015	0.880 ± 0.006 ± 0.005	0.903 ± 0.003 ± 0.004	0.930 ± 0.002 ± 0.001	0.923 ± 0.002 ± 0.001	0.925 ± 0.005 ± 0.003
[-0.1, 0]	0.882 ± 0.020 ± 0.015	0.840 ± 0.012 ± 0.011	0.879 ± 0.007 ± 0.005	0.895 ± 0.003 ± 0.004	0.920 ± 0.002 ± 0.002	0.914 ± 0.003 ± 0.003	0.920 ± 0.005 ± 0.003
[0, 0.1]	0.863 ± 0.021 ± 0.014	0.834 ± 0.013 ± 0.011	0.877 ± 0.007 ± 0.005	0.891 ± 0.003 ± 0.004	0.921 ± 0.002 ± 0.003	0.914 ± 0.003 ± 0.003	0.910 ± 0.006 ± 0.002
[0.1, 0.2]	0.890 ± 0.021 ± 0.020	0.850 ± 0.012 ± 0.015	0.891 ± 0.006 ± 0.005	0.910 ± 0.003 ± 0.003	0.930 ± 0.002 ± 0.001	0.916 ± 0.003 ± 0.002	0.918 ± 0.005 ± 0.003
[0.2, 0.3]	0.885 ± 0.020 ± 0.013	0.839 ± 0.012 ± 0.007	0.882 ± 0.007 ± 0.006	0.905 ± 0.004 ± 0.004	0.925 ± 0.002 ± 0.002	0.918 ± 0.003 ± 0.002	0.920 ± 0.005 ± 0.004
[0.3, 0.4]	0.883 ± 0.020 ± 0.014	0.833 ± 0.013 ± 0.018	0.898 ± 0.007 ± 0.006	0.910 ± 0.004 ± 0.002	0.926 ± 0.002 ± 0.002	0.913 ± 0.002 ± 0.002	0.926 ± 0.005 ± 0.002
[0.4, 0.5]	0.887 ± 0.023 ± 0.020	0.849 ± 0.013 ± 0.016	0.883 ± 0.007 ± 0.006	0.910 ± 0.004 ± 0.004	0.927 ± 0.003 ± 0.003	0.909 ± 0.003 ± 0.002	0.910 ± 0.006 ± 0.005
[0.5, 0.6]	0.892 ± 0.023 ± 0.018	0.827 ± 0.012 ± 0.011	0.889 ± 0.007 ± 0.009	0.909 ± 0.004 ± 0.004	0.920 ± 0.002 ± 0.002	0.892 ± 0.003 ± 0.002	0.897 ± 0.006 ± 0.003
[0.6, 0.7]	0.882 ± 0.023 ± 0.019	0.849 ± 0.014 ± 0.015	0.890 ± 0.007 ± 0.009	0.921 ± 0.004 ± 0.006	0.942 ± 0.003 ± 0.003	0.948 ± 0.002 ± 0.003	0.952 ± 0.006 ± 0.003
[0.7, 0.8]	0.838 ± 0.021 ± 0.018	0.786 ± 0.013 ± 0.013	0.839 ± 0.007 ± 0.007	0.880 ± 0.004 ± 0.005	0.912 ± 0.003 ± 0.002	0.924 ± 0.003 ± 0.003	0.925 ± 0.005 ± 0.005
[0.8, 0.9]	0.825 ± 0.021 ± 0.022	0.864 ± 0.015 ± 0.005	0.896 ± 0.009 ± 0.006	0.914 ± 0.005 ± 0.005	0.928 ± 0.002 ± 0.002	0.932 ± 0.003 ± 0.002	0.930 ± 0.006 ± 0.003
[0.9, 1]	0.824 ± 0.023 ± 0.019	0.844 ± 0.015 ± 0.018	0.887 ± 0.007 ± 0.006	0.904 ± 0.004 ± 0.004	0.923 ± 0.003 ± 0.003	0.939 ± 0.003 ± 0.003	0.952 ± 0.006 ± 0.004
[1, 1.1]	0.815 ± 0.022 ± 0.028	0.809 ± 0.014 ± 0.019	0.866 ± 0.007 ± 0.008	0.895 ± 0.004 ± 0.003	0.924 ± 0.003 ± 0.002	0.930 ± 0.003 ± 0.003	0.934 ± 0.006 ± 0.006
[1.1, 1.2]	0.812 ± 0.020 ± 0.026	0.804 ± 0.013 ± 0.015	0.858 ± 0.007 ± 0.010	0.879 ± 0.004 ± 0.005	0.916 ± 0.002 ± 0.003	0.931 ± 0.002 ± 0.003	0.936 ± 0.005 ± 0.008
[1.2, 1.3]	0.816 ± 0.022 ± 0.024	0.807 ± 0.014 ± 0.016	0.853 ± 0.007 ± 0.010	0.873 ± 0.004 ± 0.004	0.911 ± 0.002 ± 0.003	0.935 ± 0.003 ± 0.003	0.930 ± 0.005 ± 0.006
[1.3, 1.37]	0.848 ± 0.027 ± 0.021	0.816 ± 0.018 ± 0.015	0.846 ± 0.009 ± 0.009	0.870 ± 0.005 ± 0.004	0.903 ± 0.003 ± 0.002	0.932 ± 0.003 ± 0.002	0.938 ± 0.006 ± 0.005
[1.52, 1.6]	0.839 ± 0.028 ± 0.027	0.828 ± 0.014 ± 0.014	0.864 ± 0.008 ± 0.008	0.894 ± 0.005 ± 0.004	0.918 ± 0.004 ± 0.004	0.948 ± 0.004 ± 0.003	0.939 ± 0.009 ± 0.004
[1.6, 1.7]	0.793 ± 0.027 ± 0.016	0.751 ± 0.014 ± 0.011	0.818 ± 0.009 ± 0.005	0.855 ± 0.005 ± 0.004	0.901 ± 0.004 ± 0.003	0.926 ± 0.003 ± 0.003	0.918 ± 0.007 ± 0.007
[1.7, 1.8]	0.807 ± 0.024 ± 0.020	0.795 ± 0.016 ± 0.009	0.853 ± 0.009 ± 0.008	0.877 ± 0.005 ± 0.003	0.905 ± 0.003 ± 0.003	0.930 ± 0.003 ± 0.003	0.925 ± 0.007 ± 0.009
[1.8, 1.9]	0.789 ± 0.026 ± 0.018	0.815 ± 0.014 ± 0.009	0.846 ± 0.007 ± 0.010	0.876 ± 0.004 ± 0.005	0.902 ± 0.003 ± 0.002	0.921 ± 0.003 ± 0.004	0.923 ± 0.007 ± 0.006
[1.9, 2.01]	0.810 ± 0.026 ± 0.025	0.810 ± 0.017 ± 0.011	0.851 ± 0.009 ± 0.012	0.869 ± 0.005 ± 0.005	0.893 ± 0.003 ± 0.002	0.917 ± 0.004 ± 0.002	0.908 ± 0.009 ± 0.008
[2.01, 2.1]	0.760 ± 0.024 ± 0.023	0.735 ± 0.013 ± 0.009	0.807 ± 0.008 ± 0.011	0.844 ± 0.004 ± 0.004	0.871 ± 0.002 ± 0.002	0.903 ± 0.004 ± 0.002	0.900 ± 0.008 ± 0.008
[2.1, 2.2]	0.778 ± 0.026 ± 0.024	0.743 ± 0.013 ± 0.015	0.824 ± 0.008 ± 0.009	0.870 ± 0.004 ± 0.003	0.898 ± 0.002 ± 0.003	0.938 ± 0.003 ± 0.002	0.932 ± 0.009 ± 0.009
[2.2, 2.3]	0.763 ± 0.025 ± 0.022	0.660 ± 0.013 ± 0.012	0.740 ± 0.007 ± 0.009	0.816 ± 0.004 ± 0.004	0.854 ± 0.003 ± 0.003	0.901 ± 0.004 ± 0.003	0.900 ± 0.008 ± 0.008
[2.3, 2.4]	0.761 ± 0.028 ± 0.028	0.701 ± 0.013 ± 0.019	0.781 ± 0.009 ± 0.010	0.825 ± 0.004 ± 0.004	0.864 ± 0.003 ± 0.003	0.892 ± 0.004 ± 0.003	0.887 ± 0.009 ± 0.009
[2.4, 2.47]	0.710 ± 0.029 ± 0.018	0.684 ± 0.015 ± 0.014	0.758 ± 0.009 ± 0.007	0.809 ± 0.005 ± 0.004	0.847 ± 0.003 ± 0.003	0.888 ± 0.006 ± 0.002	0.892 ± 0.012 ± 0.010

Table A.26: MediumPP efficiencies in fine  $\eta$  granularity with their statistical and systematic uncertainties from 80 variations.

	15-20 GeV	20-25 GeV	25-30 GeV	30-35 GeV	35-40 GeV	40-45 GeV	45-50 GeV
[-2.47, -2.4]	0.746 ± 0.022 ± 0.004	0.764 ± 0.011 ± 0.006	0.819 ± 0.006 ± 0.004	0.850 ± 0.004 ± 0.001	0.869 ± 0.003 ± 0.002	0.896 ± 0.003 ± 0.001	0.902 ± 0.006 ± 0.002
[-2.4, -2.3]	0.807 ± 0.015 ± 0.003	0.785 ± 0.008 ± 0.004	0.829 ± 0.005 ± 0.001	0.864 ± 0.003 ± 0.003	0.889 ± 0.002 ± 0.001	0.913 ± 0.003 ± 0.000	0.922 ± 0.004 ± 0.001
[-2.3, -2.2]	0.838 ± 0.013 ± 0.003	0.810 ± 0.008 ± 0.002	0.850 ± 0.004 ± 0.003	0.887 ± 0.002 ± 0.002	0.911 ± 0.002 ± 0.001	0.940 ± 0.002 ± 0.000	0.951 ± 0.003 ± 0.001
[-2.2, -2.1]	0.870 ± 0.012 ± 0.006	0.840 ± 0.007 ± 0.003	0.884 ± 0.005 ± 0.002	0.908 ± 0.002 ± 0.002	0.930 ± 0.002 ± 0.000	0.947 ± 0.002 ± 0.000	0.956 ± 0.003 ± 0.002
[-2.1, -2.01]	0.802 ± 0.015 ± 0.003	0.799 ± 0.008 ± 0.004	0.835 ± 0.005 ± 0.003	0.865 ± 0.003 ± 0.002	0.896 ± 0.002 ± 0.001	0.920 ± 0.002 ± 0.001	0.924 ± 0.004 ± 0.001
[-2.01, -1.9]	0.801 ± 0.014 ± 0.004	0.814 ± 0.007 ± 0.003	0.842 ± 0.004 ± 0.001	0.861 ± 0.003 ± 0.002	0.890 ± 0.002 ± 0.000	0.906 ± 0.002 ± 0.000	0.908 ± 0.005 ± 0.002
[-1.9, -1.8]	0.785 ± 0.014 ± 0.002	0.800 ± 0.007 ± 0.003	0.840 ± 0.004 ± 0.002	0.861 ± 0.003 ± 0.001	0.892 ± 0.002 ± 0.002	0.913 ± 0.002 ± 0.001	0.926 ± 0.004 ± 0.002
[-1.8, -1.7]	0.855 ± 0.013 ± 0.002	0.841 ± 0.007 ± 0.002	0.864 ± 0.004 ± 0.003	0.882 ± 0.003 ± 0.002	0.906 ± 0.002 ± 0.001	0.935 ± 0.002 ± 0.000	0.944 ± 0.003 ± 0.001
[-1.7, -1.6]	0.828 ± 0.013 ± 0.006	0.791 ± 0.008 ± 0.002	0.846 ± 0.004 ± 0.001	0.870 ± 0.003 ± 0.001	0.899 ± 0.002 ± 0.002	0.929 ± 0.002 ± 0.001	0.935 ± 0.004 ± 0.002
[-1.6, -1.52]	0.837 ± 0.013 ± 0.002	0.832 ± 0.007 ± 0.001	0.861 ± 0.004 ± 0.003	0.880 ± 0.003 ± 0.002	0.902 ± 0.002 ± 0.001	0.927 ± 0.002 ± 0.001	0.938 ± 0.004 ± 0.001
[-1.37, -1.3]	0.835 ± 0.015 ± 0.004	0.837 ± 0.009 ± 0.002	0.869 ± 0.005 ± 0.001	0.883 ± 0.003 ± 0.003	0.917 ± 0.002 ± 0.000	0.933 ± 0.003 ± 0.001	0.940 ± 0.004 ± 0.003
[-1.3, -1.2]	0.855 ± 0.011 ± 0.002	0.824 ± 0.007 ± 0.003	0.874 ± 0.004 ± 0.003	0.892 ± 0.003 ± 0.001	0.921 ± 0.002 ± 0.002	0.939 ± 0.002 ± 0.001	0.944 ± 0.003 ± 0.002
[-1.1, -1]	0.828 ± 0.013 ± 0.001	0.836 ± 0.007 ± 0.002	0.872 ± 0.004 ± 0.004	0.900 ± 0.002 ± 0.001	0.915 ± 0.002 ± 0.001	0.933 ± 0.002 ± 0.000	0.937 ± 0.004 ± 0.002
[-1, -0.9]	0.843 ± 0.011 ± 0.004	0.836 ± 0.007 ± 0.002	0.878 ± 0.004 ± 0.002	0.900 ± 0.002 ± 0.001	0.923 ± 0.002 ± 0.001	0.936 ± 0.002 ± 0.001	0.942 ± 0.003 ± 0.001
[-0.9, -0.8]	0.857 ± 0.011 ± 0.004	0.860 ± 0.007 ± 0.002	0.889 ± 0.004 ± 0.002	0.913 ± 0.002 ± 0.002	0.927 ± 0.002 ± 0.001	0.938 ± 0.002 ± 0.001	0.946 ± 0.003 ± 0.001
[-0.8, -0.7]	0.872 ± 0.011 ± 0.002	0.882 ± 0.006 ± 0.001	0.898 ± 0.004 ± 0.004	0.908 ± 0.002 ± 0.001	0.930 ± 0.002 ± 0.000	0.932 ± 0.002 ± 0.001	0.942 ± 0.004 ± 0.001
[-0.7, -0.6]	0.832 ± 0.012 ± 0.006	0.796 ± 0.007 ± 0.002	0.855 ± 0.004 ± 0.001	0.891 ± 0.002 ± 0.001	0.915 ± 0.002 ± 0.001	0.926 ± 0.002 ± 0.001	0.933 ± 0.004 ± 0.001
[-0.6, -0.5]	0.891 ± 0.009 ± 0.005	0.888 ± 0.005 ± 0.002	0.910 ± 0.003 ± 0.001	0.930 ± 0.002 ± 0.002	0.947 ± 0.001 ± 0.000	0.955 ± 0.002 ± 0.000	0.956 ± 0.003 ± 0.001
[-0.5, -0.4]	0.901 ± 0.009 ± 0.004	0.868 ± 0.006 ± 0.002	0.902 ± 0.003 ± 0.002	0.924 ± 0.002 ± 0.001	0.936 ± 0.001 ± 0.001	0.925 ± 0.002 ± 0.001	0.931 ± 0.003 ± 0.002
[-0.4, -0.3]	0.894 ± 0.010 ± 0.003	0.863 ± 0.006 ± 0.002	0.900 ± 0.003 ± 0.002	0.917 ± 0.002 ± 0.002	0.933 ± 0.001 ± 0.001	0.927 ± 0.002 ± 0.001	0.926 ± 0.004 ± 0.002
[-0.3, -0.2]	0.884 ± 0.010 ± 0.003	0.848 ± 0.006 ± 0.003	0.893 ± 0.003 ± 0.001	0.913 ± 0.002 ± 0.001	0.933 ± 0.001 ± 0.001	0.931 ± 0.002 ± 0.001	0.937 ± 0.003 ± 0.001
[-0.2, -0.1]	0.895 ± 0.009 ± 0.001	0.852 ± 0.006 ± 0.004	0.895 ± 0.003 ± 0.002	0.915 ± 0.002 ± 0.002	0.930 ± 0.001 ± 0.001	0.927 ± 0.002 ± 0.002	0.936 ± 0.003 ± 0.001
[-0.1, 0]	0.872 ± 0.010 ± 0.002	0.846 ± 0.006 ± 0.001	0.886 ± 0.003 ± 0.000	0.912 ± 0.002 ± 0.001	0.928 ± 0.002 ± 0.001	0.927 ± 0.002 ± 0.001	0.937 ± 0.003 ± 0.001
[0, 0.1]	0.868 ± 0.010 ± 0.004	0.839 ± 0.006 ± 0.004	0.887 ± 0.003 ± 0.002	0.907 ± 0.002 ± 0.001	0.925 ± 0.002 ± 0.001	0.928 ± 0.002 ± 0.000	0.929 ± 0.004 ± 0.001
[0.1, 0.2]	0.885 ± 0.010 ± 0.002	0.844 ± 0.006 ± 0.004	0.882 ± 0.004 ± 0.002	0.902 ± 0.002 ± 0.000	0.923 ± 0.002 ± 0.001	0.920 ± 0.002 ± 0.001	0.922 ± 0.004 ± 0.001
[0.2, 0.3]	0.887 ± 0.009 ± 0.002	0.854 ± 0.006 ± 0.002	0.895 ± 0.003 ± 0.002	0.912 ± 0.002 ± 0.001	0.928 ± 0.002 ± 0.001	0.926 ± 0.002 ± 0.002	0.931 ± 0.003 ± 0.002
[0.3, 0.4]	0.881 ± 0.010 ± 0.002	0.847 ± 0.006 ± 0.003	0.898 ± 0.003 ± 0.001	0.912 ± 0.002 ± 0.002	0.930 ± 0.002 ± 0.001	0.927 ± 0.002 ± 0.001	0.933 ± 0.003 ± 0.000
[0.4, 0.5]	0.870 ± 0.011 ± 0.002	0.850 ± 0.006 ± 0.001	0.898 ± 0.003 ± 0.002	0.918 ± 0.002 ± 0.001	0.933 ± 0.001 ± 0.001	0.924 ± 0.002 ± 0.002	0.934 ± 0.003 ± 0.001
[0.5, 0.6]	0.886 ± 0.010 ± 0.004	0.852 ± 0.006 ± 0.002	0.896 ± 0.003 ± 0.001	0.919 ± 0.002 ± 0.002	0.932 ± 0.001 ± 0.002	0.925 ± 0.002 ± 0.001	0.931 ± 0.003 ± 0.001
[0.6, 0.7]	0.904 ± 0.009 ± 0.005	0.856 ± 0.006 ± 0.002	0.901 ± 0.003 ± 0.001	0.919 ± 0.002 ± 0.001	0.935 ± 0.001 ± 0.001	0.920 ± 0.002 ± 0.002	0.925 ± 0.004 ± 0.001
[0.7, 0.8]	0.879 ± 0.010 ± 0.004	0.880 ± 0.006 ± 0.001	0.917 ± 0.003 ± 0.002	0.933 ± 0.002 ± 0.002	0.948 ± 0.001 ± 0.001	0.954 ± 0.002 ± 0.001	0.959 ± 0.003 ± 0.001
[0.8, 0.9]	0.833 ± 0.012 ± 0.004	0.802 ± 0.007 ± 0.002	0.857 ± 0.004 ± 0.002	0.892 ± 0.002 ± 0.003	0.918 ± 0.002 ± 0.002	0.929 ± 0.002 ± 0.002	0.936 ± 0.004 ± 0.001
[0.9, 1]	0.837 ± 0.012 ± 0.005	0.879 ± 0.006 ± 0.001	0.903 ± 0.004 ± 0.002	0.913 ± 0.002 ± 0.001	0.934 ± 0.002 ± 0.001	0.936 ± 0.002 ± 0.000	0.942 ± 0.004 ± 0.000
[1, 1.1]	0.858 ± 0.012 ± 0.003	0.854 ± 0.007 ± 0.003	0.894 ± 0.004 ± 0.002	0.911 ± 0.002 ± 0.000	0.929 ± 0.002 ± 0.001	0.940 ± 0.002 ± 0.001	0.945 ± 0.003 ± 0.001
[1.1, 1.2]	0.836 ± 0.012 ± 0.003	0.837 ± 0.007 ± 0.004	0.880 ± 0.004 ± 0.001	0.902 ± 0.002 ± 0.002	0.925 ± 0.002 ± 0.002	0.936 ± 0.002 ± 0.001	0.942 ± 0.004 ± 0.001
[1.2, 1.3]	0.837 ± 0.012 ± 0.003	0.828 ± 0.007 ± 0.002	0.866 ± 0.004 ± 0.001	0.894 ± 0.002 ± 0.003	0.918 ± 0.002 ± 0.001	0.939 ± 0.002 ± 0.001	0.946 ± 0.003 ± 0.000
[1.3, 1.37]	0.829 ± 0.013 ± 0.004	0.834 ± 0.007 ± 0.002	0.871 ± 0.004 ± 0.001	0.891 ± 0.003 ± 0.003	0.920 ± 0.002 ± 0.002	0.934 ± 0.002 ± 0.001	0.947 ± 0.003 ± 0.002
[1.52, 1.6]	0.827 ± 0.016 ± 0.004	0.833 ± 0.009 ± 0.003	0.858 ± 0.005 ± 0.002	0.878 ± 0.003 ± 0.002	0.913 ± 0.002 ± 0.002	0.932 ± 0.003 ± 0.002	0.939 ± 0.004 ± 0.000
[1.6, 1.7]	0.846 ± 0.012 ± 0.002	0.832 ± 0.007 ± 0.002	0.866 ± 0.004 ± 0.003	0.889 ± 0.003 ± 0.001	0.910 ± 0.002 ± 0.001	0.939 ± 0.002 ± 0.000	0.941 ± 0.004 ± 0.000
[1.7, 1.8]	0.836 ± 0.012 ± 0.005	0.785 ± 0.008 ± 0.003	0.848 ± 0.004 ± 0.001	0.872 ± 0.003 ± 0.002	0.907 ± 0.002 ± 0.001	0.935 ± 0.002 ± 0.001	0.943 ± 0.004 ± 0.002
[1.8, 1.9]	0.839 ± 0.013 ± 0.004	0.831 ± 0.007 ± 0.002	0.867 ± 0.004 ± 0.002	0.882 ± 0.003 ± 0.000	0.911 ± 0.002 ± 0.001	0.933 ± 0.002 ± 0.000	0.942 ± 0.003 ± 0.001
[1.9, 2.01]	0.828 ± 0.013 ± 0.003	0.809 ± 0.007 ± 0.002	0.851 ± 0.004 ± 0.001	0.871 ± 0.003 ± 0.002	0.896 ± 0.002 ± 0.000	0.915 ± 0.002 ± 0.001	0.919 ± 0.004 ± 0.001
[2.01, 2.1]	0.819 ± 0.013 ± 0.003	0.820 ± 0.007 ± 0.001	0.844 ± 0.004 ± 0.001	0.868 ± 0.002 ± 0.002	0.893 ± 0.002 ± 0.001	0.906 ± 0.003 ± 0.000	0.908 ± 0.005 ± 0.002
[2.1, 2.2]	0.820 ± 0.014 ± 0.003	0.808 ± 0.008 ± 0.001	0.835 ± 0.004 ± 0.003	0.861 ± 0.003 ± 0.002	0.896 ± 0.002 ± 0.002	0.918 ± 0.002 ± 0.001	0.925 ± 0.004 ± 0.001
[2.2, 2.3]	0.855 ± 0.013 ± 0.004	0.834 ± 0.007 ± 0.005	0.875 ± 0.004 ± 0.002	0.903 ± 0.002 ± 0.001	0.923 ± 0.002 ± 0.001	0.947 ± 0.002 ± 0.001	0.948 ± 0.003 ± 0.000
[2.3, 2.4]	0.815 ± 0.015 ± 0.004	0.803 ± 0.008 ± 0.006	0.856 ± 0.004 ± 0.002	0.888 ± 0.002 ± 0.002	0.914 ± 0.002 ± 0.000	0.937 ± 0.002 ± 0.000	0.951 ± 0.003 ± 0.000
[2.4, 2.47]	0.829 ± 0.015 ± 0.003	0.803 ± 0.008 ± 0.005	0.854 ± 0.004 ± 0.003	0.874 ± 0.003 ± 0.003	0.898 ± 0.002 ± 0.001	0.918 ± 0.002 ± 0.001	0.928 ± 0.004 ± 0.001
[2.4, 2.47]	0.763 ± 0.021 ± 0.002	0.786 ± 0.011 ± 0.005	0.829 ± 0.006 ± 0.001	0.868 ± 0.003 ± 0.001	0.880 ± 0.003 ± 0.000	0.900 ± 0.003 ± 0.001	0.918 ± 0.006 ± 0.001

Table A.27: MediumPP Monte-Carlo efficiencies in fine  $\eta$  granularity with their statistical and systematic uncertainties from 80 variations.

	15-20 GeV	20-25 GeV	25-30 GeV	30-35 GeV	35-40 GeV	40-45 GeV	45-50 GeV
[-2.47, -2.4]	0.941 ± 0.072 ± 0.043	1.013 ± 0.037 ± 0.021	1.015 ± 0.020 ± 0.013	1.040 ± 0.012 ± 0.005	1.069 ± 0.009 ± 0.005	1.047 ± 0.012 ± 0.007	1.076 ± 0.025 ± 0.026
[-2.4, -2.3]	0.977 ± 0.053 ± 0.054	0.931 ± 0.027 ± 0.025	0.966 ± 0.015 ± 0.015	0.984 ± 0.009 ± 0.007	1.002 ± 0.006 ± 0.004	1.021 ± 0.008 ± 0.004	1.000 ± 0.015 ± 0.010
[-2.3, -2.2]	0.878 ± 0.041 ± 0.036	0.793 ± 0.021 ± 0.022	0.877 ± 0.012 ± 0.016	0.917 ± 0.007 ± 0.005	0.935 ± 0.005 ± 0.004	0.965 ± 0.006 ± 0.005	0.944 ± 0.012 ± 0.009
[-2.2, -2.1]	0.834 ± 0.035 ± 0.027	0.851 ± 0.018 ± 0.023	0.920 ± 0.011 ± 0.013	0.949 ± 0.006 ± 0.003	0.961 ± 0.004 ± 0.003	0.984 ± 0.006 ± 0.003	0.969 ± 0.011 ± 0.013
[-2.1, -2.01]	0.918 ± 0.043 ± 0.035	0.858 ± 0.020 ± 0.023	0.930 ± 0.012 ± 0.015	0.951 ± 0.007 ± 0.004	0.953 ± 0.005 ± 0.004	0.964 ± 0.006 ± 0.003	0.942 ± 0.012 ± 0.011
[-2.01, -1.9]	1.018 ± 0.045 ± 0.032	0.990 ± 0.022 ± 0.020	1.017 ± 0.013 ± 0.016	1.016 ± 0.007 ± 0.005	1.014 ± 0.005 ± 0.004	1.030 ± 0.007 ± 0.004	1.021 ± 0.014 ± 0.014
[-1.9, -1.8]	1.007 ± 0.045 ± 0.021	0.970 ± 0.023 ± 0.017	1.014 ± 0.013 ± 0.011	1.015 ± 0.007 ± 0.005	1.014 ± 0.005 ± 0.002	1.015 ± 0.007 ± 0.004	0.993 ± 0.012 ± 0.008
[-1.8, -1.7]	1.001 ± 0.043 ± 0.021	0.979 ± 0.024 ± 0.015	0.995 ± 0.013 ± 0.014	1.003 ± 0.008 ± 0.006	1.012 ± 0.006 ± 0.004	1.007 ± 0.007 ± 0.005	1.001 ± 0.011 ± 0.010
[-1.7, -1.6]	0.946 ± 0.042 ± 0.017	0.968 ± 0.023 ± 0.016	0.965 ± 0.012 ± 0.005	0.983 ± 0.008 ± 0.004	1.000 ± 0.006 ± 0.004	1.010 ± 0.007 ± 0.006	0.996 ± 0.012 ± 0.008
[-1.6, -1.52]	0.999 ± 0.044 ± 0.033	1.000 ± 0.020 ± 0.022	1.016 ± 0.012 ± 0.011	1.031 ± 0.008 ± 0.006	1.036 ± 0.006 ± 0.005	1.048 ± 0.008 ± 0.005	1.011 ± 0.012 ± 0.004
[-1.37, -1.3]	1.116 ± 0.054 ± 0.030	1.047 ± 0.024 ± 0.017	1.029 ± 0.015 ± 0.008	1.039 ± 0.009 ± 0.003	1.031 ± 0.006 ± 0.004	1.051 ± 0.008 ± 0.003	1.055 ± 0.014 ± 0.009
[-1.3, -1.2]	1.082 ± 0.039 ± 0.031	1.067 ± 0.024 ± 0.023	1.033 ± 0.012 ± 0.012	1.022 ± 0.007 ± 0.004	1.016 ± 0.005 ± 0.003	1.029 ± 0.006 ± 0.004	1.023 ± 0.010 ± 0.009
[-1.2, -1.1]	1.079 ± 0.042 ± 0.035	1.029 ± 0.022 ± 0.018	1.028 ± 0.012 ± 0.009	1.026 ± 0.007 ± 0.005	1.025 ± 0.005 ± 0.003	1.014 ± 0.006 ± 0.003	1.018 ± 0.010 ± 0.008
[-1.1, -1]	1.046 ± 0.037 ± 0.031	1.019 ± 0.021 ± 0.021	1.013 ± 0.012 ± 0.009	1.022 ± 0.007 ± 0.003	1.021 ± 0.005 ± 0.002	1.015 ± 0.005 ± 0.003	1.002 ± 0.010 ± 0.006
[-1, -0.9]	1.047 ± 0.039 ± 0.030	1.003 ± 0.021 ± 0.023	1.016 ± 0.011 ± 0.010	1.004 ± 0.006 ± 0.002	1.008 ± 0.004 ± 0.003	1.011 ± 0.005 ± 0.003	0.993 ± 0.009 ± 0.005
[-0.9, -0.8]	0.990 ± 0.030 ± 0.019	1.005 ± 0.019 ± 0.008	1.026 ± 0.012 ± 0.006	1.014 ± 0.006 ± 0.004	1.004 ± 0.004 ± 0.003	1.014 ± 0.005 ± 0.004	1.001 ± 0.009 ± 0.005
[-0.8, -0.7]	0.994 ± 0.032 ± 0.022	0.998 ± 0.019 ± 0.015	0.985 ± 0.010 ± 0.008	0.991 ± 0.006 ± 0.005	0.997 ± 0.004 ± 0.003	1.000 ± 0.005 ± 0.004	1.009 ± 0.009 ± 0.006
[-0.7, -0.6]	0.969 ± 0.029 ± 0.025	0.966 ± 0.016 ± 0.016	0.982 ± 0.009 ± 0.009	0.997 ± 0.005 ± 0.005	1.000 ± 0.004 ± 0.003	0.996 ± 0.004 ± 0.002	0.995 ± 0.008 ± 0.005
[-0.6, -0.5]	0.940 ± 0.028 ± 0.019	0.975 ± 0.016 ± 0.014	0.987 ± 0.009 ± 0.010	0.988 ± 0.005 ± 0.005	0.992 ± 0.003 ± 0.002	0.976 ± 0.004 ± 0.003	0.979 ± 0.009 ± 0.003
[-0.5, -0.4]	0.975 ± 0.029 ± 0.019	0.971 ± 0.016 ± 0.016	0.979 ± 0.009 ± 0.007	0.993 ± 0.005 ± 0.004	0.991 ± 0.004 ± 0.003	0.980 ± 0.004 ± 0.003	0.973 ± 0.008 ± 0.005
[-0.4, -0.3]	0.978 ± 0.027 ± 0.016	0.976 ± 0.016 ± 0.019	0.987 ± 0.009 ± 0.007	0.988 ± 0.005 ± 0.003	0.994 ± 0.003 ± 0.003	0.985 ± 0.004 ± 0.003	0.978 ± 0.008 ± 0.004
[-0.3, -0.2]	1.002 ± 0.027 ± 0.014	0.991 ± 0.016 ± 0.010	0.980 ± 0.009 ± 0.007	0.990 ± 0.005 ± 0.003	0.991 ± 0.003 ± 0.002	0.993 ± 0.004 ± 0.003	0.984 ± 0.008 ± 0.005
[-0.2, -0.1]	0.957 ± 0.026 ± 0.023	0.984 ± 0.017 ± 0.019	0.991 ± 0.009 ± 0.006	0.983 ± 0.005 ± 0.004	0.998 ± 0.004 ± 0.002	0.994 ± 0.004 ± 0.004	0.978 ± 0.008 ± 0.003
[-0.1, 0]	1.040 ± 0.034 ± 0.019	1.009 ± 0.019 ± 0.012	1.003 ± 0.011 ± 0.009	1.002 ± 0.006 ± 0.005	1.027 ± 0.004 ± 0.002	1.006 ± 0.006 ± 0.003	1.024 ± 0.011 ± 0.006
[0, 0.1]	1.001 ± 0.033 ± 0.020	0.995 ± 0.020 ± 0.014	1.012 ± 0.011 ± 0.006	1.011 ± 0.006 ± 0.005	1.024 ± 0.005 ± 0.003	1.023 ± 0.006 ± 0.003	1.011 ± 0.011 ± 0.004
[0.1, 0.2]	0.982 ± 0.028 ± 0.023	0.983 ± 0.017 ± 0.018	0.988 ± 0.009 ± 0.007	0.985 ± 0.005 ± 0.004	0.996 ± 0.004 ± 0.001	0.981 ± 0.004 ± 0.002	0.983 ± 0.008 ± 0.006
[0.2, 0.3]	0.983 ± 0.027 ± 0.015	0.988 ± 0.017 ± 0.009	0.982 ± 0.009 ± 0.007	0.982 ± 0.005 ± 0.003	0.987 ± 0.003 ± 0.002	0.983 ± 0.004 ± 0.002	0.974 ± 0.008 ± 0.005
[0.3, 0.4]	1.023 ± 0.029 ± 0.020	0.991 ± 0.017 ± 0.022	0.995 ± 0.009 ± 0.008	0.985 ± 0.005 ± 0.003	0.988 ± 0.003 ± 0.003	0.982 ± 0.004 ± 0.003	0.983 ± 0.008 ± 0.004
[0.4, 0.5]	1.014 ± 0.031 ± 0.024	0.992 ± 0.017 ± 0.018	0.984 ± 0.009 ± 0.007	0.990 ± 0.005 ± 0.004	0.994 ± 0.004 ± 0.003	0.982 ± 0.004 ± 0.003	0.978 ± 0.008 ± 0.005
[0.5, 0.6]	0.978 ± 0.028 ± 0.020	0.985 ± 0.017 ± 0.013	0.987 ± 0.009 ± 0.010	0.985 ± 0.005 ± 0.005	0.990 ± 0.004 ± 0.002	0.977 ± 0.005 ± 0.003	0.974 ± 0.009 ± 0.002
[0.6, 0.7]	1.010 ± 0.030 ± 0.021	0.971 ± 0.017 ± 0.017	0.977 ± 0.009 ± 0.010	0.994 ± 0.005 ± 0.005	1.002 ± 0.004 ± 0.003	1.002 ± 0.004 ± 0.002	0.991 ± 0.008 ± 0.004
[0.7, 0.8]	1.010 ± 0.033 ± 0.021	0.990 ± 0.020 ± 0.015	0.991 ± 0.010 ± 0.010	0.995 ± 0.006 ± 0.006	0.999 ± 0.004 ± 0.003	1.002 ± 0.005 ± 0.003	0.995 ± 0.009 ± 0.006
[0.8, 0.9]	1.004 ± 0.033 ± 0.026	0.997 ± 0.020 ± 0.007	1.002 ± 0.011 ± 0.006	1.020 ± 0.006 ± 0.005	1.006 ± 0.004 ± 0.002	1.009 ± 0.005 ± 0.003	0.998 ± 0.009 ± 0.004
[0.9, 1]	1.003 ± 0.035 ± 0.027	1.027 ± 0.021 ± 0.022	1.009 ± 0.010 ± 0.006	0.997 ± 0.006 ± 0.004	1.005 ± 0.004 ± 0.003	1.003 ± 0.005 ± 0.003	1.005 ± 0.009 ± 0.004
[1, 1.1]	1.044 ± 0.038 ± 0.037	1.018 ± 0.022 ± 0.023	1.013 ± 0.011 ± 0.009	1.010 ± 0.007 ± 0.004	1.012 ± 0.005 ± 0.002	1.017 ± 0.006 ± 0.003	1.005 ± 0.010 ± 0.006
[1.1, 1.2]	1.043 ± 0.037 ± 0.031	1.015 ± 0.022 ± 0.015	1.023 ± 0.012 ± 0.010	1.015 ± 0.007 ± 0.005	1.024 ± 0.005 ± 0.003	1.006 ± 0.006 ± 0.003	1.024 ± 0.011 ± 0.009
[1.2, 1.3]	1.076 ± 0.045 ± 0.031	1.027 ± 0.024 ± 0.019	1.036 ± 0.013 ± 0.011	1.023 ± 0.007 ± 0.005	1.013 ± 0.005 ± 0.004	1.041 ± 0.006 ± 0.005	1.021 ± 0.011 ± 0.007
[1.3, 1.37]	1.038 ± 0.051 ± 0.025	1.027 ± 0.030 ± 0.020	1.036 ± 0.016 ± 0.011	1.030 ± 0.009 ± 0.004	1.026 ± 0.007 ± 0.003	1.034 ± 0.007 ± 0.003	1.045 ± 0.014 ± 0.008
[1.52, 1.6]	1.025 ± 0.045 ± 0.028	1.062 ± 0.023 ± 0.016	1.028 ± 0.012 ± 0.011	1.040 ± 0.008 ± 0.006	1.035 ± 0.006 ± 0.005	1.040 ± 0.007 ± 0.004	1.032 ± 0.014 ± 0.005
[1.6, 1.7]	0.971 ± 0.043 ± 0.024	0.979 ± 0.024 ± 0.015	0.976 ± 0.013 ± 0.006	0.990 ± 0.008 ± 0.006	1.008 ± 0.006 ± 0.005	1.004 ± 0.007 ± 0.004	0.981 ± 0.011 ± 0.008
[1.7, 1.8]	0.968 ± 0.038 ± 0.028	0.968 ± 0.023 ± 0.013	0.992 ± 0.013 ± 0.014	0.996 ± 0.008 ± 0.004	0.999 ± 0.006 ± 0.005	1.005 ± 0.006 ± 0.004	0.984 ± 0.011 ± 0.011
[1.8, 1.9]	0.993 ± 0.046 ± 0.024	1.021 ± 0.023 ± 0.012	1.000 ± 0.012 ± 0.011	1.020 ± 0.007 ± 0.006	1.019 ± 0.005 ± 0.002	1.020 ± 0.007 ± 0.004	1.015 ± 0.012 ± 0.009
[1.9, 2.01]	0.987 ± 0.041 ± 0.026	1.015 ± 0.025 ± 0.017	1.028 ± 0.014 ± 0.015	1.013 ± 0.008 ± 0.005	1.011 ± 0.005 ± 0.004	1.030 ± 0.007 ± 0.004	1.018 ± 0.014 ± 0.011
[2.01, 2.1]	0.935 ± 0.042 ± 0.032	0.899 ± 0.021 ± 0.012	0.947 ± 0.012 ± 0.017	0.973 ± 0.007 ± 0.004	0.964 ± 0.005 ± 0.003	0.988 ± 0.006 ± 0.003	0.968 ± 0.012 ± 0.011
[2.1, 2.2]	0.873 ± 0.038 ± 0.034	0.873 ± 0.019 ± 0.025	0.922 ± 0.011 ± 0.011	0.960 ± 0.007 ± 0.004	0.966 ± 0.004 ± 0.004	0.974 ± 0.006 ± 0.002	0.954 ± 0.012 ± 0.010
[2.2, 2.3]	0.892 ± 0.040 ± 0.041	0.785 ± 0.020 ± 0.023	0.847 ± 0.011 ± 0.015	0.919 ± 0.007 ± 0.006	0.936 ± 0.005 ± 0.004	0.962 ± 0.006 ± 0.003	0.932 ± 0.012 ± 0.009
[2.3, 2.4]	0.923 ± 0.051 ± 0.050	0.897 ± 0.025 ± 0.041	0.946 ± 0.014 ± 0.017	0.972 ± 0.008 ± 0.008	1.001 ± 0.006 ± 0.006	1.003 ± 0.008 ± 0.004	0.987 ± 0.015 ± 0.016
[2.4, 2.47]	0.990 ± 0.068 ± 0.039	1.002 ± 0.038 ± 0.031	0.997 ± 0.019 ± 0.010	1.023 ± 0.012 ± 0.005	1.062 ± 0.009 ± 0.007	1.072 ± 0.013 ± 0.005	1.013 ± 0.023 ± 0.013

Table A.28: TightPP scale-factors in fine  $\eta$  granularity with their statistical and systematic uncertainties from 80 variations.

	15-20 GeV	20-25 GeV	25-30 GeV	30-35 GeV	35-40 GeV	40-45 GeV	45-50 GeV
[-2.47, -2.4]	0.461 ± 0.027 ± 0.018	0.514 ± 0.014 ± 0.012	0.569 ± 0.009 ± 0.007	0.608 ± 0.005 ± 0.003	0.649 ± 0.004 ± 0.003	0.687 ± 0.006 ± 0.004	0.705 ± 0.013 ± 0.016
[-2.4, -2.3]	0.527 ± 0.023 ± 0.026	0.535 ± 0.013 ± 0.015	0.596 ± 0.008 ± 0.009	0.635 ± 0.005 ± 0.003	0.679 ± 0.003 ± 0.003	0.729 ± 0.004 ± 0.003	0.728 ± 0.009 ± 0.009
[-2.3, -2.2]	0.575 ± 0.024 ± 0.023	0.522 ± 0.012 ± 0.016	0.614 ± 0.008 ± 0.010	0.675 ± 0.004 ± 0.004	0.716 ± 0.003 ± 0.003	0.777 ± 0.004 ± 0.004	0.771 ± 0.009 ± 0.008
[-2.2, -2.1]	0.608 ± 0.024 ± 0.024	0.617 ± 0.012 ± 0.018	0.696 ± 0.008 ± 0.009	0.741 ± 0.004 ± 0.003	0.776 ± 0.003 ± 0.003	0.829 ± 0.004 ± 0.003	0.823 ± 0.009 ± 0.010
[-2.1, -2.01]	0.620 ± 0.026 ± 0.024	0.599 ± 0.012 ± 0.013	0.674 ± 0.008 ± 0.008	0.707 ± 0.004 ± 0.005	0.746 ± 0.003 ± 0.002	0.797 ± 0.004 ± 0.003	0.782 ± 0.009 ± 0.009
[-2.01, -1.9]	0.615 ± 0.022 ± 0.017	0.639 ± 0.013 ± 0.013	0.672 ± 0.007 ± 0.009	0.709 ± 0.004 ± 0.003	0.741 ± 0.003 ± 0.002	0.792 ± 0.004 ± 0.002	0.784 ± 0.009 ± 0.009
[-1.9, -1.8]	0.624 ± 0.023 ± 0.013	0.626 ± 0.013 ± 0.014	0.675 ± 0.008 ± 0.006	0.719 ± 0.004 ± 0.004	0.755 ± 0.003 ± 0.002	0.797 ± 0.004 ± 0.003	0.795 ± 0.008 ± 0.005
[-1.8, -1.7]	0.667 ± 0.025 ± 0.013	0.671 ± 0.015 ± 0.009	0.706 ± 0.008 ± 0.007	0.732 ± 0.005 ± 0.003	0.767 ± 0.004 ± 0.002	0.809 ± 0.004 ± 0.003	0.808 ± 0.007 ± 0.008
[-1.7, -1.6]	0.608 ± 0.025 ± 0.013	0.632 ± 0.013 ± 0.012	0.679 ± 0.007 ± 0.005	0.723 ± 0.005 ± 0.002	0.770 ± 0.004 ± 0.002	0.816 ± 0.004 ± 0.004	0.818 ± 0.008 ± 0.007
[-1.6, -1.52]	0.619 ± 0.023 ± 0.024	0.678 ± 0.011 ± 0.018	0.718 ± 0.007 ± 0.008	0.767 ± 0.005 ± 0.005	0.794 ± 0.004 ± 0.003	0.842 ± 0.005 ± 0.003	0.831 ± 0.009 ± 0.004
[-1.52, -1.3]	0.696 ± 0.026 ± 0.024	0.695 ± 0.017 ± 0.011	0.715 ± 0.009 ± 0.006	0.760 ± 0.005 ± 0.004	0.789 ± 0.003 ± 0.003	0.820 ± 0.004 ± 0.003	0.818 ± 0.007 ± 0.006
[-1.3, -1.2]	0.713 ± 0.021 ± 0.023	0.703 ± 0.013 ± 0.013	0.733 ± 0.007 ± 0.009	0.768 ± 0.004 ± 0.004	0.804 ± 0.003 ± 0.002	0.832 ± 0.003 ± 0.003	0.831 ± 0.006 ± 0.006
[-1.2, -1.1]	0.686 ± 0.020 ± 0.025	0.687 ± 0.012 ± 0.013	0.736 ± 0.007 ± 0.008	0.772 ± 0.004 ± 0.004	0.805 ± 0.003 ± 0.004	0.824 ± 0.003 ± 0.003	0.827 ± 0.006 ± 0.007
[-1.1, -1]	0.725 ± 0.022 ± 0.024	0.715 ± 0.013 ± 0.016	0.752 ± 0.007 ± 0.006	0.793 ± 0.004 ± 0.003	0.821 ± 0.003 ± 0.003	0.835 ± 0.003 ± 0.003	0.833 ± 0.007 ± 0.005
[-1, -0.9]	0.758 ± 0.025 ± 0.017	0.754 ± 0.015 ± 0.019	0.787 ± 0.007 ± 0.006	0.822 ± 0.004 ± 0.002	0.843 ± 0.003 ± 0.003	0.862 ± 0.003 ± 0.002	0.857 ± 0.007 ± 0.003
[-0.9, -0.8]	0.750 ± 0.020 ± 0.016	0.773 ± 0.014 ± 0.008	0.806 ± 0.009 ± 0.005	0.825 ± 0.004 ± 0.004	0.843 ± 0.003 ± 0.003	0.857 ± 0.003 ± 0.003	0.862 ± 0.006 ± 0.004
[-0.8, -0.7]	0.744 ± 0.021 ± 0.016	0.708 ± 0.012 ± 0.011	0.762 ± 0.007 ± 0.007	0.810 ± 0.004 ± 0.004	0.840 ± 0.003 ± 0.003	0.856 ± 0.003 ± 0.002	0.865 ± 0.006 ± 0.005
[-0.7, -0.6]	0.759 ± 0.020 ± 0.021	0.780 ± 0.013 ± 0.013	0.806 ± 0.007 ± 0.008	0.851 ± 0.004 ± 0.005	0.873 ± 0.003 ± 0.002	0.884 ± 0.003 ± 0.002	0.886 ± 0.006 ± 0.004
[-0.6, -0.5]	0.752 ± 0.021 ± 0.015	0.760 ± 0.011 ± 0.010	0.810 ± 0.007 ± 0.008	0.840 ± 0.004 ± 0.004	0.858 ± 0.002 ± 0.002	0.842 ± 0.003 ± 0.002	0.849 ± 0.006 ± 0.002
[-0.5, -0.4]	0.778 ± 0.022 ± 0.017	0.768 ± 0.012 ± 0.013	0.805 ± 0.007 ± 0.006	0.844 ± 0.004 ± 0.004	0.862 ± 0.003 ± 0.002	0.851 ± 0.003 ± 0.003	0.846 ± 0.006 ± 0.003
[-0.4, -0.3]	0.774 ± 0.019 ± 0.013	0.754 ± 0.012 ± 0.014	0.807 ± 0.007 ± 0.005	0.840 ± 0.004 ± 0.002	0.866 ± 0.002 ± 0.002	0.858 ± 0.003 ± 0.002	0.862 ± 0.006 ± 0.004
[-0.3, -0.2]	0.794 ± 0.019 ± 0.011	0.770 ± 0.012 ± 0.008	0.806 ± 0.007 ± 0.006	0.840 ± 0.004 ± 0.003	0.860 ± 0.002 ± 0.002	0.862 ± 0.003 ± 0.002	0.861 ± 0.005 ± 0.004
[-0.2, -0.1]	0.762 ± 0.018 ± 0.018	0.752 ± 0.012 ± 0.015	0.801 ± 0.006 ± 0.005	0.833 ± 0.003 ± 0.004	0.865 ± 0.003 ± 0.002	0.859 ± 0.003 ± 0.001	0.860 ± 0.006 ± 0.003
[-0.1, 0]	0.729 ± 0.019 ± 0.015	0.711 ± 0.012 ± 0.009	0.746 ± 0.007 ± 0.005	0.771 ± 0.004 ± 0.003	0.795 ± 0.003 ± 0.002	0.798 ± 0.003 ± 0.002	0.802 ± 0.006 ± 0.004
[0, 0.1]	0.712 ± 0.020 ± 0.013	0.700 ± 0.013 ± 0.010	0.744 ± 0.007 ± 0.005	0.764 ± 0.004 ± 0.003	0.797 ± 0.003 ± 0.002	0.798 ± 0.003 ± 0.002	0.791 ± 0.006 ± 0.002
[0.1, 0.2]	0.786 ± 0.021 ± 0.018	0.771 ± 0.012 ± 0.014	0.813 ± 0.007 ± 0.006	0.835 ± 0.004 ± 0.003	0.863 ± 0.003 ± 0.002	0.851 ± 0.003 ± 0.002	0.855 ± 0.006 ± 0.003
[0.2, 0.3]	0.786 ± 0.019 ± 0.013	0.767 ± 0.012 ± 0.007	0.807 ± 0.007 ± 0.006	0.836 ± 0.004 ± 0.003	0.859 ± 0.002 ± 0.002	0.857 ± 0.003 ± 0.002	0.853 ± 0.005 ± 0.005
[0.3, 0.4]	0.795 ± 0.019 ± 0.015	0.766 ± 0.012 ± 0.017	0.821 ± 0.007 ± 0.006	0.842 ± 0.004 ± 0.002	0.862 ± 0.002 ± 0.002	0.853 ± 0.003 ± 0.003	0.865 ± 0.006 ± 0.003
[0.4, 0.5]	0.794 ± 0.022 ± 0.018	0.778 ± 0.013 ± 0.015	0.808 ± 0.007 ± 0.006	0.842 ± 0.004 ± 0.004	0.865 ± 0.003 ± 0.003	0.853 ± 0.003 ± 0.002	0.852 ± 0.006 ± 0.006
[0.5, 0.6]	0.796 ± 0.022 ± 0.018	0.756 ± 0.012 ± 0.010	0.811 ± 0.007 ± 0.008	0.838 ± 0.004 ± 0.005	0.856 ± 0.003 ± 0.002	0.836 ± 0.003 ± 0.002	0.840 ± 0.006 ± 0.002
[0.6, 0.7]	0.797 ± 0.022 ± 0.019	0.778 ± 0.013 ± 0.014	0.815 ± 0.007 ± 0.008	0.853 ± 0.004 ± 0.005	0.877 ± 0.003 ± 0.003	0.887 ± 0.003 ± 0.002	0.886 ± 0.006 ± 0.003
[0.7, 0.8]	0.738 ± 0.020 ± 0.016	0.713 ± 0.013 ± 0.012	0.768 ± 0.007 ± 0.007	0.814 ± 0.004 ± 0.005	0.848 ± 0.003 ± 0.002	0.863 ± 0.003 ± 0.003	0.863 ± 0.006 ± 0.005
[0.8, 0.9]	0.720 ± 0.020 ± 0.021	0.765 ± 0.014 ± 0.005	0.801 ± 0.008 ± 0.006	0.832 ± 0.005 ± 0.004	0.849 ± 0.003 ± 0.002	0.861 ± 0.003 ± 0.003	0.857 ± 0.006 ± 0.003
[0.9, 1]	0.739 ± 0.022 ± 0.018	0.759 ± 0.015 ± 0.018	0.790 ± 0.007 ± 0.006	0.816 ± 0.004 ± 0.004	0.841 ± 0.003 ± 0.003	0.862 ± 0.003 ± 0.003	0.863 ± 0.007 ± 0.004
[1, 1.1]	0.709 ± 0.022 ± 0.027	0.711 ± 0.013 ± 0.017	0.754 ± 0.007 ± 0.007	0.793 ± 0.004 ± 0.004	0.823 ± 0.003 ± 0.003	0.834 ± 0.003 ± 0.003	0.842 ± 0.007 ± 0.006
[1.1, 1.2]	0.689 ± 0.020 ± 0.025	0.683 ± 0.013 ± 0.013	0.736 ± 0.007 ± 0.009	0.769 ± 0.004 ± 0.005	0.807 ± 0.003 ± 0.003	0.824 ± 0.003 ± 0.003	0.834 ± 0.006 ± 0.008
[1.2, 1.3]	0.664 ± 0.020 ± 0.021	0.680 ± 0.013 ± 0.015	0.729 ± 0.007 ± 0.009	0.768 ± 0.004 ± 0.004	0.802 ± 0.003 ± 0.004	0.835 ± 0.003 ± 0.003	0.825 ± 0.006 ± 0.006
[1.3, 1.37]	0.678 ± 0.026 ± 0.020	0.679 ± 0.017 ± 0.013	0.709 ± 0.009 ± 0.008	0.750 ± 0.005 ± 0.005	0.781 ± 0.004 ± 0.003	0.814 ± 0.004 ± 0.003	0.821 ± 0.008 ± 0.005
[1.52, 1.6]	0.627 ± 0.024 ± 0.021	0.701 ± 0.013 ± 0.014	0.730 ± 0.008 ± 0.008	0.780 ± 0.005 ± 0.004	0.803 ± 0.004 ± 0.003	0.843 ± 0.005 ± 0.004	0.836 ± 0.010 ± 0.004
[1.6, 1.7]	0.627 ± 0.025 ± 0.018	0.644 ± 0.014 ± 0.010	0.699 ± 0.008 ± 0.004	0.732 ± 0.005 ± 0.003	0.779 ± 0.004 ± 0.002	0.821 ± 0.004 ± 0.003	0.820 ± 0.008 ± 0.007
[1.7, 1.8]	0.649 ± 0.022 ± 0.019	0.659 ± 0.015 ± 0.009	0.709 ± 0.008 ± 0.008	0.732 ± 0.005 ± 0.003	0.764 ± 0.003 ± 0.002	0.806 ± 0.004 ± 0.002	0.808 ± 0.007 ± 0.010
[1.8, 1.9]	0.615 ± 0.024 ± 0.016	0.659 ± 0.013 ± 0.009	0.684 ± 0.007 ± 0.008	0.729 ± 0.004 ± 0.004	0.764 ± 0.003 ± 0.002	0.803 ± 0.004 ± 0.003	0.804 ± 0.008 ± 0.007
[1.9, 2.01]	0.624 ± 0.023 ± 0.021	0.649 ± 0.015 ± 0.010	0.675 ± 0.008 ± 0.010	0.712 ± 0.005 ± 0.005	0.739 ± 0.003 ± 0.002	0.788 ± 0.005 ± 0.003	0.783 ± 0.009 ± 0.008
[2.01, 2.1]	0.618 ± 0.023 ± 0.021	0.625 ± 0.012 ± 0.009	0.683 ± 0.008 ± 0.010	0.725 ± 0.004 ± 0.004	0.754 ± 0.003 ± 0.002	0.806 ± 0.004 ± 0.003	0.791 ± 0.008 ± 0.008
[2.1, 2.2]	0.614 ± 0.024 ± 0.025	0.621 ± 0.012 ± 0.017	0.685 ± 0.007 ± 0.008	0.739 ± 0.004 ± 0.003	0.774 ± 0.003 ± 0.003	0.820 ± 0.004 ± 0.002	0.806 ± 0.009 ± 0.009
[2.2, 2.3]	0.586 ± 0.023 ± 0.027	0.526 ± 0.012 ± 0.014	0.602 ± 0.007 ± 0.010	0.672 ± 0.004 ± 0.004	0.716 ± 0.003 ± 0.003	0.774 ± 0.004 ± 0.003	0.771 ± 0.009 ± 0.009
[2.3, 2.4]	0.532 ± 0.024 ± 0.026	0.527 ± 0.012 ± 0.019	0.607 ± 0.008 ± 0.011	0.643 ± 0.004 ± 0.004	0.685 ± 0.003 ± 0.003	0.730 ± 0.004 ± 0.003	0.728 ± 0.009 ± 0.010
[2.4, 2.47]	0.498 ± 0.026 ± 0.019	0.515 ± 0.014 ± 0.012	0.567 ± 0.008 ± 0.005	0.609 ± 0.005 ± 0.003	0.650 ± 0.004 ± 0.003	0.704 ± 0.006 ± 0.004	0.679 ± 0.012 ± 0.009

Table A.29: TightPP efficiencies in fine  $\eta$  granularity with their statistical and systematic uncertainties from 80 variations.

	15-20 GeV	20-25 GeV	25-30 GeV	30-35 GeV	35-40 GeV	40-45 GeV	45-50 GeV
[-2.47, -2.4]	0.487 ± 0.025 ± 0.004	0.506 ± 0.013 ± 0.001	0.560 ± 0.008 ± 0.003	0.584 ± 0.005 ± 0.002	0.607 ± 0.004 ± 0.001	0.657 ± 0.005 ± 0.001	0.656 ± 0.010 ± 0.001
[-2.4, -2.3]	0.539 ± 0.019 ± 0.004	0.573 ± 0.010 ± 0.003	0.616 ± 0.006 ± 0.002	0.645 ± 0.004 ± 0.003	0.678 ± 0.003 ± 0.000	0.714 ± 0.004 ± 0.000	0.728 ± 0.008 ± 0.003
[-2.3, -2.2]	0.653 ± 0.017 ± 0.004	0.657 ± 0.009 ± 0.002	0.700 ± 0.005 ± 0.003	0.735 ± 0.003 ± 0.002	0.766 ± 0.003 ± 0.001	0.805 ± 0.003 ± 0.001	0.816 ± 0.006 ± 0.002
[-2.2, -2.1]	0.729 ± 0.016 ± 0.003	0.725 ± 0.009 ± 0.002	0.756 ± 0.005 ± 0.003	0.781 ± 0.003 ± 0.002	0.808 ± 0.002 ± 0.001	0.842 ± 0.003 ± 0.001	0.849 ± 0.006 ± 0.002
[-2.1, -2.0]	0.675 ± 0.017 ± 0.003	0.697 ± 0.009 ± 0.006	0.724 ± 0.005 ± 0.003	0.743 ± 0.004 ± 0.004	0.783 ± 0.003 ± 0.002	0.827 ± 0.003 ± 0.001	0.830 ± 0.006 ± 0.001
[-2.01, -1.9]	0.606 ± 0.016 ± 0.004	0.644 ± 0.008 ± 0.002	0.660 ± 0.005 ± 0.002	0.698 ± 0.003 ± 0.002	0.731 ± 0.003 ± 0.001	0.769 ± 0.004 ± 0.002	0.768 ± 0.007 ± 0.002
[-1.9, -1.8]	0.621 ± 0.017 ± 0.003	0.644 ± 0.009 ± 0.004	0.665 ± 0.005 ± 0.003	0.708 ± 0.004 ± 0.001	0.745 ± 0.003 ± 0.001	0.785 ± 0.004 ± 0.000	0.801 ± 0.006 ± 0.003
[-1.8, -1.7]	0.666 ± 0.017 ± 0.006	0.684 ± 0.008 ± 0.002	0.709 ± 0.005 ± 0.004	0.730 ± 0.003 ± 0.002	0.758 ± 0.003 ± 0.001	0.803 ± 0.003 ± 0.001	0.807 ± 0.006 ± 0.002
[-1.7, -1.6]	0.643 ± 0.016 ± 0.006	0.653 ± 0.009 ± 0.003	0.703 ± 0.005 ± 0.001	0.736 ± 0.004 ± 0.002	0.770 ± 0.003 ± 0.002	0.808 ± 0.004 ± 0.002	0.820 ± 0.007 ± 0.001
[-1.6, -1.5]	0.620 ± 0.017 ± 0.006	0.677 ± 0.008 ± 0.002	0.706 ± 0.005 ± 0.002	0.743 ± 0.004 ± 0.001	0.766 ± 0.003 ± 0.002	0.803 ± 0.004 ± 0.002	0.822 ± 0.006 ± 0.002
[-1.37, -1.3]	0.624 ± 0.020 ± 0.006	0.664 ± 0.011 ± 0.002	0.694 ± 0.007 ± 0.001	0.732 ± 0.004 ± 0.004	0.766 ± 0.003 ± 0.000	0.779 ± 0.004 ± 0.002	0.775 ± 0.008 ± 0.002
[-1.3, -1.2]	0.658 ± 0.016 ± 0.005	0.658 ± 0.009 ± 0.004	0.709 ± 0.005 ± 0.004	0.751 ± 0.003 ± 0.002	0.792 ± 0.003 ± 0.001	0.808 ± 0.003 ± 0.002	0.813 ± 0.006 ± 0.003
[-1.2, -1.1]	0.637 ± 0.016 ± 0.002	0.666 ± 0.009 ± 0.006	0.715 ± 0.005 ± 0.003	0.753 ± 0.003 ± 0.003	0.785 ± 0.003 ± 0.002	0.812 ± 0.003 ± 0.001	0.813 ± 0.006 ± 0.002
[-1.1, -1]	0.692 ± 0.015 ± 0.006	0.700 ± 0.009 ± 0.002	0.741 ± 0.005 ± 0.003	0.776 ± 0.003 ± 0.001	0.804 ± 0.003 ± 0.002	0.823 ± 0.003 ± 0.001	0.831 ± 0.006 ± 0.002
[-1, -0.9]	0.723 ± 0.015 ± 0.006	0.750 ± 0.008 ± 0.003	0.774 ± 0.005 ± 0.003	0.819 ± 0.003 ± 0.002	0.836 ± 0.002 ± 0.003	0.852 ± 0.003 ± 0.001	0.863 ± 0.005 ± 0.002
[-0.9, -0.8]	0.757 ± 0.014 ± 0.004	0.768 ± 0.008 ± 0.002	0.785 ± 0.005 ± 0.004	0.813 ± 0.003 ± 0.001	0.840 ± 0.002 ± 0.001	0.845 ± 0.003 ± 0.002	0.861 ± 0.005 ± 0.001
[-0.8, -0.7]	0.746 ± 0.014 ± 0.007	0.710 ± 0.008 ± 0.002	0.773 ± 0.005 ± 0.002	0.817 ± 0.003 ± 0.001	0.843 ± 0.002 ± 0.001	0.856 ± 0.003 ± 0.001	0.857 ± 0.005 ± 0.002
[-0.7, -0.6]	0.781 ± 0.013 ± 0.002	0.808 ± 0.007 ± 0.002	0.820 ± 0.004 ± 0.001	0.853 ± 0.003 ± 0.001	0.873 ± 0.002 ± 0.002	0.888 ± 0.002 ± 0.000	0.891 ± 0.004 ± 0.001
[-0.6, -0.5]	0.800 ± 0.012 ± 0.005	0.779 ± 0.007 ± 0.003	0.820 ± 0.004 ± 0.002	0.851 ± 0.003 ± 0.001	0.865 ± 0.002 ± 0.001	0.862 ± 0.003 ± 0.001	0.867 ± 0.005 ± 0.004
[-0.5, -0.4]	0.797 ± 0.013 ± 0.005	0.790 ± 0.007 ± 0.002	0.822 ± 0.004 ± 0.003	0.850 ± 0.003 ± 0.002	0.870 ± 0.002 ± 0.001	0.868 ± 0.003 ± 0.001	0.870 ± 0.005 ± 0.002
[-0.4, -0.3]	0.791 ± 0.012 ± 0.003	0.773 ± 0.007 ± 0.004	0.818 ± 0.004 ± 0.001	0.849 ± 0.003 ± 0.001	0.871 ± 0.002 ± 0.001	0.871 ± 0.003 ± 0.002	0.882 ± 0.004 ± 0.001
[-0.3, -0.2]	0.792 ± 0.012 ± 0.002	0.777 ± 0.007 ± 0.003	0.823 ± 0.004 ± 0.002	0.849 ± 0.003 ± 0.002	0.868 ± 0.002 ± 0.001	0.868 ± 0.003 ± 0.003	0.874 ± 0.005 ± 0.000
[-0.2, -0.1]	0.796 ± 0.013 ± 0.002	0.765 ± 0.007 ± 0.002	0.809 ± 0.004 ± 0.002	0.847 ± 0.003 ± 0.002	0.866 ± 0.002 ± 0.000	0.865 ± 0.003 ± 0.002	0.879 ± 0.004 ± 0.001
[-0.1, 0]	0.701 ± 0.014 ± 0.004	0.704 ± 0.008 ± 0.001	0.743 ± 0.005 ± 0.005	0.769 ± 0.003 ± 0.001	0.790 ± 0.002 ± 0.000	0.793 ± 0.003 ± 0.001	0.783 ± 0.006 ± 0.001
[0, 0.1]	0.711 ± 0.015 ± 0.003	0.704 ± 0.008 ± 0.002	0.735 ± 0.005 ± 0.002	0.756 ± 0.003 ± 0.001	0.778 ± 0.003 ± 0.001	0.780 ± 0.003 ± 0.001	0.782 ± 0.006 ± 0.001
[0.1, 0.2]	0.798 ± 0.012 ± 0.001	0.777 ± 0.007 ± 0.002	0.822 ± 0.004 ± 0.001	0.848 ± 0.003 ± 0.001	0.866 ± 0.002 ± 0.001	0.868 ± 0.003 ± 0.001	0.869 ± 0.005 ± 0.004
[0.2, 0.3]	0.798 ± 0.012 ± 0.002	0.776 ± 0.007 ± 0.002	0.822 ± 0.004 ± 0.002	0.851 ± 0.003 ± 0.003	0.871 ± 0.002 ± 0.001	0.872 ± 0.003 ± 0.001	0.876 ± 0.005 ± 0.001
[0.3, 0.4]	0.776 ± 0.013 ± 0.003	0.774 ± 0.007 ± 0.001	0.825 ± 0.004 ± 0.002	0.854 ± 0.003 ± 0.001	0.873 ± 0.002 ± 0.001	0.869 ± 0.003 ± 0.002	0.880 ± 0.004 ± 0.002
[0.4, 0.5]	0.782 ± 0.013 ± 0.003	0.784 ± 0.007 ± 0.002	0.821 ± 0.004 ± 0.001	0.850 ± 0.003 ± 0.002	0.870 ± 0.002 ± 0.003	0.869 ± 0.003 ± 0.001	0.871 ± 0.005 ± 0.002
[0.5, 0.6]	0.814 ± 0.012 ± 0.007	0.767 ± 0.007 ± 0.001	0.820 ± 0.004 ± 0.001	0.850 ± 0.003 ± 0.000	0.865 ± 0.002 ± 0.002	0.855 ± 0.003 ± 0.002	0.862 ± 0.005 ± 0.002
[0.6, 0.7]	0.789 ± 0.013 ± 0.005	0.802 ± 0.007 ± 0.002	0.834 ± 0.004 ± 0.002	0.858 ± 0.003 ± 0.002	0.875 ± 0.002 ± 0.001	0.885 ± 0.002 ± 0.001	0.894 ± 0.004 ± 0.002
[0.7, 0.8]	0.732 ± 0.014 ± 0.002	0.720 ± 0.008 ± 0.002	0.774 ± 0.005 ± 0.003	0.818 ± 0.003 ± 0.003	0.848 ± 0.002 ± 0.002	0.861 ± 0.003 ± 0.002	0.868 ± 0.005 ± 0.001
[0.8, 0.9]	0.717 ± 0.015 ± 0.003	0.766 ± 0.008 ± 0.002	0.799 ± 0.005 ± 0.002	0.815 ± 0.003 ± 0.002	0.843 ± 0.002 ± 0.001	0.853 ± 0.003 ± 0.002	0.859 ± 0.005 ± 0.001
[0.9, 1]	0.738 ± 0.015 ± 0.004	0.738 ± 0.008 ± 0.005	0.782 ± 0.005 ± 0.002	0.819 ± 0.003 ± 0.001	0.837 ± 0.002 ± 0.003	0.859 ± 0.003 ± 0.001	0.859 ± 0.005 ± 0.001
[1, 1.1]	0.680 ± 0.015 ± 0.003	0.697 ± 0.009 ± 0.006	0.744 ± 0.005 ± 0.001	0.785 ± 0.003 ± 0.001	0.813 ± 0.003 ± 0.002	0.820 ± 0.003 ± 0.001	0.838 ± 0.006 ± 0.001
[1.1, 1.2]	0.661 ± 0.016 ± 0.003	0.673 ± 0.009 ± 0.002	0.718 ± 0.005 ± 0.002	0.757 ± 0.003 ± 0.002	0.788 ± 0.003 ± 0.002	0.819 ± 0.003 ± 0.001	0.814 ± 0.006 ± 0.000
[1.2, 1.3]	0.618 ± 0.016 ± 0.005	0.662 ± 0.009 ± 0.002	0.703 ± 0.005 ± 0.002	0.751 ± 0.004 ± 0.002	0.791 ± 0.003 ± 0.003	0.802 ± 0.003 ± 0.001	0.808 ± 0.006 ± 0.005
[1.3, 1.37]	0.657 ± 0.020 ± 0.011	0.660 ± 0.011 ± 0.003	0.683 ± 0.007 ± 0.002	0.728 ± 0.004 ± 0.002	0.761 ± 0.004 ± 0.002	0.787 ± 0.004 ± 0.003	0.786 ± 0.008 ± 0.001
[1.52, 1.6]	0.610 ± 0.016 ± 0.006	0.660 ± 0.008 ± 0.002	0.710 ± 0.005 ± 0.003	0.750 ± 0.004 ± 0.002	0.775 ± 0.003 ± 0.001	0.810 ± 0.004 ± 0.000	0.810 ± 0.007 ± 0.001
[1.6, 1.7]	0.645 ± 0.016 ± 0.004	0.657 ± 0.009 ± 0.003	0.715 ± 0.005 ± 0.001	0.740 ± 0.003 ± 0.003	0.773 ± 0.003 ± 0.002	0.818 ± 0.004 ± 0.001	0.836 ± 0.006 ± 0.001
[1.7, 1.8]	0.672 ± 0.016 ± 0.005	0.681 ± 0.008 ± 0.002	0.715 ± 0.005 ± 0.002	0.734 ± 0.003 ± 0.001	0.764 ± 0.003 ± 0.002	0.802 ± 0.003 ± 0.002	0.821 ± 0.006 ± 0.002
[1.8, 1.9]	0.619 ± 0.016 ± 0.004	0.645 ± 0.009 ± 0.003	0.683 ± 0.005 ± 0.001	0.714 ± 0.003 ± 0.001	0.750 ± 0.003 ± 0.000	0.787 ± 0.004 ± 0.000	0.792 ± 0.007 ± 0.001
[1.9, 2.0]	0.632 ± 0.016 ± 0.006	0.639 ± 0.008 ± 0.001	0.656 ± 0.005 ± 0.001	0.703 ± 0.003 ± 0.003	0.731 ± 0.003 ± 0.001	0.765 ± 0.004 ± 0.000	0.769 ± 0.007 ± 0.001
[2.01, 2.1]	0.660 ± 0.018 ± 0.004	0.694 ± 0.009 ± 0.002	0.721 ± 0.005 ± 0.004	0.745 ± 0.004 ± 0.003	0.782 ± 0.003 ± 0.002	0.816 ± 0.003 ± 0.001	0.817 ± 0.006 ± 0.002
[2.1, 2.2]	0.705 ± 0.016 ± 0.003	0.711 ± 0.009 ± 0.004	0.742 ± 0.005 ± 0.002	0.770 ± 0.003 ± 0.002	0.801 ± 0.002 ± 0.001	0.842 ± 0.003 ± 0.001	0.845 ± 0.006 ± 0.000
[2.2, 2.3]	0.656 ± 0.018 ± 0.003	0.669 ± 0.010 ± 0.005	0.710 ± 0.005 ± 0.002	0.731 ± 0.003 ± 0.002	0.765 ± 0.003 ± 0.000	0.804 ± 0.003 ± 0.001	0.826 ± 0.006 ± 0.002
[2.3, 2.4]	0.574 ± 0.020 ± 0.005	0.586 ± 0.010 ± 0.008	0.641 ± 0.006 ± 0.001	0.661 ± 0.004 ± 0.003	0.684 ± 0.003 ± 0.002	0.727 ± 0.004 ± 0.001	0.738 ± 0.007 ± 0.002
[2.4, 2.47]	0.503 ± 0.025 ± 0.006	0.515 ± 0.013 ± 0.006	0.568 ± 0.008 ± 0.003	0.596 ± 0.005 ± 0.002	0.612 ± 0.004 ± 0.002	0.656 ± 0.005 ± 0.001	0.670 ± 0.010 ± 0.001

Table A.30: TightPP Monte-Carlo efficiencies in fine  $\eta$  granularity with their statistical and systematic uncertainties from 80 variations.

---

## B Derivation of the Statistical Formulae

---

Here, the equations used to calculate the statistical uncertainties on the efficiencies are derived, considering the correlations between the templates. The most general case used in the analysis, the statistical uncertainty on the difference between the efficiency of positive and negative charge, is deduced. The appropriate equation for a single efficiency with or without considering the correlation can easily be read off the result as special cases. Part of the notation and assumptions were used in Section 6.7, already.

We consider the sum/difference  $\bar{\varepsilon}$  of two efficiencies  $\varepsilon_+$  and  $\varepsilon_-$ .

$$\bar{\varepsilon} = \varepsilon_+ \pm \varepsilon_- \quad (\text{B.1})$$

The number of total events  $N_0$  and the number of passed events  $N_P$  for both are background contaminated

$$\varepsilon = \frac{N_{\text{Sig},P} - N_{\text{Bkg},P}}{N_{\text{Sig},0} - N_{\text{Bkg},0}} \quad (\text{B.2})$$

Following the approach given in Ref. [43] we rewrite  $N_0 = N_P + N_F$ , with  $N_F$  the number of failed events. Again, each efficiency is the function of four variables

$$\varepsilon_+ = \frac{N_{\text{Sig},P+} - N_{\text{Bkg},P+}}{N_{\text{Sig},P+} - N_{\text{Bkg},P+} + N_{\text{Sig},F+} - N_{\text{Bkg},F+}} \quad (\text{B.3})$$

$$\varepsilon_- = \frac{N_{\text{Sig},P-} - N_{\text{Bkg},P-}}{N_{\text{Sig},P-} - N_{\text{Bkg},P-} + N_{\text{Sig},F-} - N_{\text{Bkg},F-}} \quad (\text{B.4})$$

The numbers  $N_{\text{Sig}}$  are completely independent whereas the numbers  $N_{\text{Bkg}}$  are correlated. We calculate the Jacobian matrix for Eq. B.1

$$J_{\bar{\varepsilon}}(N_{\text{Sig},P+}, N_{\text{Sig},F+}, N_{\text{Bkg},P+}, N_{\text{Bkg},F+}, N_{\text{Sig},P-}, N_{\text{Sig},F-}, N_{\text{Bkg},P-}, N_{\text{Bkg},F-}) \\ = \left( \begin{array}{cccccc} \frac{(1-\varepsilon_+)}{N_{0+}} & \frac{-\varepsilon_+}{N_{0+}} & \frac{-(1-\varepsilon_+)}{N_{0+}} & \frac{\varepsilon_+}{N_{0+}} & \pm \frac{(1-\varepsilon_-)}{N_{0-}} & \mp \frac{\varepsilon_-}{N_{0-}} & \mp \frac{(1-\varepsilon_-)}{N_{0-}} & \pm \frac{\varepsilon_-}{N_{0-}} \end{array} \right) \quad (\text{B.5})$$

where  $N_0$  is short for  $N_{\text{Sig},P} - N_{\text{Bkg},P} + N_{\text{Sig},F} - N_{\text{Bkg},F}$ .

The covariance matrix is

$$C(\varepsilon_+, \varepsilon_-) \quad (\text{B.6}) \\ = \begin{pmatrix} \delta_{\text{Sig},P+}^2 & 0 & 0 & 0 & 0 & 0 & 0 & 0 \\ 0 & \delta_{\text{Sig},F+}^2 & 0 & 0 & 0 & 0 & 0 & 0 \\ 0 & 0 & \delta_{\text{Bkg},P+}^2 & \delta_{\text{Bkg}(P+,F+)} & 0 & 0 & \delta_{\text{Bkg}(P+,P-)} & \delta_{\text{Bkg}(P+,F-)} \\ 0 & 0 & \delta_{\text{Bkg}(F+,P+)} & \delta_{\text{Bkg},F+}^2 & 0 & 0 & \delta_{\text{Bkg}(F+,P-)} & \delta_{\text{Bkg}(F+,F-)} \\ 0 & 0 & 0 & 0 & \delta_{\text{Sig},P-}^2 & 0 & 0 & 0 \\ 0 & 0 & 0 & 0 & 0 & \delta_{\text{Sig},F-}^2 & 0 & 0 \\ 0 & 0 & \delta_{\text{Bkg}(P-,P+)} & \delta_{\text{Bkg}(P-,F+)} & 0 & 0 & \delta_{\text{Bkg},P-}^2 & \delta_{\text{Bkg}(P-,F-)} \\ 0 & 0 & \delta_{\text{Bkg}(F-,P+)} & \delta_{\text{Bkg}(F-,F+)} & 0 & 0 & \delta_{\text{Bkg}(F-,P-)} & \delta_{\text{Bkg},F-}^2 \end{pmatrix}$$

so there are six covariances between variables to be considered. For the uncertainty of  $\bar{\varepsilon}$  we obtain

$$\delta_{\bar{\varepsilon}}^2 = J_{\bar{\varepsilon}} \cdot C(\varepsilon_+, \varepsilon_-) \cdot J_{\bar{\varepsilon}}^T \quad (\text{B.7})$$

$$= \frac{(1 - 2\varepsilon_+) \left( \delta_{\text{Sig},\text{P}+}^2 + \delta_{\text{Bkg},\text{P}+}^2 \right) + \varepsilon_+^2 \left( \delta_{\text{Sig},0+}^2 + \delta_{\text{Bkg},0+}^2 \right)}{(N_{\text{Sig},0+} - N_{\text{Bkg},0+})^2} \quad (\text{B.8})$$

$$- 2 \frac{\varepsilon_+ (1 - \varepsilon_+)}{(N_{\text{Sig},0+} - N_{\text{Bkg},0+})^2} \cdot \delta_{\text{Bkg}(\text{P}+, \text{F}+)} \quad (\text{B.9})$$

$$+ \frac{(1 - 2\varepsilon_-) \left( \delta_{\text{Sig},\text{P}-}^2 + \delta_{\text{Bkg},\text{P}-}^2 \right) - \varepsilon_-^2 \left( \delta_{\text{Sig},0-}^2 + \delta_{\text{Bkg},0-}^2 \right)}{(N_{\text{Sig},0-} - N_{\text{Bkg},0-})^2} \quad (\text{B.10})$$

$$- 2 \frac{\varepsilon_- (1 - \varepsilon_-)}{(N_{\text{Sig},0-} - N_{\text{Bkg},0-})^2} \cdot \delta_{\text{Bkg}(\text{P}-, \text{F}-)} \quad (\text{B.11})$$

$$\pm 2 \frac{1}{(N_{\text{Sig},0+} - N_{\text{Bkg},0+}) (N_{\text{Sig},0-} - N_{\text{Bkg},0-})} \times$$

$$\left[ (1 - \varepsilon_+) (1 - \varepsilon_-) \cdot \delta_{\text{Bkg}(\text{P}+, \text{P}-)} \right.$$

$$- \varepsilon_+ (1 - \varepsilon_-) \cdot \delta_{\text{Bkg}(\text{F}+, \text{P}-)}$$

$$- (1 - \varepsilon_+) \varepsilon_- \cdot \delta_{\text{Bkg}(\text{P}+, \text{F}-)}$$

$$\left. + \varepsilon_+ \varepsilon_- \cdot \delta_{\text{Bkg}(\text{F}+, \text{F}-)} \right] \quad (\text{B.12})$$

The first equation B.7 can be found in any statistics textbook, e.g. Ref. [47]. Eq. B.8 and B.10 are the equations for the single efficiencies  $\varepsilon_+$  and  $\varepsilon_-$  that were already given in Eq. 6.25. These are the equations to be used if the templates for positive and negative charge as well as probe and ID level are uncorrelated. Eq. B.9 and B.11 account for the fact that the templates used on probe and ID level are identical. These are used when stating the efficiency for a specific charge. Finally, Eq. B.12 accounts for correlations between the templates used for positive and negative charge, where the sign has to be chosen to fit the sum and the difference.

We still need to obtain the explicit equation for the covariances. Following Section 6.7.1, the number of background events is as a function of data events in the control region and the fraction  $\beta$  of template events in signal and control region. The fraction  $\beta$  is the same in all of the four considered cases. The derivation of the covariance is given for  $\delta_{\text{Bkg}(\text{P}+, \text{F}-)}$ , the others can be obtained accordingly. With

$$N_{\text{Bkg},\text{P}+} = \beta N_{\text{dataR},\text{P}+} \quad (\text{B.13})$$

$$N_{\text{Bkg},\text{F}-} = \beta N_{\text{dataR},\text{F}-} \quad (\text{B.14})$$

the Jacobian matrix is

$$J(N_{\text{Bkg},\text{P}+}(\beta, N_{\text{dataR},\text{P}+}), N_{\text{Bkg},\text{F}-}(\beta, N_{\text{dataR},\text{F}-}))$$

$$= \begin{pmatrix} N_{\text{dataR},\text{P}+} & \beta & 0 \\ N_{\text{dataR},\text{F}-} & 0 & \beta \end{pmatrix}. \quad (\text{B.15})$$

The variables  $\beta$ ,  $N_{\text{dataR,P+}}$  and  $N_{\text{dataR,F-}}$  are uncorrelated. From the Jacobian and the covariance matrix

$$C(\beta, N_{\text{dataR,P+}}, N_{\text{dataR,F-}}) = \begin{pmatrix} \delta_\beta^2 & 0 & 0 \\ 0 & \delta_{\text{dataR,P+}}^2 & 0 \\ 0 & 0 & \delta_{\text{dataR,F-}}^2 \end{pmatrix} \quad (\text{B.16})$$

it follows that

$$\begin{aligned} C(\beta, N_{\text{Bkg,P+}}, N_{\text{Bkg,F-}}) &= J \cdot C(\beta, N_{\text{dataR,P+}}, N_{\text{dataR,F-}}) \cdot J^T \\ &= \begin{pmatrix} \delta_{\text{Bkg,P+}}^2 & N_{\text{dataR,P+}} N_{\text{dataR,F-}} \sigma_\beta^2 \\ N_{\text{dataR,P+}} N_{\text{dataR,F-}} \sigma_\beta^2 & \delta_{\text{Bkg,F-}}^2 \end{pmatrix} \end{aligned} \quad (\text{B.17})$$

using again the notation introduced in Section 6.7.1. The covariance  $\delta_{\text{Bkg(P+,F-)}}$  can just be read off the matrix and further simplified

$$\begin{aligned} \delta_{\text{Bkg(P+,F-)}} &= N_{\text{dataR,P+}} N_{\text{dataR,F-}} \sigma_\beta^2 \\ &= N_{\text{Bkg,P+}} N_{\text{Bkg,F-}} \left( \left( \frac{\delta_{\text{templL}}}{N_{\text{templL}}} \right)^2 + \left( \frac{\delta_{\text{templR}}}{N_{\text{templR}}} \right)^2 \right) \end{aligned} \quad (\text{B.18})$$



---

# C

---

# Technicalities

---

The information whether a certain identification cut was passed or failed is stored in a binary number where every digit represents a certain cut. They were used in Sections 8.2 and 9.2.2 and are therefore listed here.

ClusterEtaRange_Electron	=	0	TrackBlayer_Electron	=	16
ConversionMatch_Electron	=	1	TrackPixel_Electron	=	17
ClusterHadronicLeakage_Electron	=	2	TrackSi_Electron	=	18
ClusterMiddleEnergy_Electron	=	3	TrackA0_Electron	=	19
ClusterMiddleEratio37_Electron	=	4	TrackMatchEta_Electron	=	20
ClusterMiddleEratio33_Electron	=	5	TrackMatchPhi_Electron	=	21
ClusterMiddleWidth_Electron	=	6	TrackMatchEoverP_Electron	=	22
			TrackTRThits_Electron	=	24
ClusterStripsEratio_Electron	=	8	TrackTRTratio_Electron	=	25
ClusterStripsDeltaEmax2_Electron	=	9	TrackTRTratio90_Electron	=	26
ClusterStripsDeltaE_Electron	=	10	TrackA0Tight_Electron	=	27
ClusterStripsWtot_Electron	=	11	TrackMatchEtaTight_Electron	=	28
ClusterStripsFracm_Electron	=	12	Isolation_Electron	=	29
ClusterStripsWeta1c_Electron	=	13	ClusterIsolation_Electron	=	30
ClusterStripsDEmaxs1_Electron	=	15	TrackIsolation_Electron	=	31



---

## Bibliography

---

- [1] ATLAS Collaboration, G. Aad *et al.*, *Electron performance measurements with the ATLAS detector using the 2010 LHC proton-proton collision data*, arXiv:1110.3174 [hep-ex].
- [2] ATLAS Collaboration, *Electron performance measurements using the 2011 LHC proton-proton collision data*, ATL-COM-PHYS-2012-1024, Jul, 2012.
- [3] ATLAS Collaboration, *Supporting document on electron performance measurements using the 2011 LHC proton-proton collision data*, ATL-COM-PHYS-2012-1023, Jul, 2012.
- [4] F. Halzen and A. D. Martin, *Quarks and Leptons: An Introductory Course in Modern Particle Physics*. Wiley, 1984.
- [5] M. E. Peskin and D. V. Schroeder, *An Introduction to Quantum Field Theory*. Westview Press, 1995.
- [6] W. Buchmuller and C. Ludeling, *Field Theory and Standard Model*, arXiv:hep-ph/0609174 [hep-ph].
- [7] *CERN Press Release: CERN experiments observe particle consistent with long-sought Higgs boson*, Jul, 2012.
- [8] *Observation of an Excess of Events in the Search for the Standard Model Higgs boson with the ATLAS detector at the LHC*, ATLAS note: ATLAS-CONF-2012-093, Jul, 2012.
- [9] Particle Data Group, K. Nakamura *et al.*, *Review of particle physics*, J. Phys. **G37** (2010) 075021.
- [10] R. Ellis, W. Stirling, and B. Webber, *QCD and collider physics*, vol. 8. 1996.
- [11] A. D. Martin, W. J. Stirling, R. S. Thorne, and G. Watt, *Parton distributions for the LHC*, Eur. Phys. J. **C63** (2009) 189, arXiv:0901.0002 [hep-ph].
- [12] J. Butterworth *et al.*, *Single Boson and Diboson Production Cross Sections in pp Collisions at  $\sqrt{s} = 7$  TeV*, ATLAS internal note: ATL-COM-PHYS-2010-695.
- [13] C. Anastasiou, L. J. Dixon, K. Melnikov, and F. Petriello, *High precision QCD at hadron colliders: Electroweak gauge boson rapidity distributions at NNLO*, Phys. Rev. **D69** (2004) 094008, arXiv:hep-ph/0312266.

- [14] J. M. Campbell, J. W. Huston, and W. J. Stirling, *Hard Interactions of Quarks and Gluons: A Primer for LHC Physics*, Rept. Prog. Phys. **70** (2007) 89, [arXiv:hep-ph/0611148](#).
- [15] ATLAS Collaboration, G. Aad *et al.*, *The ATLAS Simulation Infrastructure*, Eur. Phys. J. **C70** (2010) 823, [arXiv:1005.4568 \[physics.ins-det\]](#).
- [16] S. Alioli, P. Nason, C. Oleari, and E. Re, *A general framework for implementing NLO calculations in shower Monte Carlo programs: the POWHEG BOX*, JHEP **06** (2010) 043, [arXiv:1002.2581 \[hep-ph\]](#).
- [17] T. Sjostrand, S. Mrenna, and P. Z. Skands, *PYTHIA 6.4 Physics and Manual*, JHEP **05** (2006) 026, [arXiv:hep-ph/0603175](#).
- [18] P. Golonka and Z. Was, *PHOTOS Monte Carlo: A Precision tool for QED corrections in Z and W decays*, Eur. Phys. J. **C45** (2006) 97, [arXiv:hep-ph/0506026](#).
- [19] T. Sjostrand, S. Mrenna, and P. Z. Skands, *A Brief Introduction to PYTHIA 8.1*, Comput.Phys.Comm. **178** (2008) 852–867, [arXiv:0710.3820 \[hep-ph\]](#).
- [20] GEANT4 Collaboration, S. Agostinelli *et al.*, *GEANT4: A simulation toolkit*, Nucl. Instrum. Meth. **A506** (2003) 250.
- [21] O. Brüning *et al.*, *LHC design report*, CERN-2004-003-V-1, CERN-2004-003-V-2, CERN-2004-003-V-3, 2004.
- [22] ATLAS Collaboration, G. Aad *et al.*, *The ATLAS Experiment at the CERN Large Hadron Collider*, JINST **3** (2008) S08003.
- [23] <https://twiki.cern.ch/twiki/bin/view/AtlasPublic/LuminosityPublicResults>.
- [24] T. Luminosity Group, *Improved Luminosity Determination in pp Collisions at  $\sqrt{s} = 7$  TeV using the ATLAS Detector at the LHC*, ATLAS-COM-CONF-2012-086, Jun, 2012.
- [25] J. Hartert, *Measurement of the  $W \rightarrow e\nu$  and  $Z/\gamma^* \rightarrow ee$  Production Cross-Sections in Proton-Proton Collisions at  $\sqrt{s} = 7$  TeV with the ATLAS Experiment*. PhD thesis, Freiburg U., Freiburg, 2011. Presented 20 Dec 2011.
- [26] ATLAS Collaboration, G. Aad *et al.*, *Measurement of the inclusive  $W^\pm$  and  $Z/\gamma^*$  cross sections in the electron and muon decay channels in pp collisions at  $\sqrt{s} = 7$  TeV with the ATLAS detector*, [arXiv:1109.5141 \[hep-ex\]](#).
- [27] Sasha Glazov, *Precision requirements for electrons*, Talk at the ATLAS  $e/\gamma$  workshop, 24 Oct 2011.
- [28] *Search for the Standard Model Higgs boson in the decay channel  $H \rightarrow ZZ^{(*)} \rightarrow 4\ell$  with  $4.8 \text{ fb}^{-1}$  of pp collisions at  $\sqrt{s} = 7$  TeV*, ATLAS note: ATLAS-CONF-2011-162, Dec, 2011.

- [29] ATLAS Collaboration, G. Aad *et al.*, *Expected Performance of the ATLAS Experiment - Detector, Trigger and Physics*, arXiv:0901.0512 [hep-ex].
- [30] ATLAS Collaboration, *Performance of primary vertex reconstruction in proton-proton collisions at  $\sqrt{s} = 7$  TeV in the ATLAS experiment*, ATLAS note: ATLAS-CONF-2010-069.
- [31] ATLAS Collaboration, *Expected electron performance in the ATLAS experiment*, ATLAS note: ATL-PHYS-PUB-2011-006.
- [32] <https://twiki.cern.ch/twiki/bin/viewauth/AtlasProtected/IsEMIdentification>.
- [33] <https://twiki.cern.ch/twiki/bin/viewauth/AtlasProtected/ElectronReconstruction>.
- [34] <https://svnweb.cern.ch/trac/atlasoff/browser/Reconstruction/egamma/egammaPIDTools/trunk/python>.
- [35] *Performance of the ATLAS Electron and Photon Trigger in p-p Collisions at  $\sqrt{s} = 7$  TeV in 2011*, ATLAS note: ATLAS-CONF-2012-048, May, 2012.
- [36] J. Hartert and I. Ludwig, *Electron isolation in the ATLAS experiment*, ATLAS internal note: ATL-PHYS-INT-2010-052.
- [37] *Performance of the Missing Transverse Energy Reconstruction and Calibration in Proton-Proton Collisions at a Center-of-Mass Energy of 7 TeV with the ATLAS Detector*, ATLAS note: ATLAS-CONF-2010-057, Jul, 2010.
- [38] T. Barillari *et al.*, *Local Hadronic Calibration*, ATL-LARG-PUB-2009-001, Jun, 2008.
- [39] <https://twiki.cern.ch/twiki/bin/viewauth/Atlas/AtlasHltMetSlice>.
- [40] ATLAS Collaboration, G. Aad *et al.*, *Measurement of the  $W \rightarrow l\nu$  and  $Z/\gamma^* \rightarrow ll$  production cross sections in proton-proton collisions at  $\sqrt{s} = 7$  TeV with the ATLAS detector*, JHEP **12** (2010) 060, arXiv:1010.2130 [hep-ex].
- [41] Stephen Gibson, *Update on Wenu Tag and Probe electron efficiency*, Talk in the ATLAS  $e/\gamma$  T&P meeting, 10 Dec 2010.
- [42] L. Fayard, *Private communication*, Jun, 2012.
- [43] C. Blocker, *Uncertainties on Efficiencies*, CDF/MEMO/STATISTICS/PUBLIC/7168.
- [44] <https://twiki.cern.ch/twiki/bin/viewauth/Atlas/MC11b>.
- [45] <https://twiki.cern.ch/twiki/bin/viewauth/AtlasProtected/ExtendedPileupRewighting>.

- [46] S. Resconi, D. Cavalli, S. Simoniello, *Comparison of EtMiss performance with MC11 Pythia8 and Pythia6 pile-up simulation*, Talk at the ATLAS jet/ $E_T^{\text{miss}}$  meeting, 23 Nov 2011.
- [47] V. Blobel and E. Lohrmann, *Statistische und numerische Methoden der Datenanalyse*. Teubner, 1998.